Exploring the Feasibility of Modular Hybrid Systems

Mid-Rise Buildings of Modular Housing Units with Integrated Precast Concrete Cores

Master thesis: Building Engineering

S.W.Q.S. Blanken

Delft University of Technology

TUDelft

INGENIEURSSTUDIO DCK

Exploring the Feasibility of Modular Hybrid Systems

Mid-Rise Buildings of Modular Housing Units with Integrated Precast Concrete Cores

by

S.W.Q.S. Blanken

Student Name	Student Number
S.W.Q.S. Blanken	4681924

TUDelft

Preface

The research presented in this thesis is the result of my master's study in Building Engineering at Delft University of Technology. This thesis explores the feasibility of modular hybrid systems for mid-rise buildings by integrating modular housing units with precast concrete cores. It represents the culmination of months of dedicated research, analysis, and design development, supported by industry collaboration.

The motivation for this research stems from the urgent need for innovative, efficient, and scalable housing solutions, particularly in the context of urban densification and sustainability challenges. Modular construction has emerged as a promising alternative to traditional methods, offering benefits such as reduced construction time, improved quality control, and lower environmental impact. However, structural limitations, particularly in the mid- to high-rise segment, require further investigation to unlock the full potential of this construction method.

This thesis would not have been possible without the invaluable guidance and support of my thesis committee: dr.ir. H.R. Schipper, Prof.dr.ir. M.A.N. Hendriks, dr.ir. D.C. van Keulen, and ir. C.J. Mommaas. Their expertise and critical insights have greatly contributed to shaping the direction of this research. Additionally, I would like to extend my gratitude to Daiwa Modular Europe and DCK for their collaboration, providing essential industry perspectives and technical input.

I also extend my heartfelt thanks to my parents, brothers (Sweder, Max, and Willem), sisters (Emma and Machteld), brother-in-laws (Juan and Patrick), my niece (Josephine) and the newest addition to our family (Livia) for their unwavering support throughout this journey. Their encouragement and belief in my abilities motivated me to put forth my best effort throughout this endeavour.

I hope this research contributes to the ongoing development of modular construction and inspires further advancements in the field.

S.W.Q.S. Blanken
Delft, July 2025

Abstract

The Netherlands faces an urgent housing shortage, especially in urban areas where demand outpaces supply and space for new development is limited. Modular construction presents a scalable and efficient solution, yet its application in mid-rise buildings up to 70 metres remains constrained by unresolved structural challenges, particularly regarding lateral stability, connection behaviour, and collective module behaviour. Previous research acknowledged the individual potential of outrigger elements and tie-rod connections to enhance stability, but their combined integration in a modular mid-rise context had not yet been fully explored.

This thesis addresses that gap by developing, analysing, and validating a hybrid structural concept in which corner-supported steel modules actively contribute to the building's lateral load resistance. The proposed system integrates tie-rods and steel outriggers with a precast concrete core to transform the modular units from passive vertical load carriers into active components of the lateral stability system. To assess this system, a four-phase research strategy was adopted, including a feasibility study, concept development, structural optimisation, and a final *3D* case-study application. A key methodological decision was the use of *parametric modelling* tools, *Grasshopper* and *Karamba3D*, to enable rapid iteration and flexible structural analysis across design alternatives.

The analysis demonstrated that, in a 20-storey structure, the integration of two outrigger levels (floors 7 and 14) reduced top displacement by $13.5\,\%$ compared to a *core-only* structure. The structure reached a height of $67.7\,\mathrm{m}$ while satisfying the $H/750$ serviceability criterion. Member utilisation levels remained below 1.0, and tie-rod forces stayed within feasible limits. However, the effectiveness of the proposed concept was significantly influenced by axial elongation of the tie-rods: M24 tie-rods reduced outrigger effectiveness to $17.7\,\%$ compared to $25.4\,\%$ in the idealised case without elongation, while M50 tie-rods improved performance to $20.5\,\%$. Parametric studies further showed that outrigger effectiveness depends strongly on the stiffness of the concrete core. With a flexible core, outriggers reduced lateral displacements by over $30\,\%$; this benefit dropped below $10\,\%$ for stiffer configurations, underscoring the importance of a balanced stiffness distribution between core and outriggers to maximise the effectiveness of the proposed concept.

These findings demonstrate that the proposed hybrid concept is a viable solution for modular mid-rise construction, enabling greater design heights while maintaining structural efficiency. The innovative use of parametric modelling not only enhanced design flexibility but also accelerated the evaluation process. The research contributes a validated structural concept that addresses current limitations in modular design and provides a foundation for further innovation in hybrid modular systems.

Keywords: Modular construction, hybrid system, precast concrete core, tie-rod connection, outrigger, mid-rise buildings, parametric modelling, structural feasibility

Contents

1

Introduction

1.1. Context

The Netherlands is currently experiencing a significant housing shortage, with a deficit of 279,000 homes in 2021, projected to grow to 317,000 by 2024. This housing demand is driven by several factors, including immigration, an increasing number of single-person households, and the profound impact of an ageing population. Immigration plays a pivotal role in housing demand, as newcomers typically settle in urban areas where housing shortages are already critical. Similarly, the increasing number of single-person households, attributed to societal changes such as the number of older or young professionals living alone, increases the strain on the housing market. Furthermore, the ageing population exacerbates the housing shortage, as older people live longer and tend to stay in their homes, reducing market turnover and restricting housing availability [1][2].

This trend is especially pronounced in large cities, where the demand for affordable small homes for single individuals and small families far exceeds the available supply [3]. Complementing these challenges is the limited availability of land for construction, which complicates efforts to build new housing. The construction sector also faces delays due to lengthy procedures and stringent regulations. Excessive nitrogen emissions in the Netherlands have led to restrictive environmental laws, further complicating the process of obtaining building permits for housing projects. These regulations significantly delay construction start times and increase costs [4]. In addition, high interest rates, inflation, and material shortages continue to drive up expenses in the construction industry, resulting in fewer housing developments [1].

To effectively address the housing shortage, a revolutionary shift towards efficient and industrialised construction methods is essential. Prefabrication, such as the production of concrete elements, provides a practical approach to tackling several of the previously mentioned challenges. Modular construction represents a highly advanced form of industrialised building, emerging as a promising solution. At its core, modular construction entails the off-site manufacturing one of the building components, which can range from structural elements like columns and beams to fully assembled wall, floor, and ceiling panels, as well as complete 3D modules. These modules are often integrated with building services and finishes in the factory, enabling them to arrive on-site nearly complete and ready for immediate assembly. Each module then seamlessly interlocks with the others, much like pieces of a puzzle, to form a cohesive and fully functional structure [5]. By manufacturing modules in a controlled factory environment, various stages of construction can proceed simultaneously, significantly reducing overall build time compared to traditional methods [6]. Additionally, modular construction offers benefits in terms of space and environmental efficiency, particularly in urban areas where construction sites are often constrained. These constraints include limited space for storing materials and equipment, restricted site access due to traffic, and strict regulations on noise and dust control. Since most construction occurs off-site, the impact on the surrounding environment is greatly minimized, allowing projects in densely populated areas to proceed with minimal disruption to the environment [7]. Its standardized production reduces material waste, lowers costs, and decreases nitrogen emissions, simplifying permit acquisition under strict environmental regulations [5].

Despite the numerous advantages of modular construction, certain drawbacks must also be considered when analysing this construction method. Firstly, the standardized production process, which drives down costs, can restrict design flexibility.This poses challenges for projects requiring specific architectural features or irregular geometries. Additionally, transporting modules to the construction site can be hindered by logistical constraints, especially in urban areas with limited access. Moreover, fully furnished modules are particularly vulnerable to issues during transportation or movement, such as cracking in sealants or finishes, which are highly sensitive to the additional forces involved. While these forces can be accounted for in structural design, ensuring the integrity of internal finishes remains a challenge. Modular construction often requires substantial initial investments in production facilities and specialized equipment, particularly when employing industrialized approaches such as robotic systems or carousel processes. Furthermore, this method demands a high level of precision and coordination among multiple parties, which can sometimes lead to delays if coordination is insufficient [8].

Modular construction is mostly utilized in low-rise buildings, typically defined as structures up to 35 meters in height, due to its inherent advantages such as efficiency and rapid assembly. However, extending this approach to mid-rise buildings, which range from 35 to 70 meters, introduces several significant technical challenges. These challenges include managing vertical load-bearing capacity, ensuring lateral stability, designing robust connections, and achieving effective group action of interconnected modules.

- **Vertical load capacity:** While modular buildings are highly efficient for constructing mid-rise structures within impressively short time frames, the challenge of managing vertical loads increases significantly with each additional floor. Given the slender nature of modular units, stacking multiple modules introduces concentrated point loads at the structural elements of each module. As the height of the building increases, the forces carried by the load-bearing elements in the lower modules grow significantly, as they must transfer the cumulative loads from all the floors above. In modular systems, these forces are particularly concentrated at the corners of the modules, where load transfer occurs. If not properly addressed, this can lead to structural issues such as differential settlement or local buckling of the members in these critical areas [9].

- **Lateral stability:** Mid-rise structures must resist significant lateral forces, such as wind or seismic loads, which modular units alone cannot adequately manage[10].

- **Connections:** Connections are pivotal in mid-rise modular buildings, as they must not only join individual modules but also contribute to overall structural stability. Modular construction involves a greater number of connections compared to in-situ methods [11]. These connections must handle multi-directional load transfers, such as axial forces, shear forces, bending moments, and torsional forces, all of which increase with the height of the building. Ensuring their robustness becomes increasingly demanding at greater scales [6].

- **Group Action of modules:** The collective behaviour of interconnected modules, or group action, is an important area of investigation for maintaining structural stability. Key questions include how diaphragm action distributes lateral loads and whether module interdependence could increase the risk of progressive collapse. Weak connections, inadequate load transfer, or uneven force distribution may significantly compromise stability in modular systems [12].

Addressing these challenges is essential for developing a modular construction concept capable of supporting mid-rise buildings. This research aims to explore innovative solutions to overcome these challenges, enabling the construction of taller modular structures.

1.2. Research

This section defines the research framework, presenting the problem statement, scope, main research question, and sub-questions for each phase. It establishes the key challenges and outlines the systematic approach to addressing them.

1.2.1. Problem Statement

The potential of modular construction to address the housing shortage in the Netherlands is evident, yet its application in mid-rise structures remains limited due to significant structural challenges. These challenges primarily involve the handling of vertical and lateral loads. This research seeks to bridge these gaps by exploring hybrid stability systems, such as outrigger systems combined with tie-rod connections, which integrate modular units with precast concrete elements. These systems have the potential to optimize load transfer, enhance lateral stability, and extend the feasible height of modular mid-rise buildings, paving the way for innovative applications in urban construction.

1.2.2. Scope

This study focuses on the design and evaluation of structural concepts that integrate modular units with prefabricated concrete systems for mid-rise applications. It encompasses:

1. A critical review of existing stability systems and structural limitations in modular high-rise and mid-rise buildings.
2. Development of a structural system which combines tie-rod connections and outrigger technology.
3. *Parametric* modelling and structural analysis to evaluate the feasibility of proposed designs for modular buildings up to 70 meters.
4. A case study applying the optimized structural concept to the Tang Tower, validating its practical feasibility.

1.2.3. Research Questions

The central research question guiding this thesis is:

How can the integration of hybrid stability systems be applied to the concept of modular units and precast concrete to build a mid-rise structure up to 70 meters?

To effectively address the main research question, the study is divided into four phases, each guided by specific sub-questions that contribute to answering the overarching research objective. The sub-questions addressed in each research phase are as follows:

Sub-Question Phase 1: Preliminary Research and Feasibility Assessment

- *What are the key structural limitations and possibilities of modular systems up to 70 meters, and which solutions are already proposed in literature and design practice?*

Sub-Question Phase 2: Concept Development and Initial Modelling

- *How can outrigger systems and tie-rod connections be integrated into the conceptual design of modular buildings up to 70 meters, and to what extent does this integration enhance structural performance?*

Sub-Question Phase 3: Detailed Structural Analysis

- *How can a detailed structural analysis be used to evaluate the performance of the proposed modular mid-rise concept and guide its design optimizations?*

Sub-question Phase 4: Case Study-Tang Tower

- *How can the structural concept be applied in the context of the Tang Tower to validate the proposed design solution and what is the result of this?*

1.3. Methodology
This section details the methodology employed to address the sub-questions of each research phase. For each phase, a description of the research objectives is provided, followed by the specific sub-goals. The methodology used to achieve these goals is then discussed, and the section concludes with the desired outcomes for each phase.

Phase 1: Preliminary Research and Feasibility Assessment
This phase focuses on understanding the current state of modular high-rise and mid-rise buildings, identifying challenges, and exploring potential structural innovations.

Sub-Goals Phase 1:
1. **Assess Feasibility of Modular mid-rise Systems**: Conduct a feasibility study to assess the viability of modular mid-rise buildings up to 70 meters. This includes evaluating the limitations of modular units, particularly with respect to load-bearing capacity, lateral stability systems, connection behaviour and group action of modules.

2. **Evaluate Current Modular mid-rise Stability Systems:** Examine the current stability systems used in modular mid-rise construction and assessing their effectiveness in resisting lateral loads

3. **Identify Key Influence Factors and Explore Innovative Solutions:** Examine the primary factors affecting the stability of modular mid-rise buildings and explore potential innovations that could enhance structural performance. This includes investigating novel methods to improve load distribution and lateral stability in ways not commonly employed in current modular construction practices.

Methodology Phase 1:
1. **Literature Review:** A literature review is conducted to gather insights from existing research and case studies on modular high-rise and mid-rise structures. This process involves reviewing key publications on modular construction methods, with a specific focus on vertical load-bearing capacity, lateral stability systems, and connection mechanisms. In addition, technical reports and industry standards, such as Eurocodes and other relevant modular construction guidelines, are analyzed to understand the structural requirements and limitations of these systems. Case studies of existing modular high-rise buildings are also investigated to examine the use of concrete cores, lateral stability systems, and connection technologies. These reference projects provide valuable insights into the challenges encountered in modular mid- and high-rise construction and highlight potential areas for innovation.

2. **Feasibility Assessment:**Using insights from the literature review, an initial feasibility assessment will evaluate the structural viability of modular systems for high-rise and mid-rise buildings. This process combines the review findings with basic structural analysis through simplified load models to gain preliminary understanding of modular building behaviour and the strength of individual structural elements. Preliminary structural design calculations will be used to assess load-bearing capacity, the efficiency of load transfer throughout the structure, and the relative effectiveness of various stability systems, including unbraced systems, braced systems, core systems, and outrigger systems.

The desired outcome of this phase is to understand the structural challenges of modular systems, assess their feasibility up to 70 meters, and identify limitations in current stability methods. It will also provide preliminary insights to guide the concept design, focusing on potential solutions.

Phase 2: Concept Development and Initial Modelling

This phase focuses on developing the conceptual design, which consists of various components, including the outrigger system and tie-rod connections. Once the concept is established, a structural model will be developed to represent it. This model is subsequently used to evaluate the preliminary structural feasibility of the proposed concept in achieving the target height of $70\,\mathrm{m}$.

1. **Develop the Concept for the Modular System:** Define and develop the overall concept for the modular system, incorporating key components such as tie-rod connections and outrigger systems. This includes identifying design parameters and their integration with prefabricated cores to ensure structural feasibility.

2. **Create a Preliminary Modular mid-rise Structure Model:** Create a *parametric* model for a modular mid-rise system, focusing on key structural factors such as vertical load-bearing capacity, lateral stability, and connection performance. The model will evaluate how different design choices, such as module dimensions, connection design, and choice of stability system affect the overall structural performance.

3. **Analyse the Role of Tie-Rod Connections in Modular Stability:** Investigate the effectiveness of tie rod connections within modular units, focusing on their contribution to improving lateral stability and load-bearing capacity.

4. **Develop and Analyse an Integrated Outrigger System:** Create an outrigger system that works in conjunction with modular units and prefabricated cores. Analyse how this integrated system can further enhance lateral stability and improve the overall structural resilience of the mid-rise building.

Methodology Phase 2:
1. *Parametric* **Model Development:** The *parametric* modelling process will be done using *Grasshopper* in conjunction with *Rhinoceros 3D*, enabling flexible exploration of various design configurations. The model will be designed to accommodate changes in core design, stability systems, connection detailing, and modular dimensions, allowing for rapid iteration and comparison of alternatives.

2. **Initial Structural Analysis:** After the *parametric* model is developed, an initial structural analysis will be conducted with *Karamba 3D* to gain preliminary insights into the model's performance. Simplified load assumptions will be applied to evaluate how the structure behaves under increasing building heights, particularly in terms of load transfer through the corner columns of the modular units. The lateral stability of the building will also be assessed by simulating for example wind forces.

3. **Iterative Evaluation and Comparison:** Conduct iterative tests and comparisons of different design configurations to refine the model, ensuring it accurately represents the modular system's behaviour and feasibility for buildings up to 70 meters.

The desired outcome of this phase is to establish a conceptual design for modular buildings up to 70 meters, integrating key components such as tie-rod connections and outrigger elements. This includes the development of a detailed *parametric* model that effectively represents the modular system's structural behaviour. Through initial structural analysis, the feasibility of the proposed concept will be evaluated, providing critical insights into its ability to handle vertical and lateral loads. The findings from this phase will serve as a foundation for further refinement and detailed analysis in subsequent phases.

Phase 3: Detailed Structural Analysis

This phase focuses on refining and optimizing the structural concepts developed in Phase 2 through advanced computational analysis and *parametric* modelling. The primary objective is to evaluate the structural performance of the proposed outrigger system and tie-rod connections, and to verify their feasibility in supporting a modular concept capable of reaching the target height of $70\,\mathrm{m}$.

Sub-Goals Phase 3:

1. **Refinement of the Structural Model:** Further development and adjustment of the computational model to enhance accuracy and reliability in predicting structural behaviour. This includes refining load assumptions, core refinement, and material properties to ensure that the model provides a realistic representation of actual structural performance.

2. **In-Depth Analysis of Outrigger System and Tie Rod Connection Concept:** Utilize the refined model to conduct a comprehensive structural analysis, evaluating the interaction between the outrigger system and tie rod connections. Special attention will be given to the distribution of forces, load paths, and overall structural integrity.

3. **Optimize the Structural Concept for Application:** Based on the results from the detailed analyses, refine and optimize the proposed structural concept.

Methodology Phase 3:

1. **Refinement of the Computational Model:** The structural model will be further developed using *parametric* and finite element tools to enhance its predictive capability. Adjustments will be made based on preliminary findings from Phase 2 to more accurately represent real-world structural behaviour.

2. **Inventory of Optimal Structural Configurations:** Following the detailed structural analysis, an inventory of the most effective structural configurations will be compiled. Using *parametric* modelling in *Grasshopper*, iterative simulations will be conducted to optimize the placement, dimensions, and number of outrigger arms, as well as the stiffness balance between the outriggers and the prefabricated concrete core.

The desired outcome of this phase is a refined and optimized structural concept, suitable for real-world application. The resulting model will serve as the foundation for the *3D* model developed in the following and final phase.

Phase 4: Case Study Application – Tang Tower

This final phase applies the optimized structural concept to a real-world case study, testing the validity of the research findings within a *3D* environment.

Sub-Goal Phase 4:

1. **Application of the Optimized Structural Concept to the Tang Tower Case Study:** Implement the developed structural system, including the outrigger configuration and tie-rod connections, within a real-world case study of a $70\,\text{m}$ modular mid-rise building. The Tang Tower project, developed by DCK and Daiwa House Modular Europe, will serve as the basis for this application.

Methodology Phase 4:

1. **Case Study Application:** The case study will involve applying the *parametric* model and optimization results from the previous phases within a *3D* environment. The proposed structural system will be adapted to accommodate real-world constraints and to align with the architectural design of the Tang Tower. Structural plans provided by DCK and Daiwa House Modular Europe will serve as the basis for this phase, ensuring compliance with construction practices and relevant regulatory standards.

2. **Validation and Analysis:** In this stage, the performance of the Tang Tower incorporating the optimized structural system will be evaluated against a conventional core-only design. The comparative analysis will focus on improvements in load distribution, structural stability, and overall efficiency. The findings will be reviewed by experts from Daiwa House Modular Europe, who will provide feedback on the practicality of the system and its potential for implementation in real-world modular construction projects.

The desired outcome of this final phase is to validate the optimized structural concept by applying it to the Tang Tower case study. Through its implementation in a real-world *3D* scenario, the research aims to demonstrate the concept's effectiveness in enhancing lateral stability and overall structural performance in modular mid-rise buildings designed to reach the target height of $70\,\text{m}$, thereby providing an answer to the main research question.

An overview of the four research phases is given in figure 1.1.

Phase 1: Preliminary Research and Feasibility Assessment

Sub-Question 1	What are the **key structural limitations** and **possibilities** of modular systems up to 70 meters, and which solutions are already proposed in literature and design practice?
Methodology	• Literature Review • Investigating Reference Projects • Preliminary structural design calculations
Desired Outcome	The desired outcome is to Understand the structural challenges of modular systems, assess their feasibility up to 70 meters, and also provide preliminary insights to guide the concept design, focusing on potential solutions.

Phase 2: Concept Development and Initial Modelling

Sub-Question 2	How can **outrigger systems and tie-rod connections be integrated** into the conceptual design of modular buildings up to 70 meters, and to what extent does this integration **enhance structural performance**?
Methodology	• Parametric Model Development *(Grashopper)* • Initial Structural Analysis *(Karamba 3D)* • Iterative Evaluation and Comparison
Desired Outcome	The desired outcome of this phase is to establish a comprehensive conceptual design for modular buildings up to 70 meters, integrating key components such as tie-rod connections and an outrigger system.

Phase 3: Detailed Structural Analysis

Sub-Question 3	How can a **detailed structural analysis** be used to evaluate the performance of the proposed modular mid-rise concept and **guide its design optimizations**?
Methodology	• Refinement of the structural model • Parametric Simulation of different design configurations ▪ Connection Configuration, and Outrigger Design
Desired Outcome	The desired outcome of this phase is to refine the proposed structural system and optimize its configuration. This will result in a fully developed and validated structural concept that meets the stability and performance requirements necessary for real-world application.

Phase 4: Case Study Application – Tang Tower

Sub-Question 4	How can the structural concept be applied in the context of the Tang Tower **to validate the proposed design solution** and what is the result of this?
Methodology	• Applying the developed concept to real-life conditions • Comparative Analysis (Concept against traditional modular systems) • Expert Review
Desired Outcome	The desired outcome of this phase is to refine the tie-rod connection and optimize the structural configuration of the concept. This will result in a fully developed structural concept that is ready for real-world application.

Figure 1.1: Research phases overview

2

Modular construction

This chapter introduces modular construction, highlighting its principles, advantages, and disadvantages. It reviews five reference projects showcasing modular high-rise applications and explores design options, including modular systems, connections, and stability systems. The chapter concludes by identifying the specific design options that will form the focus of this research and serve as the foundation for the proposed structural concept.

2.1. Introduction

This section begins by explaining the main principles of modular construction and its underlying design philosophy. It then discusses the key advantages and disadvantages of this construction method. Finally, it concludes with five reference projects illustrating the application of modular concepts in both high-rise and mid-rise structures.

2.1.1. Principles and Philosophy of Modular Construction

Principle of modular construction

Modular construction is a building method where components, or modules, are prefabricated in a controlled factory environment before being transported to the construction site for final assembly. This approach enhances quality control, minimizes on-site labour, and significantly accelerates construction timelines. [13].

Design Philosophy

The design philosophy of modular construction focuses on efficiency, adaptability, and sustainability. Unlike conventional construction methods, it prioritizes the repeatability of standardized units, prefabricated in controlled environments to ensure precision, minimize waste, and enhance quality control. Each module is designed and produced to exact specifications before being transported to the construction site. In high-rise construction, this philosophy evolves to balance structural integrity with modular flexibility. It emphasizes that every module must not only fulfil the building's architectural and functional requirements but also integrate seamlessly with other modules to maintain overall structural stability. Achieving this demands extensive planning and close collaboration among architects, engineers, and manufacturers to align design objectives with technical feasibility.[7] [9] [6].
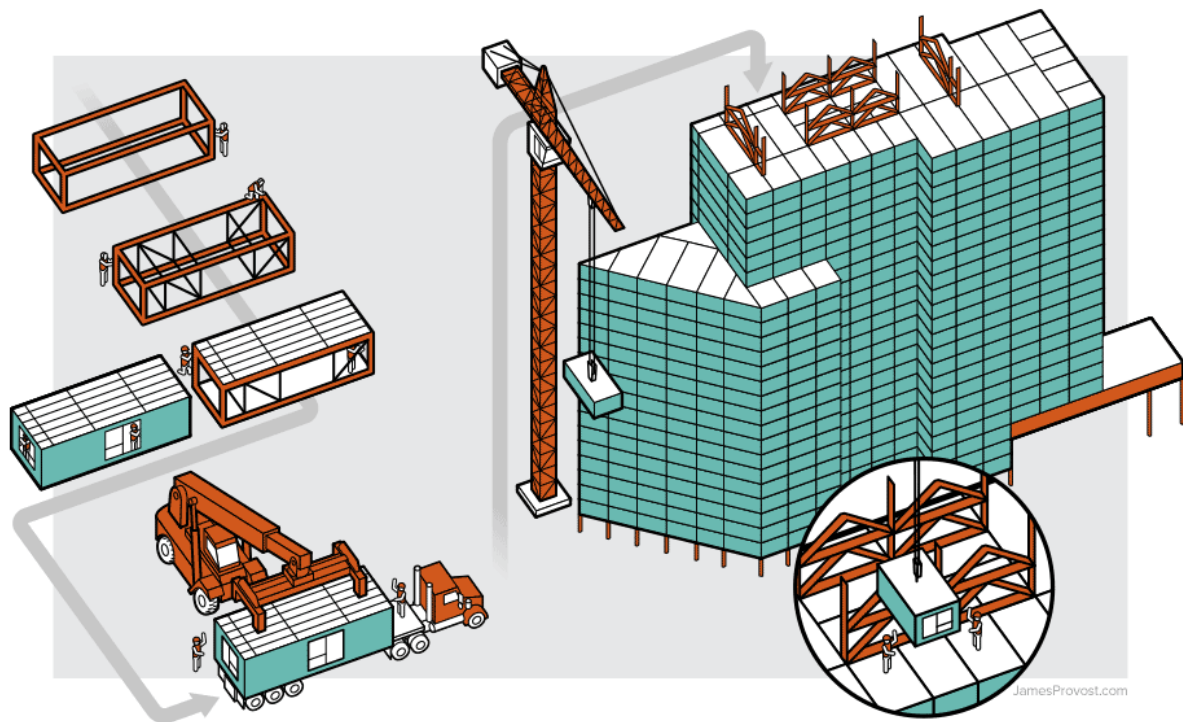
Figure 2.1: Modular Construction: from the factory to the construction site [14]

2.1.2. Advantages and Disadvantages

Advantages

Modular construction offers a range of benefits over traditional construction methods, particularly in terms of project efficiency, quality control, and environmental impact. One of the primary advantages is the significantly reduced construction time, as modular components are prefabricated off-site, enabling faster on-site assembly and reducing labour costs[6]. This acceleration in project timelines is especially beneficial in dense urban environments where logistical constraints make traditional construction more challenging. Additionally, modular construction enhances quality control through a standardized production process within a controlled factory setting, which enables rigorous inspection and adherence to high-quality standards that are more difficult to achieve with on-site methods.

Economically, modular construction is efficient due to its reliance on standardized processes and economies of scale, resulting in reduced material waste and optimized resource use, ultimately lowering costs. Environmental benefits also play a major role; modular methods generate less waste, consume fewer materials, and emit lower levels of carbon dioxide compared to traditional building practices, potentially reducing emissions by as much as 45% [15]. This method minimizes construction-related disturbances, such as noise and dust, which can be a concern in urban areas, and thus makes modular construction an attractive, sustainable option for cities. Furthermore, modular systems are adaptable and scalable, allowing flexibility in design and enabling rapid expansion or reconfiguration of the built environment. This adaptability is particularly valuable in scenarios that require rapid, large-scale construction or highly specific applications, such as hospitals, where automated manufacturing processes enable high-precision and compliance with special standards [16].

Disadvantages

Despite its advantages, modular construction faces notable challenges that hinder its broader adoption, particularly in mid-rise and high-rise applications. Key barriers include structural uncertainties, limited standardization, and design constraints. A significant issue is the lack of universally accepted design methods and guidelines, leading to complexities and hesitancy within the industry [15].

While standardization enhances efficiency in modular construction, it also restricts architectural flexibility. Achieving complex or unique designs can be challenging and costly, as modular systems are optimized for repetitive, uniform structures. Transporting large prefabricated modules to construction sites further complicates the process, particularly in densely populated or remote areas, where structural strain during transit can affect assembly quality.

In high-rise modular buildings, connection complexity becomes critical. Connections between modules and with stability systems must withstand substantial lateral and vertical loads, with demands increasing as building height grows. This requires precise engineering and robust designs, which can complicate construction and escalate costs. Moreover, the initial investment required to establish modular construction facilities, including advanced technology, equipment, and a skilled workforce, presents a financial challenge for smaller firms or projects [6] [17].

2.1.3. Application of Modular Concept for High-Rise Structures

Case 1: Apex House (London, UK)

Apex House, located on Fulton Road, Wembley, London, is a 29-storey modular student housing development, standing at 90 meters tall. It comprises 679 prefabricated steel-framed modules with concrete floors, stacked around a slip-formed concrete core. The building's modular construction was completed within just 13 weeks, demonstrating the speed and efficiency of this construction method. The modules vary in weight from 12 to 17 tons, with larger units placed at the corners of the tower for structural support. Each module was connected to adjacent units and the core using steel connectors and bolted plates. The weight of the modules, combined with their steel framing and concrete floors, provided structural integrity, while the central concrete core absorbed lateral loads such as wind and seismic forces. The façade is constructed with large-format polished white Glass Reinforced Concrete (GRC) panels, integrated with CS68-HI high-insulation windows. The GRC panels, made from a lightweight composite of cement and alkali-resistant glass fibers, reduce structural load while offering tensile strength and durability. Their lightweight design is particularly beneficial for high-rise buildings, as it optimizes material use and simplifies transportation and installation[18][19][20]. Figure 2.2 shows the Apex House [21].

Figure 2.2: Case 1: Apex House [21]

Case 2: The Paragon (West London, UK)

The Paragon project in West London serves as another notable example of modular high-rise construction stabilized by a concrete core. The development consists of several buildings ranging from 11 to 17 stories, all constructed using modules with loadbearing corner posts. Paragon's 17-story building, consisting of 413 modules, was part of a larger project that included 827 modular units in total. In this system, the modular units were designed to resist vertical loads while horizontal loads were transferred to the concrete core. The modular arrangement used in Paragon follows two key configurations: a cluster arrangement where modules are tied directly to the core using cast-in plates, and a corridor arrangement where horizontal loads are transferred via in-plane bracing in the corridors, which also connect to the core. The distance of the outermost module from the core was governed by the shear forces that could be transferred via the corridor, as well as fire evacuation considerations The core and the L-shaped floor plan with the modular arrangement of the Paragon building can be seen in figure 2.3 [9][22].
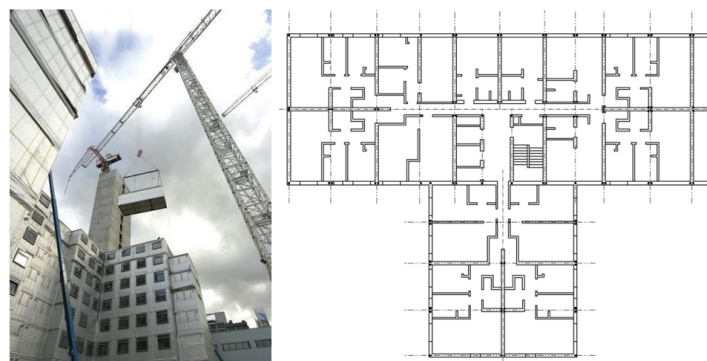

Figure 2.3: Case 2: The Paragon: Core structure (left) with modular arrangement (right)[9]

Case 3: Georgestreet 101 (Croydon, UK)

The Croydon Tower project consists of two residential towers of 44 and 38 stories, with a combined total of 546 apartments. Set to become the world's tallest modular building using the PPVC method upon completion, the project combines core- and podium-based construction. The conventionally built concrete podium, measuring 1.8 meters thick, supports 38 corner-supported steel modules per floor, each approximately 95% complete when delivered. Constructed from 1,525 modules in 23 configurations, the modules feature square hollow sections (SHS) that vary in size from 300 mm at the base to 150 mm at the top. This modular approach has reduced construction time by 30% and cut construction waste by 80%. The building's façade is finished with glazed terracotta, giving it a distinctive appearance. While it protects the structure from environmental forces, the façade is not load-bearing; the building's stability relies on its cores and internal framework. The two concrete cores are visible in figure 2.4 [6].

Figure 2.4: Case 3: Corydon Tower [6]

Case 4: B2 Tower (New York, US)

The B2 Tower in New York, a 32-story building with 363 apartments, became the world's tallest volumetric modular building upon its completion in 2016. Built using a podium-based approach, the structure includes 930 steel modules stacked on a conventional concrete podium with basement slabs, perimeter walls, and a steel frame plinth. Braced steel frames provide resistance to wind and seismic loads. Each module is built with SHS columns (150 x 150 mm), RHS floor beams (200 x 100 mm), RHS ceiling beams (100 x 100 mm), and RHS intermediate posts (50 x 75 mm), making it 65% lighter than concrete. Due to a developer dispute, construction was delayed and extended over four years. [6][23]. The structural Scheme of the B2 Tower is presented in figure 2.5.
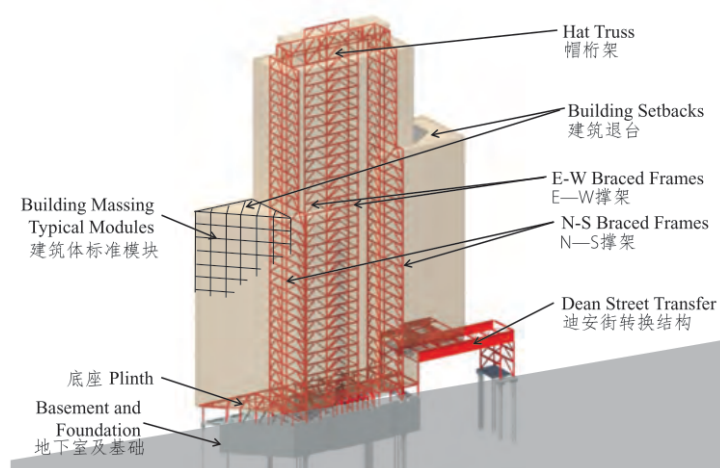

Figure 2.5: Case 4: B2 Tower structural scheme [23]

Case 5: Mini Sky City (Changsha, China)

The Mini Sky City, located in Changsha, Hunan Province, China, is a 57-story mixed-use tower completed in just 19 days by Broad Sustainable Building (BSB) in 2015. The building was constructed using a modular approach, with over 2,700 prefabricated steel modules manufactured off-site and assembled at a rate of three floors per day. This process allowed the building to be completed in a fraction of the time required for traditional construction methods.

The structural system relies on prefabricated modules that include walls, floors, and ceilings with pre-installed plumbing, electrical, and HVAC systems. These modules are tightly sealed, ensuring energy efficiency and reducing HVAC loads. The construction process was highly efficient, reducing concrete usage by approximately 15,000 truckloads, which minimized dust and environmental pollution. Mini Sky City includes 19 atriums, each 33 feet tall, and accommodates office space for 4,000 employees as well as residential units for 800 households. Despite its rapid construction, the building meets high structural and environmental standards, demonstrating the potential of modular construction to achieve sustainable and efficient urban development. The mini sky city tower is visible in figure 2.6 [24] [25] .

Figure 2.6: Case 5: Mini sky city [24] [25] .

2.2. Structural Design of Modular High-Rise structures

Modular mid-rise buildings consist of interconnected elements that form a complete structure. Designing these buildings requires strategic decisions in key areas, including modular systems, connection types, and lateral stability systems.

2.2.1. Modular Systems

Modular construction systems can be classified into three main categories: panelized, volumetric, and hybrid systems as illustrated in Figure 2.7. Each has distinct characteristics that influence its application in construction. In mid-rise modular buildings, the choice of system often depends on the need for structural integrity, speed of construction, and material efficiency [6].
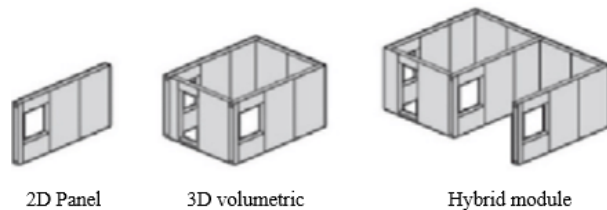

Figure 2.7: Types of modular units [6]

- **2D Panelized System:** This system consists of prefabricated panels that are assembled on-site to form a three-dimensional structure. The panels can be made from materials such as wood, concrete, or steel, and are classified into open and closed panel systems. The open system requires more on-site finishing, while the closed system is delivered fully finished. In general, 2D panelized system offers more design flexibility but demands more assembly work on-site compared to the 3D volumetric system. [26].

- **3D Volumetric System:** 3D volumetric systems consist of complete, pre-finished modules that are transported to the construction site as ready-to-install units. This method allows for rapid assembly, as the modules are fully finished in the factory, including installations and finishes. The modules are typically made from steel or concrete, with steel modules often preferred for high-rise buildings due to their durability, simpler connections, design flexibility, and a high strength-to-weight ratio. While it is also possible to use timber or cold-formed lightweight steel modules, these applications are generally limited to low-rise buildings (fewer than four stories) due to their lower load-bearing capacity. In general, 3D volumetric systems can be further categorized into two types based on their load transferring mechanism: 3D modules with load-bearing walls or 3D volumes with corner-supported frames. In load-bearing modules, the walls, typically made of concrete, transfer vertical loads to the foundation and resist lateral forces. While they provide multiple load paths, they require more complex connections to integrate vertical and horizontal loads effectively. In contrast, corner-supported modules centralize load transfer at the corners, simplifying connections but demanding robust corner designs to handle concentrated forces. This makes corner-supported modules particularly suitable for high-rise buildings due to their higher load-bearing capacity and efficient load transfer [27] [6]. The two different forms of 3D volumetric modules are shown in Figure 2.8.
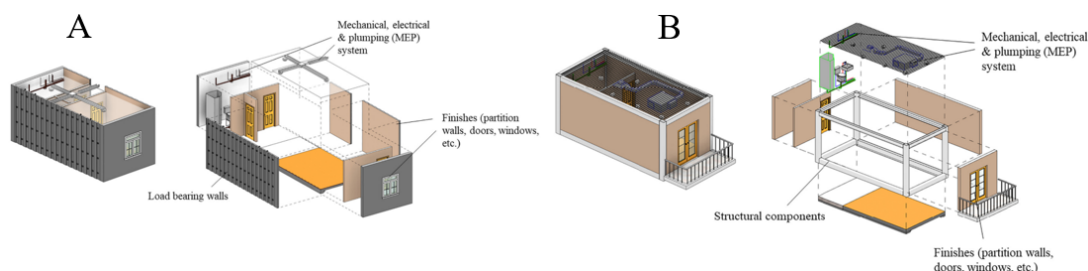

Figure 2.8: 3D Volumetric module: a) load bearing wall; b) corner supported module [27]

- **Hybrid System:** Hybrid systems combine 3D volumetric modules with 2D panels, leveraging the advantages of both approaches. In this method, 3D modules are used for complex or technically demanding sections of the building, such as bathrooms, while 2D panels are employed for the remainder of the structure. This results in faster construction times and improved transport efficiency, although coordinating between the two systems can be challenging, and costs may be higher [28].

Table 2.1 provides an overview of the different modular systems summarizing their subtypes, advantages, and limitations.

Table 2.1: Overview of modular construction systems

System	Subtype	Advantages	Limitations
2D Panelized	–	• High design flexibility • Transport efficiency • Lightweight structure	• Extensive on-site labor • More finishing required
3D Volumetric	Corner-Supported	• High load capacity • Rapid assembly • Good for high-rise	• Requires bracing or external systems for stability
3D Volumetric	Load-Bearing Wall	• Built-in lateral stability • Multiple load paths	• Heavy modules • Limited flexibility • Requires more complex connections
Hybrid	–	• Combines strengths of both systems • Flexible design and transport	• Coordination complexity • Potentially higher cost

2.2.2. Connection Types

Connections are vital in modular construction, serving to join prefabricated elements into a unified structure. This section reviews the types of connections in modular buildings, with further analysis of their impact on structural behaviour in Section 3.

The connections that are present in modular constructions can be categorized based on their location in the structure [29]:

- **Intra-module connections:** These connections form the internal framework within individual modules, linking elements such as beams, columns, floors, and walls. Intra-module connections provide stability within each module, enabling it to function as a self-contained unit that can bear loads independently before integration with other modules.

- **Inter-module connections:** Inter-module connections facilitate the integration of key structural systems by creating vertical and horizontal connections between modules.These connections can be further classified into three subtypes: (a) two-column connections, (b) four-column connections, (c) eight-column connections.

- **Module to foundation connections:** Foundation connections are responsible for anchoring the modular units to a stable foundation or support system, ensuring proper load transfer and stability at the building's base.

- **Module to external stability system connections:** In high-rise modular buildings, external stability systems, such as concrete cores, shear walls, or outrigger systems, provide additional lateral stability. Connections between modules and these systems should enable effective load distribution.

Figure 2.9 shows the key connections that are presented in a modular building.
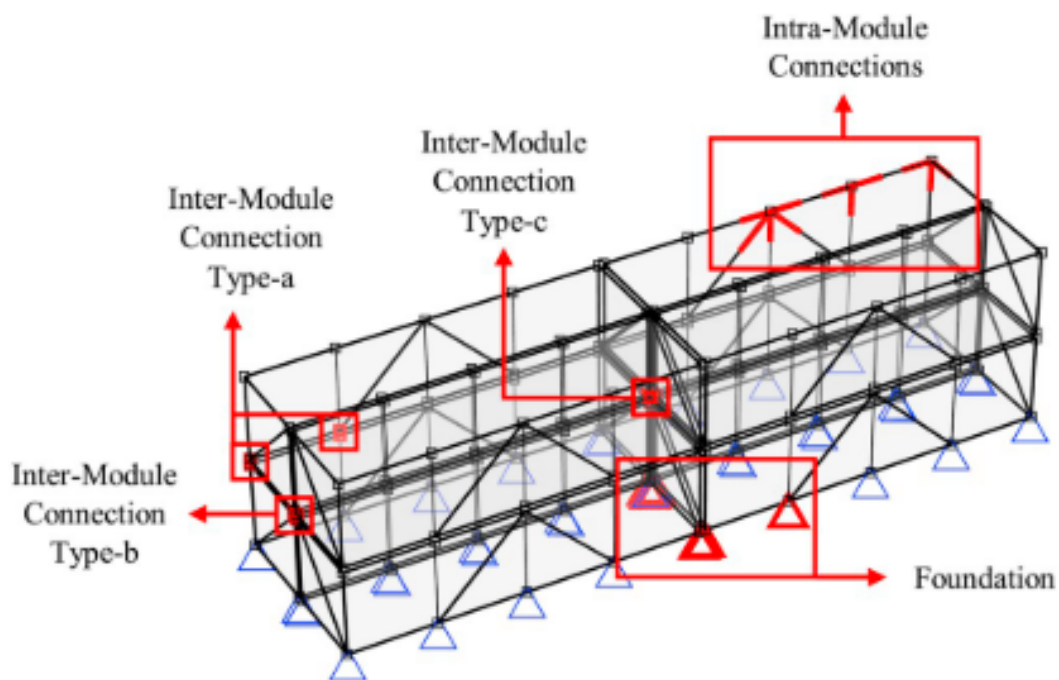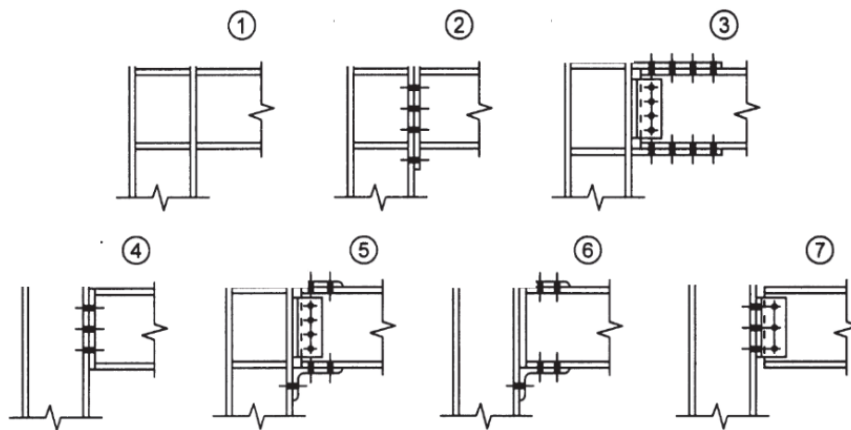

Figure 2.9: Main connections in a modular building [11]

A. Intra-Module connections

Intra-module connections vary widely in design, depending on structural materials, load demands, and the specific type of modular unit. The most commonly used connection types include bolted and welded. Bolted connections are widely used due to their ease of assembly and disassembly, making them particularly suited to the flexibility required in modular construction. These connections also allow for minor rotational movement, accommodating structural tolerances. In contrast, welded connections create rigid joints by permanently bonding steel components, providing long-term stability but at the cost of reduced flexibility [30].

In many modular systems, both bolted and welded connections are used at the interfaces between beams and columns within a module, aiming to balance ease of assembly with structural integrity. Figure 2.10 illustrates typical examples of such intra-modular connections.

Figure 2.10: Examples of typical Intra-module connections (Adjusted and retrieved from [31])

B. Inter-Module Connections

Inter-module connections are fundamental to the structural and functional performance of modular mid-rise buildings. These connections ensure the integrity of individual modules by linking them both vertically and horizontally, facilitating the load transfer and stability required for mid-rise applications. What makes inter-module connections particularly interesting is their specialised nature, arising from the unique layout of modular buildings. For instance, these connections often involve linking between four or eight columns, adding complexity and importance to their design and performance. Figure 2.11 illustrates the division into horizontal and vertical linkage components within an inter-module connection

(a) Vertical connection   (b) Horizontal connection
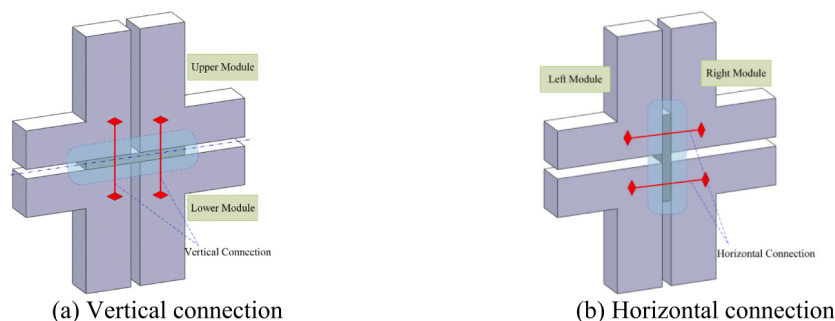
Figure 2.11: Vertical and horizontal division of inter-module connection [32]
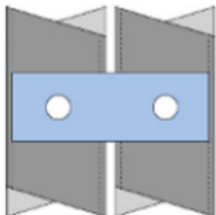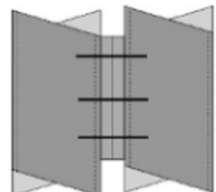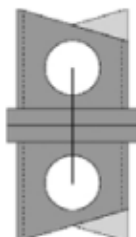
Types of Inter-Module Connections
These connections are classified based on their directional function: Horizontal Connections (HC), Vertical Connections (VC), and Horizontal-Vertical Connections (HVC) [32].

- **Horizontal Connections (HC)**: These connect adjacent modules horizontally. Commonly, shear keys, plates, and bolts are used to create a continuous horizontal plane for stability.

- **Vertical Connections (VC)**: These link stacked modules vertically. Typical components include high-strength bolts, end plates, and locking mechanisms, ensuring proper alignment and structural integrity across the module stack.

- **Horizontal-Vertical Connections (HVC)**: These combined connections integrate horizontal and vertical linkages, making them essential for managing complex load interactions and maintaining multi-plane alignment. HVCs incorporate features of both HC and VC designs.

Inter-module connections can be classified by their assembly method into welded, bolt-welded, and bolted types. While welded and bolt-welded connections provide high strength and durability, they often require extensive on-site welding, which can delay construction and complicate future disassembly. Additionally, on-site welding is generally undesirable for 3D volumetric modules, as these typically contain pre-installed insulation layers. Welding sparks can penetrate these layers, potentially compromising the building's fire safety. In contrast, bolted connections enable rapid on-site assembly and allow for straightforward disassembly over the building's lifecycle. This adaptability supports the core principles of modular construction, sustainability, reusability, and a balance between structural performance and flexibility [32].

A range of inter-module connections has been explored in the literature, with a summary presented in Table 2.2.

Table 2.2: Inter-module connection types [32][33][34]

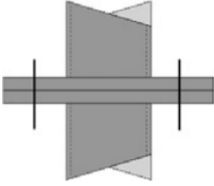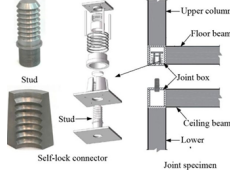| Type	Name	Illustration	Description
HC			
	Tie Plate[34]		The tie plate with bolts connects hollow steel column sections horizontally.
	Bolted Side Plate[34]		The side plate is bolted to hollow steel column sections to secure horizontal connectivity.
VC			
	Bolted End Plate[34]		A bolted end plate connects hollow column sections utilizing access holes vertically.
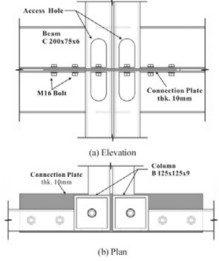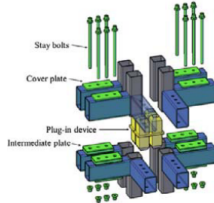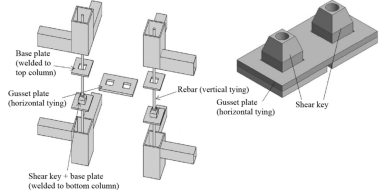
Type	Name	Illustration	Description
	Bolted End Plate (Two-Sided)[34]		A two-sided bolted end plate secures two columns vertically.
	Joint box with Stud self-lock[33][35]		Joint boxes are welded at the module corners for strength. A stud on the lower module fits into a drilled hole in the upper module's joint box, ensuring secure vertical alignment and strengthening.
HVC			
	Complex Bolted Plate[32][33]		The connection provides both vertical and horizontal load transfer by bolting adjacent module columns. The bolts resist lateral forces, but larger bolt slots can lead to increased deflections, making them unsuitable for high-rise modular buildings.
HVC (2)			
	Bolted Connection Plate[34]		The bolted connection plate provides vertical and horizontal linkage between beam and column sections.
	Bolted Plugin Device[33]		A plug-in device with four tubes for horizontal connection and high-strength bolts for vertical connection. Welding the intermediate and cover plates of the module beams prevents local buckling under bolt tension. This system eliminates the need for on-site welding.
	Rod Connection with Shear Key[33]		The steel connection plate ensures horizontal module connections, while a threaded steel bar with a nut provides vertical tension resistance, preventing separation. Columns handle compression forces, and shear keys counter shear forces.

Table 2.2 summarises conventional and innovative inter-module connections from the literature.Their impact on the structural behaviour of modular high-rise buildings is further discussed in Section 3.

C. Foundation-Module Connections

Foundation-module connections are essential for anchoring modular units to the foundation, ensuring base stability and effective load transfer. Foundations are typically prepared in advance, allowing for efficient on-site assembly. The choice of foundation system depends on site-specific conditions and soil characteristics. These connections are critical in securing the structure, as inadequate anchoring can result in issues such as overturning or slip failure, particularly in multi-storey buildings where lateral loads are significant. Common methods include chain, cable, or keeper plate connections, which are cost-effective for low-rise structures but insufficient for taller buildings. Welding modules to base plates provides high stiffness and secure anchoring but increases on-site costs and raises concerns about steel corrosion. In modular steel buildings, foundations often consist of (precast) concrete footings and bored piles, offering stability under both vertical and lateral loads[33]. An example of a foundation-to-module connection is shown in Figure 2.12.
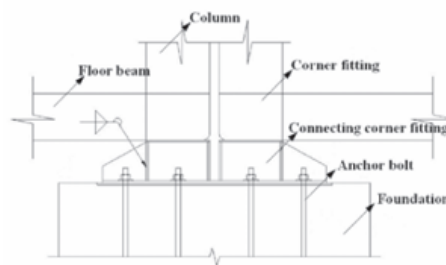
Figure 2.12: Module to foundation connection [36]

D. Module to External Stability System Connection

In modular high-rise buildings, external stability systems such as concrete cores, shear walls, or outrigger systems are crucial for lateral stability against wind and seismic forces. Connections between the modules and these systems integrate the modular structure with the overall lateral force-resisting framework, ensuring lateral loads are effectively transferred to the stability system. This prevents excessive sway or deformation and maintains structural integrity. Module-to-external stability system connections typically use bolted plates, dowels, or connectors that combine flexibility and strength. Designed to withstand shear and axial loads, these connections enable efficient force transfer without compromising the modular nature of the structure. When concrete cores or shear walls are used, modular units are anchored to the core at specific points to ensure a continuous load path, as shown in Figure 2.13.
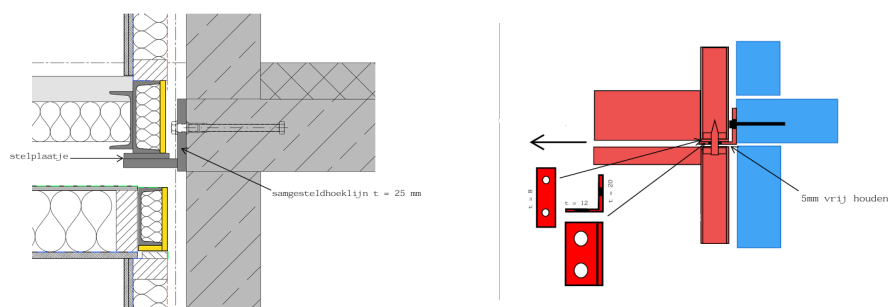
Figure 2.13: Two examples of module to core connection [35]

An example of an core to outrigger connection can be seen in figure 2.14.
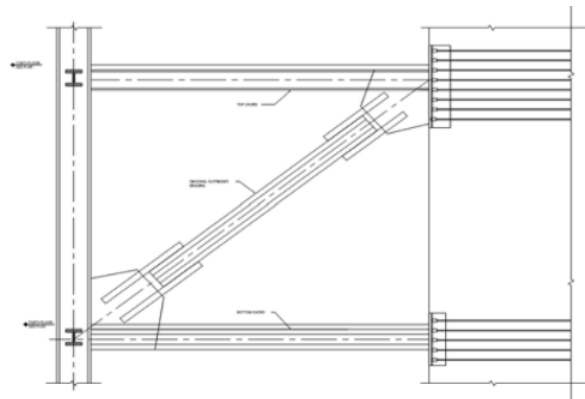
Figure 2.14: Outrigger to core connection

The connection between a steel outrigger and a concrete core can be achieved using an embedded plate that is flush with the concrete surface. Composite shear connectors, such as headed studs, are employed to transfer the vertical component of the force from the outrigger's diagonal member. To handle horizontal forces, long horizontal bolts anchored within the core wall are used, with the bolts connecting to a member end plate through threaded ends and secured with nuts. However, this method may not be suitable for situations involving high forces or reversible cyclic loads. An alternative solution is to weld deformed bar anchors to the embedded plate, which provides a more robust load path to handle such conditions [37].

2.2.3. Lateral Stability System

Lateral stability is essential in mid- to high-rise modular buildings to withstand forces from wind, earthquakes, and other environmental factors. As building height increases, these forces become more challenging, and the modular nature of construction, with its prefabricated units, often requires supplementary systems to transfer and dissipate lateral loads effectively. This section examines various lateral stability design options, ranging from simple to more complex stability systems.

Modular Buildings Without Stability Systems

Modular buildings without dedicated stability systems rely entirely on the structural capacity of the modular units. Vertical loads are carried by the modules' walls or corner posts, but lateral loads remain unaddressed. This approach limits the building's ability to resist horizontal forces, as its performance depends solely on the inherent stiffness and strength of the individual modules. While these units are efficient at handling vertical loads, they lack the rigid connections or lateral bracing needed to resist horizontal forces effectively.

Corner-supported modules, for example, are only stable on their own for one or two stories. For load-bearing wall modules arranged in a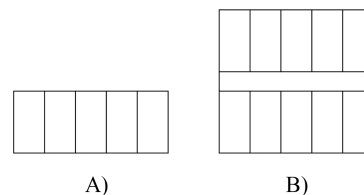 single line, a maximum of three stories can be achieved, provided there are at least five groups of modules in the line. When considering double lines of modules without additional bracing, up to six floors can be reached, but only if each line contains at least eight modules [38]. Figure 2.15 shows the different module configuration in a single and double line.

A)   B)

Figure 2.15: Top view of a single (A) and double line (B) of modules

This method may suffice for single-story or low-rise buildings where lateral forces are minimal. However, for mid- to high-rise buildings, this approach is inadequate.

Modular Buildings with Integrated Bracing

To address the limitations of unbraced modular buildings, internal bracing systems can be integrated within individual modules. These bracing elements, such as cross bracing, diagonal steel rods, or steel plates, enhance the structural integrity of each module by improving its ability to resist lateral forces. Internal bracing works by stiffening the module, allowing it to transfer horizontal forces more effectively to the foundation or adjacent structural components. This approach can significantly improve the performance of modular buildings up to a certain height, particularly when external stability systems are not feasible or cost-effective.

For example, load-bearing wall modules with additional bracing in the vertical end walls of the module can achieve up to five stories, provided the group includes at least eight modules. These braced gables increase the lateral stability of the structure. In a double-line arrangement with bracing in the gables, the number of achievable stories increases to eight, provided there are at least two lines of ten modules each[38]. Figure 2.16 shows an example of additional bracing placed in a module.
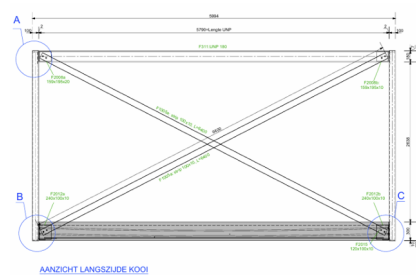
Figure 2.16: Example of module with additional bracing [35]

Highrise Stability Sytems

To construct a modular buildings that exceeds the 10 floors, which are achievable with modules and sufficient bracing, a primary supporting structure is required. The three main design options of primary structures are: core-based systems, podium-based systems, and infilled frame systems [6]. The three main types can be seen in figure 2.17.

(a) Core [32]   (b) Podium [33]   (c) Infilled frame [34]
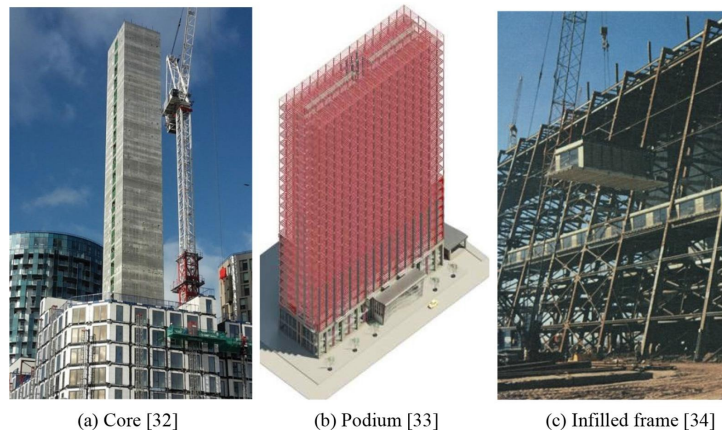
Figure 2.17: Main design options for modular high-rise structures [6]

Core-based system

The core-based system is the most widely used approach in modular construction for mid- to high-rise buildings. It places modular units around a central core, which is typically made of (prefabricated) concrete. The core plays a crucial role in managing lateral loads, such as wind and earthquake forces, ensuring the building's stability and structural integrity. In terms of load distribution, the core absorbs the majority of lateral forces, while the modular units transfer vertical loads. For corner-supported 3D modules, vertical loads transfer through the corner posts, while in load-bearing 3D modules, the loads are also transferred via the walls. The rigid connection between the core and the modular units is typically achieved via steel connectors or plates, which ensures that the modules are securely fixed to the core. Additional bracing or shear walls within the core can be used to enhance the system's capacity for resisting torsional forces, enabling the structure to reach greater heights [6].

Podium-based system

In a podium-based system, modular units are placed on top of a podium structure that acts as the foundation for the upper levels. The podium is typically a reinforced concrete or steel frame structure that supports the weight of the modular units. The podium itself provides a solid base for the modular components, allowing for more flexibility in the design and arrangement of the upper levels because the modules are designed to take less forces. The podium essentially acts as a ground-level stabilizer, reducing the structural demands on the upper modular units. Connections between the podium and the modular units are typically designed to allow some degree of flexibility to accommodate differential movements caused by various loads, ensuring the structure's durability [6][28].

Infilled frame system

The infilled frame system can be seen as a structural skeleton of the building where the modular units act as infill components that fit between the beams and columns of the frame system. the frame consists of beams and columns constructed on-site made of steel or reinforced concrete. the frame takes on most of the structural load, including gravity and lateral forces, allowing the modular units to be less structurally demanding in themselves.This system is highly adaptable because the frame can be customized to accommodate different sizes of modular units, depending on the design requirements. Connections between the modular units and the frame are typically made using steel brackets, plates, or bolts. Infilled frame systems allow for the modular units to be designed with more open spaces, as the structural support for the modules is provided externally [6][28].

Additional Stability Systems

As modular buildings grow taller, primary stability systems may require enhancements. Sole reliance on the core wall system to resist lateral forces can become uneconomical, as it would necessitate excessively large or significantly thicker core walls. Systems like outriggers and belt trusses can connect the core to exterior columns. The implementation of stiff horizontal members could complement the primary systems in order to let the entire structure become more efficient[39].

Outrigger System

The outrigger system connects the central core to the perimeter columns using horizontal trusses or beams, creating a wider structural base to resist lateral loads. These outriggers act as structural "arms," tying the core to the surrounding structure and effectively distributing lateral forces. This configuration reduces the overturning moments caused by lateral forces and increases the building's overall stiffness.Strategically positioning outriggers at specific levels increases rigidity, significantly minimizing lateral sway. Various types of outriggers, such as concrete, steel, hybrid, and damped systems, can be employed, but figure 2.18 illustrates the basic configuration of an outrigger [39][40].
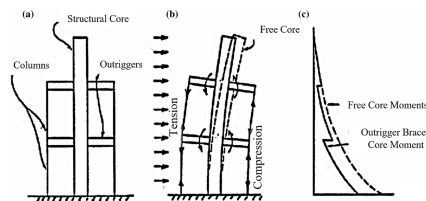
Figure 2.18: Outrigger system [40]

One of the primary advantages of incorporating an outrigger system in modular construction is its ability to counteract the lower stiffness often associated with precast concrete cores. Precast cores, while efficient and fast to assemble, are generally less stiff compared to cast-in-situ concrete cores. By transferring lateral forces from the core to the perimeter columns or modules, the outrigger system compensates for this limitation, allowing the structure to maintain its stability and resist torsional forces. However, the integration of outriggers in modular construction also poses challenges. Achieving the necessary rigidity in the connections between outriggers, the core, and the modules requires precise engineering and high-quality material[39][40].

Belt System

The belt truss system is another example of an additional structural system to enhance lateral stability. It works by connecting the perimeter columns of a building at specific levels using trusses.While outriggers extend horizontally from the core to connect directly to perimeter columns, belt trusses are located at the building's perimeter and rely on the floor diaphragm to bridge the transfer of forces to the core. This eliminates the need for direct connections between the core and outriggers, simplifying construction and preserving the building's interior space. Additionally, belt trusses avoid issues related to differential shortening between the core and outer columns, a common challenge in outrigger systems. However, Belt trusses are most effective when paired with stiff floor diaphragms, but achieving this is challenging due to the inherent discontinuities in modular construction. Figure 2.19 shows the an example of such a belt system without a direct connection to the core via an outrigger[39][41].

Figure 2.19: Example of a belt truss system without outrigger[41]

2.3. Selection of Design Focus

Type of Modular System: Steel Corner Post Module

The previous sections showed that the 3D volumetric modular system utilizing steel corner-supported modules is one of the most efficient solutions for high-rise construction. This system combines structural robustness, rap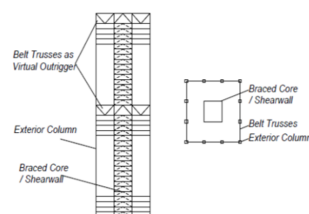id assembly, and a high strength-to-weight ratio with simplified connections, making it ideal for modular high-rise buildings. Loads are primarily transferred through steel components such as Square Hollow Section (SHS) columns and Parallel Flange Channel (PFC) beams. The floor cassettes are supported by edge beam. This system is particularly advantageous for high-rise buildings that demand adaptability, efficient load distribution, and minimal on-site construction. Additionally, this choice aligns with the expertise of Daiwa Modular Europe, the industrial partner for this research, which specializes in manufacturing these corner-supported modules.

Type of Connection: Tie-Rod Connection

This research focuses on tie rod connections as an inter-module connection, which use high-strength steel rods to link modules vertically. These connections enhance stiffness of the modules, resist tensile forces, and reduce lateral deflections. By improving module stability, tie rod connections demonstrate significant potential as a complementary component to an outrigger system, optimising load transfer and maximising the efficiency of the core-based stability framework.

Type of Stability System: Precast Core With Outriggers

Given that the focus of this thesis is to explore the possibilities of modular high-rise structures with precast concrete, the core-based system is the most relevant option for further investigation. This system could provide the required structural stability for buildings exceeding 10 floors and also aligns seamlessly with the modular construction approach by employing prefabricated components. In comparison, the podium and infill frame systems demand a substantial amount of on-site construction, which goes against the philosophy of the modular concept. Furthermore, integrating an outrigger system into the core-based approach could enhance the reduced stiffness of using a precast core by connecting the central core to perimeter modules or columns, effectively reducing sway and optimizing load distribution. Despite its potential, this type of system remains largely unexplored in modular construction. Investigating the use of a precast concrete core in combination with outriggers could introduce a novel stability concept.

Conclusion

The research centres on three key components: corner post modular systems, tie rod inter-module connections, and a precast concrete core with outriggers. These elements form the foundation for the proposed concept to be developed in subsequent phases of this research. Figure 2.20 summarises the research focus moving forward.

Steel Corner-Post Module Tie-rod Inter-Module Connection Precast Concrete Core with Outrigger
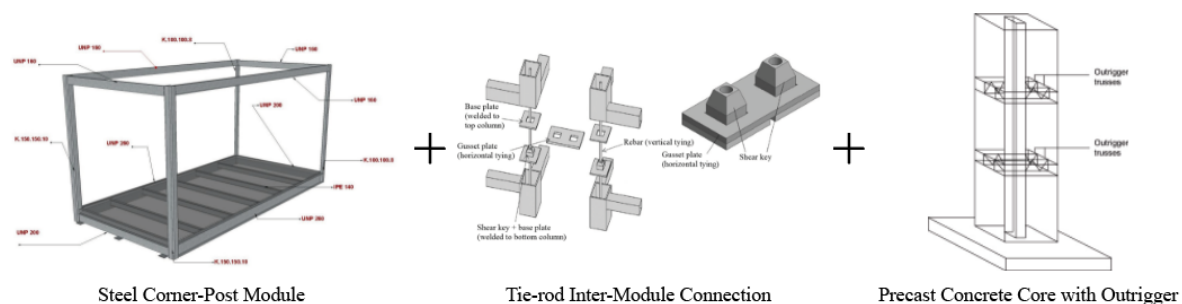
Figure 2.20: Selected design options for further research.

3

Structural Performance of Modular buildings

The structural performance of modular buildings differs significantly from conventional construction due to the segmented nature of their design and reliance on prefabricated components. Understanding these differences is essential for optimising modular constructions and addressing their unique challenges. This chapter investigates key aspects of structural performance critical to the stability and resilience of modular mid- or high-rise buildings.

The analysis begins with an evaluation of the vertical load capacity of the columns, exploring how modular systems manage concentrated loads at connection points. It then examines various lateral stability systems, including unbraced, braced, core and outrigger systems, using simplified models to assess their effectiveness in resisting lateral forces such as wind and seismic loads. Finally, the chapter explores the group action of modules, focusing on how interconnected modular units behave collectively to maintain overall structural integrity.

3.1. Vertical Load-Bearing Capacity

In modular buildings the vertical loads are primary transferred through the corner-post columns of the module. These steel corner-posts must be designed with sufficient axial compressive capacity to prevent buckling or localized failure. The nature of modular construction often requires these sections to be as lightweight as possible. This results in smaller sized columns, which can affect their load-bearing capacity, especially in the lower stories where the load is greatest.

In a mid- or high-rise structure, the columns in the lower levels are subjected to significantly higher compression forces, yet increasing their size to accommodate these loads is not preferable. Making the lower-level columns larger would compromise the modular system's flexibility and replace ability, as uniform module sizes are essential for efficient fabrication, construction, and logistics. Increasing the size of all modules would also make the building less efficient and heavier, creating additional challenges for the cranes required to lift the modules to the higher levels of the building[6].

To assess the feasibility of modular mid-rise construction, initial hand calculations are performed to evaluate the load-bearing capacity of corner columns. These calculations provide insights into the structural performance of the modular units under vertical loads, particularly as building height increases.

Simple hand calculation

For this preliminary design calculation, a typical module with dimensions of 4.5 x 6.4 meters is chosen. The module's total self-weight is estimated at 126.4 kN, which is assumed to be evenly distributed across the four corner-posts, resulting in a concentrated load at each connection point. When modules are stacked, this weight is transferred progressively through the columns down to the foundation. The additional imposed live load for a residential or living space, classified under Class A occupancy, is considered. According to EN 1991-1-1, the variable load for such spaces is 1.75 kN/m^2. Furthermore, a load of 0.5 kN/m^2 is included for partition walls, along with a roof load of 1.0 kN/m^2, which contributes additional load on the lower levels. This calculation accounts only for the specified loads, omitting the weight of the façade and other architectural elements to ensure simplicity in this preliminary research phase. The relevant loads are summarized in Table 3.1.

Parameter	Value
Module dimensions	4.5×6.4 m
Self- Weight Load per corner-post (perm. load)	31.6 kN
Variable load (residential Class A)	1.75 kN/m^2
Partition wall load (var. load)	0.5 kN/m^2
Roof load (var. load)	1.0 kN/m^2

Table 3.1: Parameters for load calculation

Design Load

In accordance with the Eurocode 0, the design load P_d on the columns includes both permanent and variable actions, with partial safety factors and combination factors applied as required. The design load is calculated as: 6.10A and 6.10B.

Formula 6.10A:

$$P_d = \gamma_G \cdot G + \gamma_Q \cdot \psi_0 \cdot Q \tag{6.10A}$$

For floors 1 to n, where:

- P_d: Design load on the column
- $\gamma_G = 1.35$: Partial safety factor for permanent loads (self-weight)
- G: Permanent load or self-weight of the modular unit
- $\gamma_Q = 1.5$: Partial safety factor for variable loads (live loads)
- $\psi_0 = 0.4$: Combination factor for variable loads (residential buildings, Class A)
- Q: Total variable load, including live load, partition load, and roof load

Formula 6.10B:

- **Floors 1–3:**

$$P_d = \gamma_G \cdot G + \gamma_Q \cdot Q \tag{6.10B-1}$$

- **Floors 4–n:**

$$P_d = \gamma_G \cdot G + \alpha_n \cdot Q \tag{6.10B-2}$$

Where:

- $\gamma_G = 1.2$: Partial safety factor for permanent loads (self-weight)
- G: Permanent load or self-weight of the modular unit
- $\gamma_Q = 1.5$: Partial safety factor for variable loads (live loads)
- α_n: Reduction factor for variable loads based on the number of floors n, given by:

$$\alpha_n = \frac{2 + (n - 2) \times \gamma_Q}{n} \tag{6.2}$$

- Q: Total variable load, including live load, partition load, and roof load

Because the goal of this research is to investigate the feasibility of using the modular building concept for a mid-rise structure up to 70 meters, it is estimated that there will be 23 modules stacked on top of each other. This is an overstatement of the height because the modules are higher than 3 meters in total height, but for this phase of the research, this estimation will be sufficient. Based on the previously mentioned formulas, it is estimated that to reach a height of 70 meters, only taking vertical load into account, the columns of the bottom module will need to resist 1152 kN.

Capacity of the column member
To evaluate the capacity of various column members, four widely used column types made of S355 steel are investigated. An overview of the investigated cross-sections is provided in Table 3.2.

Table 3.2: Overview of investigated cross-sections

Cross-Section	Type	Range
Square Hollow Section (SHS)	Hot-Formed (HF)	20/2.6 - 400/20
	Cold-Formed (CF)	20/2 - 600/20
Rectangle Hollow Section (RHS)	Hot-Formed (HF)	50x30/2.6/2 - 500x300/20
	Cold-Formed (CF)	40x20/2 - 400x300/16

For this calculation, the column length is estimated to be 3 meters, which is the typical size used for column members in corner-post modules. The boundary condition is assumed to be pinned, reflecting the rotational flexibility at the beam-column connection in modular systems. The maximum buckling resistance is then calculated for each cross-section. These calculations are performed in accordance with Eurocode 3: Design of Steel Structures [42]. The used formulas are:

$$N_{\text{Ed}} \leq \frac{N_{\text{b,Rd}}}{1.0} \tag{6.46}$$

The design buckling resistance of a compression member for Class 1, 2, and 3 cross-sections is:

$$N_{\text{b,Rd}} = \frac{\chi\, A\, f_{\text{y}}}{\gamma_{\text{M1}}} \tag{6.47}$$

For Class 4 cross-sections, the design buckling resistance is:

$$N_{\text{b,Rd}} = \frac{\chi\, A_{\text{eff}}\, f_{\text{y}}}{\gamma_{\text{M1}}} \tag{6.48}$$

Where:

- N_{Ed}: Design value of the compression force,
- $N_{b,Rd}$: Design buckling resistance of the compression member.
- χ: Reduction factor for buckling,
- A: Cross-sectional area,
- A_{eff}: Effective cross-sectional area for Class 4 sections,
- f_y: Yield strength of the material,
- γ_{M1}: Partial safety factor for resistance of members to instability.

Feasibility Results

In Figure 3.1, the column load per floor is plotted as the blue line. The horizontal lines represent the maximum buckling capacity of a selection of commonly used cross-sections.

(a) Setup of the hand-calculation model

(b) Plot of column axial compression force (kN) with the capacity selection of SHS profiles (HF and CF)
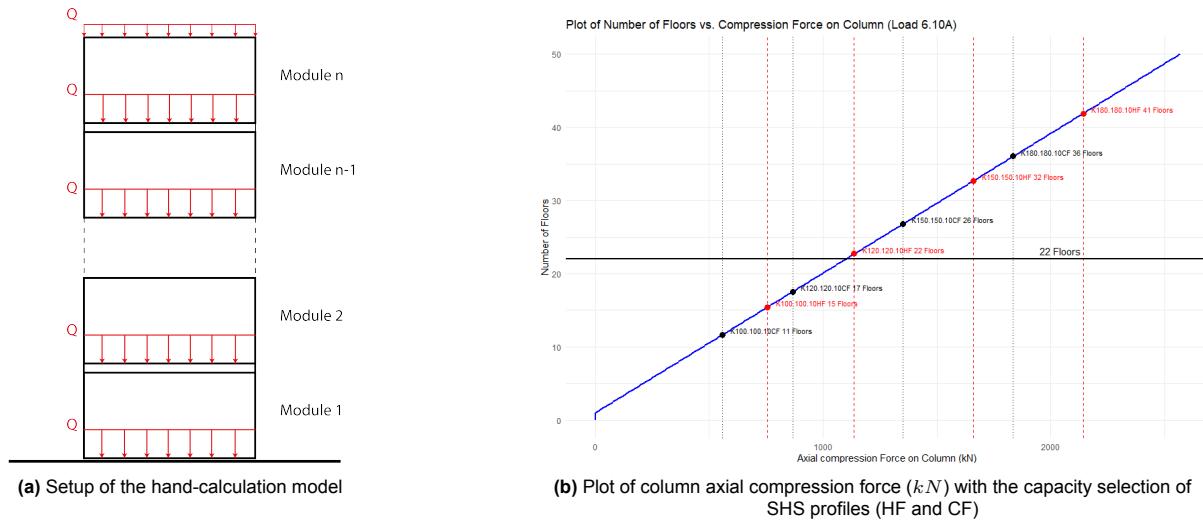
Figure 3.1: Comparison of the hand-calculation setup and the plot of compression force.

As shown in the graph, not all cross-sections provide sufficient buckling resistance to withstand the compression forces generated when 23 modules (22 floors) are stacked. For instance, the SHS100.10 Cf cross-section can only support up to 11 stacked modules, which falls short of the desired height of 70 meters. The first cross-section approaching the desired height is the SHS120.120.10 HF profile, which can support up to 22 stacked modules. The buckling resistance of this cross-section is calculated to be 1137.11 kN.

Table 3.3 provides an overview of the first cross-section from each of the four types that is sufficiently strong to withstand the estimated design load of 23 stacked modules.

Table 3.3: Buckling capacity of selected cross-sections

Cross-Section	Type	Axial compression capacity (kN)	Reachable Height
SHS 140 / 10	Cold-Formed (CF)	1189	23 floors (69 meter)
SHS 120 / 10	Hot-Formed (HF)	1137	22 floors (66 meter)
RHS 200x100 / 12.5	Cold-Formed (CF)	1144	22 floors (66 meter)
RHS 180x100 / 10	Hot-Formed (HF)	1205	24 floors (72 meter)

Appendix A includes a detailed sheet listing all the calculated column capacities

3.2. Lateral Stability in Modular Buildings

Lateral forces such as wind and seismic activity present significant challenges for mid or high-rise modular buildings. As mentioned before unlike traditional monolithic structures, modular systems often exhibit segmented behaviour due to their reliance on discrete components. This segmentation can lead to increased deformation under lateral loads, as discontinuities between modules and connections influence the overall structural response.

3.2.1. Lateral Loads

Wind Loads

The wind load acting on a structure can be calculated according to the provisions of NEN-EN Euro-Code 1: General Actions: Wind Actions [43]. The magnitude of this load depends on the building's height, which, for modular structures, corresponds to the number of stacked modules. The wind force is calculated using the following equation:

$$F_w = c_s c_d \cdot c_f \cdot q_p(z) \cdot A_{\text{ref}} \tag{3.1}$$

where:

- $c_s c_d$ is the structural factor accounting for dynamic effects and the overall stability of the structure,
- c_f is the force coefficient, representing the aerodynamic characteristics of the building,
- $q_p(z)$ is the peak velocity pressure of the wind at a specific height z, and
- A_{ref} is the reference area exposed to the wind.

The distribution of wind force on a building depends on its geometry, particularly the height-to-width ratio. For buildings where the height is less than or equal to the width, wind pressure is evenly distributed across the structure. When the height is between one and two times the width, the wind pressure divides into two zones along the building's height. For buildings where the height exceeds twice the width, the wind pressure is distributed into three distinct zones [43]. Figure 3.2 illustrates these variations in wind load distribution based on building proportions.
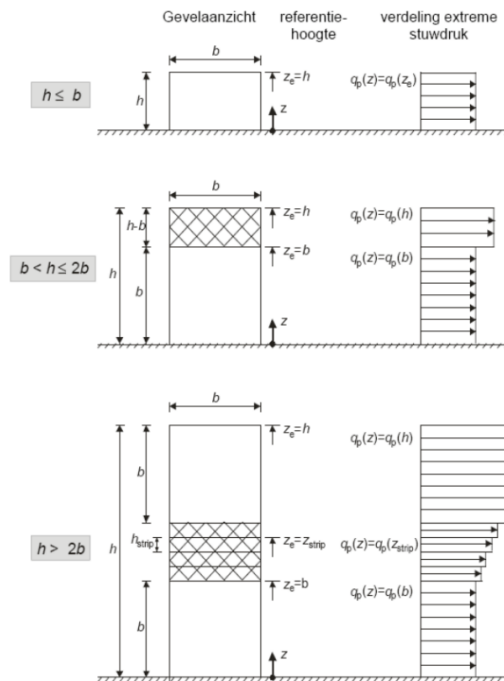

Figure 3.2: Wind loads from Eurocode[43]

3.2.2. Lateral Deflection

The total lateral deflection in a modular building is the sum of all the individual contributions of all the segmented components. Figure 3.3 illustrates the process of calculating total deflection results from inter-story drift and the cumulative effect caused by the horizontal rotation of lower stories. This rotation creates an angle θ, which, when multiplied by the story height, determines the additional displacement.

For constructions with more than two storeys, the horizontal displacement limits, as specified in the Dutch National Annex to EN 1990 (Eurocode), are $u \leq \frac{H}{500}$ for the entire building with foundation, $u \leq \frac{H}{750}$ without foundation, and $u \leq \frac{H}{300}$ per storey [44].
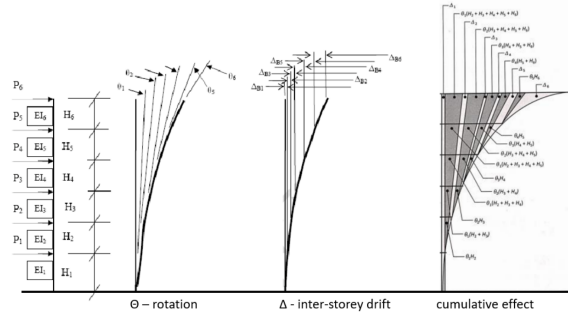
Figure 3.3: Bending deformation with cumulative effect on a modular building [45]

The total lateral deflection at a given level consists of contributions from the following deformation components:

$$\Delta_{\text{storey},i} = \Delta_{\text{storey},V,i} + \Delta_{\text{storey},B,i} + \Delta_{\text{storey},T,i} \tag{3.2}$$

the components of the lateral deflection are [46][45]:

1. $\Delta_{\text{storey},V,i}$: Horizontal deflection due to Shear
2. $\Delta_{\text{storey},B,i}$: Horizontal deflection due to Bending (including Vertical deformation)*
3. $\Delta_{\text{storey},T,i}$: Horizontal deflection due to Translational

*The bending and vertical deformation components introduce an additional rotation angle, which contributes to further lateral displacement at higher levels.

Shear Deformation

Displacement caused by shear action occurs within structural components such as beams and inter-module connections. This deformation mechanism is influenced by the material properties, stiffness, and the design of intra-module connections within the modules. Figure 3.4 illustrates the cumulative shear deflection in a stacked modular building, with increasing shear displacement towards the base due to higher shear forces in the lower modules.
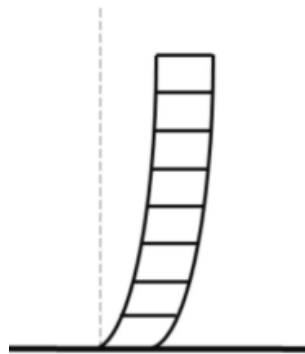
Figure 3.4: Deflection due to shear deformation[47]

This representation aligns with the expected behaviour, where the lower levels experience greater deformation. Notably, this type of deformation does not induce any additional rotation, as the displacement remains confined to the horizontal shear deformation of the components [46].

Bending Deformation

Lateral displacement due to flexural bending arises from the deformation of columns and beams under lateral loads. This deformation mechanism is primarily influenced by the stiffness and geometry of the structural components. As the structure bends, an additional rotational angle θ is introduced, which contributes to cumulative lateral displacement in the upper stories. Figure 3.5 illustrates the deflection pattern of a modular building due to bending deformation[46].
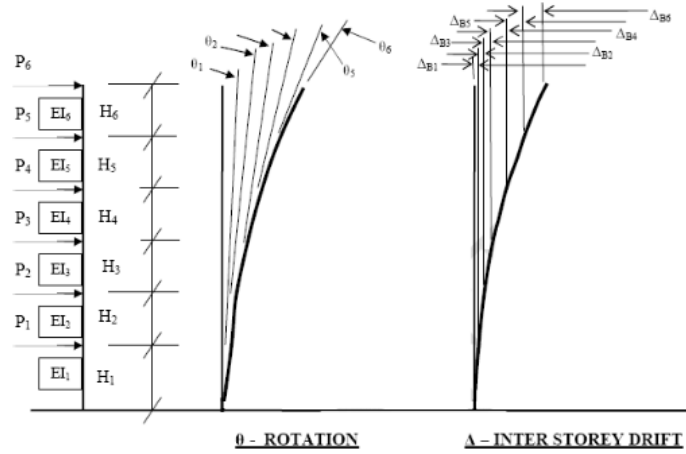
Figure 3.5: Deflection due to bending deformation[46]

Part of the total bending deformation occurs as axial deformation, which involves either the elongation or shortening of the columns and inter-module connections. These vertical deformations are caused by the axial forces that arise from the global bending moment, and they contribute to lateral displacement through a rotational tilt of the structure. This effect is especially relevant in stacked systems, where the flexibility of the inter-module joints and the stiffness of the columns influence how the structure responds to bending. Figure 3.6 illustrates how both the elongation of inter-module connections (A) and the deformation of columns (B) contribute to this behaviour [46].

Figure 3.6 illustrates the deformation caused by the elongation of the inter-module connections and the deflection resulting from the elongation of the module columns.

A)   B)
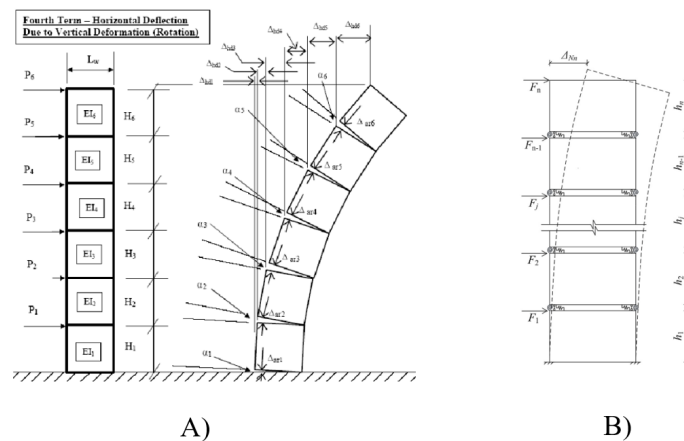
Figure 3.6: Deflection due to deformation of inter-module connections (A) and deformation of the columns (B) [46]

Translational Deformation

Translational deformation occurs due to the horizontal movement of inter-module connections, columns, and foundations under lateral loads. This mechanism directly contributes to the lateral displacement of the structure without inducing rotation. The degree of translational deformation is determined by the stiffness and alignment of the inter-module connections and the overall stability of the supporting columns and foundation. The translation deformation is presented in figure 3.7 [46].
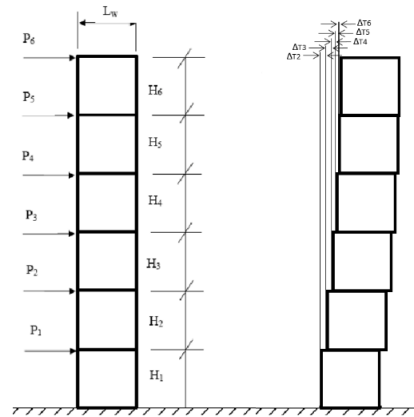
Figure 3.7: Deflection due to the translation deformation[46]

3.2.3. Stability Systems

To evaluate the structural behaviour of various stability systems, a *2D* model is developed using *Grasshopper*.

Simple Grasshopper Models

The model incorporates four distinct stability configurations for analysis:

1. **Unstabilized Structure**: A modular structure without any additional stability systems, relying solely on the modules for lateral stability.

2. **Braced Structure**: A modular structure with bracing elements incorporated in the middle modules to enhance lateral stability.

3. **Core-Based System**: A modular structure with a centrally positioned core to resist lateral forces.

4. **Core with Outrigger System**: A modular structure combining a central core with an outrigger system to improve load distribution and lateral stiffness.

The model is *parametric*, allowing key variables to be adjusted. These variables include the number of floors and the number of modules in the width of the structure. By employing this *parametric* approach, it becomes possible to systematically compare the effectiveness of different stability systems under varying configurations, providing insights into their performance across different building layouts.

Figure 3.8 shows the geometrical set-up of the four different stability systems.
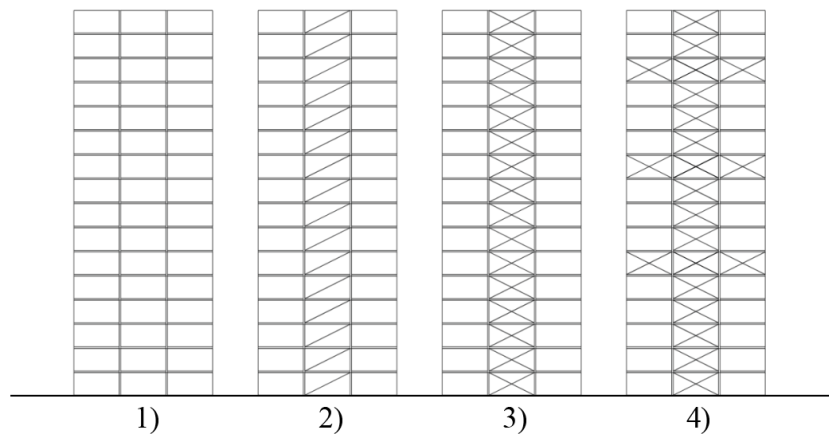
Figure 3.8: *Grasshopper 2D* Stability Models

For the purposes of these simplified models, intra- and inter-module connections are assumed to be rigid. While this assumption oversimplifies real-world conditions, where connections exhibit semi-rigid behaviour, it is deemed acceptable for this preliminary phase. The connections are now modeled in as a vertical element for a vertical connection and as a horizontal element. this configuration can be seen in figure 3.9.
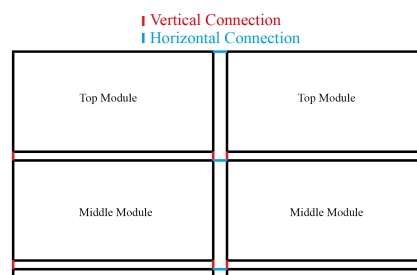
Figure 3.9: Simplified Connection Set-up

The primary goal of this section is to gain an initial understanding of how the different stability systems perform, rather than to provide a detailed analysis of connection behaviour. This simplification allows for a focus on comparing overall system performance without delving into the complexity of connection mechanics.

Lateral Deformation Results

The preliminary results provide an overview of the lateral stability of three distinct structural systems, braced frames, core-based systems, and outrigger systems,applied to modular mid-rise construction. as said before, the aim of this phase was not to determine exact values for design implementation but rather to validate the conceptual feasibility of each system and their relative performance. The *parametric* model allows variations in the number of floors and modules in width. The maximum lateral displacement is used as the primary performance metric, and the load applied to these models is a horizontal Q load of $5\,\mathrm{kN/m}$.

The maximum lateral displacements for each stability system were recorded across various configurations, with the preliminary results presented in Figure 3.10. The deformations for the different stability systems, modelled at a height of 22 floors (approximately 70 meters) with a width of 5 modules, are illustrated in Figure 3.10a. Additionally, figure 3.10b shows a plot of the lateral displacement of the three stability systems with an increasing height with a constant width of 5 modules.

(a) Deformed Stability Systems

(b) Displacement plots
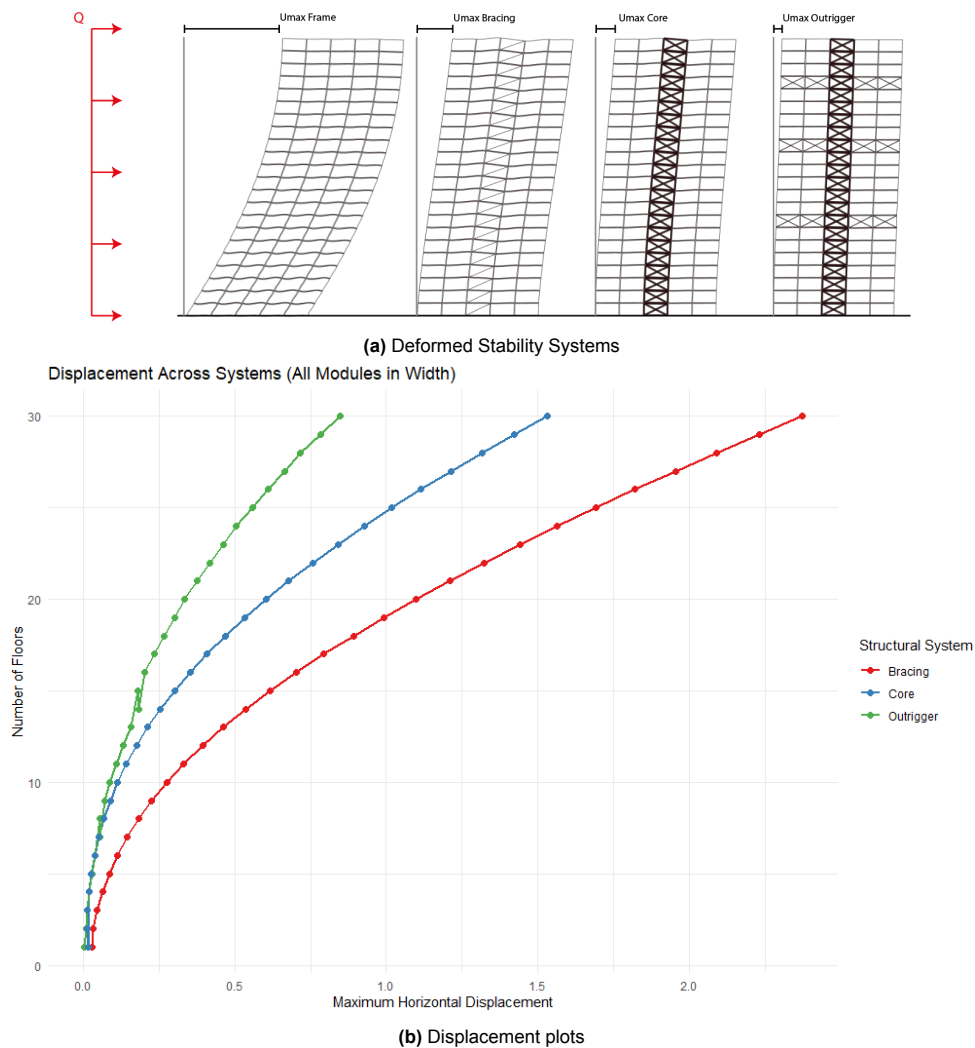
Figure 3.10: Side-by-side comparison of deformed stability systems and displacement performance.

The deformation profiles, illustrated in Figure 3.10a, reveal significant differences in the performance of the stability systems under lateral loads. Among the systems evaluated, the framed system performed the worst, exhibiting the highest lateral displacement. The braced frame system demonstrated better resistance but still experienced substantial displacement. While this system may be effective in low-rise modular construction, its limitations in providing adequate lateral resistance for mid- or high-rise configurations are cleary visible from these figures.

The core-based system showed a significant improvement in stability compared to the braced frame, with significantly lower maximum lateral displacement, as highlighted in Figure 3.10b. The core effectively resisted lateral forces, particularly at lower levels, reducing overall deformation. However, its deformation profile, shown in Figure 3.10a, revealed moderate deflection at the upper levels, indicating limitations in stiffness at greater heights.

The outrigger system proved to be an effective strategy for improving lateral stiffness, achieving reduced horizontal displacement and a relatively uniform deformation profile across the height of the structure. As illustrated in Figures 3.10a and 3.10b, the outriggers link the central core to the perimeter modules, thereby activating tensile and compressive forces in the façade zone through the rotational response of the core. This mechanism becomes particularly effective when the core experiences flexural deformation, allowing the outriggers to function similarly to stiff arms that redistribute bending effects. In contrast, if the structure primarily resists lateral loads through shear (as in a pure frame without a stiff core), outriggers would have little to no effect, since no significant rotation occurs to engage the axial forces in the perimeter.

A notable and somewhat unexpected feature in the displacement plot is the observed reduction in horizontal displacement between floors 7 and 8 and again between floors 13 and 14. This behaviour stems from predefined geometrical criteria in the *Grasshopper* script: when the number of floors reaches 7, a second outrigger is added to the structure, and when it reaches 14 floors, a third outrigger is introduced. Each additional outrigger substantially increases the global stiffness, resulting in the observed drop in lateral displacement at those levels.

It is important to note that the comparison between stability systems also reflects a progressive addition of material and structural elements. Moving from a simple frame to a core, and finally to a core with one or more outriggers, naturally increases the stiffness because additional load paths and stiffness contributions are introduced. While the outrigger system demonstrates a notable reduction in displacement, this result should be viewed in the context of the additional structural elements and material invested to achieve this improvement.

3.3. Connection Behaviour

The structural performance of modular mid- or high-rise buildings is significantly influenced by the behaviour of their connections. Connections, both within individual modules and between adjacent ones or between modules and external stability systems, are fundamental to the transfer of loads, control of deformation, and maintenance of overall stability. This chapter discusses the implications of connection behaviour on structural performance and illustrates how connections can be realistically modelled using *Karamba3D*. An example of transitioning a horizontal connection from rigid to pinned is provided to highlight the potential impact of connection properties on structural performance of a modular building.

3.3.1. Impact on Structural Performance

Connections in modular buildings play a crucial role in ensuring structural efficiency and safety. Their behaviour under various loading conditions shapes the overall performance of the building, from load distribution to resistance against deformation and collapse.

Key Aspects of Connection Behaviour

- **Moment-Rotation Behaviour:** Connections experience rotational forces due to lateral loads like wind. Fully rigid connections resist these forces but may create stress concentrations at critical points. Semi-rigid connections allow for a controlled amount of rotation, reducing the likelihood of brittle failure. Pinned connections, by contrast, are assumed to offer no rotational resistance and are typically used when moment transfer is not required.

- **Deformation Behaviour:** The stiffness of a connection affects the deformation of the structure. Flexible connections can result in excessive lateral displacement, increasing the risk of instability. In contrast, overly stiff connections can restrict necessary movements, leading to stress accumulation and potential failure.

- **Robustness and Failure Resistance:** Connections play a key role in the building's ability to prevent progressive collapse. Weak or poorly designed connections can propagate failure throughout the structure. Incorporating redundancy and secondary load paths into the connection design enhances robustness and mitigates the risk of catastrophic failure.

Given these critical aspects of how connections influence the performance of a modular building, it is essential to represent connections in the models as realistically as possible.

Modelling Connections with Beam Joint Elements

The behaviour of connections, as outlined in the key aspects, should be effectively represented in a *parametric* modelling environment to assess their impact on the structural performance of modular buildings. In *Karamba3D*, all connection types, whether intra-module or inter-module can be realistically modelled using *beam joint element* component. These elements provide a versatile framework for representing the mechanical properties of connections, including their rotational and translational stiffness, allowing the model to simulate various types of connections found in modular construction, such as bolted, welded, semi-rigid, or pinned joints.

The *Beam joint elements* in *Karamba3D* are defined by two primary parameters that govern connection behaviour:

- **Rotational Spring Stiffness:** This parameter represents the connection's ability to resist bending moments, simulating how the connection behaves under rotational forces.

- **Translational Spring Stiffness:** This parameter quantifies the resistance of the connection to axial and shear forces. It reflects the connection's capacity to transfer loads between modules and maintain structural continuity.

By assigning values to these stiffness parameters, the model can simulate different types of connection behaviours. This enables the representation of various connection types in modular buildings, making the model adaptable to specific structural designs and supporting further developments in this research.

Illustrative Example: Transitioning from Rigid to Pinned Horizontal Connections

To illustrate the impact of connection modelling, a horizontal inter-module connection was analysed in *Karamba3D*, transitioning between rigid and pinned configurations. Figure 3.11 shows the setup of the beam to joint component and its effect on structural deformation at connection level.
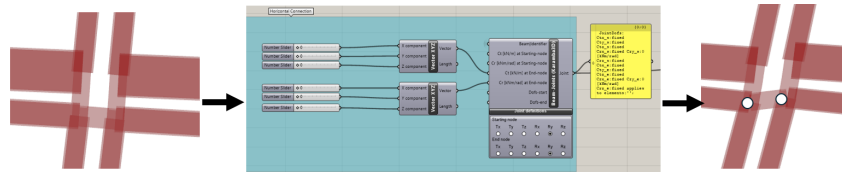
Figure 3.11: *Karamba3D* setup: rigid to pinned horizontal connection

In the rigid configuration, the connection restricts rotational movement, resulting in significantly lower lateral displacement compared to the hinged configuration, which allows rotational freedom and leads to increased lateral displacement. This contrast is clearly illustrated in Figure 3.12 and Figure 3.13, highlighting the superior control over deformation exhibited by the rigid connection in the braced model, configured with a width of 3 modules and a varying number of floors.

Rigid Horizontal Connection   Pinned Horizontal Connection
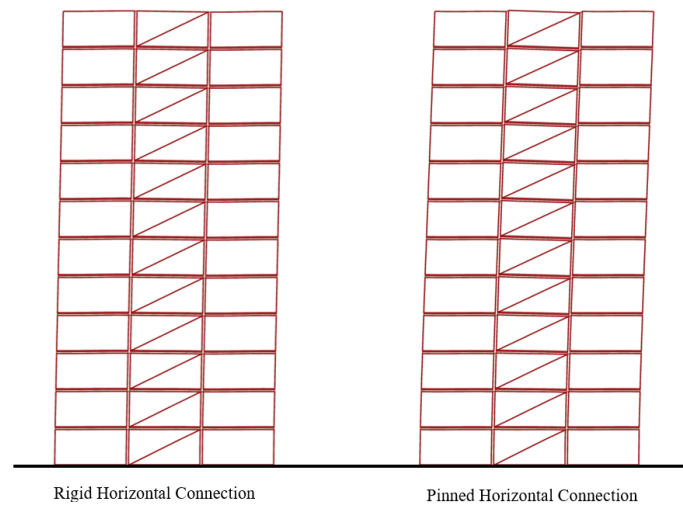
Figure 3.12: Effect of connection type on global deformation
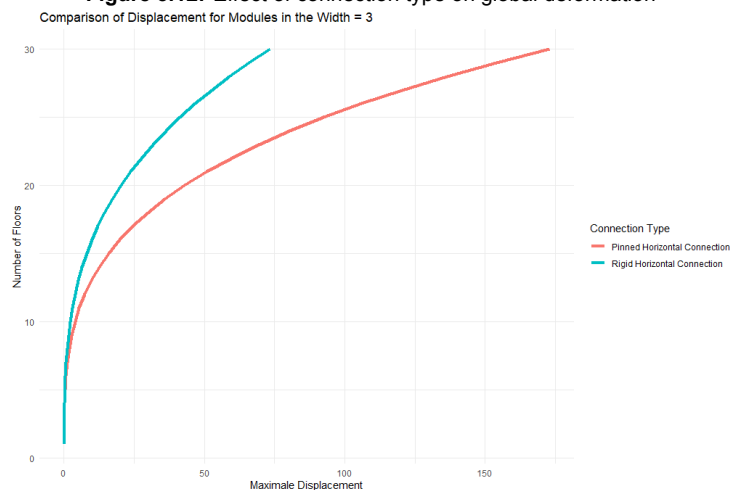
Figure 3.13: Displacement plot of pinned and rigid horizontal connection

This example highlights the importance of accurately modelling connections, as they have a significant impact on structural behaviour and are crucial for ensuring realistic simulation results. Properly capturing the effects of connection stiffness enables models to more reliably predict deformation patterns and stress distribution.

3.4. Structural Group Action of Modules

In modular mid- or high-rise buildings, the structural behaviour of grouped modules presents unique challenges due to their interconnected nature and the variety of forces acting on them. Each group of modules must function cohesively to support vertical and lateral loads. This structural behaviour is influenced by several critical factors, including modular arrangement and diaphragm action.

3.4.1. Impact of Modular Arrangement

The arrangement of modules within a modular mid- or high-rise building significantly influences the structural performance. Modules must be placed strategically to optimize load transfer and stability. Symmetrical arrangements typically result in more uniform load distribution, reducing stress concentrations on specific modules or connections. Conversely, asymmetrical arrangements could introduce uneven forces, increasing the likelihood of deformation or failure. Effective modular arrangement requires careful consideration of the interplay between vertical and lateral load paths. Proper alignment of modules around the core and along the building's perimeter can enhance the overall stability of the structure. An example of this approach can be seen in Chapter 2.1.3. In Case study 2 (The Paragon) the modules are symmetrically placed and clustered around the core.Figure 3.14 shows the optimized modular arrangement.
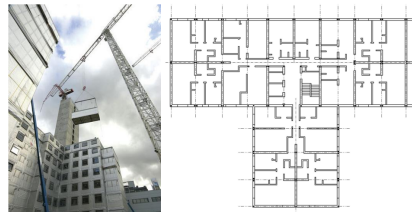
Figure 3.14: Example of optimized Core structure (left) with modular arrangement (right)[9]

3.4.2. Role of Diaphragm Action

Diaphragms are critical components for transferring lateral loads to the stability system and connecting vertical elements. In conventional buildings, diaphragms made of cast-in-situ concrete or concrete-filled metal decking are typically rigid and continuous, ensuring efficient lateral load distribution when span-to-depth ratios meet specific design criteria. However, in modular steel modular buildings, diaphragms often exhibit flexible behaviour due to the discontinuities inherent in modularisation, such as gaps between prefabricated units. These flexible diaphragms behave like deep beams, distributing loads across tributary areas but with reduced stiffness. This flexibility can cause uneven load distribution, increased drifts, and potential instability, especially during seismic or wind events. To mitigate these challenges, it is crucial to assess diaphragm stiffness during the design phase and implement measures to enhance stiffness where needed [48][49].

Figure 3.15 illustrates the classification of diaphragms based on their stiffness, highlighting the distinction between rigid, stiff, and flexible diaphragms and Figure 3.16 provides an example of a discrete floor diaphragm in a modular system, showcasing the segmentation and gaps present in modular structures.
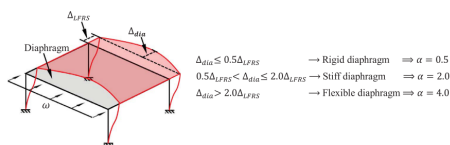
Figure 3.15: Diaphragm classifications [48]
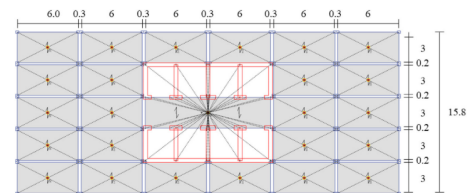
Figure 3.16: Example of a discrete floor diaphragm[49]

3.5. Conclusion

The findings of this chapter provide an understanding of the structural challenges and opportunities in modular mid-rise construction.

- **Vertical Load Capacity** : Modular mid-rise buildings rely heavily on corner-post columns to transfer vertical loads through stacked units. The analyses demonstrated that achieving sufficient axial capacity in these columns presents a significant challenge. Columns in the lower levels are subjected to the highest compressive forces, which necessitates careful cross-section optimization to prevent buckling.

- **Lateral Stability**: Addressing lateral loads requires specialized stability systems tailored to the segmented nature of modular construction. The comparative analysis of braced frames, core-based systems, and outrigger systems revealed that outrigger systems provide superior performance. They minimize lateral displacements, ensure uniform deformation patterns, and effectively engage the entire structural system in resisting lateral forces, making them suitable for mid-rise modular applications. However, this superior performance is partly attributed to the additional structural material introduced by the outriggers, which may result in increased construction costs and complexity.

- **Connection Behaviour**: The behaviour of both intra-module and inter-module connections was found to significantly influence the structural performance of modular mid-rises. Inter-module connections, modelled as beam-joint elements in *Karamba3D*, were shown to play a crucial role in determining the overall deformation behaviour of the structure. The flexibility or stiffness of these connections can greatly affect the lateral displacement and rotational behaviour of modular units, highlighting the need for robust connection design to ensure structural integrity.

- **Group Behaviour**: The collective behaviour of the modular units contributes to the overall stability of the building. highlighting the importance of considering how individual modules interact within the group. Uniform deformation patterns and effective load sharing between modules are essential for achieving a stable and resilient structure.

This chapter has established the foundation for understanding the structural performance of modular mid-rise buildings. In the following section the concept for the modular construction will be developed.

4

Concept Development

This chapter presents the conceptual development of a structural system for a modular mid-rise building. It begins with the design of the floor plan and a *3D* structural configuration, which combines a precast concrete core with modular corner-post units and outriggers. The *3D* concept is then translated into a representative *2D* model, allowing for simplified analysis of structural behaviour and critical interface forces.

Subsequently, a *parametric* model is constructed in *Grasshopper*. The model is used to assess structural performance of the proposed concept under vertical and wind loads, evaluate displacement behaviour, and analyse the effect of varying connection stiffness. Results are validated using analytical methods and matrix-frame models, ensuring the reliability of the proposed approach.

4.1. Concept Overview

This section outlines the foundational layout and structural principles of the proposed modular concept. It begins with the design of a floorplan, followed by a *3D* structural overview that integrates a concrete core, modular units, and outrigger elements.

4.1.1. Floorpan Design

The first step in creating the concept was to design the floor plan of the concept. The floor plan design philosophy was guided by the previously outlined optimal layout for the modules. The design began with arranging modules based on the optimal layout to ensure efficient load paths. Corner-post modules were aligned to create direct and effective load transfer, promoting structural performance. A symmetrical layout was prioritized to ensure uniform load distribution, minimizing stress concentrations and enhancing stability.

To assess the effectiveness of the proposed concept, a comparative stability model supported solely by a concrete core has been developed. This model serves as a benchmark for evaluating the structural performance of the outrigger-enhanced design. A basic stacked modular system without external stability mechanisms was initially considered but ultimately excluded from the comparison, as the focus is on assessing the added value of the outrigger system relative to a conventional core-only structure.

For the two models with a core, the modules were aligned so the columns of the module are connected directly to the core perimeter, ensuring effective load transfer. Figure 4.1 illustrates the floor plan layout for the three systems.
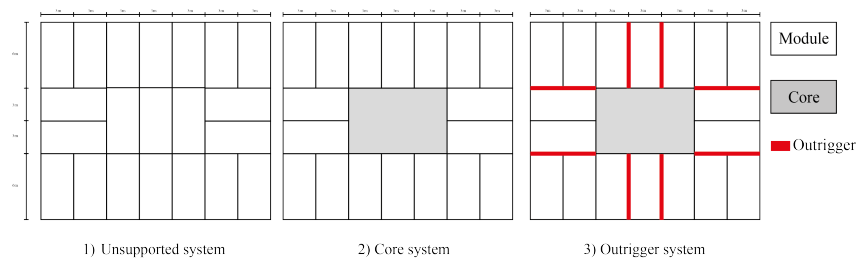
Figure 4.1: Floor plan design

Figure 4.2 illustrates a potential room layout within the modular design. The green modules represent student rooms, the yellow modules correspond to medium-sized rooms, and the red modules denote the larger rooms.
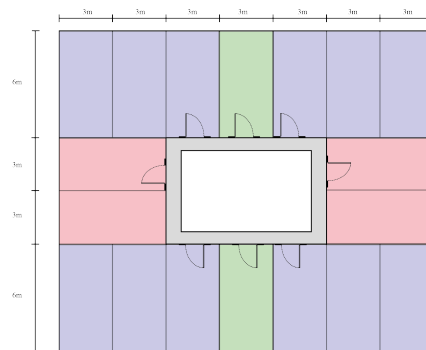
Figure 4.2: Potential room division

The floor plans for the three models were designed to cover a total area of $378 \ \mathrm{m}^2$. Modules with dimensions of $6 \times 3, \mathrm{m}$ were selected, and the layout was based on the principle of aligning the module corners to connect directly with one another. For the models incorporating a core as part of their stability system, the core size was estimated at $54 \ \mathrm{m}^2$. This area was calculated to provide sufficient space for essential functionalities, including staircases and elevators, for a building height of up to $70 \ \mathrm{m}$.

4.1.2. 3D Structural Overview

The proposed concept is a hybrid structural system combining a precast concrete core, outrigger elements on three floors, and modular corner-post units. The system operates as follows:

The precast core acts as the primary vertical load-resisting and lateral stability element, carrying significant axial loads and resisting overturning moments. Outriggers are strategically placed at three levels, extending from the core to engage with the modules. These outriggers distribute lateral forces and enhance the overall stiffness of the structure by creating a coupling effect between the core and the exterior columns. The modules are connected to the outriggers at the columns of the modules. This configuration ensures that the modules contribute to lateral and gravity load resistance. The outriggers link directly to a single stack of modules underneath, effectively transferring loads and engaging the modules in the structural system.

Based on the previously designed floorplan a *3D* concept is made. The elements of the proposed concept are presented in a series of figures to illustrate the progression of the hybrid structure. This progression can be seen in figure 4.3.
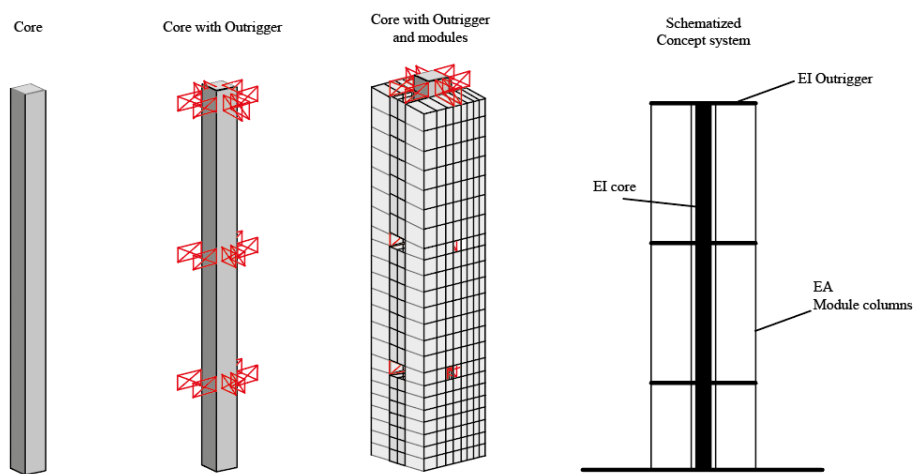
Figure 4.3: Overview of the concept with a simplified structural mechanical scheme

The first figure shows the precast concrete core alone, highlighting its role as the primary vertical and lateral load-resisting element. The second figure builds on this by incorporating the outriggers, which extend horizontally from the core to engage with the modules, demonstrating their function in coupling the core to other structural components. In the third figure, the modules are added to the system, showing how the outriggers connect the core to the modular corner-post units, completing the visualization of the *3D* hybrid structure.

The fourth figure transitions to a simplified structural mechanical scheme, which represents the system in a *2D* schematic form. This schema is designed to simplify the analysis and focus on the mechanical behaviour of the structure. It shows how the core, outriggers, and modules work together to resist loads and maintain stability. The structural mechanical scheme illustrates the locations of the most critical material properties that enable the concept to function effectively. These properties include the flexural rigidity EI of the core, the flexural rigidity EI of the outriggers, and the axial stiffness EA of the columns. The EI of the core is critical as it determines the core's ability to resist bending and lateral deformations, which are essential for stability under lateral loads. The EI of the outriggers is crucial because it governs their capacity to transfer forces between the core and other structural components, ensuring the entire structure participates in resisting loads. The EA of the columns is equally important as it influences their ability to carry vertical loads and resist the axial forces generated by the coupling action of the outriggers. These properties collectively define the structural behaviour and performance of the hybrid system, which is simplified in the structural mechanical scheme.

4.1.3. Structural Stability Systems

To gain a clear understanding of the proposed concept, the hybrid structure can be divided into three distinct stability systems: the frame, the core, and the core with outriggers. Before examining how these systems interact and function together within the hybrid structure, each stability system is analysed individually to evaluate its performance and contribution to overall stability.

Figure 4.4 illustrates a schematic representation of these three stability systems.
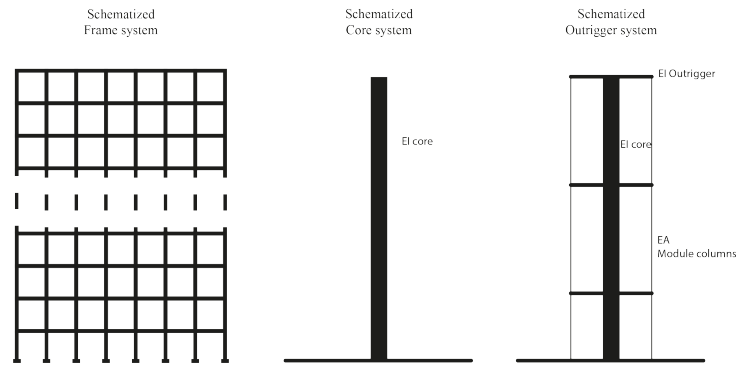
Figure 4.4: Three different stability systems schematized

In the following sections, each stability system is analysed using analytical expressions and simplified models to capture its individual structural behaviour. These serve as a theoretical basis for understanding the system response and provide a reference for validating the results from the *Karamba3D* structural analysis, as discussed in Section 4.3.

Rigid Frame model

The first stability system is the frame system, which resists lateral loads through the stiffness of its beam and column connections. These elements work together to form a continuous and stable framework. When the portals of the modules are considered stiff, and when the inter-modular connections are assumed to behave as rigid connections, the overall assembly can function as a stiff frame. However, an important distinction must be made: the portals along the short sides of the modules can be assumed to function as rigid frames, whereas the portals along the length of the modules cannot be regarded as rigid frames due to their configuration. The portals along the short sides of the modules are characterized by shorter spans between columns, which result in increased stiffness and reduced deflection, allowing them to function effectively as rigid frames.

To evaluate the performance of this system, a *Matrix-frame* model has been developed to analyse the load distribution and deformation characteristics. The rigid frames along the short sides have been modelled using a four-by-three module configuration, with the same cross-sections applied in the *Grasshopper models*. For this analysis, a dummy load of $10\,kN/m$ has been applied to the left side of the structure. Both the intra-modular and inter-modular connections are behave as stiff connections. An overview of the resulting forces is presented in figure 4.5.
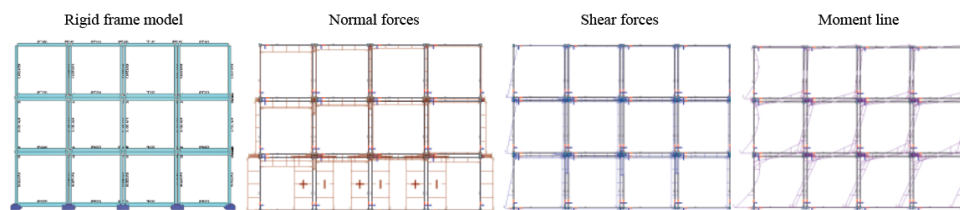
Figure 4.5: *Matrix-frame* overview of stiff portal frame

Enlarged figures of the *MatrixFrame* results for internal forces in a rigid frame are provided in Appendix B.

Core System

In models that include a core, the core is designed as a rectangular hollow section. At this stage, any openings in the core, such as doorways, are disregarded. The core has a length of $9\,m$ in the x-direction and a width of $6\,m$ in the y-direction, with walls assumed to have a thickness of $0.3\,m$. The design of the core, including its dimensions, is illustrated in Figure 4.6.
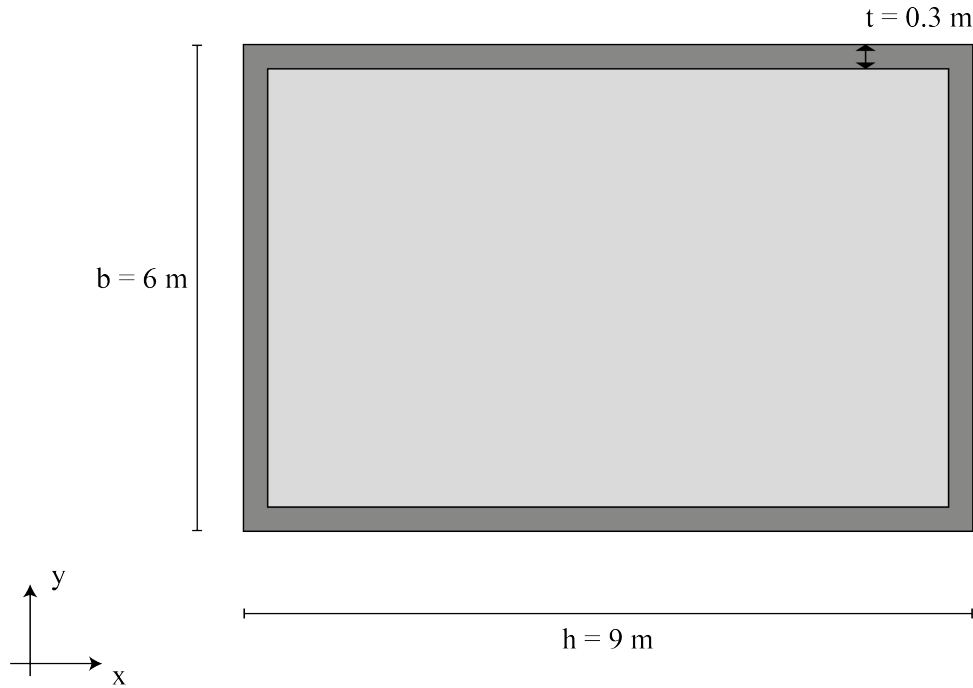
Figure 4.6: Core dimensions

The moments of inertia of the core in both directions are calculated using the following formulae:

For bending about the x-axis (I_{xx}):

$$I_{xx} = \frac{b \cdot h^3}{12} - \frac{(b - 2t) \cdot (h - 2t)^3}{12} \tag{4.1}$$

For bending about the y-axis (I_{yy}):

$$I_{yy} = \frac{h \cdot b^3}{12} - \frac{(h - 2t) \cdot (b - 2t)^3}{12} \tag{4.2}$$

Where:

- b: Length of the core in the x-direction ($9\,m$),
- h: Width of the core in the y-direction ($6\,m$),
- t: Wall thickness ($0.3\,m$).

The calculated moments of inertia are: The calculated moments of inertia are:

$$I_{xx} = 51.8\,\mathrm{m}^4, \quad I_{yy} = 97.8\,\mathrm{m}^4$$

The elastic modulus (E) of the core, made from precast concrete, should be determined based on the concrete mix, production process, and supplier specifications. Standard values from design codes can be used for preliminary analysis, but precise values should be verified and will be incorporated in later stages of this research.

First order effect analytical approach

A core, when subjected only to horizontal loading (e.g., wind), can be simplified and schematized as a cantilever beam with one fixed support. This is visualised on the left side of figure 4.7. The bending moments at the base of the cantilever beam, representing the core, can be calculated using the formula for the bending moment. The deflection of the cantilever beam due to horizontal loading can also be calculated, providing insights into the maximum deflection at the top of the cantilever.

$$M = \frac{1}{2} \cdot q \cdot l^2 \quad ; \quad \delta = \frac{1 \cdot q \cdot l^4}{8 \cdot E \cdot I} \tag{4.3}$$

where M is the bending moment at the base of the core, q is the horizontal force per unit length, l is the height of the cantilever beam, δ is the maximum deflection at the top of the cantilever, E is the modulus of elasticity of the material, and I is the moment of inertia of the cross-section.

As an illustrative example, with the previously defined moments of inertia in the y- and x-directions, and assuming a distributed load ($q = 10\,\mathrm{kN/m}$), a modulus of elasticity ($E = 3.3 \times 10^7\,\mathrm{kN/m^2}$), and a building height of $H = 70\,\mathrm{m}$, the total moment at the base of the core is calculated as $M = 24,500\,\mathrm{kNm}$. The corresponding deflection at the top of the core is approximately $\delta_x = 0.0092\,\mathrm{m}$ in the x-direction and $\delta_y = 0.0176\,\mathrm{m}$ in the y-direction. It is evident that the y-direction is the weak side of the building, as the deflection in this direction is significantly higher compared to other directions.

Second order effect

When the core is subjected to both horizontal loading and vertical loading (e.g., normal forces from floors), the interaction between these forces significantly influences its stability. Horizontal loads cause deflection, resulting in a bending moment, while vertical loads acting on the deflected core create additional bending moments through second-order effects. These combined effects determine the core's ability to resist instability [50].

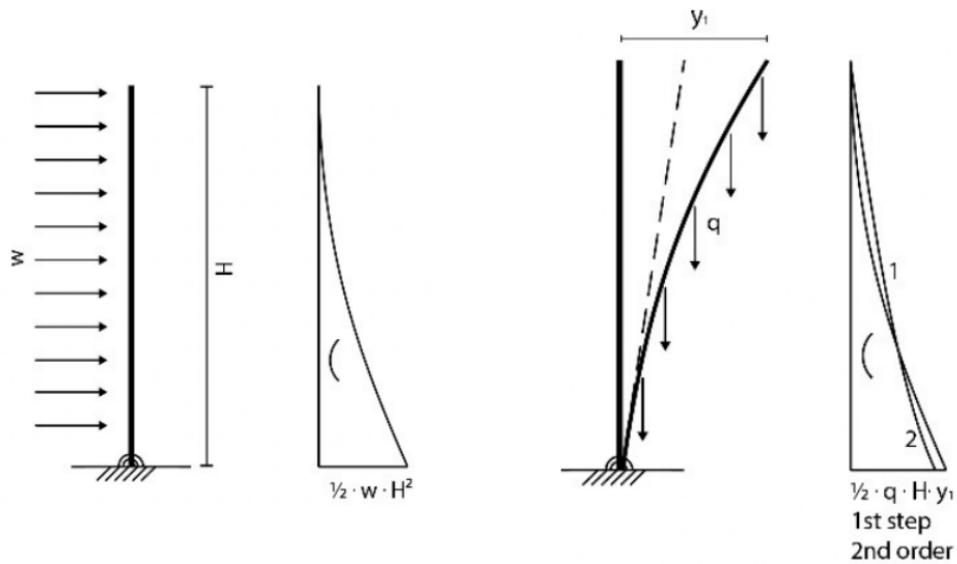Figure 4.7 illustrates the first-order and second-order effects of loads acting on the core.

Figure 4.7: First and second order effect on core system [50]

Outrigger
Incorporating an outrigger system into the structural design requires careful consideration of several
critical design options. The most important options to take into account for the designing the concept
are the type of outrigger, outrigger placement and the number of outriggers.

- The type of outrigger selected significantly influences its structural performance and architectural
  integration. Common types of outrigger configurations are conventional, virtual, and offset systems.
  For the proposed concept the choice has been made to develop a conventional outriggers system.
  These are rigid horizontal structures that connect the building's core in normal cases to perimeter
  columns, enhancing lateral stiffness and strength by creating a unified structural system [51]. In the
  proposed concept, the outrigger system will be directly connected to the columns of the modules
  rather than being exclusively attached to the perimeter columns, as is traditional.

- The vertical placement of outriggers plays a critical role in their effectiveness as a stability sys-
  tem. A uniformly distributed lateral load causes the structure to rotate, with exterior columns act-
  ing as elastic springs to counteract this motion, thereby reducing deflections and base moments.
  Columns beneath lower outriggers provide greater stiffness due to their shorter length, but rota-
  tional deflection of the core is highest near the top. To balance these opposing effects, the optimal
  placement of a single outrigger is approximately $0.455\,H$, where H is the total building height.
  For two outriggers, ideal positions are located at $H/3$ and $2H/3$, with similar proportional logic
  applicable for additional outriggers. In practice, architectural constraints often govern outrigger
  placement, as they occupy usable floor space. As a result, outriggers are typically located on me-
  chanical floors designated for elevator shafts or ventilation systems to minimize disruption while
  maintaining structural efficiency [52].

- The number of outriggers incorporated into a building's design directly affects its lateral load resis-
  tance and overall stability. Implementing multiple outriggers can significantly enhance a structure's
  stiffness and reduce lateral deflections. For instance, utilizing two outriggers optimally placed at
  one-third and two-thirds of the building's height can effectively control lateral displacements and
  improve load distribution. However, increasing the number of outriggers beyond two may yield di-
  minishing returns in terms of additional stiffness and can introduce complexities in construction and
  architectural design. Therefore, determining the optimal number of outriggers involves balancing
  structural benefits with practical considerations, ensuring that each additional outrigger contributes
  meaningfully to the building's performance [51].

Figure 4.8 illustrates the impact of various outrigger configurations (number and placement of outriggers)
on the bending moment distribution in a structure. The figure clearly demonstrates a reduction in bending
moments at the points where the outriggers are positioned.
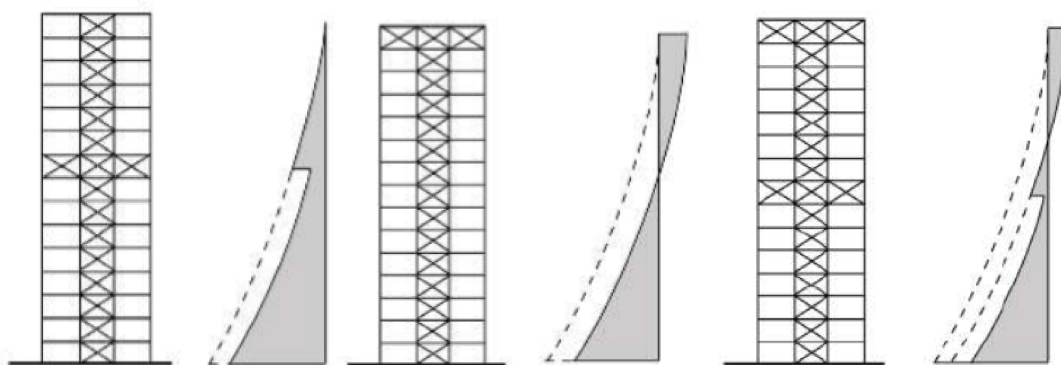
Figure 4.8: Effect of different outrigger configurations on the bending moment (*Retrieved and adjusted from [50]*)

The design choices for the outrigger elements in the initial iteration of the concept are described in detail
in Section 4.3.

Example Analytical approach outrigger

In order to be able to get an idea of the effectiveness of the outrigger, a simple method of calculation is applied based on the examples of Structural Calculations of High Rise Structures (Version: 26-4-2017, Authors: ir. P.H. Ham and dr. ir. K.C. Terwel) [50]. The set-up for this calculation can be seen in figure 4.9.
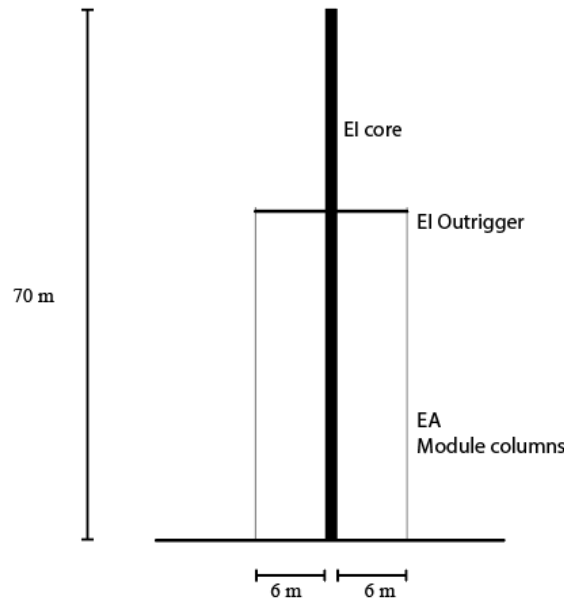
Figure 4.9: Simplified outrigger calculation set-up

The following formulas are used to determine the flexural rigidity and deflection of the structure:

Moment of Inertia for the Core:

$$I_{core}$$

Outrigger System Contribution:

$$I_{outrigger} = c \cdot n \cdot 2 \cdot z^2 \cdot A$$

Where:

- c: Reduction factor for the effectiveness of the outrigger system, depending on position and stiffness ($0.3 < c \leq 0.6$), for optimized location take $c = 0.6$.
- n: Number of columns per façade.
- z: Distance from the core to the centre of the column.
- A: Cross-sectional area of the column.

Combined Flexural Rigidity (EI):

$$(EI)_{structure} = I_{core} \cdot E_{concrete} + I_{outrigger} \cdot E_{steel}$$

Combines the contributions of the concrete core and the steel outrigger system, accounting for their respective moduli of elasticity.

Deflection of the Structure:

$$\delta = \frac{q \cdot L^4}{8 \cdot (EI)_{structure}}$$

With the columns made of *SHS HF 120×10*, the cross-sectional area is $A = 4293 \, \text{mm}^2$ ($0.004293 \, \text{m}^2$). Assuming $n = 1$, corresponding to the outrigger being connected to a single column of the stacked modules, the moment arm is taken as $z = 10.5 \, \text{m}$. This value represents the distance between the perimeter column and the centreline of the core, based on the assumption that plane sections remain plane, following Bernoulli's hypothesis. A reduction factor of $c = 0.6$ is applied, reflecting the assumption that the outrigger is positioned at its optimal location.

The moment of inertia of the outrigger ($I_{\text{outrigger}}$) is calculated as $0.57\,\text{m}^4$. Given a modulus of elasticity for steel of $E_{\text{steel}} = 210{,}000\,\text{N/mm}^2$, the resulting flexural rigidity of the outrigger system becomes $EI_{\text{outrigger}} = 0.120 \times 10^9\,\text{kNm}^2$.

For the concrete core, assuming uncracked behaviour and a modulus of elasticity corresponding to concrete class *C20/25*, $E_{\text{concrete}} = 19.997{,}500\,\text{kN/m}^2$, the resulting flexural rigidities are:

$$EI_{yy} = 0.976 \times 10^9\,\text{kNm}^2, \quad EI_{xx} = 0.517 \times 10^9\,\text{kNm}^2.$$

By adding the outrigger's contribution to the total flexural rigidity of the system, the horizontal displacements are reduced to $\delta_x = 0.0471\,\text{m}$ and $\delta_y = 0.027\,\text{m}$. These values show an improvement compared to the displacements of the core-only configuration, which exhibited $\delta_x = 0.058\,\text{m}$ and $\delta_y = 0.031\,\text{m}$.

Table 4.1 summarizes the computed lateral displacements for the core-only and outrigger-enhanced systems, along with the resulting percentage reductions.

Table 4.1: Reduction in Lateral Displacement Due to Outrigger Contribution

Direction	Core Only (δ [m])	With Outrigger (δ [m])	Reduction (%)
x-direction	0.058	0.047	19%
y-direction	0.031	0.027	11%

This limited enhancement can be attributed to several factors: only a single outrigger is implemented, and it connects to just one line of module columns. These columns, having relatively small cross-sectional areas, lack the necessary stiffness and strength to effectively counteract the coupling action of the outriggers. As a result, the overall contribution of the outrigger to structural performance is constrained.

4.2. Concept from 3D to 2D

A *3D* model has been created to represent the concept, serving as the foundation for further investigation. The *3D* model will be translated into a representative *2D* cross-sectional model. By making informed and reasonable assumptions, the *2D* model will be designed to closely resemble the structural behaviour of the original *3D* concept. The purpose of this approach is to provide insight into the feasibility and performance of the proposed system without introducing unnecessary complexity during this stages of analysis.

4.2.1. Development of the 2D Cross-section

The floor plan of the concept is dual symmetrical as can be seen in figure 4.10. the first step into making a *2D* model of the concept is by halving the floorplan in two.
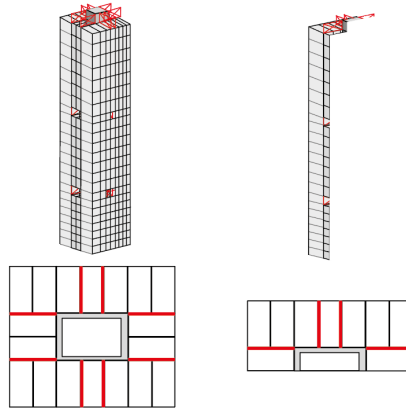
Figure 4.10: Division of the floor plan in symmetrical parts

Figure 4.11 presents the selected cross-section of the building, representing half of the structure along its length. This cross-section has been chosen as the initial focus for analysis. However, since this cross-section corresponds to the long side of the building, where the core exhibits higher stiffness, an additional cross-section will be developed for the short side of the building. The same procedure, as outlined in the following sections, will be applied to analyse this alternative cross-section to ensure a comprehensive evaluation of the concept.
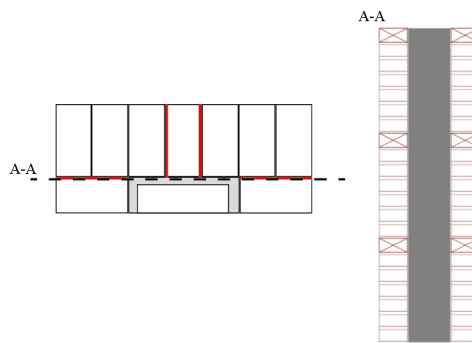
Figure 4.11: *2D* Cross-section of the building in long side of the building

To ensure that the cross-section provides an accurate representation of the entire building, certain critical aspects must be carefully addressed. These include the connections of the core, the core stiffness, the stiffness of the portals of the modules, and the transfer of loads within this cross-section. Each of these points will be discussed in detail in the following sections.

4.2.2. Critical Points

The transition from the *3D* structural concept to a simplified *2D* analysis model introduces several critical modelling considerations. This section identifies and discusses the key aspects that require careful treatment to ensure the *2D* model accurately captures the structural behaviour of the original system. These include the representation of module to core connections, the adjustment of core stiffness due to symmetry, the estimation of interface forces arising from deformation differences, and the modelling of vertical and horizontal load transfer mechanisms.

Core connections

To investigate the effect of the rotational stiffness of the connections on the overall stability of the structure, it is essential to thoroughly examine how the connections in the *2D* concept represent the connections in the *3D* model. The exact method of modelling the module to core connection will be discussed in detail in Section 4.3.

This module to core connection is present twice on each side of the core. To illustrate the location and arrangement of these connections, an exploded view of the floor plan has been created. In this exploded view, the modules are separated, and the connections between them are represented by lines. The module to core connections are visualized in the exploded floor plan using green lines in figure 4.12.
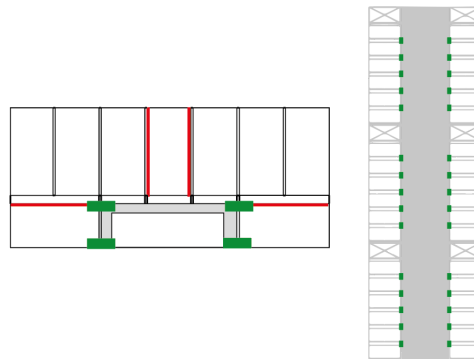
Figure 4.12: Core to module connections in the exploded floor plan (left) and in *2D* cross-section (right)

It is important to note that in the *2D* cross-section, on the right side of the figure 4.12, this connection is represented as a single element, effectively combining the two connections due to the nature of *2D* modelling. When estimating the effect of varying the stiffness of this connection, it must be understood that the representation in the *2D* cross-section inherently includes the contribution of both connections, necessitating careful consideration of this factor to achieve a realistic assessment.

Core Stiffness

Since the *2D* cross-section represents half of the building, due to its symmetrical layout, the stiffness of the core must also be considered as half of the total core stiffness. As a result, the calculated moments of inertia provided in Section 4.1.3 should be halved. Figure 4.13 shows the conversion from the *3D* moments of inertia to the *2D* model.

3D Model   2D Model

Iyy = Iyy full core   Iyy = 1/2 * Iyy full core
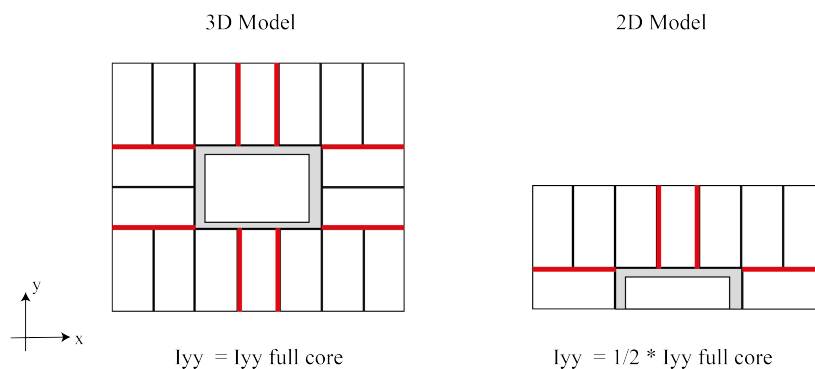
Figure 4.13: Moments of inertia in *3D* and *2D* model

Interface Forces due to deformation differences Core and Modules

As mentioned before the core provides the primary source of lateral stability. While the modules contain portal frames at their ends, these frames are primarily intended to ensure sufficient transport stiffness and have a significantly lower lateral stiffness compared to the concrete core[6].

Because the modules are physically connected to the core, they are required to follow its deformation. This becomes particularly relevant when the core deforms laterally due to horizontal loads. Since the modules themselves deform differently then the core, this mismatch in deformation will lead to to forces at the interface between the modules and the core. These forces are especially significant near the base and the top of the structure, where bending curvature of the core is largest.

Since this interaction cannot be captured within the two-dimensional cross-sectional model, an alternative approach is required to estimate the magnitude and distribution of the interface forces. Figure 4.14 shows the location of the portals that need to follow the deformation of the core.
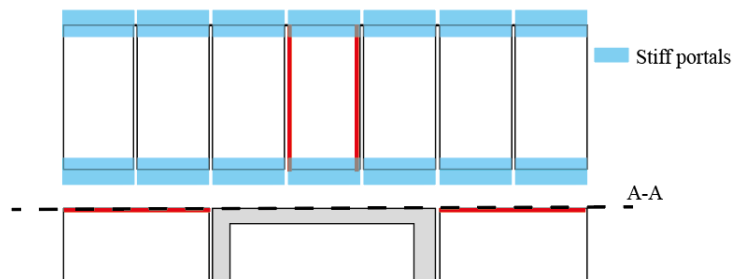
Figure 4.14: Location of the stiff portals in the floorplan

Figure 4.15 shows a dedicated *Grasshopper* model developed to investigate the interaction between the portal frames, previously introduced in Figure 4.14 and an adjacent core wall.
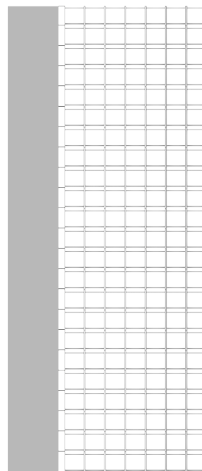
Figure 4.15: *Grasshopper*-model for interface forces due to deformation differences

In this model, the wind load acting on that portion of the structure is applied directly to the core wall. A connection is introduced between the core and the stacked modules, allowing for direct evaluation of the resulting axial forces at the interface. These interface forces will be of key importance later in this research, when the proposed concept is applied in the case study presented in Chapter 6, focusing on connection detailing and the transfer of forces between the modules and the core.

Load Transfer

Lastly, an important aspect of converting the *3D* concept into a *2D* structure is defining how load transfer occurs in both vertical and horizontal directions, and how the structure responds to the applied loads within the *2D* model.

Vertical load transfer

Because the modules are corner-post modules, the vertical loads from the self-weight of the material are primarily transferred through the columns of the modules to the foundation. However, when the modules are connected to the core, an additional load transfer mechanism must be considered and incorporated into the *2D* model. Specifically, the vertical loads of the modules are distributed such that half of the load is carried by the columns on the side not connected to the core, while the other half is transferred through the module-to-core connection into the core.

For modules not directly visible in the *2D* cross-section, their contribution to the vertical load transfer is represented by applying point loads to the core at the locations where these modules are connected. This approach ensures that the *2D* model accurately reflects the vertical load distribution in the *3D* concept. Figure 4.16 illustrates the points where vertical load transfer occurs to the core.
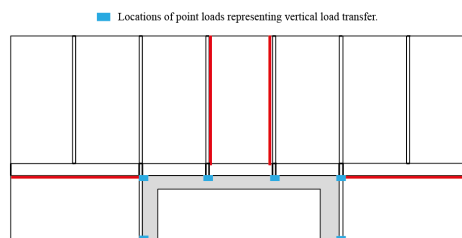
Figure 4.16: Points of vertical load transfer to the core

An important assumption in modelling the distribution of live loads on the roofs and floors of the modules is that they behave as one-way slabs. Under this assumption, the live loads are evenly distributed along the long sides of the modules, ensuring a simplified and consistent load path. This distribution is illustrated in Figure 4.17, complementing the representation of vertical load transfer to the core described earlier.
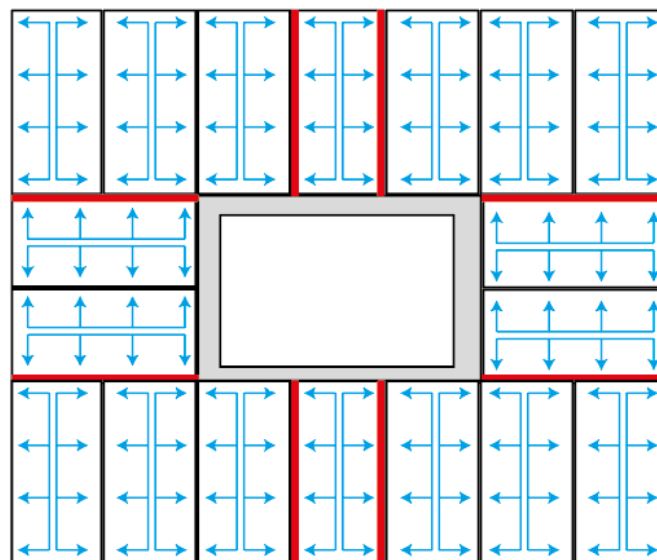
Figure 4.17: Vertical load transfer path on module floor

Figure 4.18 illustrates the positions of the point loads representing the load transfer from the modules to the core at a typical floor level in the *2D* cross-section. At locations where two modules connect to the core, there are two point loads positioned closely together. In the *2D* model, these are simplified and combined into a single point load with twice the magnitude to accurately represent the total transferred load.
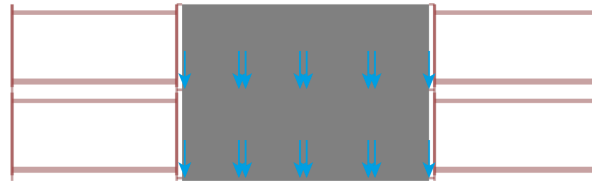
Figure 4.18: Point loads of the vertical load transfer

Horizontal load transfer

In the *2D* model, horizontal loads are applied to the beams of the modules as point loads rather than directly to the columns. This approach reflects how the façade would realistically transfer horizontal forces, such as wind loads, to the structural system. The façade, acting as a cladding system, distributes the loads to the beams, which then transfer them to the columns and the core. Figure 4.19 illustrates how the horizontal loads are modelled in the *2D* model.
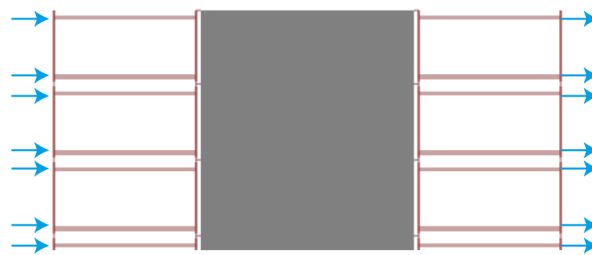
Figure 4.19: Vertical Loads modelling

The exact values for the horizontal and vertical loads used in the model are determined in Section 4.4.1.

4.3. Grashopper Model

To assess these structural systems and evaluate the viability of the proposed concept, models were developed using *Grasshopper*. The approach and methodology employed in creating these models will be detailed in the following section.

4.3.1. Components

Module

The module used in the concept is based on commonly used corner-post designs. As illustrated in Figure 4.20, the module measures $6\,m$ in length, $3\,m$ in width, and $3\,m$ in height.
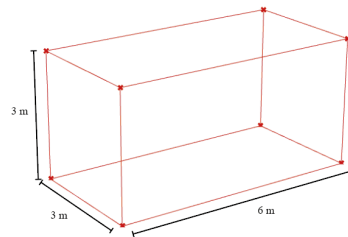
Figure 4.20: The concept module

The columns in a corner-post module typically feature SHS or RHS cross-sections, while the beams are commonly UNP. However, the *Grasshopper* plug-in *Karamba* supports only symmetrical cross-sections, making it impossible to use UNP directly in the model. To address this, a cross-section for the beams is chosen based on similar moments of inertia and cross-sectional area. These parameters are critical because the moment of inertia determines the beam's resistance to bending, while the cross-sectional area influences its axial load-bearing capacity and overall structural stability, ensuring the substitute section closely replicates the behaviour of the original UNP beams.

The top beam is specified as a UNP 160; however, an IPE 160 is selected as a suitable alternative. Similarly, the bottom beam is originally designed as a UNP 200 but is replaced with an IPE 220. For the columns, an SHS 120/10 HF profile is selected based on calculations in Section 3.1, which demonstrate that these columns can support the vertical load of up to 22 floors, considering only the self-weight of the modules. Table 4.2 summarises the configuration of the cross-sections chosen for this stage of development.

Table 4.2: Beam and column profiles of the modules used in the model

Component	Specified Profile	Chosen Profile
Top Beam	UNP 160	IPE 160
Bottom Beam	UNP 200	IPE 220
Columns	SHS 120/10 HF	SHS 120/10 HF

These cross-sections serve as the baseline for the concept development; however, they may be revised at a later stage of this research if structural analysis indicates that the selected cross-sections are unable to resist the required loads.

Core modelling

For this stage, it is modelled as a single continuous shell element, providing an idealized version of the core's structural behaviour. This approach represents an intentional overstatement of the real-world situation, as the actual core consists of precast concrete segments rather than monolithic in-situ concrete. Additionally, openings such as doorways and service passages are not included in the model. These simplifications allow for a focused study of the structural performance and stability of the concept, without the additional complexity introduced by detailed core segmentations and openings. Such refinements will be incorporated in subsequent phases of this research to enhance the model's realism once the fundamental design principles are validated.

Verification of Shell Behaviour: Karamba Model vs. Analytical Approach

To verify if the core in the model would behave as what would be expected, both a *Karamba* model in *Grasshopper* and an analytical approach were used. The set-up for both can be seen in figure 4.21.

$$\theta_2 = \frac{F\ell^2}{2EI}; \quad w_2 = \frac{F\ell^3}{3EI}$$

Analytical Model   Karamba Model
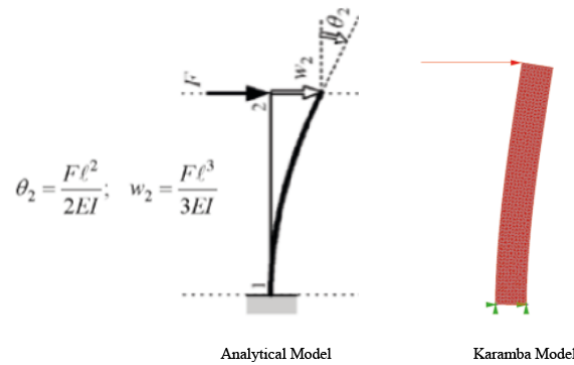
Figure 4.21: Core modelling in *Karamba*

The shell, with a height of 70 meters, width of 9 meters, and thickness of 1 cm, was modelled in *Karamba* using the material properties of concrete C12/15 ($E = 2.7 \times 10^7 \, \text{kN/m}^2$, $\nu = 0.2$). A horizontal point load of $10 \, \text{kN}$ was applied at the top of the shell, resulting in a maximum displacement of $7.84 \, \text{cm}$ according to *Karamba*'s finite element solver.

For the analytical approach, the shell was approximated as a vertical cantilever beam using $\Delta = \frac{FL^3}{3EI}$, where $I = \frac{Bt^3}{12}$. The calculated maximum displacement was $6.97 \, \text{cm}$, which differs the *Karamba* result by approximately 12%. The difference arises from the analytical method's simplifications, the analytical approach assumes uniform bending behaviour, while the finite element solver accounts for complex interactions such as local deformations, shell effects, and potential stress concentrations.

Outrigger Modelling
For the first iteration of the concept the following design options are made regarding the outrigger element. The setup of the outriggers involves specifying the cross-sectional properties of the outrigger components and determining their placement across the building height based on a strategic logic.

The cross-sectional properties of the columns, beams, and diagonals used in the outrigger system are outlined in Table 4.3. The columns and beams are modelled as Square Hollow Sections (SHS) with dimensions of $200 \times 10 \, \text{mm}$, while the diagonals are also SHS but with slightly reduced dimensions of $180 \times 10 \, \text{mm}$.

Component	Type	Cross-Section (SHS)
Columns	Square Hollow Section	SHS 200x10
Beams	Square Hollow Section	SHS 200x10
Diagonals	Square Hollow Section	SHS 180x10

Table 4.3: Specifications of the cross-sections used in the outrigger design.

As the number of floor in the structure increases, outriggers are placed following a *parametric* logic: for structures up to 7 floors, an outrigger is placed at the top floor. For structures with 8 to 14 floors, outriggers are positioned at the 7th floor and the top floor of this range. For structures taller than 14 floors, outriggers are placed at the 7th floor, the 14th floor, and the topmost floor. This placement approach is designed to enhance structural efficiency as the height of the structure increases. However, this placement logic is flexible and can be adjusted in subsequent iterations if analysis of this initial configuration indicates the need for changes. For the first iteration of the concept, the outriggers are on floor 7,14 and 20.

Connections
This section outlines the modelling strategy for the various structural connections implemented in the *2D Grasshopper* model. Particular attention is given to intra-modular, inter-modular, module-to-core, and outrigger connections, each of which plays a critical role in accurately representing the global behaviour and stability of the structural system.

Intra-module connections
In modular steel buildings, the structural behaviour of intra-modular connections is important to ensuring the overall stability and robustness of the system. Previous research has demonstrated that assuming the moment–rotation (M-θ) behaviour of intra-modular connections to be fully rigid significantly overestimates their stiffness [15]. In reality, the intra-modular connections within the corner-supported modules are unable to rigidly transfer the moments generated in the beams to the square hollow section (SHS) columns.

To better reflect this behaviours, a simplified modelling assumption is made: the short side of the module is considered rigid due to its assumed stiff portal, while in the long cross-section of the module, the connections between the columns and beams are assumed to be hinged. This approach acknowledges the absence of a stiff portal frame along the length of the module, where rotational flexibility is more pronounced. By incorporating these connection properties, the model captures the realistic force redistribution and bending behaviours, ensuring a more accurate representation of the structural response under loading conditions. Figure 4.22 illustrates the simplified intra-connections and how they are incorporated into the first iteration of the concept.
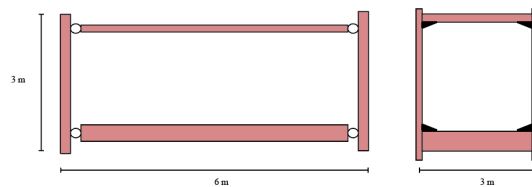
Figure 4.22: Cross-section of the portals of the modules with the simplified intra-connections

Inter-module connection
In the proposed concept, a tie-rod connection type has been adopted for the inter-module connections. The vertical connection between the upper and lower modules relies on a tension rod, which resists tensile forces and prevents vertical separation under high lateral loads and the columns are designed to carry compressive forces. The horizontal connection involves the transfer of shear forces between the upper and lower modules through the bearing action of the top plate of the upper column on a shear key. Additionally, the horizontal force between adjacent modules is transmitted via a horizontal tie plate, which bears against the shear key to provide lateral stability.

Figure 4.23 illustrates the model implemented in *Grasshopper* to simulate the tie-rod connection. This model is adapted from the reference study by Chua et al. (2020) [49].
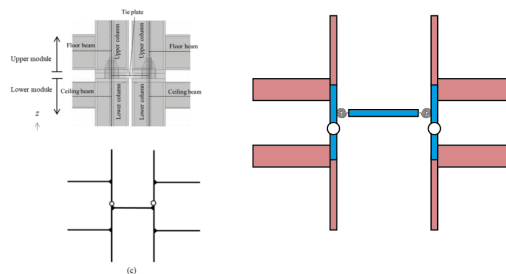
Figure 4.23: Inter-module connection based on tie-rod theory

A key modification made to the original model is the addition of rotational springs at the ends of the horizontal connection between the two modules. This adjustment was introduced to enable the analysis of various stiffness configurations and their impact on the overall stability of the structure.

Module to core connection
Figure 4.24, shows the reference model of the connection from literature (left) illustrates this approach. On the right side of the figure the connection that is used in the *Grashopper* model is show.
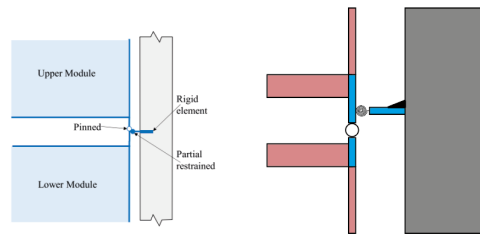
Figure 4.24: Module-to-Core connection models: Reference model (left) and *Grasshopper* model (right)

The connection between the modules and the core wall is a critical component in ensuring the stability and structural performance of modular mid-rise buildings. The proposed concept builds on the reference study by Shan et al. (2024) ([53]. This connection was modelled using macro finite element (FE) methods to accurately simulate its mechanical behaviour. In the reference design, the stacked modules were assumed to be pinned to each other to replicate their bolted connections. A partial restraint link was introduced to represent the interface between the core wall and the modules. The vertical rotational stiffness of these links was released to allow free rotation on the vertical plane, while horizontal rotational springs were incorporated to account for rotational stiffness on the horizontal plane. Furthermore, the segment of the restraint link embedded within the core wall was modelled as a rigid element to accurately represent its mechanical behaviour.

To recreate this model, a connection element was implemented in *Grasshopper* to connect the stacked modules vertically. A hinge was placed at the connection points to replicate the bolted connections, mirroring the reference model. The modules were then linked to the core wall through a horizontal connection element, which featured a rigid connection to the core. At the end connected to the modules, a rotational spring was introduced to permit rotations and to enable the analysis of various stiffness configurations and their impact on the overall stability of the structure. A modification was made to the original model by introducing a rotational spring at the connection between the horizontal and vertical elements. This addition allows again for the analysis of various stiffness configurations and their influence on the overall stability of the structure.

Outrigger-to-Core and Outrigger-to-Module Connections
Figure 4.25 illustrates how the outrigger connections are modelled within the structural concept.
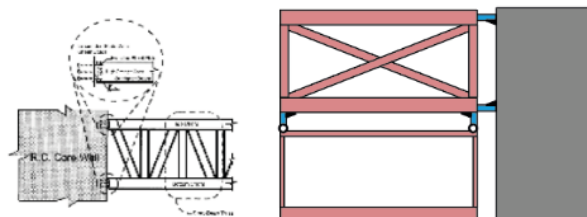
Figure 4.25: Outrigger-to-core connection: Reference model (left) and *Grasshopper* implementation (right)

In the *Grasshopper* model, the outrigger-to-core and outrigger-to-module connections are modelled to account for the transfer of significant bending moments and shear forces. These connections are critical for ensuring continuity in lateral force distribution and maintaining global stability. To simplify the modelling while preserving structural realism, the outrigger-to-core connection is assumed to be fully rigid, allowing for complete moment transfer. In contrast, the outrigger-to-module connection is modelled as pinned in the vertical direction, thereby allowing rotation and preventing moment transfer between the outrigger and the module columns. This modelling strategy ensures that the outriggers effectively engage with the core for lateral stiffness, without imposing unrealistic rotational constraints on the modules.

4.3.2. Model Overview

Figure 4.26 provides a overview of these components as represented in the *parametric* model.
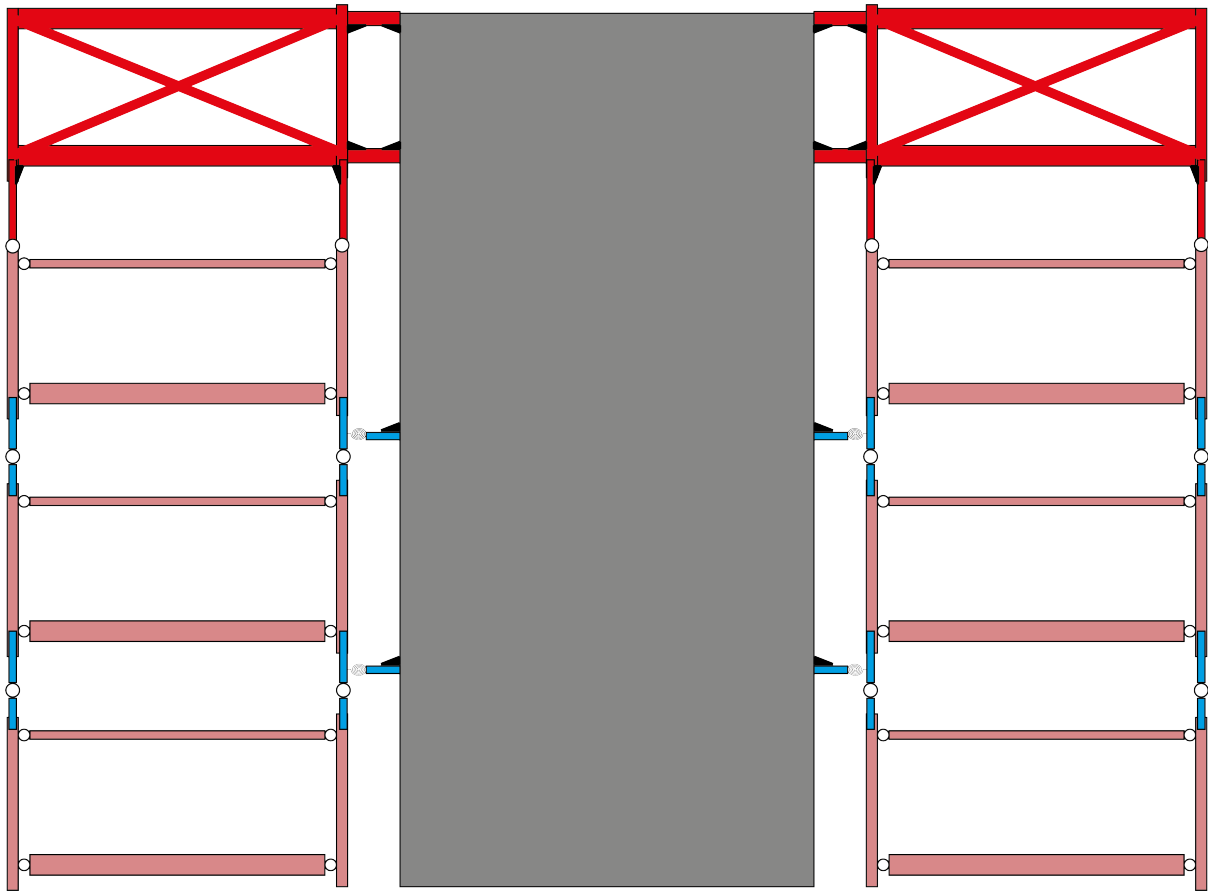
Figure 4.26: Overview the *parametric* Model

This overview illustrates the interconnected elements and their configuration within the *Grasshopper* framework, setting the foundation for structural analysis and optimization of the proposed concept.

4.4. Structural Performance

To assess the structural performance of the *2D* model, the applied loads are first calculated, followed by the presentation of the analysis results.

4.4.1. Applied Loads

Vertical loads
Permanent load

The permanent load applied in the model is calculated based on the weight of the structural elements present in the modules. The module dimensions are $6\,\text{m} \times 3\,\text{m}$. Each module consists of four columns, four top beams, and four bottom beams. The floor is assumed to be made of concrete with a self-weight G of $1.75\,\text{kN/m}^2$, while the roof is assumed to have a load of $0.4\,\text{kN/m}^2$. The specific values of the weights of these components are provided in Table 4.4.

Table 4.4: Calculation of total weight for a $6\,\text{m} \times 3\,\text{m}$ module

Type	Profile	G (kN/m)	Length (m)	Amount	Weight (kN)
columns	SHS 120 10 HF	0.31	3	4	3.74
Top Beam (trans. direction)	IPE 160	0.15	3	2	0.93
Top Beam (Long. direction)	IPE 160	0.15	6	2	1.86
Bottom Beam (trans. direction)	IPE 220	0.25	3	2	1.54
Bottom Beam (Long. direction)	IPE 220	0.25	6	2	3.08
Type	**size**	G **(kN/m2)**	**area (m2)**	**Amount**	**Weight (kN)**
concrete floor	b = 3m and l = 6m	1.75	18.00	1	31.50
ceiling	b = 3m and l = 6m	0.4	18.00	1	7.20
walls (Long. direction)	h = 3m and l = 6m	0.5	18.00	2	18.00
walls (trans. direction)	h = 3m and l = 3m	0.5	9.00	2	9.00
Total					**76.86**

Variable load

An overview of the variable loads applied in the analysis is provided in Table 4.5.

Table 4.5: Variable load calculations for the modules

Variable	Area (m^2 (A)	Load (kN/m^2 (Q)	Total Load (kN)
Variable load (residential Class A)	18	1.75	31.5
Partition wall load (variable load)	18	0.5	9.0
Roof load (variable load)	18	1.0	18.0
Total for Roof Module			**58.5**
Total for Normal Module			**40.5**

The variable loads considered in the analysis include the imposed live loads and partition wall loads, as specified for residential spaces under Class A occupancy. The live load of $1.75\,\text{kN/m}^2$ and the partition wall load of $0.5\,\text{kN/m}^2$ are distributed evenly across the floor area of the module. For the *Grasshopper* models, these loads are assumed to be shared equally between the two sides of the module in the longitudinal direction. They are applied as linear loads along the bottom beams for the floor loads and along the top beams for the roof load.

Figure 4.27 illustrates the approach used to model vertical loads realistically within the *2D* cross-section. Modules not directly visible in the cross-section are connected to the core, influencing the overall performance of the structure. The loads acting on these modules are transferred to the core at the location of their respective connections.
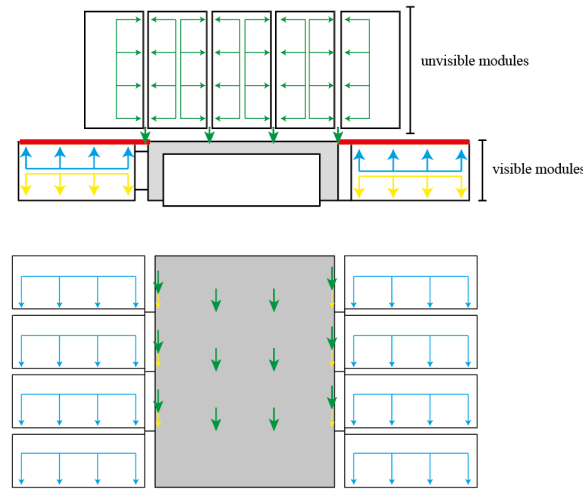
Figure 4.27: Vertical load modelling in 2D

The vertical loads acting on the modules behind the *2D* model, visualised as the green distributed load, represent the total loads applied to these modules that need to be transferred to the *2D* cross-section. These distributed loads are transferred to the core through the connections between the modules and the core. The green arrows indicate the load transfer from the columns of the modules, with each arrow corresponding to $\frac{1}{4}$ of the total load acting on two modules. Based on the current floor plan, each green arrow represents the load transferred from two columns, one from each module connected to the core at that location. These arrows are positioned on the core at the points where the modules connect to it. The values of the green point loads are equal to $\frac{1}{4} \cdot$ load on module $\cdot 2$ (two modules). For permanent loads, each arrow represents $38.43\,\mathrm{kN}$, which is half of the module's total weight. For variable loads, the arrow represents $29.25\,\mathrm{kN}$ for a roof module and $20.25\,\mathrm{kN}$ for a standard floor module.

The yellow vectors in Figure 4.27 represent the loads from the half of the module that is visible in the *2D* cross-section, including both permanent and variable loads. These yellow vectors are applied at the core, specifically at the locations at the core where the module is horizontal connected two. The value of this load is equal to one-quarter of the total permanent and variable load of the module. For the permanent load, this value is $19.22\,\mathrm{kN}$. For the variable load, the value is $14.63\,\mathrm{kN}$ for a roof module and $10.13\,\mathrm{kN}$ for a normal module. These are summed up with the green point loads that are also at this location in the *2D* model

The blue distributed load in Figure 4.27 represents the variable loads acting on the half of the module. These are modelled as line loads applied to the bottom beam in the 2D cross-section for normal floor modules or the top beam in the case of roof modules. The permanent load from this half of the module is already considered in the model, and therefore these values are excluded from the distributed loads to avoid double counting. For a normal floor module, the distributed load applied to the bottom beam consists of the variable floor load $1.75\,\mathrm{kN/m}^2$ and the partition wall load $0.5\,\mathrm{kN/m}^2$, giving a total load of:$2.25\,\mathrm{kN/m}^2$, The distributed load is then calculated as the half-width of the module $(1.5\,\mathrm{m})$ multiplied by this total equalling $(3.375\,\mathrm{kN/m})$For a roof module, the distributed load is split into two parts. The variable floor load and partition wall load act on the bottom beam, as in the normal floor module, contributing $3.375\,\mathrm{kN}$. Additionally, the roof load $1.0\,\mathrm{kN/m}^2$ acts on the top beam. This roof load is equal to $1.5\,\mathrm{kN/m}$.

Table 4.6 summarizes the vertical loads acting on the structure as represented in the *2D* model. It categorizes the load types, their sources, and the corresponding permanent and variable loads applied to the core and beams.

Table 4.6: Vertical loads represented in the *2D* model

Load Type	Description	Permanent Load (kN)	Variable Load
Green point load	From two columns of modules behind the core	38.43	29.25 (roof) 20.25 (floor)
Yellow point load	From one-fourth of the visible module	19.22	14.63 (roof) 10.13 (floor)
Blue line load	Variable loads on half a module applied to beams	*Excluded*	3.375 kN/m (bottom beam) 1.5 kN/m (top beam, roof only)

Wind load on the structure
As described in chapter 3.2.1 in order to determine the wind load on a structure the following equation can be used:

$$F_w = c_s c_d \cdot c_f \cdot q_p(z) \cdot A_{\text{ref}} \tag{4.4}$$

To calculate this force, the dimensions of the building must be determined. The structure's height in the current setup is 70 meters, with a rectangular floorplans measuring 21 by $18\,\text{m}$ and a flat roof. Depending on the wind direction, the effective dimension e is either 21 or $18\,\text{m}$, as both values are less than twice the building's height. For the analysed *2D* model the effective dimension is equal to $21\,\text{m}$ meter. It is assumed that the concept is located in reference area II in a urban area. The described building dimensions are visualised in figure 4.28. The calculations have been done according to the NEN-EN Euro-Code 1: General Actions: Wind Actions [43].
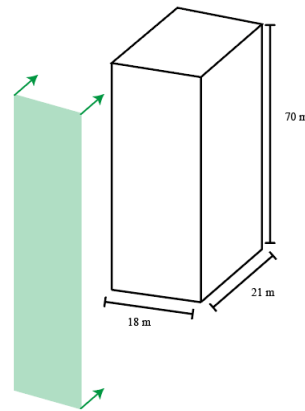
Figure 4.28: The considered wind load with the building dimensions

To calculate the wind force acting on the building the following parameters need to be calculated:

- The $c_s c_d$ factor represents the structural factor of the building. Since the height of the building is less than 4 times the in-wind depth, this factor may be taken as 1 [43].

- The velocity pressure of the wind, $q_p(z)$ on the building depends on the velocity pressure profile. For buildings where the height exceeds twice the width, the wind pressure is distributed into three distinct zones. The velocity pressure profile is shown in Figure 4.29. For the chosen 2D cross-section of the building. the first part of the velocity pressure (from height 0 to 21 meters) is $0.9\,\text{kN/m}^2$ (reference height of $20\,\text{m}$). For the strip section, the value is assumed to be $1.21\,\text{kN/m}^2$ (reference height of $50\,\text{m}$). This assumption represents an overestimation; further refinement can be achieved by dividing the profile into additional strips. Currently, the maximum value is used for simplicity. For the top section, the wind velocity pressure is $1.34\,\text{kN/m}^2$ (reference height of $70\,\text{m}$) *(values retrieved from Quick-reference)*.

- To calculate the forces on the façade of the building in this wind direction, the force coefficients c_f must be determined. Since the effective depth is smaller than the building's dimensions in the wind direction, the façade is divided into three distinct wind zones, as illustrated in Figure 4.30. The ratio of the building's height to its dimension in the wind direction exceeds is equal to 3.33. However, to take a conservative approach, a height-to-depth ratio of 1 is selected, and the corresponding force coefficient is used for the analysis. The corresponding force coefficients for this scenario are provided in Table 4.7.

- Since the cross-section of the building represents half of the structure, the reference area subjected to wind loads is halved. With the total building width being $18\,\text{m}$, the reference width for the wind load in the 2D model is $18/2 = 9\,\text{m}$
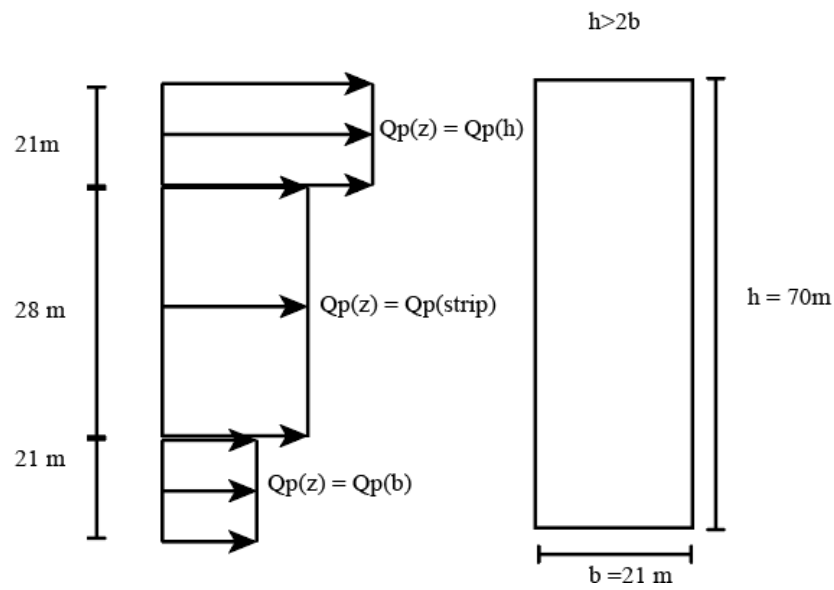
Figure 4.29: Wind velocity pressure profile of the building
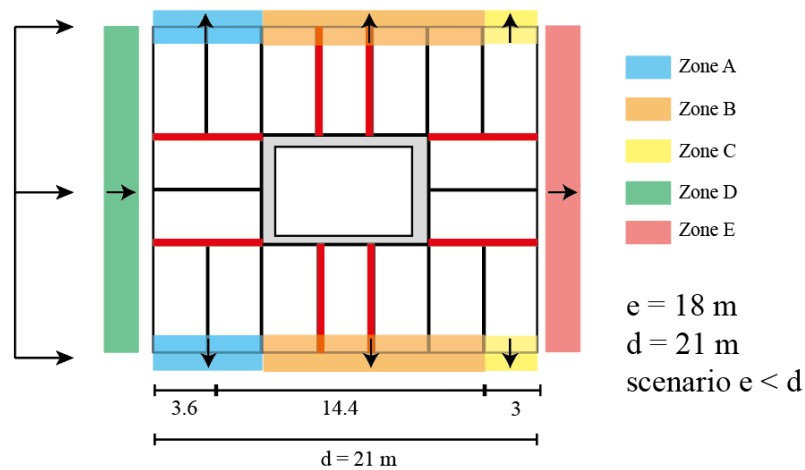
Figure 4.30: Wind zones on the facade

h/d ratio	Zone A	Zone B	Zone C	Zone D	Zone E
5	-1.2	-0.8	-0.5	+0.8	-0.3
1	-1.2	-0.8	-0.5	+0.8	-0.5

Table 4.7: c_f for different zones and height-to-depth ratios, *(retrieved from Euro-Code 1)*

Using the previously determined parameters, the wind loads on the *2D* structure can be calculated using the formulas presented in figure 4.31.
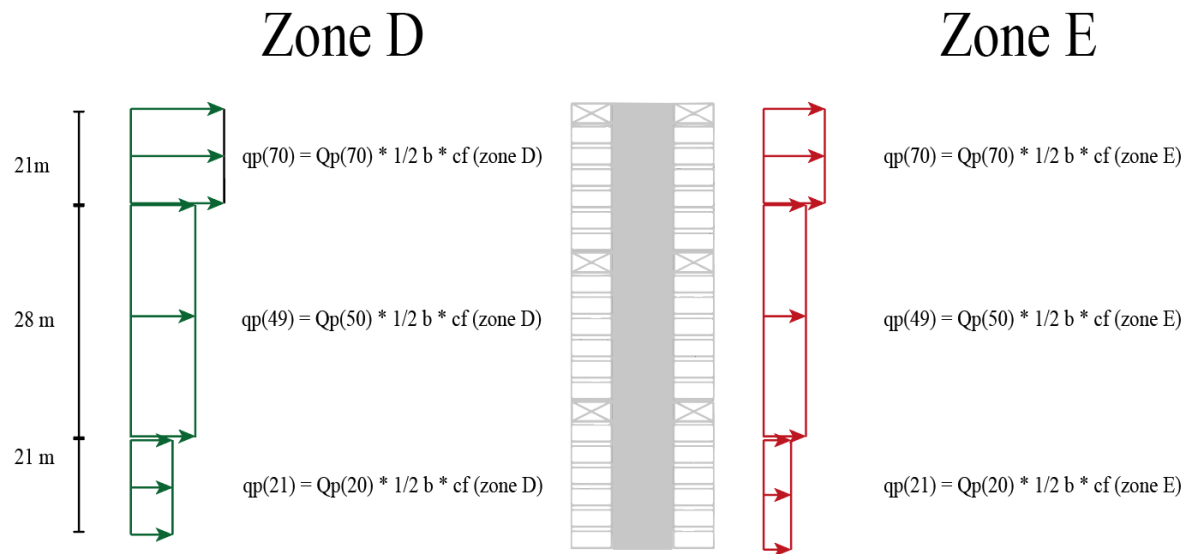
Figure 4.31: Direction and formulas of the wind load on the *2D* model

As mentioned in section 4.2, the calculated horizontal loads, which are applied to the beams of the modules as point loads to reflect the realistic transfer of façade forces to the structural system, are determined by multiplying the line load by the module height of 3 meters and then dividing by two. This accounts for the equal distribution of the load between the top and bottom beams of the module. The calculated loads can be seen in Table 4.8.

Table 4.8: Wind load calculations values

Zone	z (m)	$Q_p(z)$ (kN/m^2)	$1/2B$ (m)	C_f	q_p (kN/m)	Load on Beam (kN)
Zone D	49–70	1.34	9	0.8	9.648	14.5
	21–49	1.21	9	0.8	8.712	13.1
	0–21	0.90	9	0.8	6.48	9.7
Zone E	49–70	1.34	9	-0.5	-6.03	-9.1
	21–49	1.21	9	-0.5	-5.45	-8.2
	0–21	0.90	9	-0.5	-4.05	-6.1

4.4.2. Results

This section presents the analysis results from the *Grasshopper* models. For each aspect analyzed, a conclusion will be provided to highlight key points of interest and guide targeted improvements for the next iteration of the concept.

Normal Force

The first step in analysing the proposed concept involves examining the force distribution within the structure. This is done by evaluating the normal force lines. This assessments is crucial for understanding how forces are transferred throughout the structure and identifying critical load paths. Figure 4.32 illustrates the normal force distribution under lateral wind loading. For clarity and to provide a more focused visualization of the normal forces within the modular structure, the core has been removed from the figure.
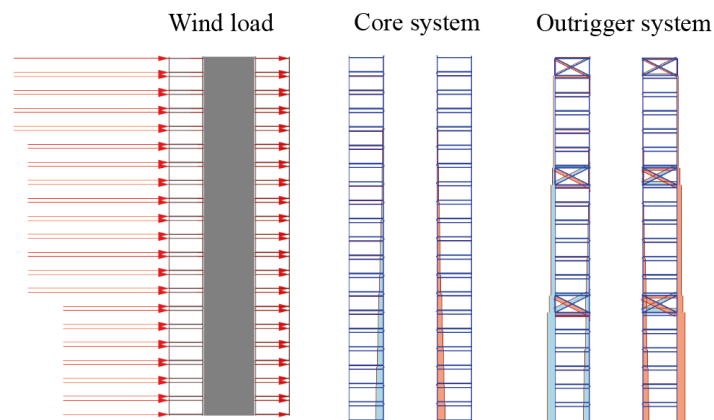
Figure 4.32: Normal force distribution under wind load

In the core-only system, the normal forces are low in the perimeter columns and significantly higher in the columns adjacent to the core. Tension is observed on the left side of the core, while compression is concentrated on the right side. This behaviour is expected, when subjected to lateral wind loading, the core undergoes bending, causing it to transfer forces to the adjacent columns. These columns, being directly connected to the core, experience the highest normal forces due to their proximity to the core. The lateral load creates tension in the columns on the windward side and compression in the columns on the leeward side, consistent with the deformation patterns caused by bending moments in the core. The perimeter columns, being farther from the core, contribute less to resisting lateral loads, resulting in lower normal forces in these columns.

The system with the outrigger exhibits a noticeably different force distribution. While tension remains in the module members on the left side of the core and compression on the right of the core, the inclusion of the outrigger introduces compression and tension forces in the perimeter columns as well. This behaviour aligns with expectations, as the outrigger system is designed to engage the perimeter columns more effectively, redistributing forces across the structure and enhancing overall lateral stability.

Figure 4.33 shows the normal force under the vertical load.
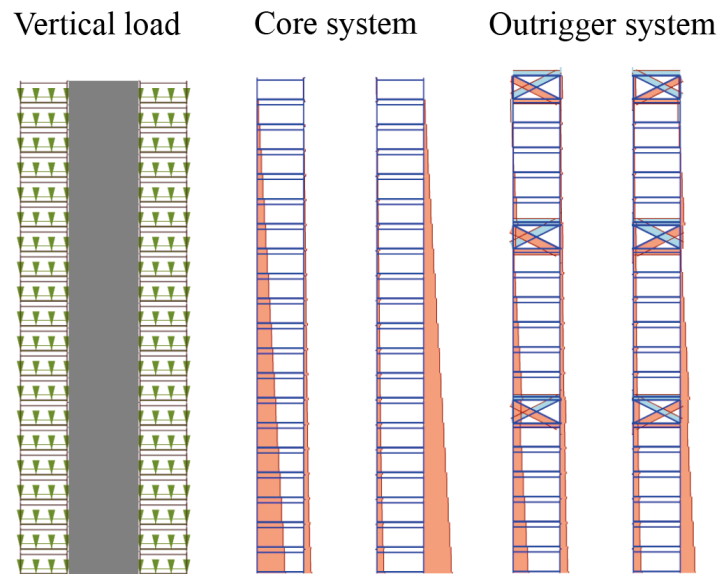
Figure 4.33: Normal force distribution under Vertical load

In the core system, it can be seen that the normal force in the perimeter columns is significantly higher than in the columns close to the core, as the core primarily absorbs this portion of the vertical load. When comparing the normal force distribution to the outrigger system, a similar pattern is observed, but the outriggers introduce a notable effect on the perimeter columns. In the outrigger system, the stiff horizontal members create an additional load path by coupling the perimeter columns to the core. This coupling allows part of the vertical load in the perimeter columns above the outrigger level to be redirected into the core through the stiff outrigger elements. As the outriggers act to stiffen the frame and transfer forces laterally, they reduce the vertical load directly passing through the perimeter columns above these levels. Consequently, the core absorbs a greater share of the vertical load redistributed from the perimeter columns.

Conclusion

The analysis of normal forces reveals that the inclusion of outriggers significantly affects the load distribution within the structure. The outrigger system redistributes vertical loads by engaging the perimeter columns and transferring part of their load into the core. This redistribution results in reduced normal forces in the perimeter columns above while increasing the forces absorbed by the core.

This redistribution is critical to the overall structural performance, as it creates increased stresses at the connections between the outriggers and the core, necessitating careful design to handle these forces.

An additional takeaway is that when the outrigger is connected to only one side of a module, an uneven force distribution develops within the modules. The forces in the members connected to the outrigger differ from those in the unconnected members, potentially introducing displacement differences and localized stress concentrations that could compromise the stability of the structure.

Displacement
The displacement analysis under the combined vertical and horizontal loads shows a significant differ-ence between the core-only system and the outrigger system. The deformation of the two systems can be seen in figure 4.34.
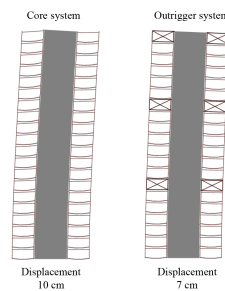
Figure 4.34: Displacement of the core and outrigger

In the core-only system, the maximum displacement is $10\,\mathrm{cm}$, indicating limited lateral stiffness and a concentration of deformations at the upper levels. In contrast, the outrigger system achieves a maximum displacement of $7\,\mathrm{cm}$, demonstrating improved structural performance. This reduction is attributed to the outriggers, which enhance stiffness by engaging the perimeter columns and redistributing forces more effectively.

Conclusion

The inclusion of outriggers reduces maximum displacement by $30\,\%$, highlighting their effectiveness in improving the system's lateral stability. Optimizing the stiffness and placement of the outriggers will be a key focus for the next iteration to further enhance structural performance.

Core analysis
The core was modelled as a *2D* shell element for both the core-only and outrigger stability systems. To explore the effects of reduced stiffness, the core was modelled with a stiffness lower than that of in-situ concrete, serving as a proof of concept to simulate the expected behaviour of a precast concrete core. A utilization plot of the core shell with a deformed geometry was generated to visualize the stress distribution within the shell element. In this plot, the blue areas indicate regions in tension, where the core is subjected to pulling forces and the red areas indicate regions in compression, where the core is under compressive forces.

The utilization plot in figure 4.35 highlights significant stress concentrations at the module-to-core con-nections in both systems. These concentrations are particularly pronounced in the outrigger system due to the stiff outriggers transferring large forces and moments into the core.
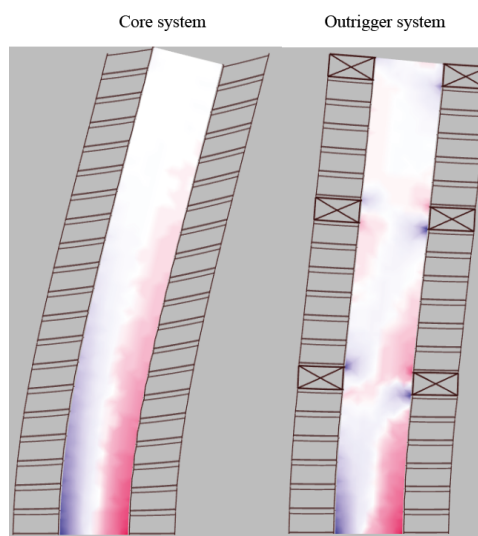
Figure 4.35: Utilization plot of the core

Conclusion

Currently, the core is modelled as a continuous shell element, which does not capture the segmental nature and structural behaviour of a precast core. This simplification provides useful insights but does not account for the stress distribution unique to a precast system. The analysis highlights significant stress concentrations at the outrigger-to-core connections. The results indicate that the connection between the outriggers and the precast core is likely to be a critical component of the system.

Varying Connection stiffness

To evaluate the effect of varying rotational stiffness on the overall stability of the system, the rotational spring stiffness at the module-to-core connection was modified and analysed. The maximum displacement of the structure was recorded as a performance criterion to assess the impact. Figure 4.36 visually illustrates the bandwidth of the connection stiffness that was analysed. It is important to note that these connections represent two connections on either side of the core. However, due to the 2D modelling approach, they are modelled as a single connection.
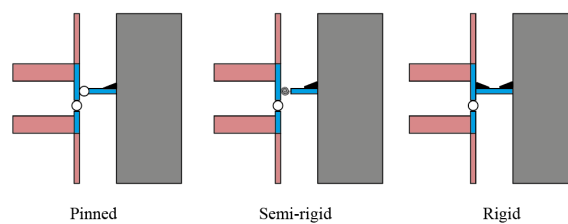
Figure 4.36: Bandwidth of the module to core connection

Figure 4.37 illustrates the relationship between the displacement of the structure and the rotational stiffness of the connections between the modules and the core. As the rotational stiffness increases, the maximum displacement of the structure decreases. The stiffness is plotted on a logarithmic scale in the figure, highlighting the exponential sensitivity of displacement to changes in stiffness at lower values and the diminishing effect at higher stiffness values.
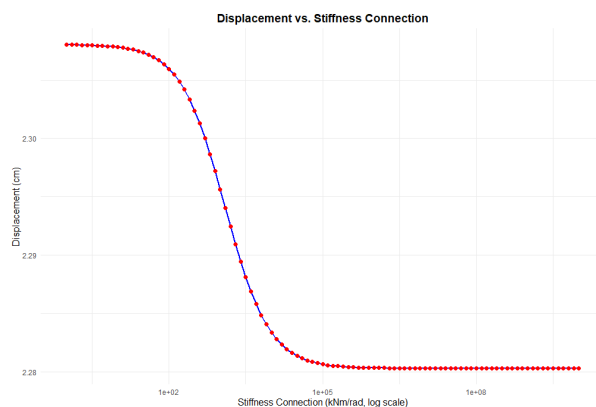
Figure 4.37: Displacement with varying rotational stiffness of the module to core connection

At low stiffness values, such as 100 kNm/rad to 1000 kNm/rad, the displacement decreases significantly, indicating that the structural performance is highly sensitive to changes in stiffness in this range. Even small increases in the rotational stiffness lead to noticeable improvements in stability. However, as the stiffness increases further, beyond approximately 10^5 kNm/rad, the displacement stabilizes and becomes almost constant. This indicates that, at higher stiffness values, the connection begins to behave nearly as a fully rigid joint, and further increases in stiffness have a negligible effect on the displacement.

Conclusion

These results demonstrate that the rotational stiffness of the module-to-core connection has a significant influence on the displacement of the structure, particularly at lower stiffness ranges. Beyond a certain threshold, around 10^5 kNm/rad, further increases in stiffness provide minimal benefits to stability.

4.4.3. Model Validation

This section applies the validation methods outlined in Section 4.1.3 to assess whether the *parametric* model exhibits the expected structural behaviour.

Frame Model Validation
Validation Set-Up

To validate the frame system's behaviour in the *Grasshopper* model, a *Matrix-Frame* model has been made. A specific configuration was selected, consisting of a stacked arrangement of four modules in width and three modules in height. Two types of loads are applied to both models: a horizontal Q-load of $10\,kN$ applied to the left side of the stacked modules, and a uniform dummy load of $7\,kN/m$ applied to the floor beams and $3\,kN/m$ applied to the roof beams to evaluate vertical load transfer. The comparison is conducted under two different connection conditions: rigid inter-modular connections (A) and pinned inter-modular connections (B). Figure 4.38 presents the setup of the *Grasshopper* and *Matrix-frame* models side by side, including the displacement patterns of both models to illustrate their structural response.
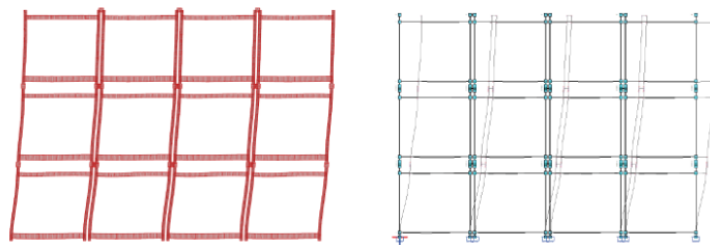
Figure 4.38: Frame Validation Set-up

Validation Results

Table 4.9 presents a comparison of the maximum force and displacement values between the *Matrix-Frame* and *Grasshopper* models. Appendix C presents a comparison between different modelling software used for structural analysis, supporting the validation of the results obtained from the later *Grasshopper* models. The corresponding *Matrix-Frame* force diagrams are provided in Appendix D.

Table 4.9: Comparison of frame system results

	Matrix-Frame **model**				*Grasshopper* **model**			
	N (kN)	V (kN)	M (kNm)	w (mm)	N (kN)	V (kN)	M (kNm)	w (mm)
A (Rigid)	-64.8	28.55	17.2	21.5	-63.78	25.47	17.25	22.678
B (Pinned)	-67.19	-29.83	19.05	24.3	-67.02	-26.58	19.03	25.35

Conclusion

The validation results confirm that the *Grasshopper* model effectively replicates the structural behaviour of modular frames under different connection conditions. Both the rigid and pinned connection scenarios show strong agreement between the *Grasshopper* model and the *Matrix-Frame* model, with only minor discrepancies. It is assumed that this due to differences in numerical computation methods. The normal force and moment diagrams align well in both models, while the shear force diagram exhibits slight computational differences. Additionally, the displacement results highlight the expected increase in deformation for the pinned connection scenario compared to the rigid frame. Despite the minor variations, the *Grasshopper* model accurately captures the key structural responses, confirming its reliability for further structural analysis and optimization.

Core Model Validation
Validation Set-up

To validate the behavior of the core, *analytical* calculations are performed to assess its response in the *Grasshopper* model. The validation focuses on evaluating the flexural behavior of the core and ensuring that the *parametric* model aligns with theoretical predictions. Figure 4.39 illustrates the validation setup, with the *analytical* model shown on the left and the *parametric* core model in *Grasshopper* displayed on the right.
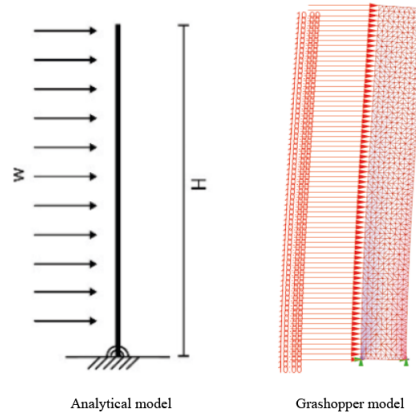
Figure 4.39: Validation set-up of the core

Table 4.10 summarizes the input variables for both methods.

Table 4.10: Input Variables for *Analytical* and *Grasshopper* Models

Parameter	*Analytical* Method	*Grasshopper* Model
Applied Lateral Load (Q)	10 kN/m	10 kN/m
Core Height (H)	70 m	70 m
Core Width (B)	-	9 m
Shell Thickness (t)	-	0.3 m
Modulus of Elasticity (E)	19975×10^3 kN/m^2	53595.47×10^3 kN/m^2
Second Moment of Area (I_{yy})	48.9 m^4	18.225 m^4
Flexural Stiffness (EI_{yy})	976777500 kNm^2	976777500 kNm^2

Since the *Grasshopper* model in *Karamba3D* inherently relies on different modelling assumptions, a direct match of I_{yy} between the *Grasshopper* and Analytical calculation was not feasible while maintaining the correct structural representation. To achieve consistency in flexural stiffness (EI_{yy}), the modulus of elasticity (E) for the *Grasshopper* model has been adjusted to $53595.47 \ kN/m^2$. This ensures that the behaviour of the core in the *parametric* model remains comparable to the *analytical* solution.

Validation Results

The lateral displacement at the top of the core is determined using both the analytical method and the *Grasshopper* model. The *analytical* method yields a displacement of $W_y = 0.031 \ m$, while the *Grasshopper* model produces a displacement of $W_y = 0.036 \ m$.

Conclusion

The validation results demonstrate that the *Grasshopper* model accurately captures the structural behaviour of the core. The minor deviation between *analytical* and computational results falls within an acceptable range, confirming the model's reliability. This ensures that the *parametric* approach can be used confidently in further structural optimization and refinement.

Outrigger Validation
Validation Set-up

The objective is to assess the effectiveness of the outriggers in enhancing structural stiffness and reducing lateral displacements. The analytical calculations serve as a benchmark to validate the results obtained from the *Grasshopper* model, ensuring its accuracy and realistic behaviour. The analytical validation follows the methodology presented in section 4.1.3. The setup of this calculation is illustrated in Figure 4.40.
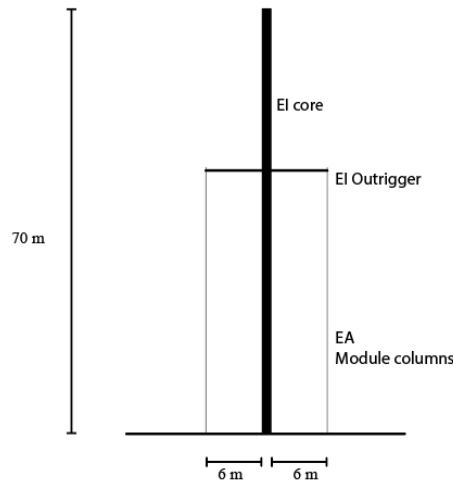
Figure 4.40: Simplified outrigger calculation set-up

The flexural rigidity of the structure, incorporating the contribution of the outrigger system, is determined using the following formulation:

$$I_{\text{outrigger}} = c \cdot n \cdot 2 \cdot z^2 \cdot A \tag{4.5}$$

where:

- c = 0.6 (reduction factor for outrigger efficiency)
- n = 1 (number of columns per façade)
- $z = 10.5\ m$ (distance from the centre of the core to the centre of the column)
- A = 0.004293 m^2 (cross-sectional area of the column)

The calculated moment of inertia for the outrigger is $I_{\text{outrigger}} = 0.56796\ m^4$. The modulus of elasticity of steel is taken as $E_{\text{steel}} = 210000\ N/mm^2$. The resulting flexural rigidity contribution from the outrigger system is:

$$EI_{\text{outrigger}} = 119272419\,\text{kNm}^2 \tag{4.6}$$

The combined flexural rigidity of the structure, incorporating both the core and the outrigger contribution, is used to compute the lateral displacements under the applied loads.

Validation Results

The displacement results obtained from the analytical method are presented in Table 4.11, and the displacement results from the *Grasshopper* model (with only 1 outrigger) are summarized in Table 4.12.

Table 4.11: *Analytical* Approach - Displacement Results

Condition	δ_{yy} (m)	δ_{xx} (m)
Without Outrigger	0.0307	0.0580
With Outrigger	0.0274	0.0471
Improvement Percentage	11 %	19 %

Table 4.12: *Grasshopper* model - Displacement Results

Condition	δ_{yy} (m)
Core Only	0.01253
With Outrigger	0.01129
Improvement Percentage	10 %

Conclusion

The validation results indicate that the addition of an outrigger leads to a reduction in lateral displacements. The *analytical* approach predicts improvements of 11% in the yy-direction and 19% in the xx-direction, whereas the *Grasshopper* model shows a 10% reduction in the yy-direction. These results suggest that the *analytical* method provides a reasonable approximation of the structural behaviour when compared with *Grasshopper* simulations. The slight differences between the *analytical* and *Grasshopper* results remain within an acceptable margin, validating the model's accuracy.

4.5. Conclusion

This chapter presented the conceptual development of a structural system for a modular mid-rise building. The primary focus was on establishing a stable and efficient modular mid-rise building through a core-outrigger hybrid system.

The concept was developed starting with the floor plan and a *3D* structural overview, followed by a transition to a simplified *2D* model for *analytical* and *parametric* analysis. The *2D* representation facilitated a clearer understanding of load paths and structural behaviours while allowing for computational efficiency in evaluating different configurations.

Key findings from the analysis indicate that:

- The core-alone system experiences significant lateral displacement under wind loading, demonstrating the need for additional lateral stability measures.
- The inclusion of outriggers reduced the lateral displacement by approximately $30\,\%$.
- The module-to-core connection stiffness impacts the structural behaviour, particularly in displacement reduction.
- The stress distribution analysis highlighted significant force concentrations at outrigger-to-core connections, emphasizing the necessity of careful connection design and detailing to prevent local failures.
- The validation of the *parametric* model using *analytical* approaches and *Matrix-Frame* models confirmed its reliability.

While the initial concept demonstrates promising results, several aspects require further optimization. The effectiveness of the outrigger system can be improved by refining the number and vertical placement of the outriggers. Additionally, the core should be modelled more realistically as a segmented precast element with openings to capture its true structural behaviour.

5

Detailed Structural Analysis and Optimizing Concept

To ensure the feasibility and performance of the proposed modular concept, a detailed structural analysis is required. This chapter focuses on refining and optimizing the structural system.

The analysis begins with the refinement of the *Grasshopper* model, enhancing its accuracy through adjustments to material properties and load assumptions. Subsequently, *parametric* simulations are conducted to evaluate the influence of different design configurations, including the placement and number of outriggers. The final stage of this chapter focuses on optimizing the structural configuration, ensuring a balance between material efficiency, stability, and overall structural performance.

5.1. Refinements in Modelling

To improve the accuracy and reliability of the structural analysis, several refinements have been introduced in the modelling process. These adjustments focus on enhancing the representation of critical structural components. The refinements include the incorporation of core modifications, improved load calculations, and the determination of the governing load combinations.

5.1.1. Core Refinement

As previously discussed, the core was initially modelled as a monolithic slab without openings for doors and without accounting for the modulus of elasticity of cracked concrete, leading to an overestimation of its stiffness. This section refines the core model by incorporating these elements, ensuring a more accurate and realistic structural analysis.

Modulus of Elasticity for Cracked Concrete

To improve the accuracy of the structural behaviour representation in the *Grasshopper* model, the modulus of elasticity (E) of the core shell is adjusted to account for the effects of cracking in precast concrete. Since *Karamba3D* operates under the *linear elasticity* (LE) theory, it assumes that concrete remains elastic. However, this simplification does not accurately represent the behaviour of concrete in reality, where tensile stresses lead to cracking, significantly reducing the stiffness of the concrete element.

To address this limitation and align the model with *engineering best practices*, a reduced modulus of elasticity is introduced to account for the loss of stiffness due to cracking. Values from literature can be used to determine the modulus of elasticity of cracked concrete [54]. Table 5.1 presents these values for different concrete strength classes.

Table 5.1: Modulus of elasticity for cracked and uncracked concrete [54]

Concrete Strength Class	$E_{cd,\text{cracked}}$ (N/mm^2)	$E_{cd,\text{uncracked}}$ (N/mm^2)
C20/25	9987	19975
C25/33	10492	20984
C30/37	10946	21891
C35/45	11359	22718
C40/50	11740	23480
C45/55	12094	24189
C50/60	12426	24852
C55/67	12738	25476
C60/75	13033	26067
C70/85	13581	27162
C80/95	14081	28163
C90/105	14544	29087

The values presented in Table 5.1 are utilized in the analysis to assess the impact of different concrete strength classes on the structural performance of the proposed concept. Since the cracked E-modulus of concrete is not a standard parameter in *Grasshopper*, these values have been imported into the model. These imported values have been applied to the core elements via the *Material Properties* component, as illustrated in Figure 5.1.
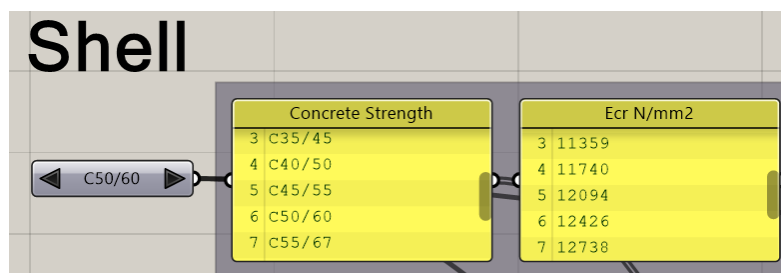
Figure 5.1: Refinement of *modulus of elasticity*

Openings in the Core

To incorporate openings in the core, the moment of inertia must be recalculated while considering the impact of these openings on the flexural stiffness of the core. Figure 5.2 illustrates the distribution of the openings within the core.
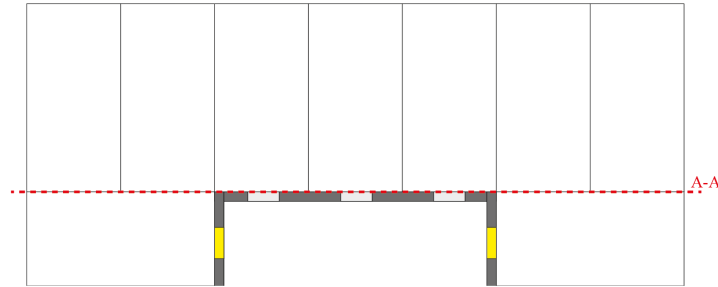
Figure 5.2: Floor plan of the building highlighting core openings

As shown in the figure, a distinction can be made between different types of openings. The openings located on the *A-A* cross-section, which corresponds to the cross-section used for the *2D* model, can be directly incorporated into the model, allowing their effect on flexural stiffness to be accurately considered. However, the openings highlighted in yellow, which are not visible in the *A-A* cross-section, cannot be directly included in the *2D* model.

Figure 5.3 illustrates the process of translating the core flanges from a *3D* representation to a *2D* model while incorporating the effects of the openings in these flanges. The door openings are assumed to have a width of $1.0\,\text{m}$.
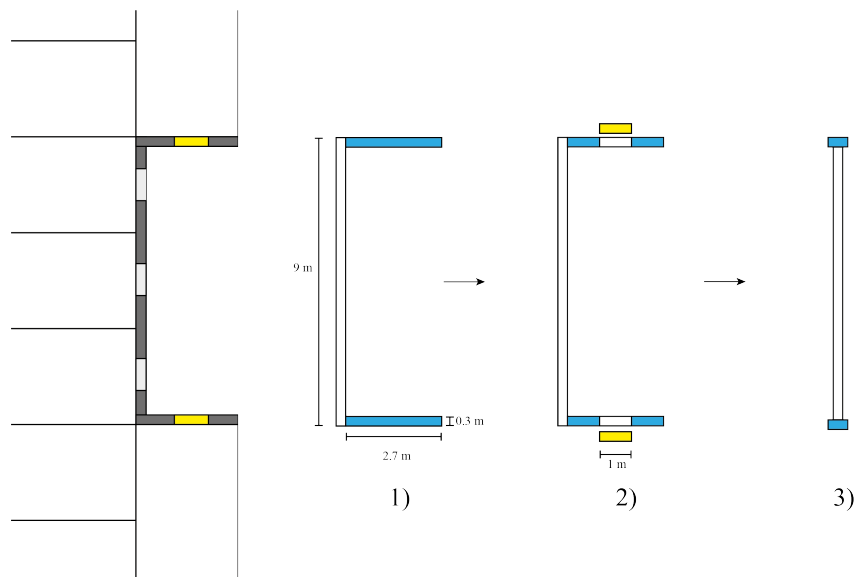
Figure 5.3: Translation of Core Flanges (including openings) to 2D

On the left side of the figure, the floor plan is displayed, including the core and modular units. The yellow-highlighted rectangles indicate the openings in the core flange, which must be accurately accounted for in the *2D* model since they are not directly visible in the *2D* cross-section. The process of incorporating these openings consists of three main steps: calculating the second moment of inertia of the core flanges, determining the reduction in moment of inertia due to the door openings, and finally, adjusting the core thickness in the model to accurately represent the contribution of the core flanges while excluding the openings.

Step 1:

The first step involves calculating the second moment of inertia I_{yy} of the core flanges. These flanges, highlighted in blue in Figure 5.3, must be considered separately as they do not share the same neutral axis as the entire cross-section. Therefore, the *parallel axis theorem (Steiner's rule)* is applied:

$$I' = I + Ad^2, \tag{5.1}$$

The dimensions of each blue rectangular flange are: Width: $2.7\ m$ and Height: $0.3\ m$. The second moment of inertia of a single flange is calculated as $I_{yy} = 0.00608\ m^4$. Additionally, the area of each flange is $A = 0.81\ m^2$. The distance from the neutral axis to the centroid of each flange is $4.35\ m$. Applying Steiner's rule shows that the contribution of one flange to the total second moment of inertia is $15.33\ m^4$. Since there are two flanges symmetrically positioned on either side of the neutral axis, their total contribution is $30.66\ m^4$.

Step 2:

The second step accounts for the reduction in moment of inertia caused by the door openings. Given the door dimensions ($1.0\ m$ width), the moment of inertia of a single opening is 0.00225 m^4. Using Steiner's rule, the reduction in moment of inertia due to each door opening is calculated as $5.679\ m^4$. With one door opening per flange, the total reduction in I_{yy} is $11.358\ m^4$.

Step 3:

The final step involves adjusting the core thickness in the model to accurately account for the contribution of the core flanges, excluding the openings. The net contribution of a single flange to I_{yy} is determined to be $0.00383\ m^4$. Given a predefined segment length of $0.3\ m$, the necessary width of the additional section is calculated as $1.70\ m$. To ensure the correct representation of the structural behaviour, the existing core thickness of $0.3\ m$ must be added, resulting in a total required thickness of $2.0\ m$ over a $0.3\ m$ length on both sides of the core.

Figure 5.4 shows the original simple core on the left and the redefined core model on the right. From the figure, the local thickness increase to $2.0\ m$ for a segment of $0.3\ m$ on each side of the core is clearly visible. The remaining sections of the core retain their original thickness of $0.3\ m$. Additionally, the openings that are visible in *2D* cross-section are added. The mesh size is chosen to be equal to $0.3\ m$. The reason behind this mesh size is explain in Appendix F, where a mesh sensitivity study is done.

a) Original Core   b) Redefined Core
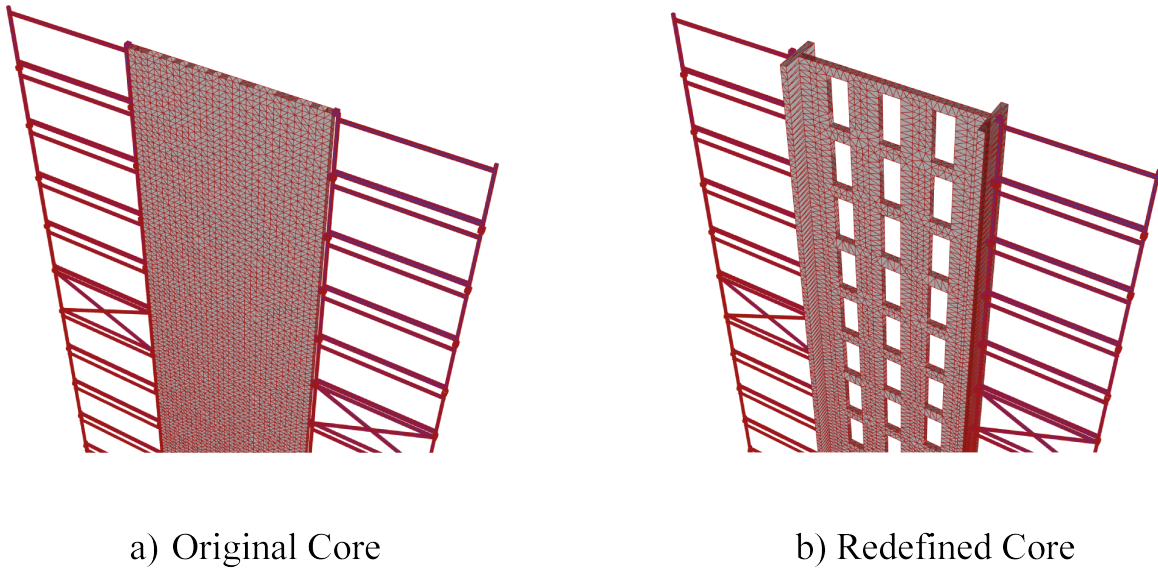
Figure 5.4: Original simplified core (left) and redefined core (right)

5.1.2. Load Calculations Refinement

Governing Load Combination

The following governing load combinations are used for the detailed analysis:

$$L_{01} = 1.2 \cdot G_{k/sup} + 1.5 \cdot F_w + 1.5 \cdot \psi_0 \cdot Q_{K1} \tag{5.2}$$

$$L_{02} = 0.9 \cdot G_{k/inf} + 1.5 \cdot F_w + 0 \tag{5.3}$$

It is expected that the maximum compression forces in the structural elements will result from the first equation, as it considers the amplified permanent and imposed loads in combination with wind forces. In contrast, the second equation is expected to govern the maximum tension forces in the structure due to the reduced permanent load factor and the elimination of the other variable loads. The results from this load case will be used to assess the maximum tensile forces in the tie-rod connections, ensuring that the connections can effectively transfer these forces without exceeding their design capacity.

Additional Self-Weight load

In addition to the self-weight loads of the modules presented in Table 4.4, additional self-weight must be incorporated into the model. The current model only accounts for the self-weight of the visible structural members. Since it is a *2D* representation, the floor, ceiling, and half of the short-side module portal are not directly visible but must still be included, as their loads are transferred to the visible module within the model. Figure 5.5 shows the location of the added forces that represent the additional self-weight loads.
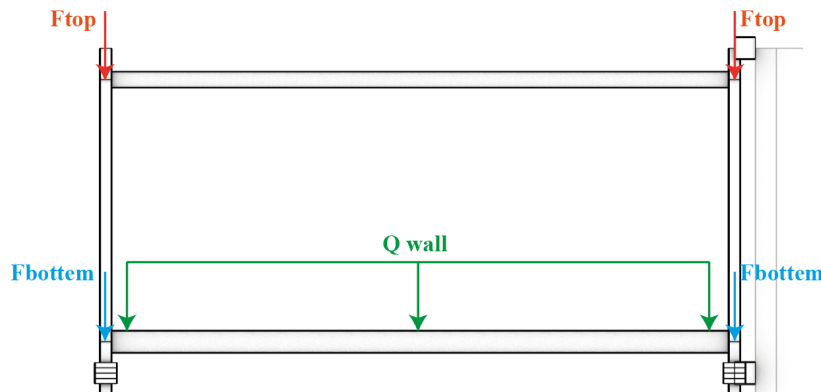
Figure 5.5: Additional self-weight loads on the modules

The point load F_{top} is calculated as one-fourth of the self-weight of the roof and half of the self-weight of the top beam on the short side of the module. Similarly, the point load F_{bottom} is determined as one-fourth of the self-weight of the floor, half of the load of the wall in the short direction of the module, and half of the self-weight of the bottom beam. Additionally, the distributed load Q_{wall} corresponds to the self-weight of the wall along the long side of the module.

Table 5.2 presents the values of these additional loads.

Load Symbol	Value	Unit
F_{top}	3.83	kN
F_{bottom}	10.51	kN
Q_{wall}	1.50	kN/m

Table 5.2: Additional self-weight loads

Overview of the applied Loads

This section provides an overview of the applied loads, categorized into permanent loads, variable loads, and wind loads. It is important to note that the presented values do not include any safety factors or combination factors; they represent solely the calculated values of the applied loads.

Overview of the permanent loads
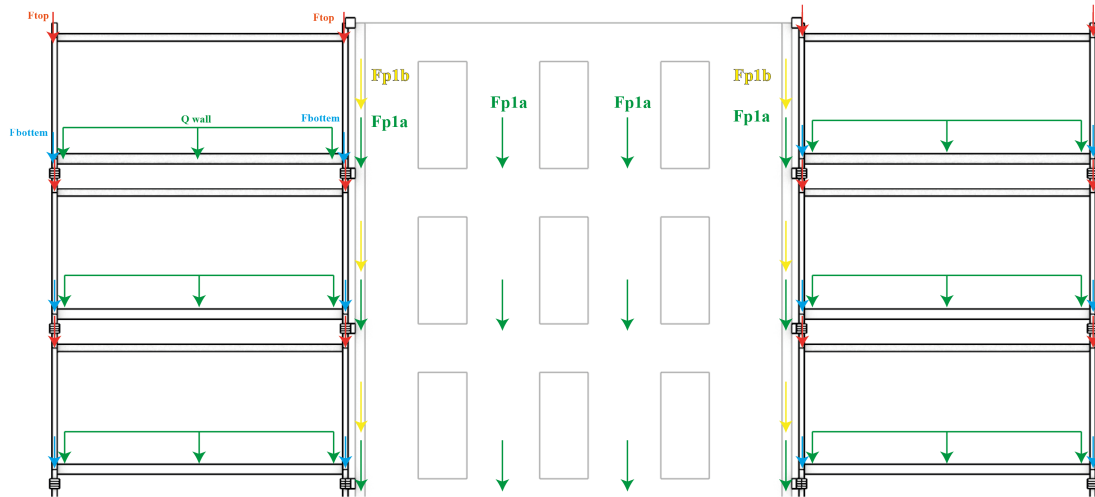
Figure 5.6: Overview of all the permanent loads

Load Symbol	Value	Unit
F_{top}	3.83	kN
F_{bottom}	10.51	kN
Q_{wall}	1.50	kN/m
F_{p1a}	38.43	kN
F_{p1b}	19.215	kN

Table 5.3: Overview of permanent load forces

Overview of the variable loads
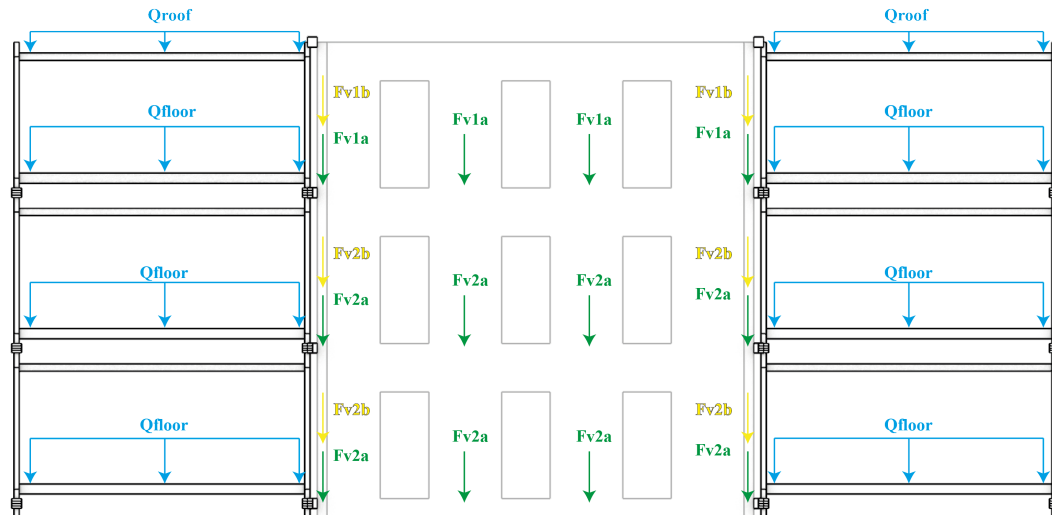
Figure 5.7: Overview of all the variable loads

Load Symbol	Value	Unit
Q_{roof}	1.5	kN/m
Q_{floor}	3.75	kN/m
F_{v1a}	29.25	kN
F_{v1b}	14.63	kN
F_{v2a}	20.25	kN
F_{v2b}	10.13	kN

Table 5.4: Overview of variable load forces

Overview wind load
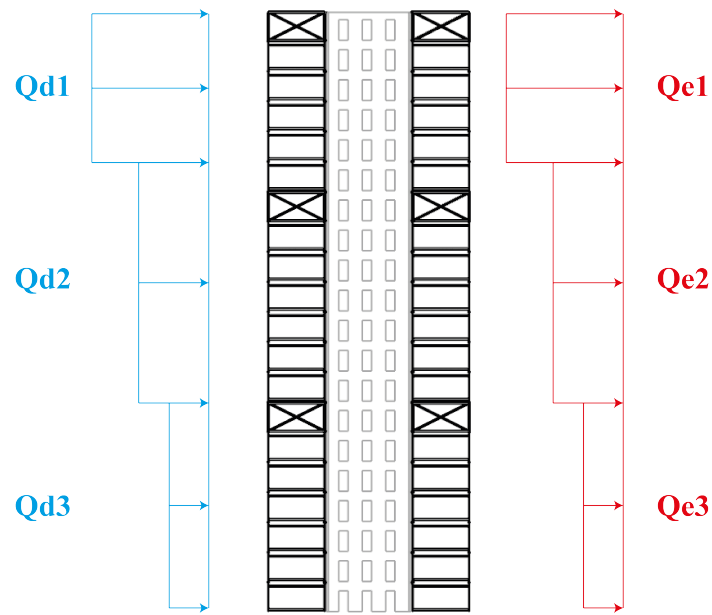
Figure 5.8: Overview windload

Table 5.5: Wind load calculations values

Load symbol	z (m)	$Q_p(z)$ (kN/m^2)	$1/2B$ (m)	C_f	q_p (kN/m)	Load on Beam (kN)
Qd1	49–70	1.34	9	0.8	9.648	14.5
Qd2	21–49	1.21	9	0.8	8.712	13.1
Qd3	0–21	0.90	9	0.8	6.48	9.7
Qe1	49–70	1.34	9	-0.5	-6.03	-9.1
Qe2	21–49	1.21	9	-0.5	-5.45	-8.2
Qe3	0–21	0.90	9	-0.5	-4.05	- 6.1

5.2. Performance Criteria

To ensure the structural feasibility of the proposed concept and its various configurations, key performance criteria must be determined. These criteria will provide a clear and objective framework for a fair comparison between different design iterations. The following subsections outline the performance criteria employed in this research.

5.2.1. Lateral Deflection Criteria

Lateral deflection limits are essential in ensuring the serviceability and structural integrity of mid-rise buildings. *Structural Calculations of High Rise Structures* by Ham and Terwel (2017) [50], suggest that the maximum allowable lateral displacement at the top of the structure should be:

$$\delta_{\text{max}} \leq \frac{H}{500} \tag{5.4}$$

where:

- H = total building height (m)
- δ_{max} = maximum lateral displacement (m)

However, if the foundation is excluded from the structural model, the overall stiffness of the system increases artificially, leading to an overestimation of lateral stability. To account for this modelling assumption, a stricter deflection criterion is recommended:

$$\delta_{\text{max}} \leq \frac{H}{750} \tag{5.5}$$

5.2.2. Maximum Tension Capacity of Tie-rod

The maximum allowable tension in the tie-rod is an important limitation of the proposed concept, serving as a key performance criterion in evaluating its structural feasibility.

To determine the maximum tensile force that a tie-rod connection can withstand, the following calculation method is applied. As an example, an M22 threaded rod made of 8.8-grade steel is used. The core cross-sectional area of the threaded rod governs its tensile strength. Although the nominal diameter of the rod is 22 mm, the effective cross-section at the root of the thread is reduced. Based on standard threading specifications, the core diameter is determined to be 19.2 mm, resulting in a cross-sectional area of $A_s = 289.53$ mm^2.

The nominal ultimate tensile strength (f_u) for 8.8-grade steel is given as $f_u = 800$ N/mm^2, while the yield strength (f_y) is calculated as $f_y = 640$ N/mm^2. Using these values, the maximum tensile force that the tie-rod can withstand before ultimate failure is calculated as $F_u = A_s \cdot f_u = 289.53 \times 800 = 231.62$ kN. Similarly, the force at yield is determined as $F_y = A_s \cdot f_y = 289.53 \times 640 = 185.30$ kN.

The same methodology is applied to other tie-rod diameters. The results are summarised in Table 5.6, where additional diameters are added for comparison.

Table 5.6: Tensile strength of tie-rods

M	d_s (mm)	A_s (mm^2)	F_u (kN)	F_y (kN)
20	17.3	234.79	187.83	150.27
22	19.2	289.53	231.62	185.30
24	20.7	336.56	269.23	215.38
27	23.8	443.01	354.41	283.53

In appendix G various dimensions of the tie-rods can be found, which are used for the previously described calculation.

5.2.3. Utilisation of the Structural Members

To ensure efficient material use and structural safety, the utilization factor (η) of each structural member is evaluated. It is defined as:

$$\eta = \frac{S_{Ed}}{S_{Rd}} \tag{5.6}$$

where:

- S_{Ed} = applied design effect (e.g., axial force, shear force, bending moment) (kN, kNm)
- S_{Rd} = corresponding design resistance of the member (kN, kNm)

A utilization ratio below 1.0 ensures that no structural component exceeds its capacity.

The *Karamba3D Utilization* component is used to assess the performance of beams and shells in the model. For beams, it evaluates utilization based on axial forces, shear forces, bending moments, and torsion. For shells, utilization is determined based on comparative stress criteria such as *Von Mises* and *Rankine*. The results provide insight into critical load cases and overstressed regions, guiding design refinements. figure 5.9 presets the *Grasshopper Utilization* component.
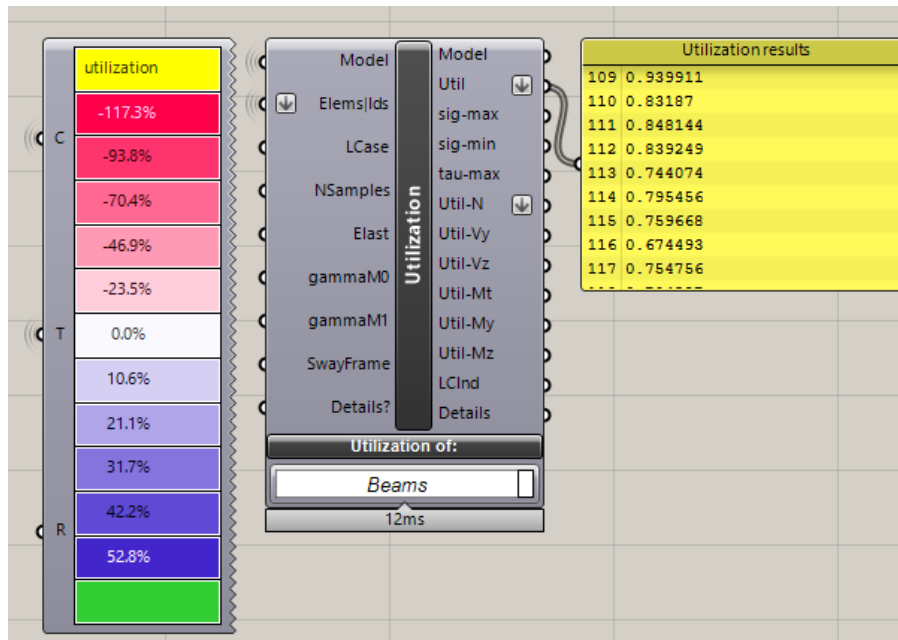
Figure 5.9: *Grashopper Utilization* component

The evaluation is applied to key structural elements, including core walls, outrigger diagonals and beams, as well as the beams and columns of the modules, ensuring an optimized and code-compliant structural design.

A detailed explanation of the theoretical background, and a validaton example of the *Karamba3D utilisation* component can be found in Appendix K.

5.3. Detailed Structural Analysis of the Concept

This section analyses the proposed concept and compares it to a core-only system. In this analysis, the original outrigger placement is set at floors 6, 13, and 22. The height of the structures are increased with two floors in order to reach the desired height of 70 meters (total 22 floors). The modulus of elasticity (E) of the core slab is chosen as Cracked C50/60, with a value of 1242.6 kN/cm². Figure 5.10a illustrates both systems along with their respective configurations.

The performance criteria described in Section 5.2 include lateral deflection, the utilization of structural members, and the maximum allowable tension force in the tie-rod connections will be used to compare the two systems. To determine the maximum forces present in the structure, the normal force values must be extracted from the *Grasshopper* model. To maintain a structured and clear analysis, the columns are divided into four groups: two groups on the left side of the core and two groups on the right side of the core. This division can be seen in figure 5.10b.

Core System   Outrigger System

(a) Core and Outrigger system at 70m

Group 1
Group 2
Group 3
Group 4
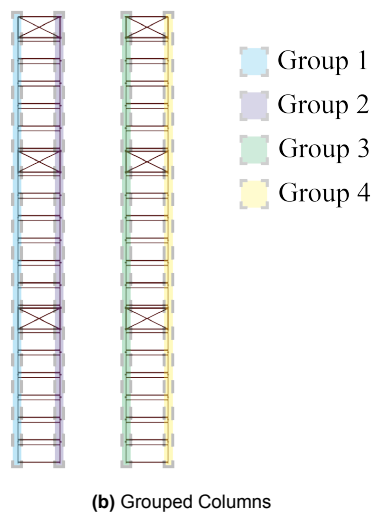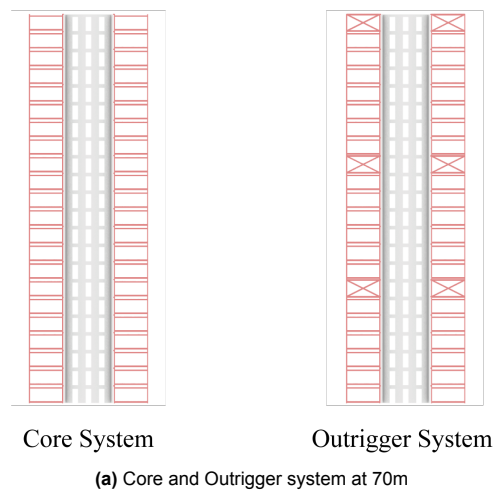
(b) Grouped Columns

Figure 5.10: Advanced analysis set-up

In the following section, the normal forces in the columns will first be analysed for the core-only system and the original outrigger configuration, using the previously defined grouped division. This analysis aims to identify the maximum force present in the structure.

Subsequently, the utilization of all structural members will be calculated to compare the structural performance of the components in both the core and outrigger system.

Finally, the lateral deflection of both systems will be evaluated and compared against the previously established lateral deflection limit.

5.3.1. Maximum Column Forces

This section presents the maximum tension and compression forces in the structural system. The governing load combinations largely determine these forces, with the L_{01} load combination expected to produce the maximum compression and the L_{02} load combination governing the maximum tension. To avoid excessive visualization, only the force distribution for the L_{01} load combination is plotted, while the maximum tension forces from the L_{02} load combination are analyzed at the end of this subsection to assess tie-rod connection capacity.

Core system

Figure 5.11 illustrates the normal force distribution in the four predefined column groups of the core-only system. Enlarged versions of the figures are included in Appendix E.

(a) Normal force group 1

(b) Normal force group 2

(c) Normal force group 3

(d) Normal force group 4

(e) Group division of the core system
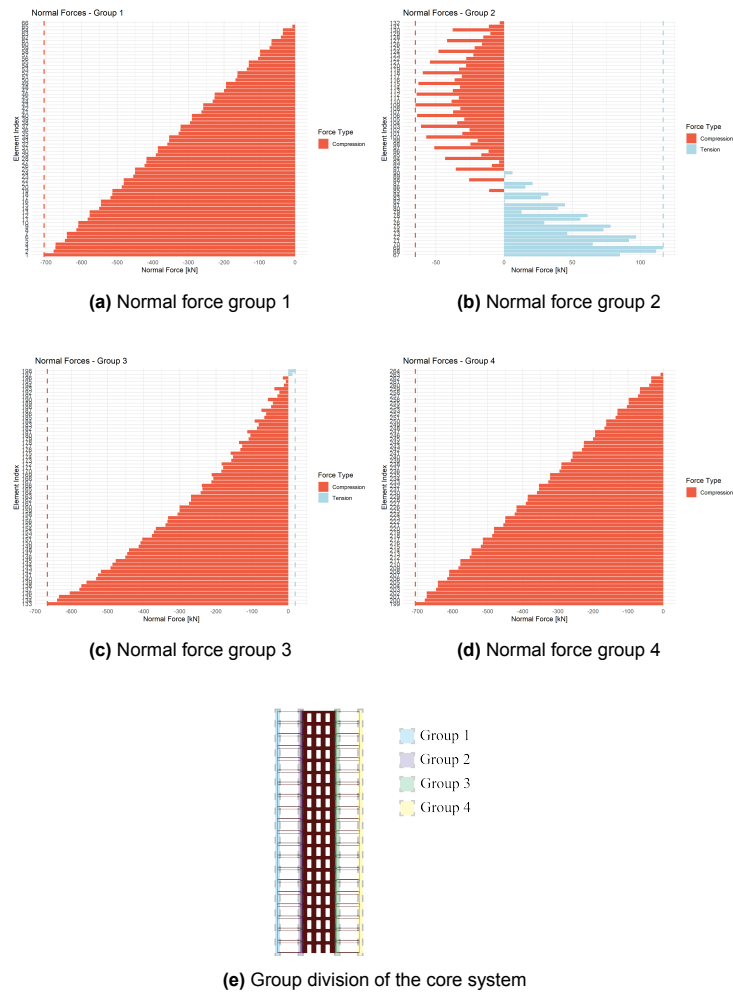
Figure 5.11: Normal force distribution for all four groups in the core system (L_{01} load combination)

Table 5.7 presents the maximum tension and compression forces observed in each group. The table includes the element index where the maximum values occur, allowing for a detailed assessment of the most critical structural members.

Table 5.7: Index and value of maximum tension and compression elements per group of the core system (L_{01} load combination)

Group	Max Ten. Index	Max Ten. Value [kN]	Max Comp. Index	Max Comp. Value [kN]
1	-	-	1	-705.33
2	69	116.78	109	-64.94
3	198	19.43	133	-666.31
4	-	-	199	-705.33

Original Outrigger Configuration

Figure 5.12 illustrates the normal force distribution in the four predefined column groups of the original outrigger configuration, where outriggers are positioned on floors 6, 13, and 19. Enlarged versions of the figures are included in Appendix E.

(a) Normal force group 1

(b) Normal force group 2

(c) Normal force group 3

(d) Normal force group 4

(e) Group division of the core system
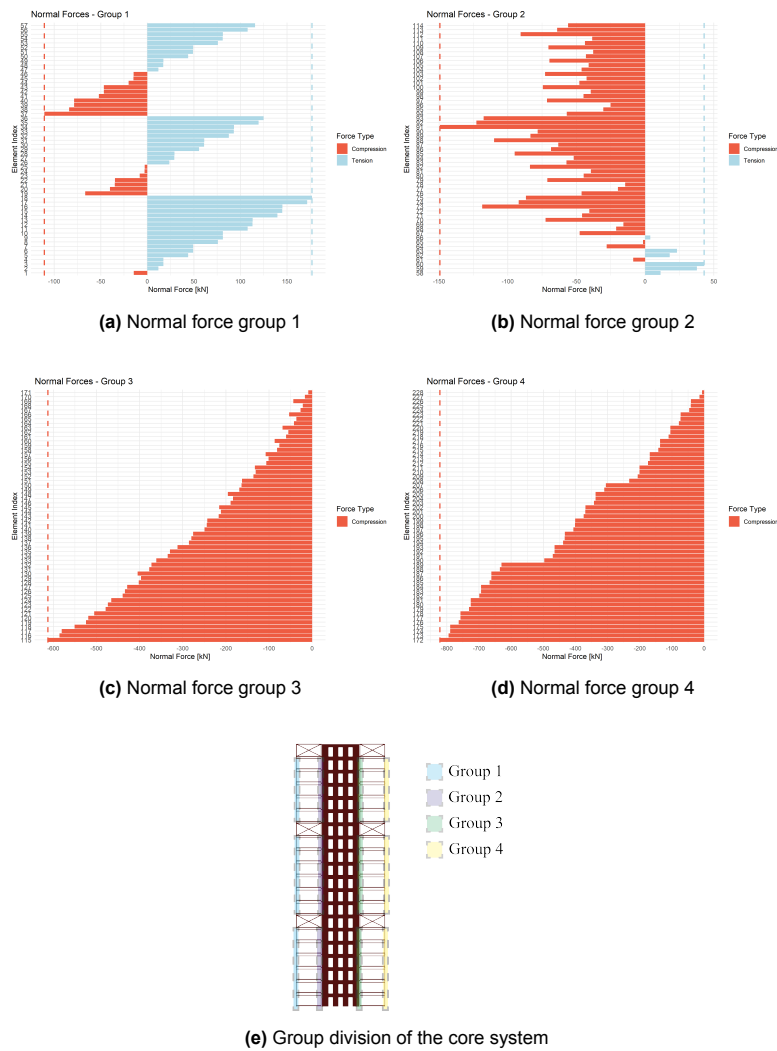
Figure 5.12: Normal force distribution for all four groups original outrigger configuration (L_{01} load combination)

Table 5.8 presents the maximum tension and compression forces observed in each group in the original outrigger configuration.

Table 5.8: Index and value of maximum tension and compression elements per group (L_{01} load combination)

Group	Max Ten. Index	Max Ten. Value [kN]	Max Comp. Index	Max Comp. Value [kN]
1	18	176.89	37	-110.5
2	60	43.05	91	-149.36
3	-	-	115	-612.33
4	-	-	172	-821.46

Conclusion

A comparison of the normal force distributions between the core-only system and the original outrigger configuration reveals a significant shift in load transfer behaviour. The incorporation of outriggers leads to a redistribution of axial forces across the structural system, altering both the location and magnitude of critical tension and compression forces.

In the core-only system, the highest compression force is recorded in groups 1 and 4, both reaching a value of $-705.33\,\text{kN}$. These extreme values occur in columns positioned near the base of the structure, where gravitational and lateral effects accumulate. The maximum tensile force in this configuration is considerably lower, with a peak value of $116.78\,\text{kN}$ occurring in group 2, which contains columns positioned adjacent to the core.

In contrast, the original outrigger configuration demonstrates a distinct redistribution of internal forces. The maximum compression force increases slightly to $-821.46\,\text{kN}$ in group 4, indicating an increase of axial compression forces in columns situated toward the perimeter and below the outrigger floors. This change can be attributed to the introduction of outriggers, which redirect axial loads through the perimeter columns. Meanwhile, the highest tension force is observed in group 1, reaching a value of $176.89\,\text{kN}$, which represents an increase relative to the core-only system and reflects the enhanced engagement of perimeter columns.

Overall, the data confirms that the outrigger system effectively alters the axial load path by engaging both core-adjacent and perimeter structural elements. While this improves the distribution of normal forces throughout the building, it also introduces new zones of concentrated stress, particularly in the lower perimeter columns. These findings underscore the need for careful tie-rod and column capacity verification in proposed concept.

Evaluation of Maximum Tension Force Against Tie-rod Capacity

To evaluate the structural feasibility of the tie-rod connections, the maximum tension force is determined using the L_{02} load combination. The maximum tension force under this load combination is in the core system 207 kN in the outrigger system is 260 kN.

The tie-rod connections, modelled with an M22 threaded rod (8.8-grade steel), have an ultimate tensile capacity of 231.62 kN and a yield strength limit of 185.30 kN as shown in Table 5.6. Since the maximum observed tension force exceeds both the ultimate failure capacity and the yield strength of an M22 tie-rod, this indicates that the current tie-rod configuration is insufficient to withstand the expected forces.

Some possible design solutions can be implemented to overcome the insufficient capacity of the current tie-rod system to withstand the expected forces. These include:

- **Increasing the tie-rod diameter:** A larger tie-rod, such as an M30 or higher, would provide greater tensile capacity.
- **Using higher-grade steel:** By selecting a steel grade with a higher ultimate tensile strength, the tie-rod's capacity can be improved without necessarily increasing its diameter. This would allow for better performance while maintaining constructability.

Implementing one or a combination of these solutions would enhance the structural performance and ensure the system can safely accommodate the expected forces.

5.3.2. Member Utilization

This section analyzes the utilization of structural members, starting with the core-only system, followed by the original outrigger configuration. The focus is primarily on the columns of the modules, as the utilization results show that these elements govern the structural performance in terms of utilization. For this analysis the L_{01} load combination is used.

Core system

Figure 5.13 presents the utilization distribution for the four predefined column groups in the core-only system. Each subfigure illustrates the utilization levels within a specific group, providing insight into the variation of load-bearing capacity across the structure. The final subfigure shows the group division used in the analysis. Enlarged versions of the figures are included in Appendix E.

(a) Utilization group 1

(b) Utilization group 2

(c) Utilization group 3

(d) Utilization group 4

(e) Group division of the core system
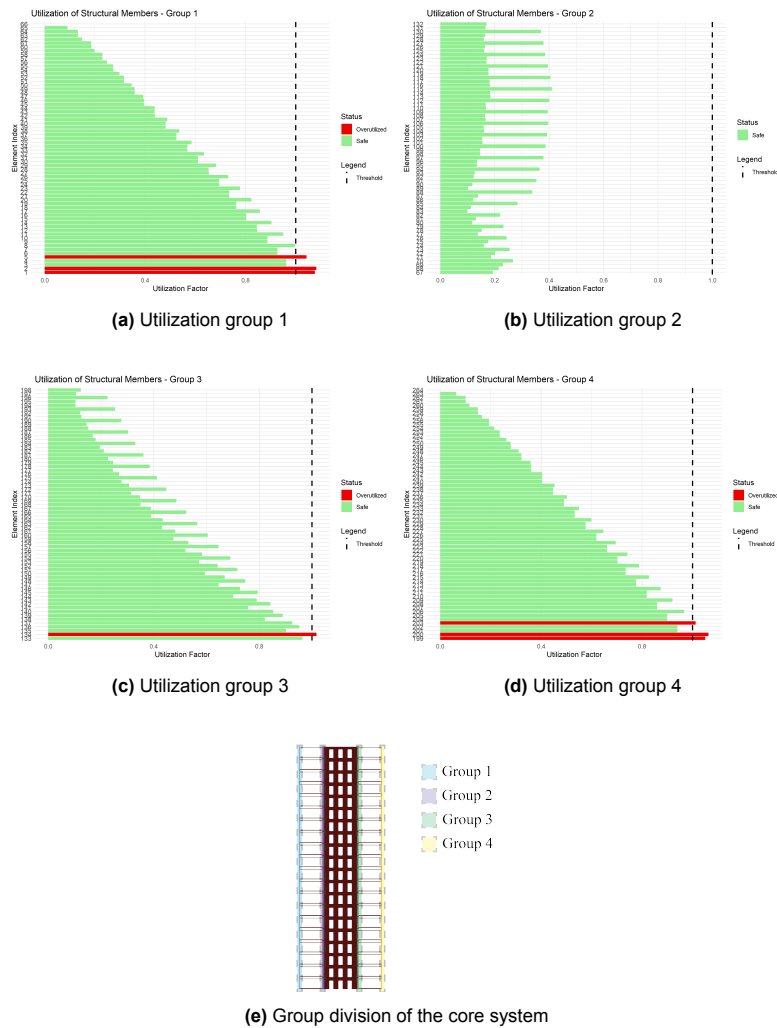
Figure 5.13: Utilization for all four groups for the core system (L_{01} load combination)

Table 5.9 summarizes the number of overutilized members, along with the maximum utilization values observed in each group.

Table 5.9: Summary of overutilized members and maximum utilization values of core (L_{01} load combination)

Group	Overutilized Members	Max Utilization Index	Max Utilization Value
1	3	2	1.08
2	0	115	0.41
3	1	134	1.02
4	3	200	1.06

Figure 5.14 provides a visual representation of the overall utilization distribution across the core system.
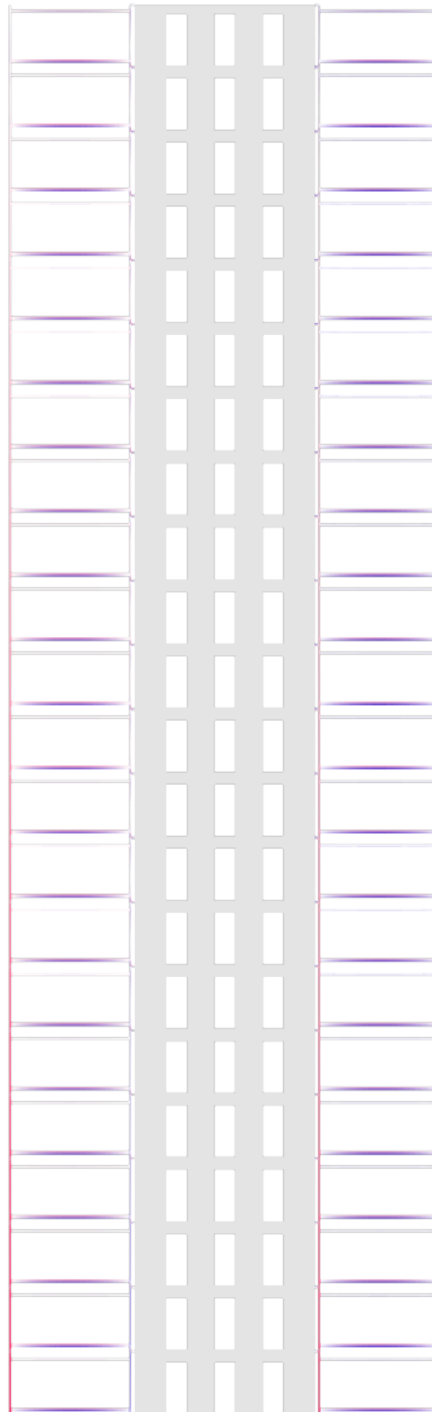
Figure 5.14: Utilization plot core (L_{01} load combination)

Original outrigger configuration

Figure 5.15 presents the utilization distribution for the four predefined column groups in the original outrigger system with the original configuration.

(a) Utilization group 1

(b) Utilization group 2

(c) Utilization group 3

(d) Utilization group 4

(e) Group division of the core system

Figure 5.15: Utilization for all four groups Original Outrigger (L_{01} load combination)

Table 5.10 summarizes the number of overutilized members in the outrigger system with the original configuration.

Table 5.10: Summary of overutilized members and maximum utilization values original outrigger (L_{01} load combination)

Group	Overutilized Members	Max Utilization Index	Max Utilization Value
1	0	37	0.36
2	0	91	0.56
3	0	116	0.94
4	12	173	1.24

Figure 5.16 provides a visual representation of the overall utilization distribution across the original outrigger system.
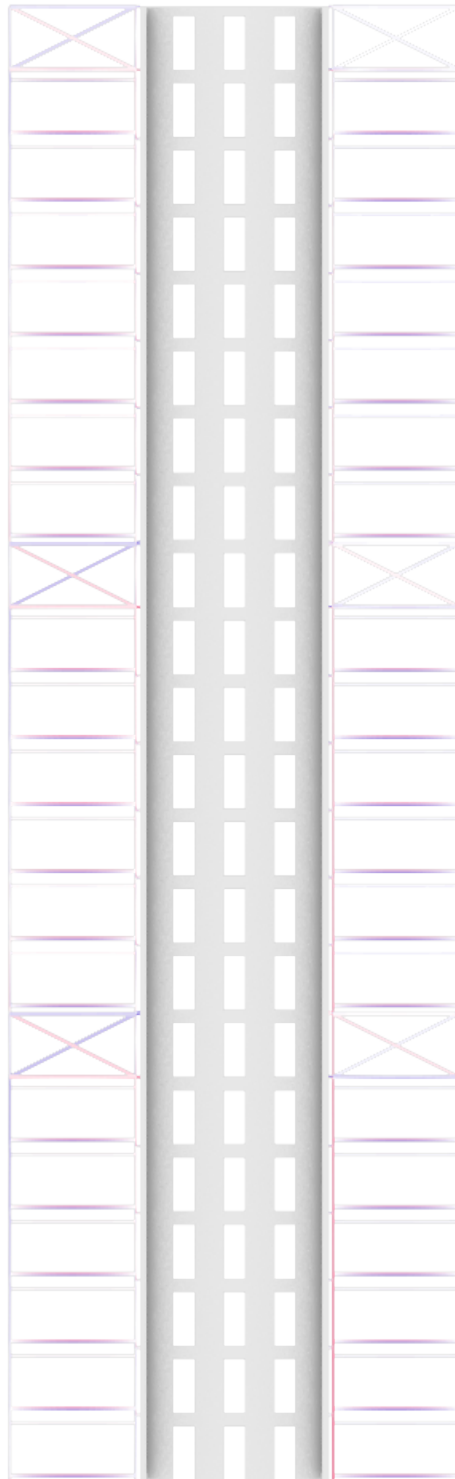
Figure 5.16: Utilization plot original outrigger (L_{01} load combination)

Conclusion

After introducing the original outrigger configuration, the maximum utilization increases to 1.24, located in group 4. While this value is higher than the core-only maximum, it reflects a redistribution of internal forces.

The outrigger system enhances the engagement of perimeter columns, which results in a noticeable decrease of stress in the central, core-connected members. This effect is most evident in group 1, where the number of overutilized members drops from three in the core-only configuration to zero in the outrigger system, accompanied by a reduction in maximum utilization from 1.08 to 0.36. Part of the compression forces in group 1 is redistributed by the outrigger to the core.

However, this redistribution also introduces new stress concentrations at the periphery of the structure, particularly in group 4, where the number of overutilized members increases from three to twelve and the maximum utilization rises from 1.06 to 1.24. this is due to the increased compression force coming from the outriggers.

These outcomes highlight the dual nature of the outrigger system: while it effectively spreads lateral loads and mitigates core-localized overstressing, it simultaneously demands careful design attention to the perimeter regions, where new critical points of utilization emerge.

Evaluation Against the Utilization Limit

To ensure structural integrity, all members should remain within an acceptable utilization limit, generally set at <1.0. Exceeding this threshold indicates overstressed elements that may require reinforcement or design modifications.

Possible design modifications to mitigate overutilization include:

- **Using Higher-Strength Materials:** Selecting a material with superior mechanical properties increases the allowable stress limits. The existing columns are made of *S235* steel, which could be upgraded to *S355* steel for enhanced strength and durability.
- **Increasing Column Dimensions:** Enlarging the cross-sectional area of overstressed members enhances their load-bearing capacity. In the current design, all module columns are *SHS 120×10*, which can be increased to a larger size to improve structural performance.
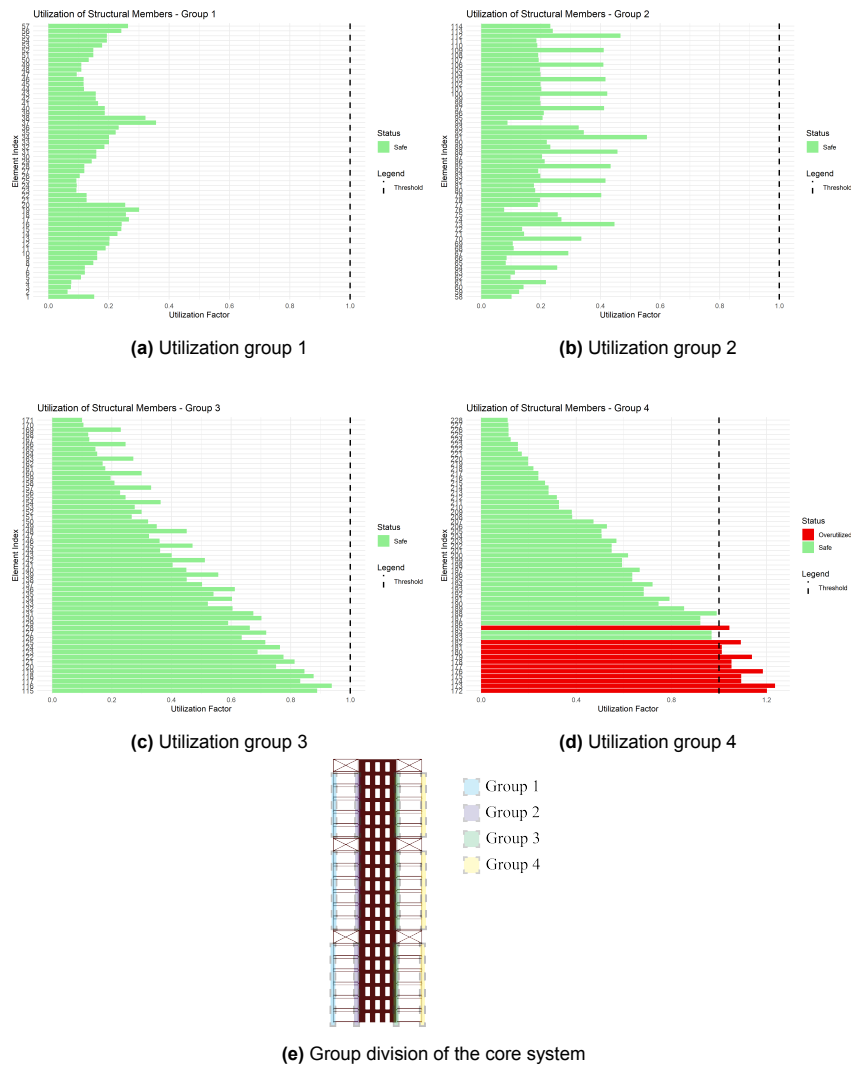- **Optimizing outrigger placement:** Adjusting the vertical positioning of the outriggers may improve force redistribution.

Implementing one or a combination of these solutions would enhance the overall performance and ensure compliance with utilization limits.

5.3.3. Lateral Deflection Limit

As previously established in Section 5.2, the maximum allowable lateral displacement is governed by the building height (H) and the inclusion or exclusion of the foundation in the model. In the *Grasshopper* model, no foundation is explicitly modelled, and the supports are simplified as fully fixed. For the analysed structure with a building height of $H = 70.3$ m, the deflection limits are defined as follows:

- Allowable deflection with foundation: $\delta_{\text{max}} = \frac{70.3}{500} = 0.1406$ m
- Allowable deflection without foundation: $\delta_{\text{max}} = \frac{70.3}{750} = 0.0937$ m

For this analysis, the *parametric* models structures are increased by two floors to reach the target height of 70 meters.

Table 5.11 presents the lateral displacement results obtained for the core-only system and the original outrigger configuration, compared against the respective deflection limits. Figure 5.17 illustrates the deformation pattern of both configurations. For this analysis the L_{01} load combination is used.

Table 5.11: Comparison of lateral displacement against deflection limits (L_{01} load combination)

Configuration	Lateral Displacement (m)
Core-Only System	0.153
Original Outrigger	0.118
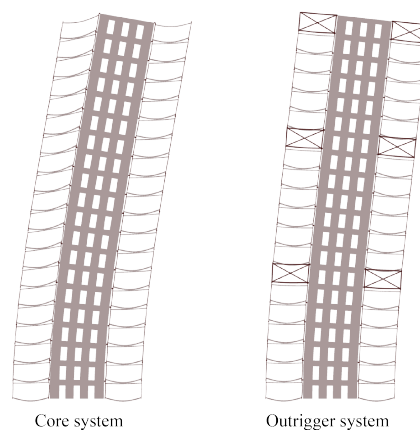
Figure 5.17: Displacement core and outrigger system (L_{01} load combination)

The results indicate that the core-only system exceeds the deflection limit, with a lateral displacement of 0.153 m, surpassing both the allowable 0.1406 m (with foundation) and the stricter limit of 0.0937 m (without foundation). This confirms that the core alone lacks sufficient stiffness to meet the serviceability requirements. In contrast, the original outrigger configuration reduces the lateral displacement to 0.118 m, which satisfies the allowable limit with foundation but exceeds the stricter limit without foundation.

Implications and Design Considerations
To further optimize lateral stiffness and ensure compliance with stricter deflection limits, the following refinements could be considered:

- **Adjusting outrigger placement**: Optimizing the vertical positioning of outriggers to maximize their contribution to lateral stiffness.
- **Enhancing outrigger stiffness**: Increasing the cross-section or material strength of the outrigger elements to improve their contribution to the stiffness of the structure.
- **Enhancing core-wall stiffness**: Increasing the thickness or material strength of the core walls to improve their inherent resistance to lateral displacement.

5.4. Design Adjustments Based on Results

Based on the findings in Section 5.3, it is evident that the current outrigger concept enhances the structural performance of a modular mid-rise system compared to a core-only configuration. However, despite the improvements, the existing concept does not fully meet all structural requirements, particularly in terms of lateral stiffness, material utilization, and tie-rod capacity.

To address these limitations, several design adjustments are proposed. These refinements aim to further optimize the outrigger configuration, improve material efficiency, and develop a more effective tie-rod force transfer mechanism to ensure all structural elements remain within safe utilization limits.

5.4.1. Various Outrigger Configurations and Optimization

The effectiveness of an outrigger system is highly dependent on its positioning, number, and stiffness contribution to the overall structural system. While the original outrigger configuration has proven beneficial in reducing lateral deflections and redistributing forces, further optimization is required to maximize its efficiency. This subsection explores alternative outrigger placement strategies, including adjustments in vertical positioning and additional outrigger levels, to improve lateral stiffness. For this analysis the L_{01} load combination is used.

To determine the most effective outrigger placement, the *Opossum* plugin in *Grasshopper* was utilized. *Opossum* employs an optimization algorithm that allows for the predefinition of adjustable parameters, which, in this case, was the vertical placement of the outrigger levels. By iteratively adjusting these variables, the algorithm aims to identify the optimal outrigger placement that results in the smallest lateral displacement at the top of the structure. The optimized configurations were subsequently compared to both the core-only system and the original outrigger configuration. Figure 5.18 illustrates the optimal vertical placement for configurations with one, two, and three outriggers.

n = 1   n = 2   n = 3
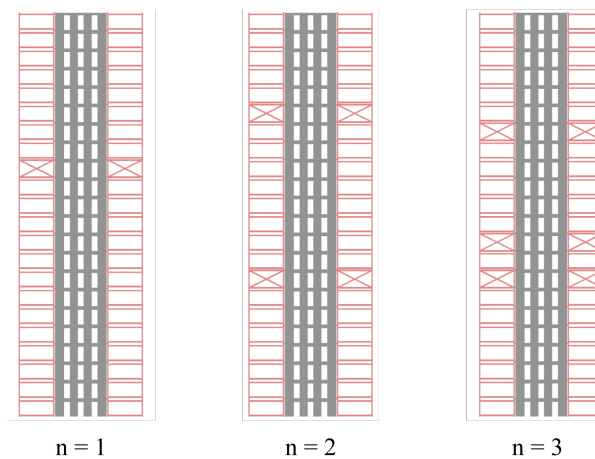
Figure 5.18: Optimal outrigger placement for (L_{01} load combination)

Table 5.12 presents the key results for each configuration, including maximum displacement, maximum normal force, and the percentage reduction in lateral displacement compared to the core-only system.

Table 5.12: Top displacement comparison of outrigger configurations (L_{01} load combination)

Configuration	Outrigger level(s)	Top displacement w_{top} (m)	Reduction (%)
Core Only	-	0.153	–
Original Outrigger	6, 14, 21	0.118	22.9
Opt. 1 Outrigger	13	0.127	17.0
Opt. 2 Outriggers	7, 16	0.122	20.3
Opt. 3 Outriggers	7, 9, 15	0.117	23.5

Table 5.12 presents the top displacement values for the core-only structure and several outrigger configurations under the L_{01} load combination. The core-only system exhibits the highest top displacement, with a peak value of 0.153 meters. When outriggers are introduced, a consistent reduction in top displacement is observed across all configurations.

The original outrigger configuration, with outriggers placed at levels 6, 14, and 21, reduces the top displacement to 0.118 meters. The optimized single-outrigger scheme (*Opt. 1*), located at level 13, yields a slightly higher top displacement of 0.127 meters. The dual-outrigger setup (*Opt. 2*), with outriggers at levels 7 and 16, further improves performance, reducing top displacement to 0.122 meters. The lowest value is achieved with the triple-outrigger configuration (*Opt. 3*), where outriggers are placed at levels 7, 9, and 15, resulting in a top displacement of 0.117 meters.

While the triple-outrigger configuration offers the greatest absolute reduction in top displacement, the improvement over the dual-outrigger case is marginal. This suggests that beyond two well-placed outriggers, the structural benefit of adding additional outriggers diminishes, particularly when considering practical constraints such as cost, complexity, and space requirements. Based on this balance, the dual-outrigger configuration (*Opt. 2*) is selected for continued analysis in the subsequent sections.

Opt.2 Outrigger configuration

The performance of the optimized two-outrigger configuration (*Opt. 2*) is assessed based on both utilization levels and internal force demands in the modular column groups. Table 5.13 summarizes the number of overutilized members, the maximum utilization indices, and the corresponding utilization values for each group under load combination L_{01}, which governs compressive behaviour.

Table 5.13: Summary of overutilized members and maximum utilization values for *Opt. 2* (L_{01} load combination)

Group	Overutilized Members	Max Utilization Index	Max Utilization Value
1	0	22	0.42
2	0	103	0.57
3	0	122	0.94
4	10	182	1.22

As shown in Table 5.13, groups 1 through 3 exhibit no overutilized members, with maximum utilization values remaining well below the critical threshold of 1.0. In contrast, group 4 exhibits significant stress concentrations, with ten members exceeding the utilization limit and a peak utilization value of 1.22, located at element index 182.

Table 5.14 further details the maximum internal forces recorded within each group under load combination L_{01}. The table identifies the indices and magnitudes of both the most heavily loaded compressive and tensile members.

Table 5.14: Index and value of maximum tension and compression elements per group for *Opt. 2* (L_{01} load combination)

Group	Max Ten. Index	Max Ten. Value [kN]	Max Comp. Index	Max Comp. Value [kN]
1	21	159.37	46	-162.28
2	63	48.38	103	-149.11
3	180	19.44	121	-617.12
4	–	–	181	-808.97

The most critical compressive force, $-808.97\,\text{kN}$, is observed in group 4, which aligns with the high utilization recorded in that same group. The maximum tensile force under load combination L_{01} is $159.37\,\text{kN}$, found in group 1. However, for assessing tie-rod demands, load combination L_{02} is considered more appropriate, as it governs the tensile behaviour. Under this loading, the maximum observed tensile force increases to $238.00\,\text{kN}$, indicating the design demand that must be resisted by the vertical tie-rod connections within the inter-modular connection.

5.4.2. Material Optimization

To further enhance the structural performance of the optimized two-outrigger configuration, this section examines material optimization strategies aimed at reducing overutilization in critical structural members while maintaining overall efficiency. The primary objectives are to ensure compliance with utilization limits and to reduce the lateral deflection to remain within the allowable deflection limit. The structural analysis in Section 5.4.1 highlighted that specific members in group 4 remain overutilized, with maximum utilization value of 1.12, respectively. These overutilized members are primarily located in the perimeter columns, which experience increased forces due to the redistribution of loads via the outrigger system.

Optimization strategies

The focus of the material optimization is on reducing overutilization in the cross-sections of the columns. The L_{01} load combination has been chosen for this analysis as it induces the highest normal forces in the columns. Subsequently, the L_{02} load combination will be used to verify whether the optimized cross-sections remain within the acceptable utilization limits.

Using Higher-Strength Materials

The first optimization strategy involves upgrading the material of the columns from S235 to S355 structural steel. This change enhances the yield strength of the columns, thereby increasing their load-bearing capacity without necessitating any changes in cross-sectional geometry.

Table 5.15 summarizes the utilization results for the configuration using S235 steel. Although groups 1 through 3 exhibit acceptable utilization levels (with maximum values well below the critical threshold of 1.0) group 4 contains ten overutilized members, with a maximum utilization value of 1.22. This highlights a localized overstressing in the upper column zones.

Table 5.15: Summary of overutilized members with S235 steel

Group	Overutilized Members	Max Utilization Index	Max Utilization Value
1	0	22	0.42
2	0	103	0.57
3	0	122	0.94
4	10	182	1.22

After upgrading the material to S355 steel, the overall utilization across all groups is reduced significantly, as shown in Table 5.16. Most notably, the overutilized members in group 4 are entirely eliminated, and the maximum utilization in that group drops to 0.85, comfortably below the critical threshold. Similar improvements are seen in the other groups, where maximum utilization values decline to 0.66 in group 3 and below 0.4 in groups 1 and 2.

Table 5.16: Summary of overutilized members with S355 steel

Group	Overutilized Members	Max Utilization Index	Max Utilization Value
1	0	22	0.27
2	0	103	0.37
3	0	122	0.66
4	0	182	0.85

These results confirm that the material upgrade from S235 to S355 steel is an effective and efficient strategy for resolving overutilization without altering the structural layout or geometry or the proposed concept.

Increasing Column Cross-Section Dimensions

Following the material upgrade, the next step is to adjust the cross-sectional dimensions of the columns.

To optimize the cross-section dynamically, the *Optimize Cross Section* component in Karamba is utilized. This component allows for real-time adjustments to the cross-sections in response to design modifications of the overall structure, ensuring that the most efficient structural configuration is selected. The *Optimize Cross Section* component automates the selection of optimal cross-sections for beams and shell elements by considering their load-bearing capacity and, optionally, the maximum allowable deflection of the structure.

To promote standardization of the members and connection details, a consistent column size was adopted throughout the building height. A uniform rectangular steel section was used for the columns, with variations only in wall thickness, to facilitate ease of connection between modules in the vertical direction. This approach not only simplifies the design and manufacturing process but also enhances structural efficiency [49]. The available column cross-sections are categorized into subgroups where only the thickness varies while maintaining a consistent external column size. The division of column cross-sections is illustrated in Figure H.1 in Appendix H.

To ensure proper connection of the outriggers and to prevent any discontinuity in force transmission, For each configuration, the columns of the outriggers, are assigned the cross-section with the greatest thickness within each subgroup. This approach ensures that the load transfer remains uniform and minimizing stress concentrations at the connection between the outrigger and module columns.

Using an optimization target of 0.9 utilization, the maximum top displacement values for different column cross-sections were obtained through the optimization component. It is important to note that in this illustrative example, the self-weight applied to the core has not been adjusted to account for the point loads transferred by the units behind the core. Nevertheless, the results provide an indication of how structural displacements evolve as cross-sections are increased. Table 5.17 shows the maximum top displacement of the building with an increase column cross-section.

Table 5.17: Maximum top displacement for different cross-sections

Cross-Section	Maximum Top Displacement (m)
SHS 120	0.121
SHS 140	0.116
SHS 150	0.107
SHS 160	0.104
SHS 180	0.100
SHS 200	0.096
SHS 220	0.093
SHS 250	0.086
SHS 260	0.084
SHS 300	0.079
SHS 350	0.073
SHS 400	0.064

From table 5.17, it is evident that increasing the cross-section size leads to a clear and gradual reduction in top displacement. Between SHS 120 and SHS 200, the displacement decreases from 0.0121 m to 0.0096 m, an improvement of approximately 21%. Beyond that, the reductions become even more pronounced. For example, moving from SHS 220 (0.0093 m) to SHS 400 (0.0064 m) results in a displacement reduction of around 31%.

While increasing cross-section sizes provides measurable benefits in reducing lateral displacement, it is crucial to acknowledge practical and economic limitations. Very large cross-sections, such as SHS 350 and SHS 400, may not be realistic or feasible for modular construction, as they would require excessive material usage and could complicate fabrication, transportation, and assembly. Selecting an optimal cross-section size should be based on achieving sufficient displacement reduction without excessive material costs.

5.4.3. Enhanced Tie-rod Capacity

As established in Section 5.4.1, the maximum tensile force observed in the optimized outrigger configuration (Opti.2) under the L_{02} load combination is $238.00\,\text{kN}$. This force exceeds the capacity of the originally specified tie-rod connection, which utilized an M24 threaded rod (steel grade 8.8) with a yield strength of $230.82\,\text{kN}$. As a result, a revised connection strategy is required to ensure safe and sufficient capacity under service conditions.

The existing tie-rod configuration, based on an M22 rod in 8.8-grade steel, has an ultimate tensile capacity of $231.62\,\text{kN}$ and a yield capacity of only $185.30\,\text{kN}$. Both values fall short of the required $238\,\text{kN}$, confirming the need for a more robust solution.

To support the design evaluation, an *Excel* sheet was developed containing the cross-sectional properties and strength capacities of threaded tie-rods across a range of diameters (M8 to M68) and steel grades (4.8, 8.8, 10.9, and 12.9). Instructions for accessing and using this *Excel* sheet are provided in Appendix I.

Increasing Tie-rod Diameter
The first strategy is to increase the nominal diameter of the tie-rod. Larger diameters yield greater effective core areas, and thus higher tensile and yield capacities.

As shown in Figure 5.19, increasing the rod size from M24 to M27 (while maintaining grade 8.8 steel) boosts the yield capacity from $230.82\,\text{kN}$ to $263.14\,\text{kN}$. This value exceeds the required tensile force of $238\,\text{kN}$, confirming that the tie-rod can safely resist the applied load. Further increases in diameter, such as M30 or M33, provide additional safety margin but may introduce geometric or cost constraints.
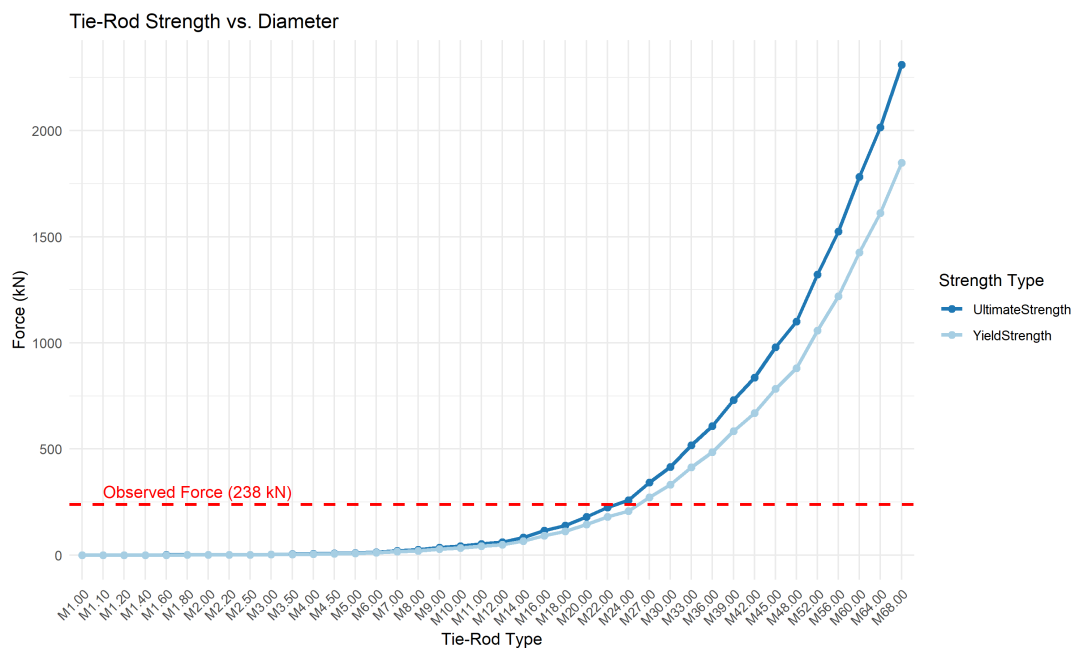
Figure 5.19: Tensile and yield strength capacities for various tie-rod diameters (steel grade 8.8).

Upgrading Steel Grade
An alternative approach is to retain the existing tie-rod diameter while increasing the steel grade. Figure 5.20 illustrates the influence of steel grade on yield strength for a range of tie-rod diameters.
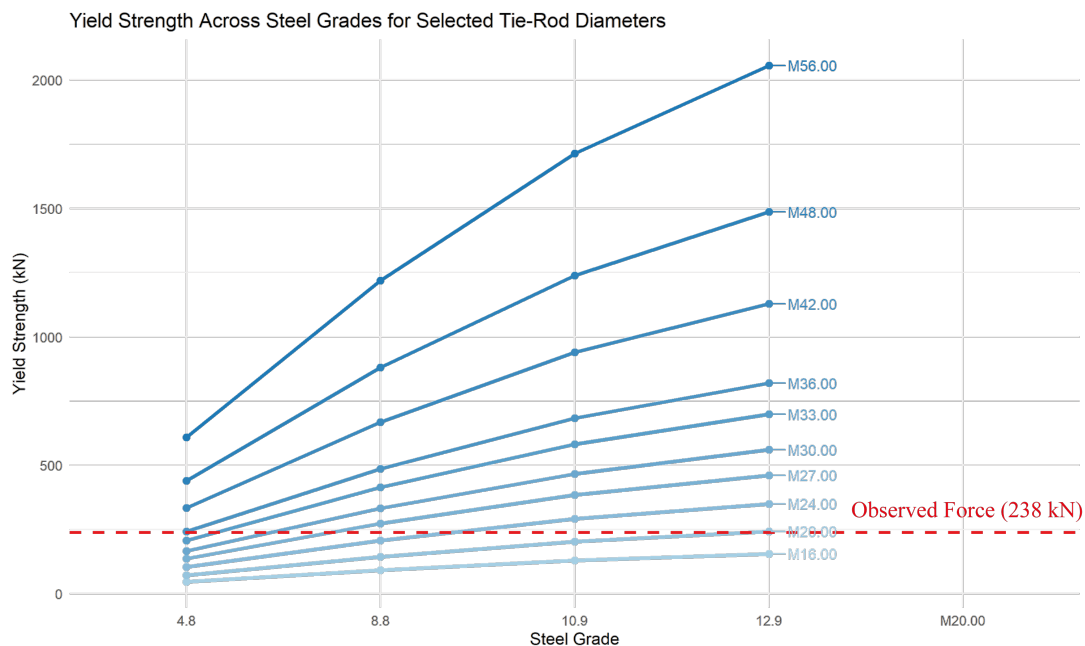
Figure 5.20: Yield strength progression across steel grades (4.8–12.9) for selected tie-rod diameters.

For example, an M24 rod made from grade 10.9 steel has a yield capacity of approximately $289.74\,\mathrm{kN}$, which exceeds the demand. Similarly, an M22 rod in grade 12.9 steel reaches $312.34\,\mathrm{kN}$, comfortably surpassing the required $238\,\mathrm{kN}$ without increasing diameter. This strategy may be preferable in cases where space or interface constraints make larger diameters impractical.

Conclusion
Both proposed strategies, enlarging the rod diameter or increasing the steel grade, provide feasible and effective methods to ensure the tie-rod connection can resist the observed tensile force. From a structural safety perspective, an M27 rod in grade 8.8 steel or an M24 rod in grade 10.9 or higher is sufficient.

5.4.4. Enhancing Lateral Displacement Resistance

To ensure compliance with lateral deflection limits it is necessary to evaluate and improve the global lateral stiffness of the structural system of the concept. This section estimates the required global stiffness of the core-outrigger system. The resulting reference stiffness will serve as a design target for the case study developed in Chapter 6.

Estimating Required Global Stiffness Using the Analytical Outrigger Method

The analytical method employed is based on simplified models described in section 3.2.3, where the building is idealised as a cantilever beam stiffened by discrete lateral elements. This method enables the estimation of the total required flexural rigidity EI_{total} to satisfy a predefined maximum lateral displacement under uniform wind loading. For this analysis, a total building height of $70\,m$ is assumed. As discussed in Section 5.3.3, the stricter deflection criterion of $H/750$ results in a maximum allowable top displacement of $0.093\,m$.

Loads applied L02   Recorded displacement   Set Displacement limit
Known EI   Estimated uniform Q load   Estimated Required EItotal for the Case study
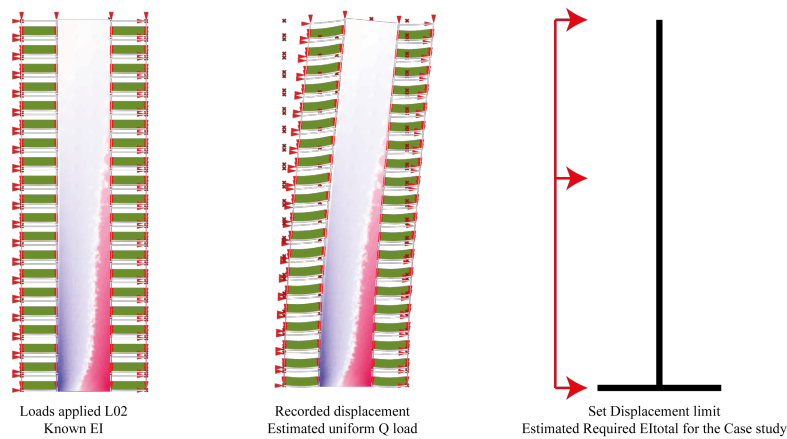
Figure 5.21: Estimated strategy for global stiffness

To estimate the stiffness requirement, the governing loads in the structural model must be simplified to a uniform distributed load q, which can then be used in the analytical expression for displacement. An iterative process was carried out in *Grasshopper* to achieve this simplification. In this process, all permanent, variable, and wind loads applied to the structure were summarised into an equivalent line load q acting over the full height of the structure. The simplified core-only system, modelled without openings or segmentation, served as the reference configuration. By analysing the displacement response of the structure under known stiffness conditions, the equivalent distributed load was determined such that it resulted in the same top displacement as observed in the full load model.

This iterative procedure yielded a representative uniform load of approximately 33.1 kN/m. With this value, the required flexural stiffness could be estimated using the displacement equation for a cantilever beam subjected to a uniform load:

$$\delta_{\text{top}} = \frac{qH^4}{8EI}$$

Substituting the known values, including the deflection limit of $0.093\,m$ and the equivalent load of $33.1\,kN/m$, the required flexural stiffness for one side of the structure was found to be approximately $1.06 \times 10^9\,\text{kNm}^2$. It is important to recognise that the calculated stiffness value corresponds to only one half of the building in the y-direction, since the *Grasshopper* model represents only the half of the structure in this direction. Therefore, the total required flexural rigidity in the y-direction, EI_{yy}, must be at least twice the initially estimated value. Consequently, the combined stiffness of the core and outrigger system should exceed $2.12 \times 10^9\,\text{kNm}^2$ to ensure that the structure remains within the limits of the stricter deflection criterion.

Applying the Calculated Required Stiffness
To evaluate whether the analytically derived flexural stiffness is a valid design target, the estimated value of $1.06 \times 10^9 \, \text{kNm}^2$ was applied in the *Grasshopper* model.

In the first scenario, a core-only system was modelled, with the modulus of elasticity for cracked concrete set to $E_{cr} = 1242.6 \, \text{kN/cm}^2$ (cracked concrete C50/60). To match the target stiffness, the core wall thickness was increased to $1.4 \, m$ over an effective length of 9 meters in the y-direction. Under load combinations L_{01} and L_{02}, the resulting lateral displacement at the top remained below $0.093 \, m$, confirming that the estimated stiffness leads to acceptable structural performance. In the second scenario, two outrigger levels were added to the same core configuration. This resulted in a further reduction of the top displacement to $0.076 \, m$.

These results validate the analytical estimation and confirm that the simplified line load approach provides a robust target for stiffness-based design within the deflection criteria.

Optimising the Balance Between Core and Outrigger Stiffness
The results of the previous sections show that both the core and the outriggers contribute to the overall lateral stiffness of the structure. However, their interaction must be investigated: a more flexible core tends to increase outrigger effectiveness, while a stiffer core can reduce the relative deformation required to activate the outriggers. This trade-off opens the possibility to optimise both elements jointly, rather than over-designing one at the expense of the other.

To explore this balance systematically, three different *parametric* investigations are done:

1. **Effect of elastic modulus of the core on outrigger efficiency:** By adjusting the modulus of elasticity of the concrete, the relative effectiveness of the outrigger system can be assessed for different levels of core stiffness.

2. **Effect of the moment of inertia of the core on outrigger Efficiency):** Instead of varying the material stiffness, the geometric stiffness of the core can be adjusted by changing its cross-sectional thickness.

3. **Effect of the varying outrigger stiffness on outrigger efficiency:** Lastly, the cross-sections of the outrigger elements themselves will be altered, while keeping the core properties constant. This will help determine whether increasing outrigger stiffness significantly improves performance, or if diminishing returns are observed.

1. Effect of Core Elastic Modulus on Outrigger Efficiency

In the first analysis, the elastic modulus E of the concrete core was varied by considering different concrete strength classes, ranging from C20/25 to C90/105 in cracked and uncracked condition. The table of the values can be found in Appendix J in table J.1. This variation simulates how changes in material stiffness affect both the overall lateral performance of the structure and the relative contribution of the outriggers. To assess this interaction, the maximum lateral displacement at the top of the structure was calculated for both a core-only system and the two outrigger system (*Opt. 2*). As shown in Figure 5.22a, increasing the elastic modulus E of the core leads to a consistent reduction in lateral displacement for both systems.

(a) Top displacement vs. elastic modulus for core-only and outrigger systems.

(b) Relative reduction in top displacement due to outriggers.
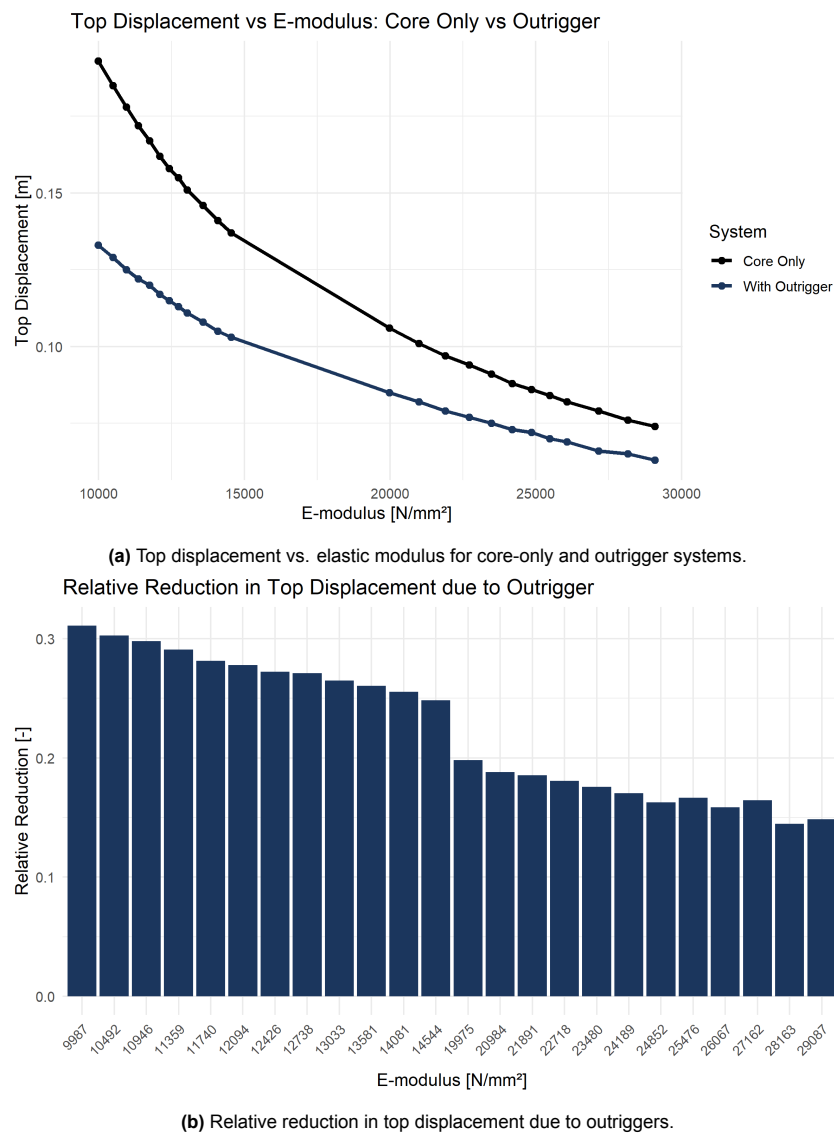
Figure 5.22: Effect of varying core stiffness on total displacement and outrigger efficiency.

However, the relative benefit of the outriggers becomes smaller as the core becomes stiffer. This trend is further illustrated in Figure 5.22b, which shows the relative reduction in top displacement due to the outriggers as a function of the elastic modulus. For low-strength concrete, the outriggers contribute to a displacement reduction of over $30\,\%$. As the E-modulus increases, this benefit gradually declines to below $20\,\%$, indicating diminishing returns. This confirms that the outrigger effect is more pronounced when the core is more flexible, due to greater rotational deformation at the outrigger levels.

2. Effect of the Moment of Inertia on Outrigger Efficiency

In this analysis, the focus is shifted from material to geometric stiffness by varying the core's moment of inertia I, achieved through adjustments in its cross-sectional thickness. The core is modelled as a solid concrete slab with a constant width and variable thickness, allowing for systematic control over its flexural rigidity. Openings in the core were not included to isolate the influence of geometric stiffness. For consistency across all iterations, the modulus of elasticity E was fixed to that of cracked concrete of strength class C50/60, with a value of $1242.6\,\text{kN/cm}^2$. Figure 5.23 shows the results of this analysis.

(a) Top displacement vs. moment of inertia for core-only and outrigger systems.

(b) Relative reduction in top displacement due to outriggers.
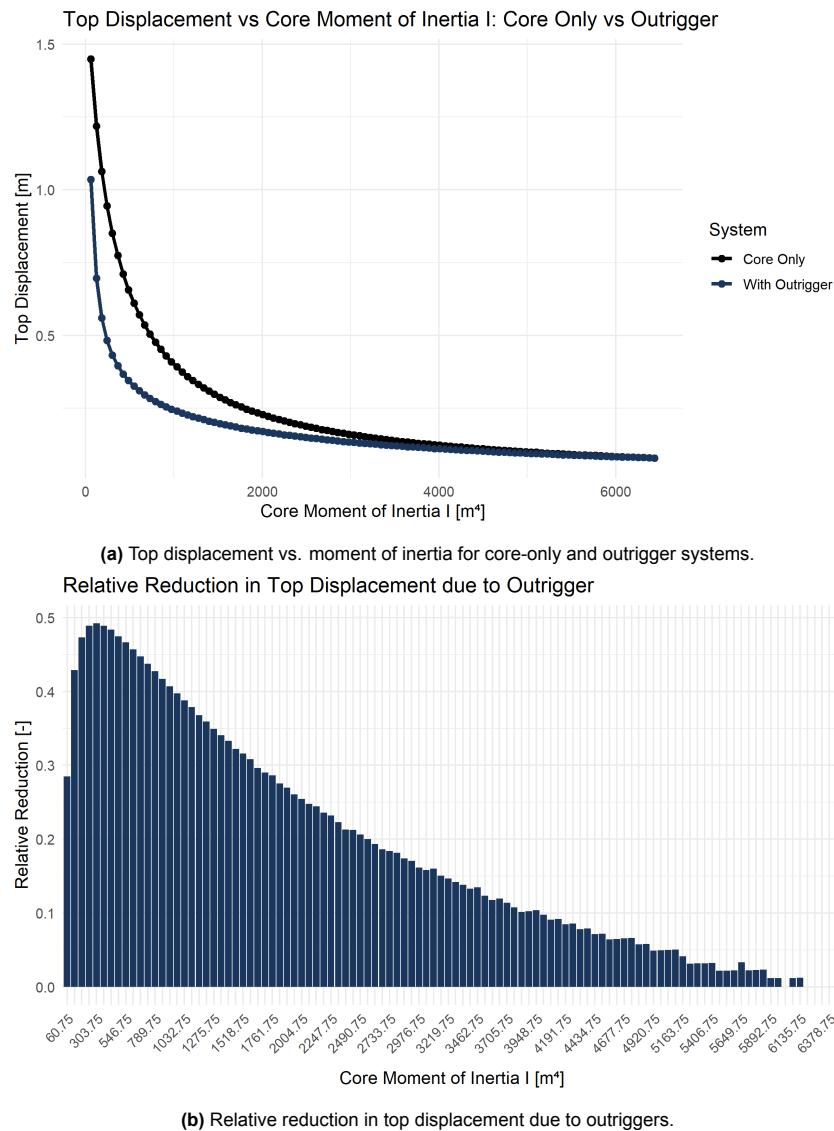
Figure 5.23: Influence of core moment of inertia on top displacement and outrigger effectiveness.

The results show a clear trend: as the moment of inertia of the core increases, the lateral displacement at the top of the structure decreases significantly for both core-only system and the two outrigger system (*Opt. 2*). This is shown in Figure 5.23a. However, similar to the behaviour observed in the previous section, the relative benefit of the outriggers diminishes as the core becomes stiffer. This is because the more rigid the core, the less it rotates under lateral load, reducing the load redistribution through the outriggers. Figure 5.23b quantifies this effect by presenting the relative reduction in displacement due to the outriggers. For cores with low stiffness, the relative reduction exceeds $45\,\%$, while this value gradually drops below $10\,\%$ for cores with high moment of inertia. This again highlights the importance of tuning the balance between core and outrigger stiffness to maximise structural efficiency.

3. Effect of Varying Outrigger Stiffness on Outrigger Efficiency

To evaluate the impact of outrigger stiffness on lateral displacement, a *parametric* analysis was conducted on the two outrigger system (*Opt. 2*). In the first, only the top and bottom beams of the outrigger truss were varied, while diagonals and columns remained constant. In the second, the same cross-section was applied to all outrigger members. The SHS profiles considered are listed in Appendix J, Table J.2. This distinction between the two configurations is logical from both a structural and a practical design perspective. The beams at the top and bottom of the outrigger truss are primarily responsible for transferring bending moments between the core and perimeter columns. As such, they play a dominant role in controlling relative rotation at the outrigger levels and in mobilising axial forces in the outer columns. Therefore, it is reasonable to first isolate and study the effect of varying only these elements. Once the influence of beam stiffness is understood, extending the variation to include all outrigger members provides insight into the full system potential. While diagonals and verticals contribute less directly to moment transfer, they affect the global stiffness of the truss and the ability of the outrigger to deform compatibly with the core.

Figure 5.24 compares top displacements for both configurations. Increasing the member size consistently reduces displacement, but the reduction is more pronounced when all outrigger elements are stiffened.

(a) Top displacement vs. outrigger beam cross-section stiffness.

(b) Top displacement vs. total outrigger cross-section stiffness (all members).
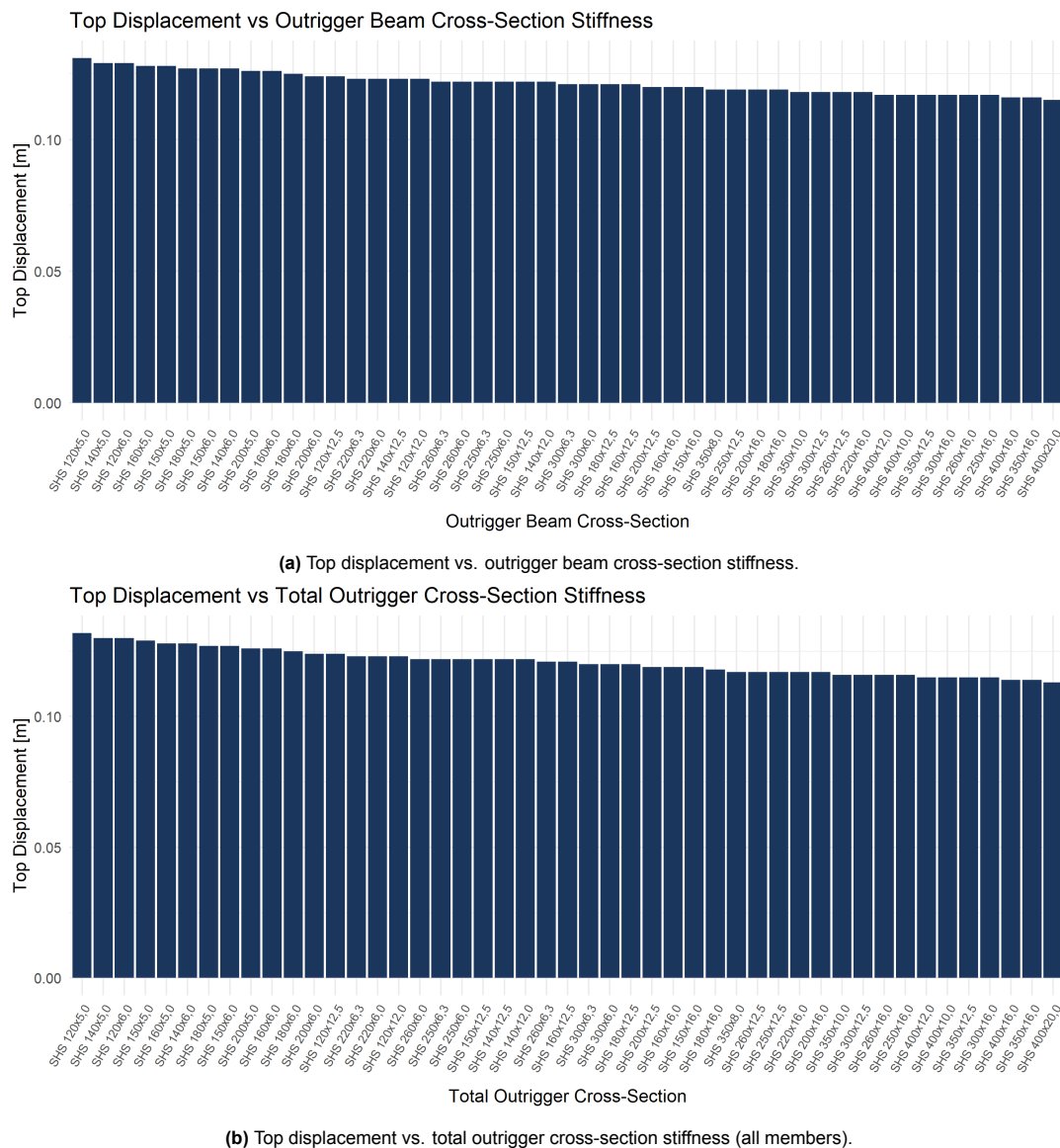
Figure 5.24: Comparison of top displacement for two outrigger stiffening strategies.

As shown in Table 5.18, the top displacement of the structural system decreases as the cross-section of the outrigger elements increases.

Table 5.18: Top displacement for different outrigger configurations and cross-sections

Configuration	Cross-Section	Top Displacement [m]
Beam-only	SHS 120x5.0	0.131 (Maximum)
Beam-only	SHS 400x20.0	0.115 (Minimum)
Total Outrigger	SHS 120x5.0	0.132 (Maximum)
Total Outrigger	SHS 400x20.0	0.113 (Minimum)

This results in a relative reduction in top displacement of approximately $12.2\,\%$ when only the top and bottom outrigger beams are stiffened from SHS 120x5.0 to SHS 400x20.0. Applying the same stiffening approach to all outrigger members further reduces the displacement to $0.113\,\mathrm{m}$, yielding a total improvement of $13.7\,\%$. However, this additional reduction comes at the expense of significantly increased material usage, which may not be justified given the relatively modest gain in performance.

Conclusion
The results of this section showed the importance of carefully balancing core and outrigger stiffness to achieve efficient lateral displacement. Using a simplified analytical method, a target global flexural stiffness of $2.12 \times 10^9\,\mathrm{kNm^2}$ was established to meet the deflection limit of $H/750$.

The subsequent investigations showed that both material stiffness (via the elastic modulus E) and geometric stiffness (via the moment of inertia I) of the core have a significant influence on overall lateral performance. However, as the core becomes stiffer, the relative effectiveness of outriggers diminishes due to reduced rotational deformation at outrigger levels. The stiffness of the outriggers themselves was also found to be a key parameter. While increasing only the top and bottom beam stiffness already yields a displacement reduction of $12.2\,\%$, extending this stiffening strategy to all outrigger members further reduces displacement to a total of $13.7\,\%$.

These insights form a foundation for the case study in Chapter 6. The derived stiffness requirements and observed interactions between core and outrigger properties will be used to guide the configuration and sizing of the structural elements in the Tang Tower concept.

5.5. Conclusion

This chapter has presented a comprehensive analysis of the structural behaviour of the proposed concept and the design modifications required to meet serviceability criteria.

The assessment began with evaluating the lateral displacement response, revealing that the initially modelled system did not satisfy the deflection limit of $H/750$. To resolve this, an analytical method was applied to estimate the required global stiffness, resulting in a target flexural rigidity of at least 2.12×10^9 kNm^2 for the combined core–outrigger system.

A subsequent *parametric* study was conducted to investigate the interaction between core stiffness and outrigger efficiency. The results demonstrated that while both components contribute to improved lateral performance, their effectiveness is interdependent. A more flexible core benefits significantly from the presence of outriggers, whereas a stiffer core reduces the reliance on additional lateral support.

The final part of the analysis focused on the influence of outrigger stiffness. Increasing the stiffness of the top and bottom beams led to a notable reduction in lateral displacement. However, extending this stiffening strategy to all outrigger members provided only marginal additional benefit while substantially increasing material use.

These findings indicate that, although outrigger stiffness contributes to the effectiveness of the proposed system, overall performance is primarily governed by the stiffness of the core.

The insights gained in this chapter regarding stiffness distribution and the interaction between core and outrigger elements provide a solid foundation for the application of the proposed structural concept in Chapter 6, where these principles will be tested and validated through a case study.

6

Case Study – Tang Tower

This chapter presents the final phase of the research: the application of the optimized structural concept to a real-world-inspired case study. The selected project, Tang Tower, is a conceptual design for a modular mid-rise residential building that was developed but never realised. The aim of this phase is to evaluate whether the proposed structural system can be successfully implemented within a realistic modular design and whether it effectively enhances lateral stability and overall structural performance. The case study is represented by a full *3D* model in which the proposed concept is applied and tested under realistic conditions.

6.1. Project Description

Tang Tower was selected as a representative case study for modular mid-rise construction. The design, developed in 2022 by Daiwa House Modular Europe in collaboration with Mirck Architecture and engineers from Ingenieursstudio DCK, was created for a $13\,storey$ residential building in Almere, the Netherlands. Although the project was never realised, the extensive structural documentation provides a realistic foundation for applying and validating the proposed structural concept in this research [35].

The Tang Tower features a hybrid construction system that combines prefabricated steel-framed modular units with a central precast concrete core. The upper twelve storeys consist of vertically stacked modular units, primarily measuring $6.0\times3.0\,m$. To meet spatial requirements, several units are designed in alternative sizes of $6.4\times3.0\,m$ and $8.5\times3.0\,m$. All modules are arranged on a regular grid and stacked in consistent vertical alignment. The ground floor and basement are constructed using cast-in-place concrete.

Each unit incorporates a composite floor system (Movixvloer), consisting of IPE beams integrated into a $70mm$ concrete topping. These beams span between UNP profiles along the long sides of the module, transferring loads to corner columns made of cold-formed hollow steel sections. Horizontal connections between modules are realised using tie-plate connections at ceiling level, while vertical continuity is ensured through bolted connections and dowel systems.

Figure 6.1 provides a visual overview of the Tang Tower.

(a) Exterior view of Tang Tower (Artist impression)   **(b)** Typical floor plan showing unit arrangement around core

Figure 6.1: Visualisation of the Tang Tower case study

The left image shows the complete tower, highlighting the repetitive modular configuration above the concrete base. The right image illustrates a typical floor plan, showing the arrangement of prefabricated units around the centrally located core.

Lateral stability is provided by a concrete core composed of two U-shaped shear wall segments (indicated in red and blue in Figure 6.1b), coupled by diaphragm action through the prefabricated floors. Due to functional openings at critical locations, the core does not form a fully continuous element. Consequently, lateral loads are distributed according to the relative stiffness of each wall segment. The overall structural stability depends on the interaction between the core and the foundation, with partial rotational restraint assumed at the base as a result of the pile foundation's stiffness.

6.2. Application of the Proposed Concept

This section presents the implementation of the optimized structural concept developed in the previous chapters. The design integrates three key components: a continuous concrete core, fixed outrigger levels, and enhanced vertical connections between modular units.

In the original Tang Tower design, the core was segmented into two separate U-shaped walls due to functional openings at critical locations, which reduced its effectiveness in distributing lateral loads. In the revised concept, the placement and geometry of these openings are strategically adjusted to preserve core functionality while enabling it to act more as a single, continuous structural element.

To further enhance lateral stability, fixed outrigger levels are introduced at predetermined heights. These outriggers establish structural linkages between the core and the exterior columns of the modular façade, enabling a more efficient transfer of lateral forces and reducing overall deformation.

A final refinement addresses the vertical load transfer mechanism between stacked modules. In the original Tang Tower concept, vertical forces were entirely carried by the corner columns of each module. In the proposed system, tensile forces resulting from outrigger action are redirected into designated tie-rod connections. These tie-rods are responsible for resisting tension, while compressive forces continue to be transferred through direct contact between the module columns.

The following sections of this chapter consolidate these conceptual enhancements into a fully developed *3D* model.

6.2.1. Core and Floorplan Design

To support the structural efficiency targets established in Section 5.4.4, the geometric layout and floorplan of the tower are refined in this section. The objective is to achieve an optimal balance between core stiffness and outrigger efficiency, while maintaining functional and architectural requirements. The core layout is designed with the same usable area as the Tang Tower for staircases and vertical shafts, ensuring comparability in terms of service integration and fire safety.

Required moment of inertia of the core

According to the analytical estimation in Section 5.4.4, the required total flexural stiffness EI_{total} was found to be

$$EI_{\text{total}} = 2.12 \times 10^9 \, \text{kNm}^2.$$

However, prior simulations have shown that the inclusion of two outrigger levels can reduce the lateral displacement by approximately 25–50%. Based on this, the required flexural stiffness of the core-only system may be conservatively reduced by 25%, resulting in a revised target stiffness of

$$EI_{\text{core,target}} = 0.75 \cdot 2.12 \times 10^9 = 1.59 \times 10^9 \, \text{kNm}^2.$$

Assuming a modulus of elasticity for cracked concrete of strength class C50/60 equal to $E_{\text{cr}} = 1242.6 \, \text{kN/cm}^2 = 12426000 \, \text{kN/m}^2$, the required moment of inertia I_{core} can be estimated as:

$$I_{\text{core}} = \frac{EI_{\text{core,target}}}{E_{\text{cr}}} = \frac{1.59 \times 10^9}{1.2426 \times 10^7} \approx 128 \, \text{m}^4.$$

This indicates that the redesigned square core should provide a flexural rigidity corresponding to a moment of inertia of approximately $128 \, \text{m}^4$ to meet the lateral displacement limit.

Redesigned Floorplan

Figure 6.2 illustrates the typical floor layout of the original Tang Tower design.
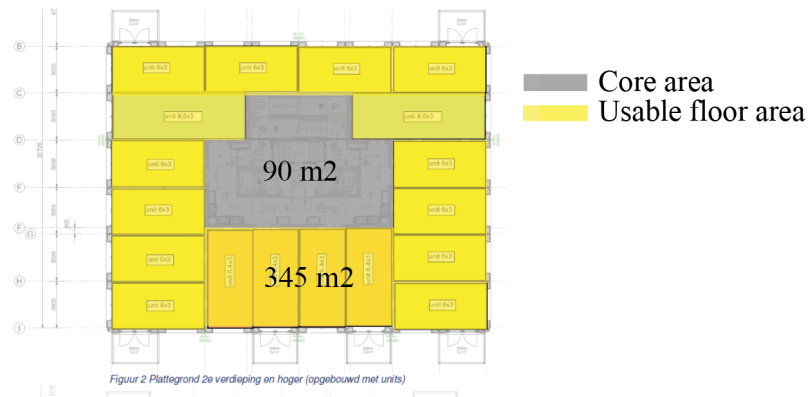

Figure 6.2: Floorplan of the original Tang Tower design showing the core area (grey) and usable living area (yellow).

The highlighted areas show the division between the central core (in grey) and the surrounding usable living area (in yellow). Analysis of this floorplan indicates that the core occupies approximately $90 \, \text{m}^2$ per floor, while the usable living area amounts to roughly $345 \, \text{m}^2$.

The existing core has an irregular shape, which is suboptimal from a structural stability perspective, particularly in terms of lateral stiffness and symmetric load distribution. In the revised design, the core is reconfigured into a square shape to enhance structural performance. This square geometry provides a more uniform distribution of stiffness and mass, which improves the structure's resistance to lateral loads and reduces torsional effects under lateral loading.

Surrounding this central core, the modules are arranged to maintain a comparable usable floor area as in the original Tang Tower design. The redesigned floorplan is shown in Figure 6.3, which presents both a typical floor (left) and an outrigger floor (right). The new square core has a side length of $9.44\,\mathrm{m}$.

Normal Floorplan   Outrigger Floorplan
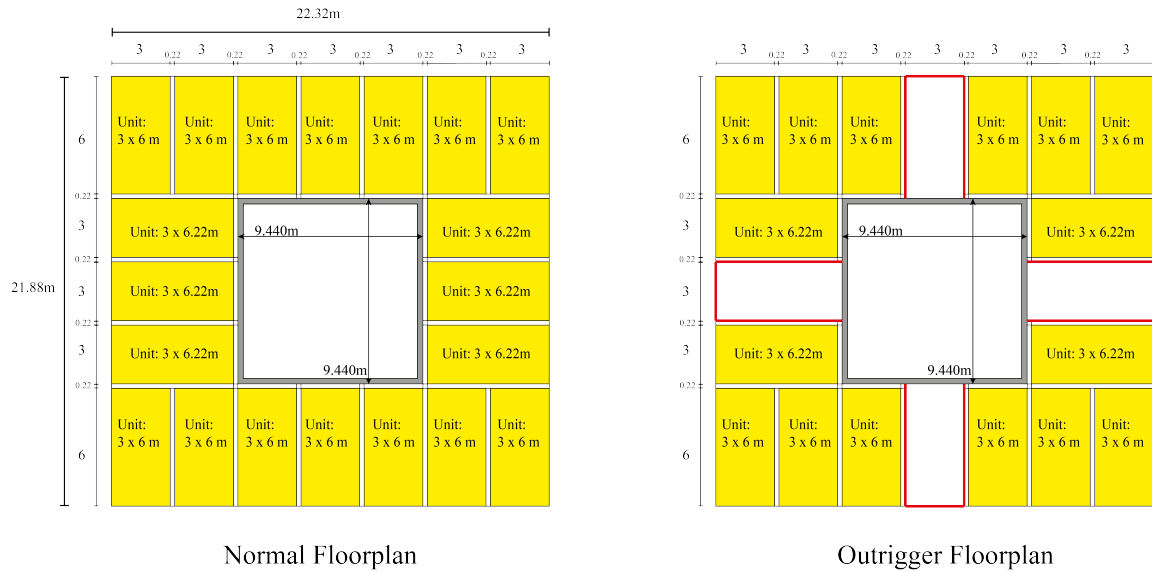
Figure 6.3: Redesigned floor layouts: typical floor without outriggers (left), and outrigger floor (right).

Each module was modelled with a spacing of $220\,\mathrm{mm}$ in both the x- and y-directions, which accounts for the centre-line offset of perimeter columns and a construction tolerance of approximately $20\,\mathrm{mm}$ between adjacent elements [49]. Two standard module types are used in the floorplan: $3 \times 6.0\,\mathrm{m}$ modules and slightly elongated $3 \times 6.22\,\mathrm{m}$ modules to account for spacing requirements. Each floor consists of 20 prefabricated modules, arranged symmetrically around the core.

On the outrigger floors, specific areas within the floorplan are reserved to accommodate the integration of outrigger elements. Each outrigger beam connects directly to a single vertical stack of modules and is highlighted in red in Figure 6.3 (right).

Figure 6.4 presents the redesigned core layout, reflecting a realistic configuration suitable for a modular mid-rise residential structure.
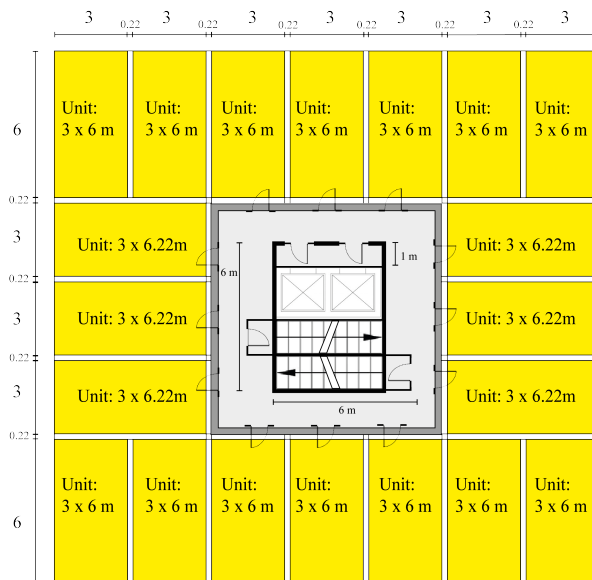
Figure 6.4: Floorplan with stairs and elevators

The core includes two spiral staircases (*wokkeltrappen*) and two elevators, ensuring vertical circulation and compliance with accessibility and evacuation requirements for buildings of this scale. The symmetrical positioning of these elements further contributes to balanced load distribution and efficient use of space within the core.

An example of the designated emergency walking paths within the redesigned floorplan is shown in Figure 6.5.
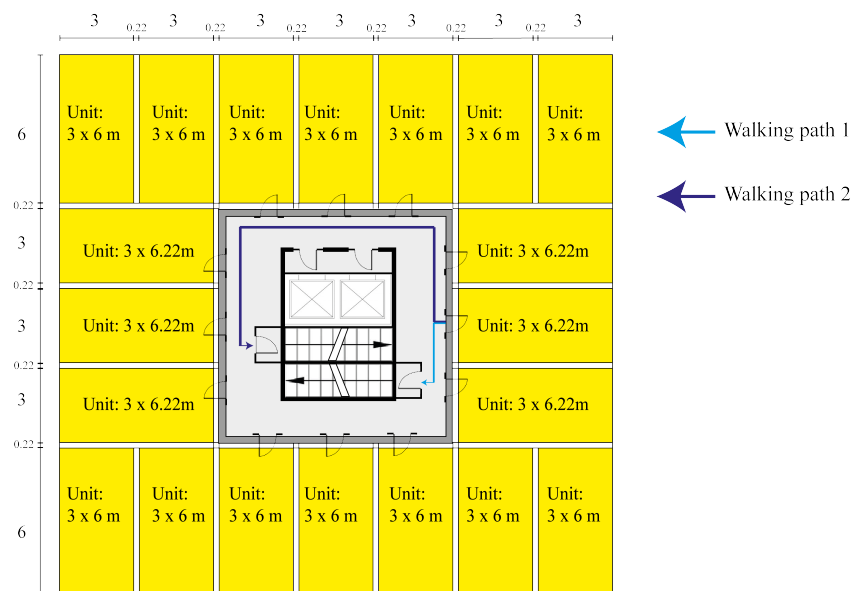
Figure 6.5: Example of designated emergency walking paths connecting rooms to stairwells.

Fire safety is addressed by ensuring that each room has access to the central stairwells via two independent walking paths. This redundant layout provides reliable and safe evacuation routes in the event of an emergency, in line with regulatory requirements for mid-rise residential buildings.

Stiffness Calculation of the Core

In the redesigned floorplan, the usable area on a normal floor is approximately $363.96\,\text{m}^2$, while the core area is $89.11\,\text{m}^2$. On the outrigger floors, the core size remains unchanged, but the usable area is reduced to $290.64\,\text{m}^2$ due to the integration of structural outrigger.

Assuming a uniform core wall thickness of $0.30\,\text{m}$, the total moment of inertia of the core in both principal directions is calculated to be approximately:

$$I_{\text{core}} = 152.87\,\text{m}^4,$$

which exceeds the previously estimated target value of $128\,\text{m}^4$. However, it is anticipated that this value will significantly decrease once openings for doors are introduced into the core walls. To quantify the effect of these reductions, the core was modelled as a *3D* volume with the same external dimensions, incorporating all functional openings. This model will serve to more accurately estimate the effective moment of inertia and validate whether the structural performance remains within the required displacement limits.

To evaluate the reduction in lateral stiffness, a uniform lateral load of $10\,\text{kN}$ was applied to one face of the core, and the resulting displacement response was used to back-calculate the effective flexural rigidity. From this analysis, the effective moment of inertia in the x- and y-direction was determined to be

$$I_{xx,\text{eff}} = I_{yy,\text{eff}} = 112.317\,\text{m}^4.$$

This result lies approximately 12% below the target value of $128\,\text{m}^4$ when the assumption is made that the outriggers will have a $25\,\%$ this moment of inertia will not be sufficient. Although this reduction may be critical, previous results have shown that the introduction of outriggers can reduce lateral displacement by as much as $50\,\%$ for low values of I, as discussed in Section 5.4.4.

Nevertheless, should subsequent analyses indicate that the combined core and outrigger system fails to meet displacement limits, there remain viable design adaptations. One option is to reduce the number of door openings in the core by consolidating access points, thereby increasing the net effective stiffness. However, this comes at the expense of architectural flexibility and reduces usable floor area. A more structurally and spatially efficient alternative is to increase the thickness of the core walls, thereby improving stiffness without compromising usable interior space. This solution, however, must be balanced against constructibility and cost, as increasing wall thicknesses beyond practical limits may lead to excessive self-weight and material use, as well as complicate reinforcement detailing and formwork logistics.

Figure 6.6 presents a *3D* view of the core. On typical floors, an opening is provided at each location where a module connects to the core.
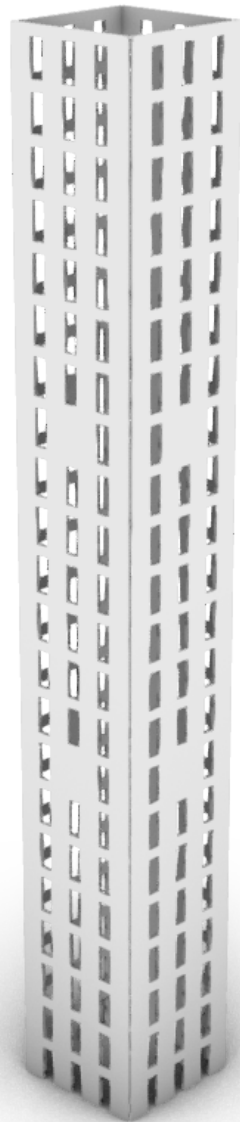
Figure 6.6: Three-dimensional model of the structural core including all functional door openings ($1.0\,\mathrm{m} \times 2.5\,\mathrm{m}$ each).

6.2.2. Outrigger Placement

For the case study model with 20 floors, the optimal locations for the outrigger levels were identified at floors 7 and 14. These positions were determined based on the *parametric* strategy outlined in Section 5.4. Figure 6.7 illustrates the integration of the outrigger and modular floors within the three-dimensional model.
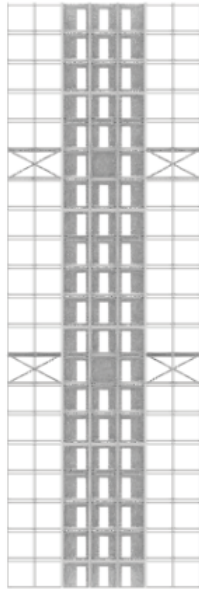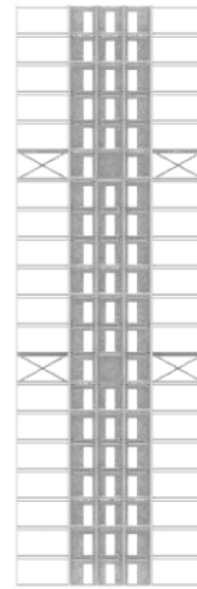
Right View   Front View
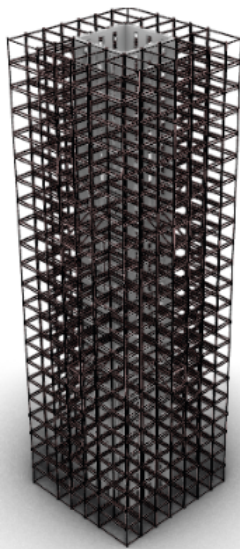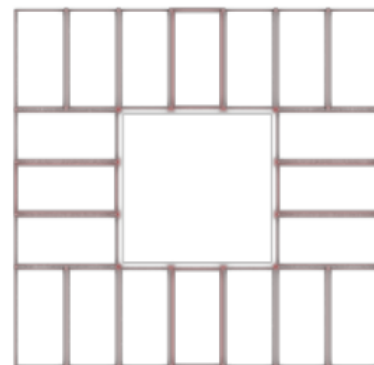
Perspective View   Top View

Figure 6.7: *3D model* with Modules and Outriggers floors

6.2.3. Core-Floor

At each outrigger level, core floors are implemented to enable effective force transfer between the core and the outriggers.

A) Core floor locations   B)   Force distribution in floor

Figure 6.8: Core floors: elevation view (left) and plan view (right).

As illustrated in Figure 6.8, the elevation view shows the vertical placement of these floors at the top and bottom of each outrigger zone. This configuration ensures that the axial forces introduced by the outrigger to core connections are properly anchored and spread across the entire core. The plan view illustrates the load paths, with the outrigger arms (highlighted in red) transferring tension forces into the floor plate, which in turn distributes these forces toward adjacent core wall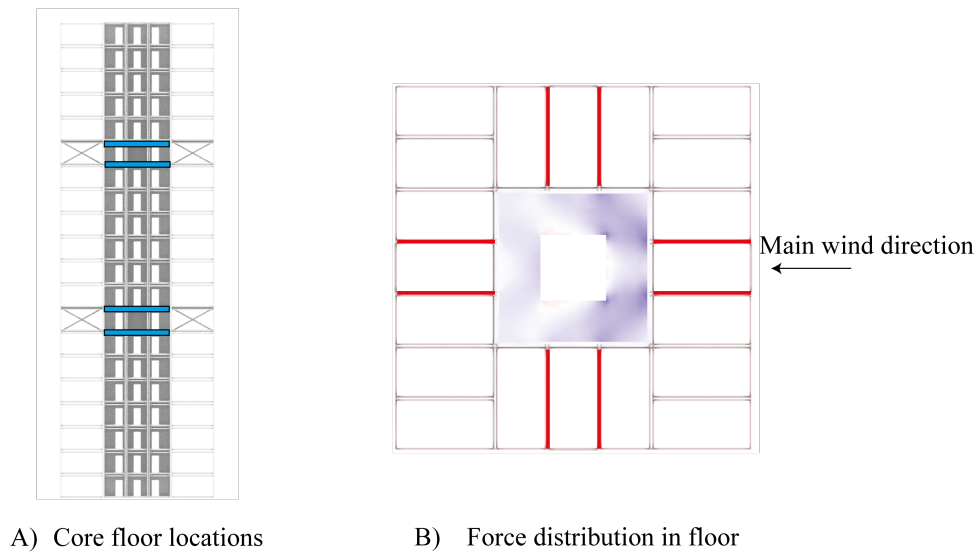s. The blue-shaded areas indicate the magnitude of tension forces within the slab, originating from the windward side of the building.

Structurally, these floors behave as in-plane diaphragms and are therefore capable of redistributing horizontal forces. However, they are unable to transfer bending moments from the core due to their construction with precast concrete elements, which lack sufficient out-of-plane stiffness. To reflect this limitation in the structural model, the connection between the core walls and the core floors is modelled using line hinges. This allows for horizontal force transfer while preventing the floors from contributing to the bending stiffness of the core.

For consistency across the *core-only*-model and *outrigger*-model, these four core floors are also included in the *core-only* configuration, even though they serve no structural purpose in that case. Their inclusion ensures that the *core-only* and *outrigger* models remain geometrically and *parametrically* equivalent, allowing for a fair comparison of system performance.

6.2.4. Connection Modelling

This section provides a visual overview of all connection types implemented in the case study model. The same connection modelling strategy used in the *2D* model has been applied. A detailed explanation of the underlying modelling principles and assumptions is provided in Section 4.3.

Intra-Modular Connection

The short-side portals of the modules are assumed to be rigid, providing significant lateral stiffness. In contrast, the intra-modular connections between columns and beams on the long-side portals are modelled as hinged. Figure 6.9 illustrates the modelling approach for the intra-modular connections. The white circles indicate the hinges introduced in the long-side portals, while the short-side portals are modelled as rigid connections.
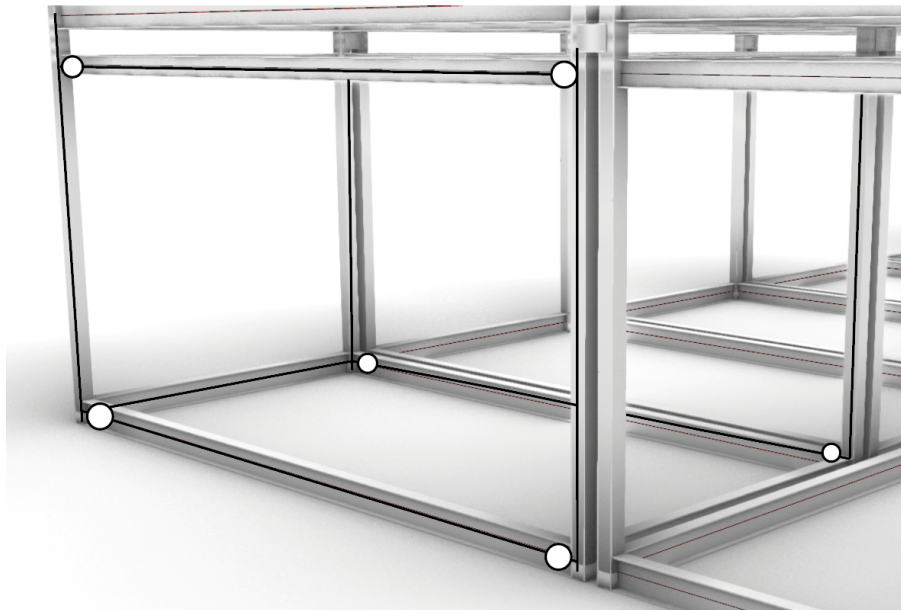
Figure 6.9: Intra-modular connection

Inter-Modular Connection

The inter-modular connection is modelled using both horizontal and vertical components. The horizontal connection is represented by a steel plate placed between adjacent modules. At the ends of this plate, rotational springs are introduced to simulate various levels of rotational stiffness. This allows for a *parametric* analysis of different connection stiffness configurations and their influence on the global stability of the structure.

The vertical connection is modelled as a direct extension of the column element. In reality, however, the connection between the upper and lower modules includes a tension rod, which resists vertical separation under lateral loading by carrying tensile forces, while the columns continue to carry compressive loads.

Since the vertical connection is modelled as a column extension with the same cross-section and material properties, the differential elongation of the tie-rod under tension is not captured. This simplification stems from a limitation in *Karamba3D*, which does not allow a single element to switch its elastic modulus depending on the direction of the internal force (tension vs. compression). To address this, a separate analysis focusing on the effect of tie-rod elongation is presented in Section 6.7.1.

Figure 6.10 shows the two types of inter-modular connections used in the model.
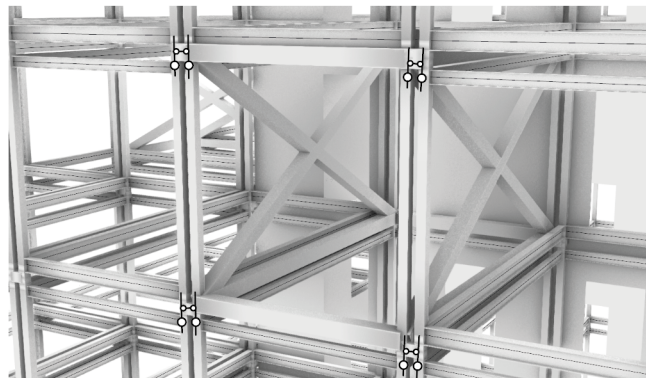

Figure 6.10: Inter-modular connection

The left side of the figure illustrates the first type of inter-modular connection, which consists solely of a vertical connection between the columns of two stacked modules. A hinge is introduced at this joint to prevent the transfer of bending moments, accurately representing the bolted nature of the real connection.

The right side of the figure shows the second type of inter-modular connection. Similar to the first type, it provides a vertical connection between stacked modules, but it also includes a horizontal connection via a steel plate. Rotational springs are placed at both ends of this horizontal plate to simulate varying connection stiffnesses; in this particular example, they are configured as fully hinged.

Module to Outrigger Connection
Figure 6.11 presents the module-to-outrigger connection.

Figure 6.11: Outrigger to module connection

As shown in Figure 6.11, the modelling approach is similar to that of the inter-modular connections. However, a key difference is that no rotational springs are applied at the ends of the horizontal steel plates in the outrigger connections; instead, these ends are modelled as hinges. This is a deliberate design choice.

By modelling the ends of the horizontal plates as hinged, the forces from the outriggers are transferred solely through the vertical stack of modules located directly above and below the outrigger level. The hinges prevent moment transfer into the horizontally adjacent modules, thereby avoiding unintended force paths. If these hinges were replaced by rigid connections, the outrigger forces would partially redistribute through neighbouring modules placed beside the outrigger floor. This would introduce eccentric load paths and torsional effects, leading to inefficient force distribution and additional stresses in parts of the structure that are not intended to carry these forces. By confining the vertical force path to a single aligned stack of modules, the outrigger loads are transferred efficiently and directly to the foundation, enhancing both structural clarity and performance.

Core Connections
Figures 6.12 and 6.13 show the two types of core connections present in the *3D* model.
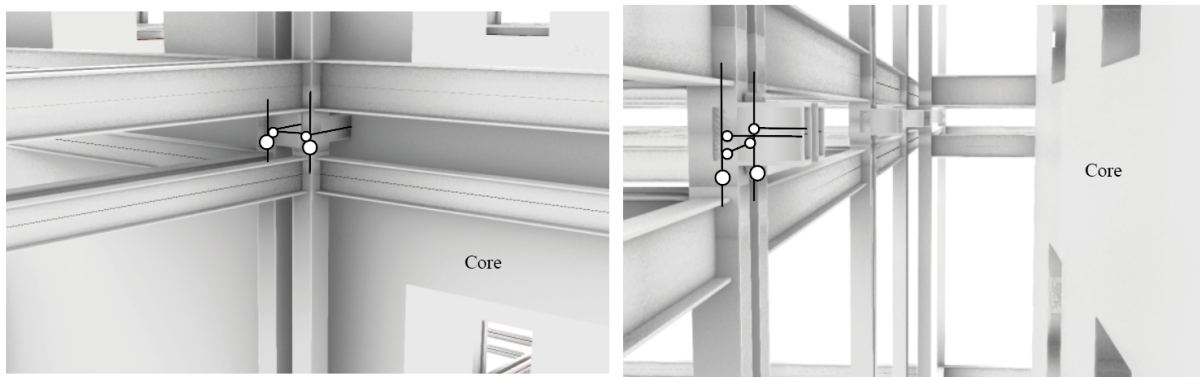
Figure 6.12: Module to core connection
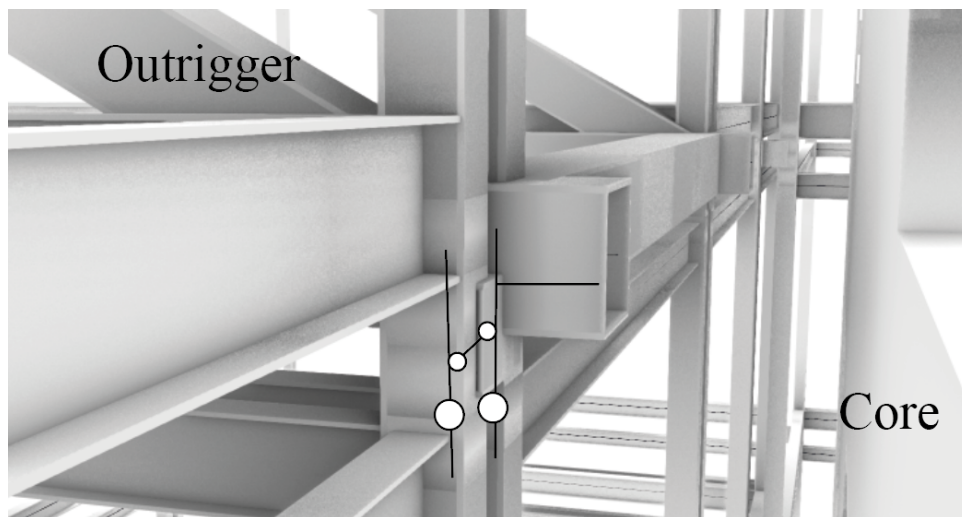
Figure 6.13: Outrigger to core connection

These connections are particularly interesting because they serve a dual purpose. As shown in Figures 6.12 and 6.13, the goal of these connections is not only to link the modules to each other or the outriggers to the modules, but also to ensure that structural loads are effectively transferred to the core.

In the case of the module to core connection, the primary function is to transfer lateral forces from the modular façade into the central core, allowing the core to act as the primary lateral load-resisting element.

By contrast, the outrigger to core connection serves a different structural role: it couples the rotational deformation of the core to axial forces in the perimeter columns. This mechanism enables the outriggers to reduce lateral displacement by converting core bending into tension and compression forces in the outer modules.

In the module to core connection (Figure 6.12), the horizontal plate is rigidly connected to the core and linked to the inter-modular connection via a rotational spring. In the configuration shown, the rotational springs are modelled as hinges; however, their stiffness can be adjusted to study the effect of varying connection rigidities on the global lateral stiffness of the building.

In the outrigger to core connection (Figure 6.13), a similar approach is applied. However, in this case, the horizontal connection with the core is directly connected to the outrigger beams, and no rotational spring is included. The connection between the outrigger and the core is assumed to be fully rigid.

6.3. Structural Component Overview

This section provides an integrated overview of the main structural components.

6.3.1. Structural Elements

Table 6.1 lists all primary load-bearing components by subsystem, including their materials, strengths, and cross-sectional specifications.

Component	Material	Steel Grade	Strength	Cross-section / t
Modular Unit Elements				
Column	Steel	S355	–	SHSH120x12.0
Top Beam	Steel	S355	–	IPE160
Bottom Beam	Steel	S355	–	IPE220
Floor	Concrete	–	C35/45	6 cm
Roof	Wood		E1/E2	1.2 cm
	(OSB/3)		350/140 $\mathrm{kN/cm^2}$ [55]	
Outrigger Elements				
Column	Steel	S355	–	SHSH120x12.0
Diagonal	Steel	S355	–	SHSH200x10.0
Top Beam	Steel	S355	–	SHSH200x10.0
Bottom Beam	Steel	S355	–	SHSH200x10.0
Core				
Walls	Concrete	–	CR50/60	30 cm

Table 6.1: Overview of structural elements by subsystem

6.3.2. Structural Connections

Table 6.2 provides an overview of the structural connections between modular units, outriggers, and the central core. These include both horizontal and vertical links, with material and steel grade specifications.

Connection Type	Material	Steel Grade	Cross-section
Module to Module connection			
Horizontal	Steel	S355	FL 120X15
Vertical	Steel	S355	SHSH120x12.0
Module to Outrigger connection			
Horizontal	Steel	S355	FL 120X15
Vertical	Steel	S355	SHSH120x12.0
Core connection			
Module to Core	Steel	S355	FL 120X40
Outrigger to Core	Steel	S355	FL 120X40

Table 6.2: Overview of structural connection types and properties

6.4. Applied loads

This section will give an overview of the applied loads in the *3D* model.

6.4.1. Wind Loads

The wind loads applied to the *3D* model are determined using a simplified method derived from Eurocode 1 (EN 1991-1-4), which governs wind actions on rectangular buildings. A detailed overview of the load calculation procedure is provided in Section 4.4.1. The building parameters are visualised in Figure 6.14 and the values of the parameters are summarised in Table 6.3.
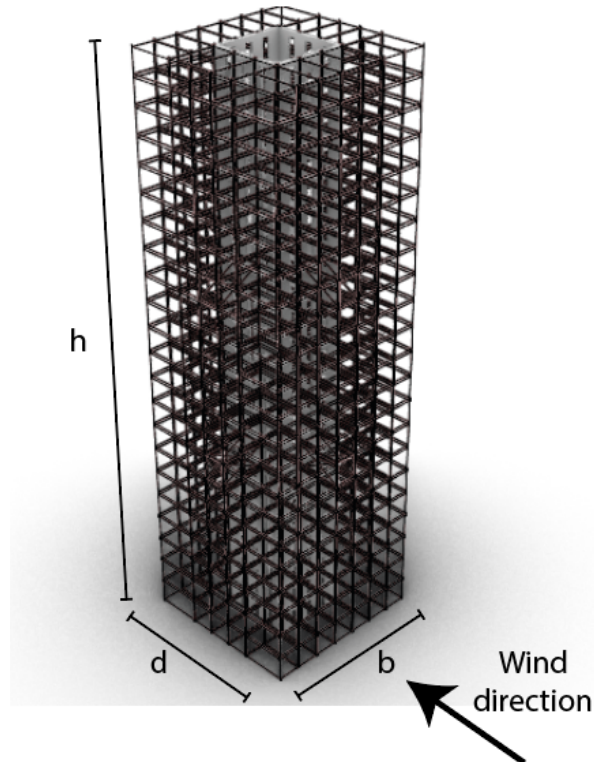
Figure 6.14: The building parameters of *3D* model

Parameter	Description	Value [m]
h	Total height of the building	67.7
d	Length in wind direction	21.88
b	Length perpendicular to wind direction	22.32
h/d	Slenderness ratio	3.10
e	Reference façade width (min(b, $2h$))	22.32

Table 6.3: Overview of geometric building parameters used for wind load calculations.

The structure is located in wind region 2 with open terrain exposure, where the Dutch National Annex specifies peak velocity pressures for different height intervals. With a height of 67.7 m and a windward length of 21.88 m, the building has an h/d ratio of approximately 3.1.

Accordingly, façade wind zones are defined using the Eurocode configuration for wide buildings. The corresponding external pressure coefficients c_f are linearly interpolated between the values for $h/d = 1$ and $h/d = 5$, as shown in Table 6.4, and are used to convert wind pressures into equivalent façade forces.

h/d ratio	Zone A	Zone B	Zone C	Zone D	Zone E
3.1	-1.2	-0.8	-0.5	+0.8	-0.63

Table 6.4: External pressure coefficients c_f for different façade zones at $h/d \approx 3.1$

Because the building height exceeds twice its width perpendicular to the wind direction, the façade is vertically subdivided into three strips. The first and third zones each have a height equal to the building width ($b = 22.32$ m), while the middle zone occupies the remaining height ($h - 2b = 23.06$ m). This results in the following vertical divisions:

Zone	Height range [m]	Peak velocity pressure $q_{p,ze}$ [kN/m^2]
1	0.00 – 22.32	1.07
2	22.32 – 45.38	1.38
3	45.38 – 67.7	1.50

Table 6.5: Vertical subdivision of the façade and corresponding peak velocity pressures for wind region 2.

To model wind action on the façade, the surface is subdivided both horizontally and vertically. Since the façade width e is greater than its depth d, only zones A, B, D, and E are considered; zone C is excluded from the analysis. Horizontally, the façade is segmented into these four wind zones based on the geometry-dependent pressure coefficients. Vertically, the façade is divided into three height strips that correspond to variations in wind pressure along the height.
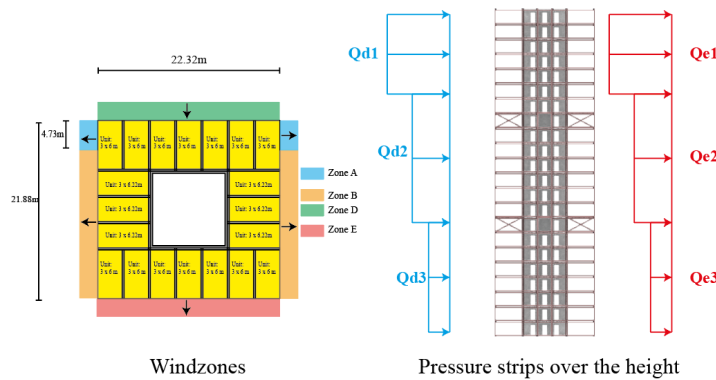
Figure 6.15: Eurocode-based façade wind zones (left) and vertical pressure strips (right).

For each façade and height zone, the reference area A_{ref} is determined by multiplying the façade zone width with the corresponding height strip. These areas serve as input for calculating the wind forces acting on each zone. The calculated reference areas are summarised in Table 6.6.

Height zone (height [m])	Zone A A_{ref} [m^2]	Zone B A_{ref} [m^2]	Zone D A_{ref} [m^2]	Zone E A_{ref} [m^2]
0–22.32	97.67	390.68	498.18	498.18
22.32–45.38	100.91	403.64	514.70	514.70
45.38–67.70	97.67	390.69	498.18	498.18

Table 6.6: Updated reference areas A_{ref} per façade zone and height zone, based on corrected geometry.

Wind forces are determined separately for each façade and height zone using the simplified wind load equation from Section 4.4.1. Zone D is subject to positive pressure on the windward side, while zones A, B, and E experience suction. Table 6.7 presents the resulting wind forces per façade and height segment.

Height zone [m]	Zone A [kN]	Zone B [kN]	Zone D [kN]	Zone E [kN]
0–21	-125.41	-334.43	426.44	-335.82
21–49	-167.11	-445.62	568.23	-447.48
49–70	-175.81	-468.83	597.82	-470.78

Table 6.7: Wind force per façade zone and vertical height segment.

The resulting point loads are then distributed over the top and bottom façade beams at the column-beam intersections, as outlined in Section 4.4.1.

6.4.2. Permanent and Variable Loads

In the *3D* structural model, the modular unit is fully represented, and all primary structural elements of the modules are explicitly modelled. Therefore, most self-weight contributions are inherently included through the material properties and geometry of the elements. However, some components, such as the ceiling, walls, and floor, as well as additional partitioning and variable loads, are introduced separately.

Self-weight of the components present

The self-weight of the components that are explicitly modelled in the *3D* model is summarised in Table 6.8. This includes columns, beams in both directions.

Table 6.8: Self-weight of modelled structural components per column

Component	G (kg/m or kN/m^2)	Dim. (m)	Amount	A (m^2)	Total G (kN)
Columns	40.90 kg/m	3.00	4	–	4.81
Top beam (trans.)	15.80 kg/m	3.00	2	–	0.93
Top beam (long.)	15.80 kg/m	6.00	2	–	1.86
Bottom beam (trans.)	26.20 kg/m	3.00	2	–	1.54
Bottom beam (long.)	26.20 kg/m	6.00	2	–	3.08
			Total self-weight		12.23 kN
			Weight per column		3.06 kN

When applying the gravity load in the *Grasshopper* model, the resulting value is approximately $3.12\,kN$, which is sufficiently accurate.

Additional Self-weight

The self-weight of the floor, ceiling, and walls is applied as vertical point loads on the columns. Table 6.9 shows the distributed weight per component, divided over the top and bottom column intersections.

Table 6.9: Self-weight of non-structural components per column

Component	Location	Area (m^2)	G (kN/m^2)	Total (kN)	Per column (kN)
Ceiling	Top	18.00	0.40	7.20	1.80
Floor	Bottom	18.00	1.75	31.50	7.88
Walls (longitudinal)	Bottom	18.00	0.50	18.00	4.50
Walls (transverse)	Bottom	9.00	0.50	9.00	2.25
			Total on one top column		1.8 kN
			Total on one bottom column		14.63 kN

Variable loading

Variable loads are applied according to residential Class A occupancy. A live load of $1.75\,kN/m$ is applied on the floor area, together with a partition wall load of $0.5\,kN/m$ to account for interior separations. These loads act on the bottom beam–column intersections. Additionally, a roof live load of $1.0\,kN/m$ is applied.

Table 6.10: Variable loads per column

Load type	Location	Area (m^2)	Q (kN/m^2)	Total (kN)	Applied at	Per column (kN)
Live load (Class A)	Floor	18.00	1.75	31.50	Bottom	7.875
Partition wall load	Floor	18.00	0.50	9.00	Bottom	2.25
Roof load	Roof	18.00	1.00	18.00	Top	4.50
			Total bottom load per column			10.125 kN
			Total top load per column			4.50 kN

Governing Load Combination

The same governing load combinations that were used for the *2D* analysis are also applied in the *3D* model.

$$L_{01} = 1.2 \cdot G_{k/sup} + 1.5 \cdot F_w + 1.5 \cdot \psi_0 \cdot Q_{K1} \tag{6.1}$$

$$L_{02} = 0.9 \cdot G_{k/inf} + 1.5 \cdot F_w + 0 \tag{6.2}$$

It is expected that the maximum compression forces in the structural elements will still result from the first combination and that the second combination is likely to govern the maximum tensile forces in the structure, due to the reduced permanent load factor and the exclusion of other variable actions.

6.5. Performance Evaluation and Structural Analysis

This section presents the structural performance evaluation of the case study building using the *3D* model. The aim is to assess the global behaviour of the optimized structural concept and to compare it with trends identified in the *2D* analysis. A key addition in this phase is the evaluation of vertical displacement differences between adjacent stacks of modules, which could not be captured in the *2D* model.

6.5.1. Global Analysis

The global analysis first examines the load transfer mechanism, followed by the lateral deformation behaviour of the structure. This includes the top deflection, inter-story drift, and the vertical displacement difference between stacked vertical modules.

Load Transfer Mechanism
Figure 6.16 shows the distribution of normal forces in the *3D* model under load combination L_{02}.
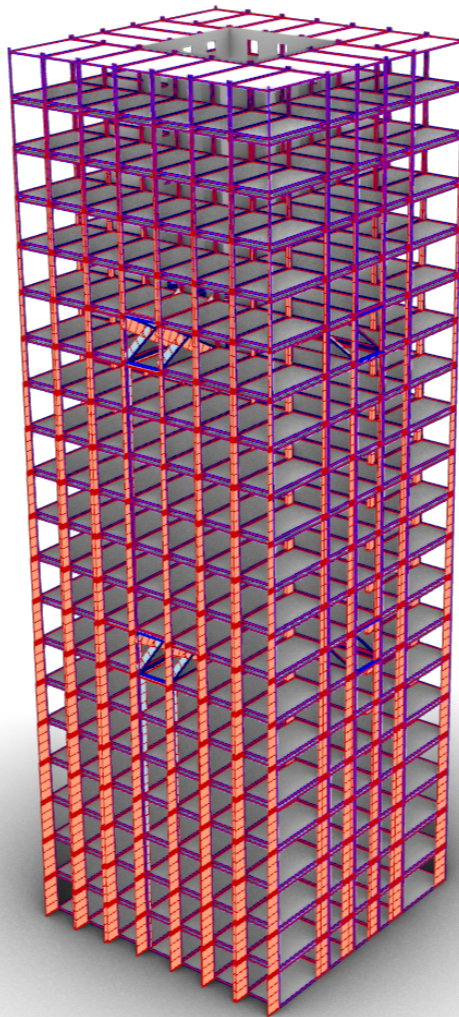
Figure 6.16: Global normal force distribution under load combination L_{02}.

As observed in the *2D* model, the outriggers redistribute vertical forces within the stack of modules located directly beneath each outrigger. This region again experiences the highest tension force in the structure, with a peak value of $187\,\text{kN}$.

Figure 6.17 highlights the region where the outrigger introduces normal forces into a single vertical stack of modules.
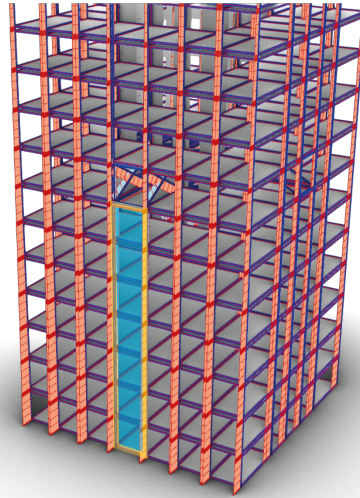
Figure 6.17: Zoomed-in view of activated vertical modules under the outriggers.

The figure shows that only the vertical modules located directly beneath the outriggers are activated in tension. This behaviour confirms the intended load path of the concept: the forces introduced by the outriggers are concentrated along a single, continuous stack of modules extending down to the foundation, thereby minimising load redistribution to adjacent vertical module stacks.
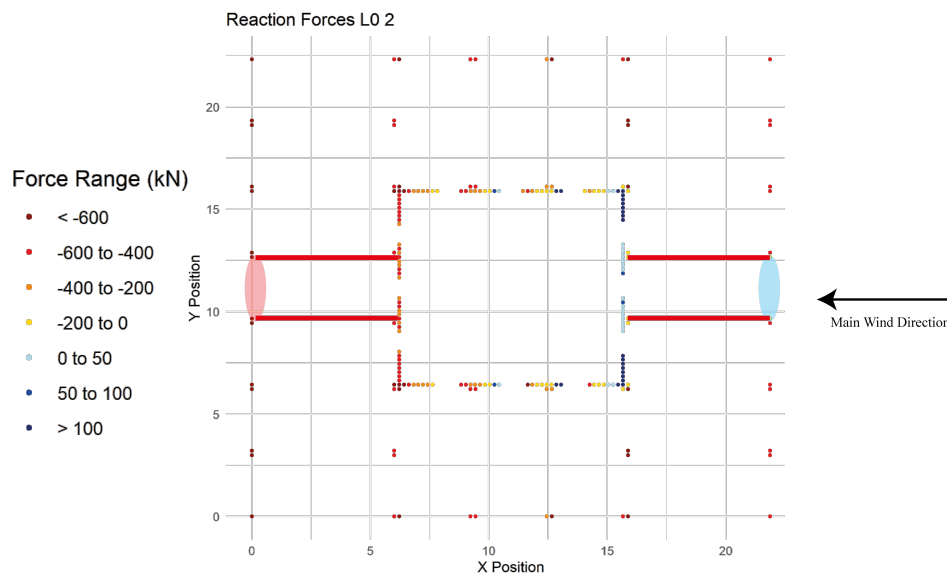
Figure 6.18 shows the distribution of vertical support reactions in the *3D* model under load combination L_{02}.

Figure 6.18: Vertical support reactions under load combination L_{02}.

The figure reveals a clear contrast in vertical support reactions between module stacks connected to an outrigger and those that are not. On the windward side, compressive reactions decrease beneath the outrigger-connected modules (blue zone), while on the leeward side, vertical support reactions increase (red zone). Support reactions in adjacent, non-connected stacks remain largely unchanged. This indicates that axial forces from the outriggers are transmitted vertically through the connected stack, with minimal redistribution to neighbouring columns. This confirms the intended behaviour of a concentrated load transfer path.

Comparison with 2D Results

To investigate whether the results of the *3D* model are comparable to those of the earlier *2D* analysis, a new comparison model was developed. Since the geometry of the original *2D* models did not directly correspond to the *3D* case study, a revised *2D* model was created with matching characteristics. This model includes 20 floors, outrigger levels at floors 7 and 14, and identical cross-sections to those used in the *3D* model.

Figure 6.19 shows a side-by-side comparison of the newly created *2D* model and the original *3D* case study model.

Case study-model
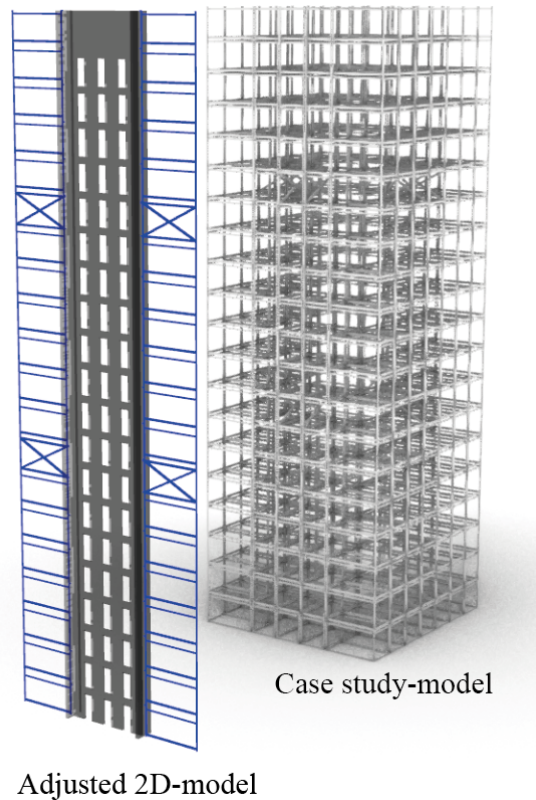
Adjusted 2D-model

Figure 6.19: Comparison between the updated *2D* model (left) and the *3D* case study model (right).

In the adjusted *2D* model, the maximum axial tension force in the module columns was $214\,\mathrm{kN}$ under load combination L_{02}, while the maximum compression force reached $846\,\mathrm{kN}$ under load combination L_{01}.

By comparison, the *3D* model exhibits a lower peak tension force of $187\,\mathrm{kN}$, occurring in the module column directly beneath the outrigger on the windward side. The maximum compression force is $747\,\mathrm{kN}$, located in the corresponding column on the leeward side at ground level.

This reduction in both tension and compression forces can be attributed to the increased stiffness of the core in the *3D* model. Owing to its greater flexural rigidity, the core absorbs a larger portion of the lateral loads, thereby reducing the contribution required from the outrigger system. As a result, the axial forces induced in the module columns are lower than those observed in the *2D* model.

6.5.2. Deformation Behaviour

Lateral Deformation Behaviour

Figure 6.20 presents the side view of the deformed *3D* model under load combination L_{02}, comparing the *core-only* configuration with the proposed *outrigger* system.
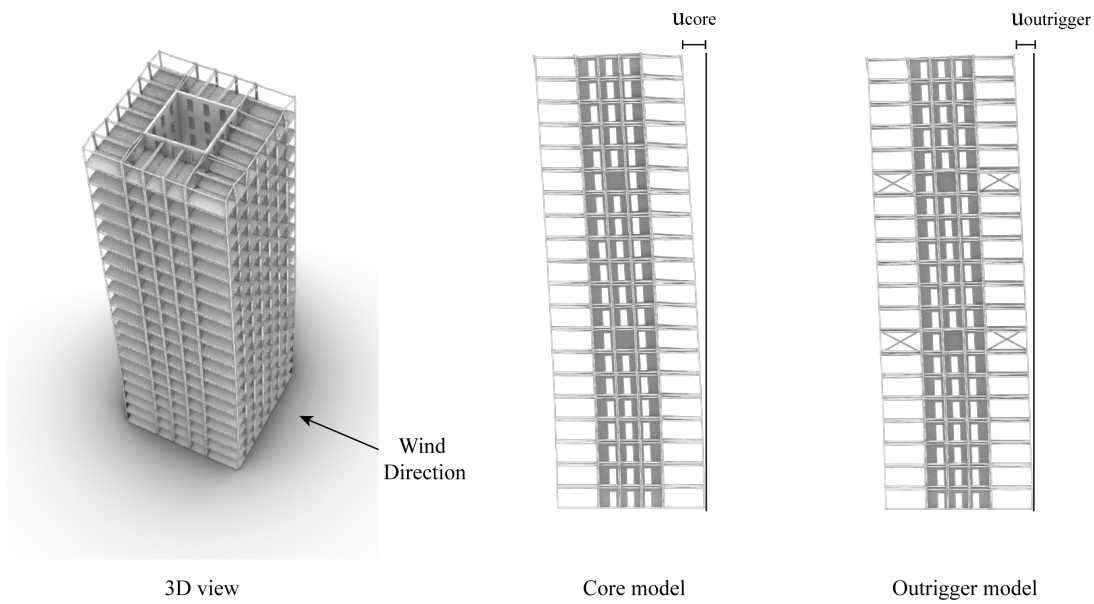
Figure 6.20: Overview of lateral displacement for *core-only* and *outrigger* system.

Top deflection

Figure 6.21 shows on the left side the global deformation pattern of the *core-only* system and on the right side the *outrigger* system.
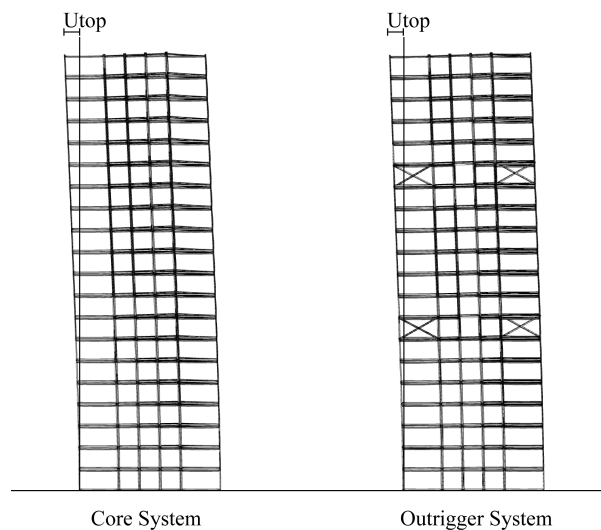
Figure 6.21: Top deflection of the *core-only* and the proposed *outrigger* system.

The maximum top displacement is recorded under load combination L_{02}. The top displacement of the *core-only* model is $0.01\,\mathrm{m}$, while the displacement in the *outrigger* system is reduced to $0.088\,\mathrm{m}$. This corresponds to an approximate $13.6\,\%$ decrease in top displacement, highlighting the improved lateral stiffness provided by the *outrigger* system.

Inter-story Deflection

Inter-story drift refers to the relative horizontal displacement between two consecutive floors and serves as a key indicator of a structure's deformation response under lateral loading. Excessive inter-story drift can lead to non-structural damage, such as façade cracking, partition failure, and occupant discomfort [56].

The drift is calculated as the difference in lateral displacement between adjacent floor levels, normalized by the inter-story height:

$$\text{Interstory Drift} = \frac{\Delta_i - \Delta_{i-1}}{h} \tag{6.3}$$

where Δ_i and Δ_{i-1} are the lateral displacements of the upper and lower floors, respectively, and h is the inter-story height.

Figure 6.22 indicates the location at which the inter-story drift was evaluated in the model.
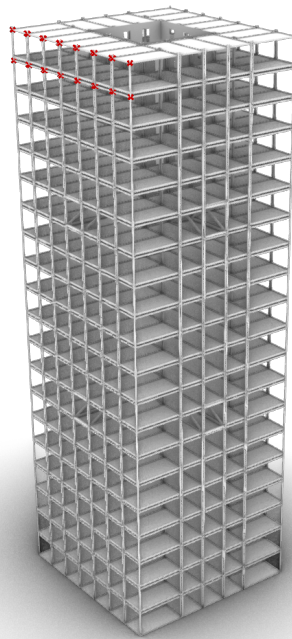
Figure 6.22: Location of inter-story drift evaluation (red points on the structure).

The largest inter-story drift occurs at the uppermost levels of the structure. In the proposed *outrigger* system, the lateral displacement at the top floor is $0.088\,\text{m}$, while the floor below displaces $0.083\,\text{m}$. Given an inter-story height of $3.0\,\text{m}$, the resulting drift is:

$$\text{Drift} = \frac{0.088 - 0.083}{3.0} = 0.00167$$

This corresponds to a drift ratio of approximately $\frac{1}{599}$, which is well within the commonly accepted serviceability limit of $\frac{1}{300}$.

Interestingly, the maximum inter-story drift occurs at the top of the structure, which is somewhat counterintuitive. Typically, peak drift is expected at mid-height or lower, where curvature in the lateral displacement profile is greatest. However, the inclusion of fixed outrigger floors significantly alters the deformation shape, stiffening the structure at intermediate levels and shifting the maximum inter-story drift towards the top.

Vertical Displacement Difference

An important phenomenon not captured in the earlier *2D* models is the vertical displacement mismatch between adjacent stacks of modules. These differences arise from variations in deformation behaviour between different structural components within the system. In the *3D* model, two primary factors contribute to these mismatches.

First, the deformation of the core induces vertical movement in the directly connected modules. Second, there is a deflection difference between module stacks that include outrigger levels and those that do not.

Vertical Deflection Due to Core Deformation

Figure 6.23 illustrates the first cause of vertical displacement differences between adjacent stacked modules.

A)Core Deflection Pattern   B) Modules with and without core connection
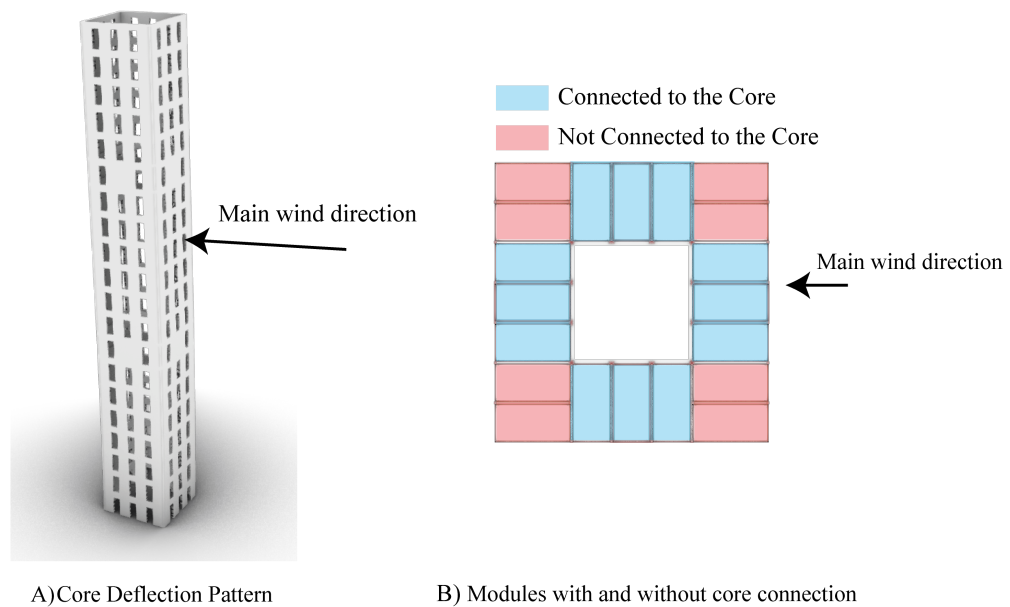
Figure 6.23: Core deformation and location of core-connected modules (blue) and unconnected modules (red).

The image on the left shows the horizontal deformation of the core, and the right side presents the floorplan, highlighting modules that are directly connected to the core in blue, and those not connected in red.

Under load combinations L_{01} and L_{02}, the core undergoes horizontal displacement in the direction of the wind. Modules directly attached to the core are forced to follow this movement. However, the corner modules are not physically connected to the core and thus do not experience the same displacement. This deformation difference leads to relative vertical displacements between adjacent modules and is one of the primary causes of the vertical mismatch observed in the case study model.

Figure 6.24 shows the division between the two groups of vertically stacked modules in a *3D* view.
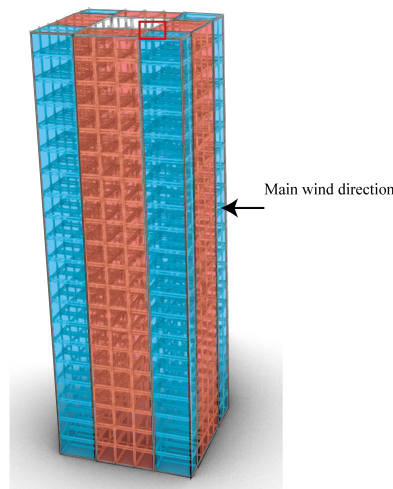
Figure 6.24: 3D visualization of vertically stacked module groups.

Figure 6.25 illustrates the vertical displacement difference on the windward side under load combination L_{02}.

A) Corner Modules   B) Vertical deflection Difference
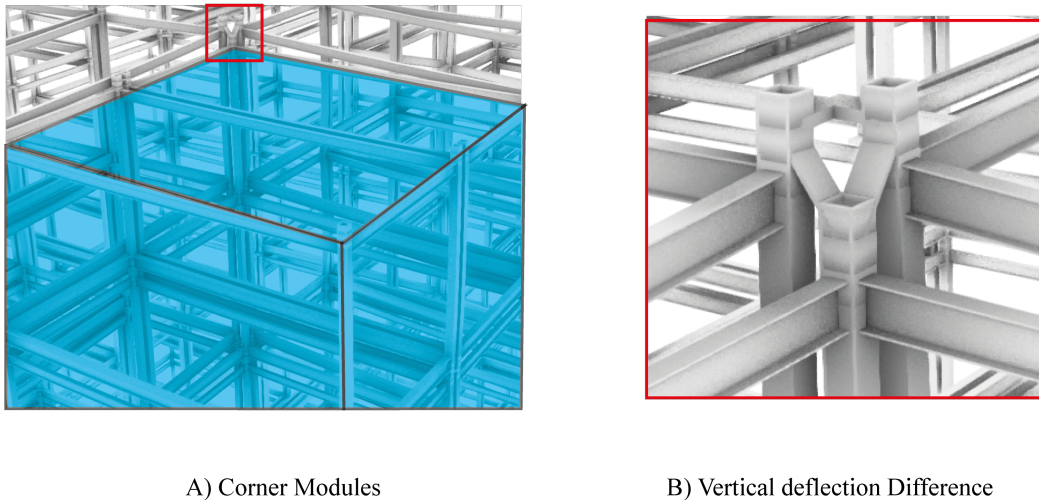
Figure 6.25: Vertical displacement difference between connected and unconnected modules on the windward side.

On the windward side, the stack of modules not connected to the core is positioned lower than the core-connected stack. This occurs because the core deforms in the direction of the wind and pulls the attached modules upward. The unconnected modules are not subjected to this movement and therefore remain lower, resulting in a vertical displacement mismatch between adjacent stacks of modules.

On the leeward side, the opposite effect is observed. The core deformation pushes the connected modules downward, creating a compressive effect. The adjacent unconnected modules do not follow this displacement and consequently appear higher than the core-connected modules next to them.

Figure 6.26 shows the locations of the maximum vertical deflection differences caused by core deformation. These critical locations are highlighted with red boxes.
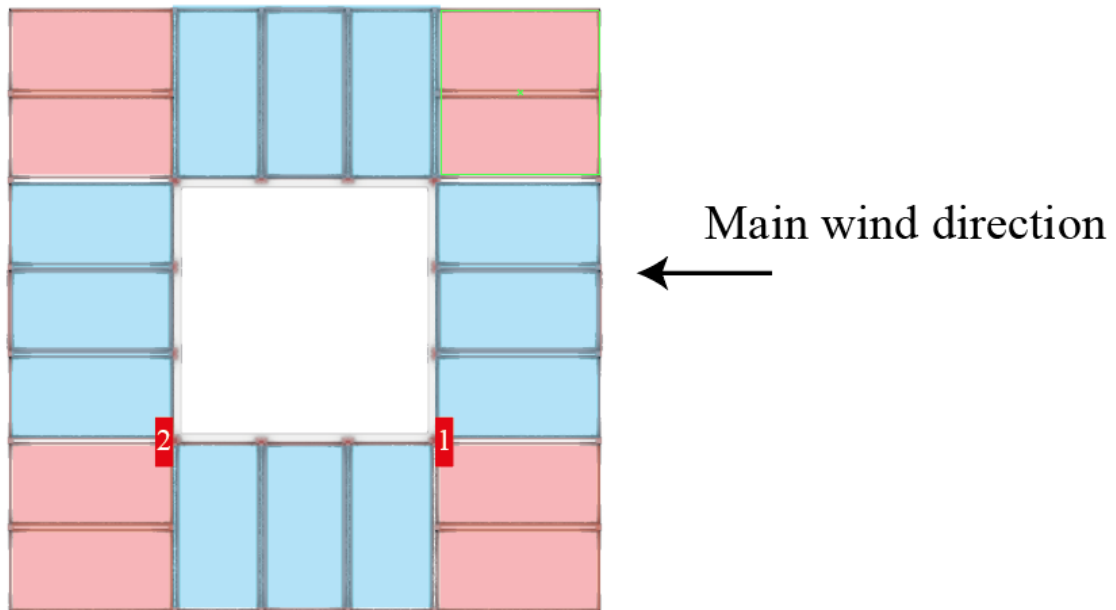
Figure 6.26: Location of maximum vertical displacement difference due to core deformation

Table 6.11 summarizes the corresponding values of the vertical displacement difference on both the windward and leeward sides.

Table 6.11: Maximum vertical displacement differences caused by core deformation

Location	Vertical Displacement Difference [m]
Windward side (Red box 1)	- 0.017
Leeward side (Red box 2)	0.002

The results show that the vertical displacement difference is most pronounced on the windward side of the structure, with a maximum value of $17\,mm$. This displacement is relatively high when considering typical finishing tolerances. Such differential displacements can lead to issues with the alignment of interior finishes, floor coverings, and the performance of the inter-modular connections. On the leeward side, the mismatch is considerably smaller with the maximum value equal to $2\,mm$.

These findings emphasize the need to carefully address differential vertical displacements in the design phase, especially at module interfaces where finish continuity is required.

Vertical Displacement Difference Due to Outrigger Presence

The second cause of vertical displacement differences in the case study arises from the presence of outriggers within vertically stacked modules.

Figure 6.27 shows the division between vertical module stacks that include outriggers and those that do not.
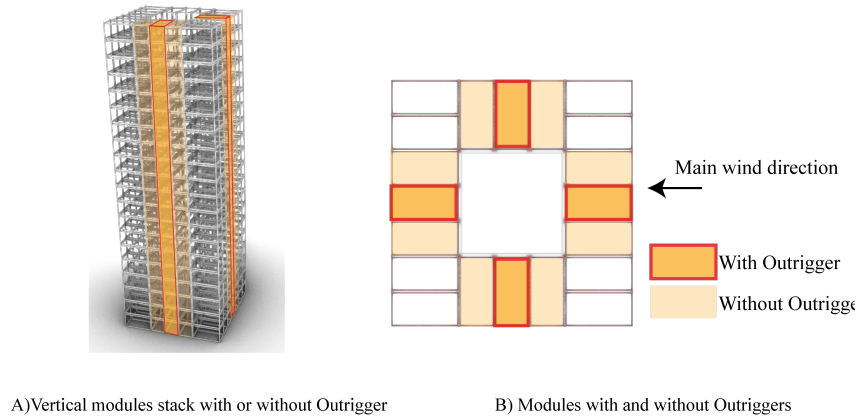
A)Vertical modules stack with or without Outrigger   B) Modules with and without Outriggers

Figure 6.27: *3D* view and floorplan indicating vertical stacks with and without outriggers.

On the left, a *3D* representation distinguishes between stacks with and without outriggers. The corresponding floorplan on the right highlights the same distinction.

Figure 6.28 visualizes the vertical deflection differences at the top of the structure between module stacks with and without outriggers.
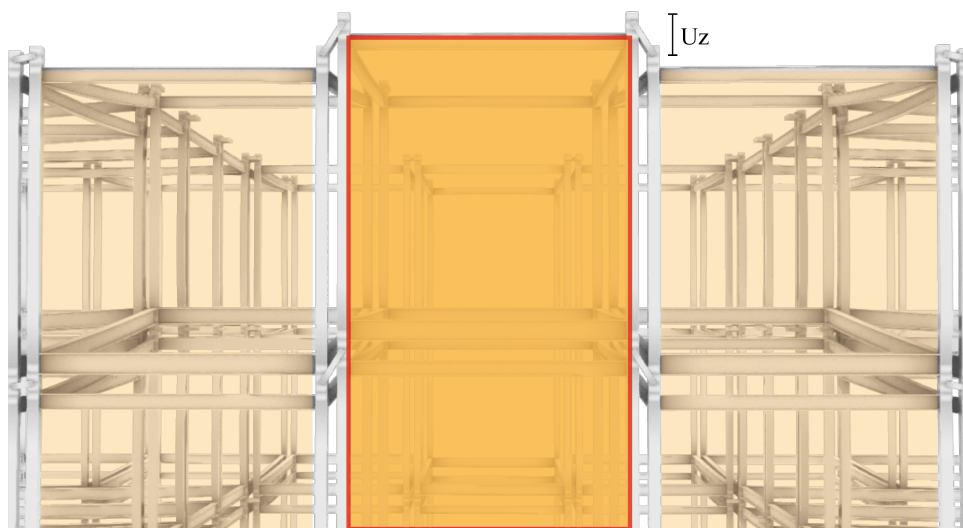
Figure 6.28: Vertical displacement difference between stacked modules on the windward side.

The presence of outriggers increases the vertical stiffness of the stacks in which they are installed. On the windward side, this added stiffness is associated with tensile forces transmitted from the core to the perimeter, resulting in an upward vertical displacement. On the leeward side, the outriggers induce compressive forces, which lead to additional downward displacement.

As a result, the modules in outrigger-aligned stacks are vertically offset relative to adjacent stacks without outriggers: they are slightly higher on the windward side and lower on the leeward side.

Figure 6.29 shows the locations where the maximum vertical displacement differences occur between stacks with and without outriggers.
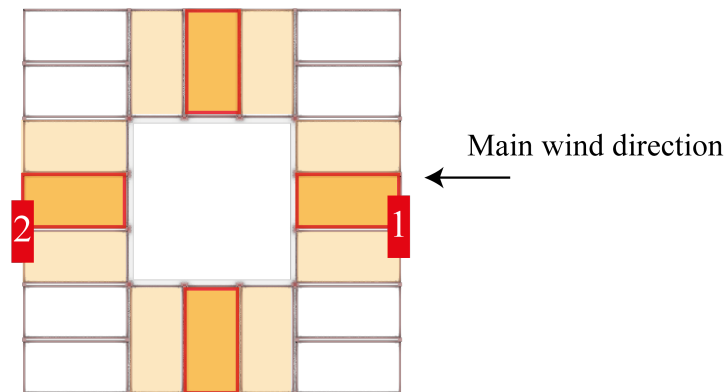
Figure 6.29: Locations of maximum vertical displacement differences between stacks with and without outriggers.

The measured differences under load combinations L_{01} and L_{02} are summarized in Table 6.12.

Table 6.12: Maximum vertical displacement differences caused by outriggers.

Location	L_{01} [m]	L_{02} [m]
Windward side (Red box 1)	0.016	0.013
Leeward side (Red box 2)	-0.004	-0.007

The results indicate that vertical displacement differences due to the presence of outriggers can reach up to $16\,\mathrm{mm}$ on the windward side. On the leeward side, differences between stacks with and without outriggers range from 4 to $7\,\mathrm{mm}$.

Both sources of vertical displacement mismatch, core deformation and outrigger presence, can lead to misalignment between adjacent modules if not properly addressed. Section 6.7.3 will explore potential strategies to mitigate these mismatches and reduce them to more acceptable levels through connection design.

6.6. Performance Criteria

This section evaluates the case study model against the performance criteria defined in Section 5.2. It assesses lateral top displacement, tie-rod tension capacity under load case L_{02}, and the utilisation of key structural members.

6.6.1. Lateral Displacement Criteria

Figure 6.30 shows the top displacement of the *core-only* and *outrigger* models under load case L_{02}.

Ucore   Uoutrigger

Wind
Direction

3D view   Core model   Outrigger model
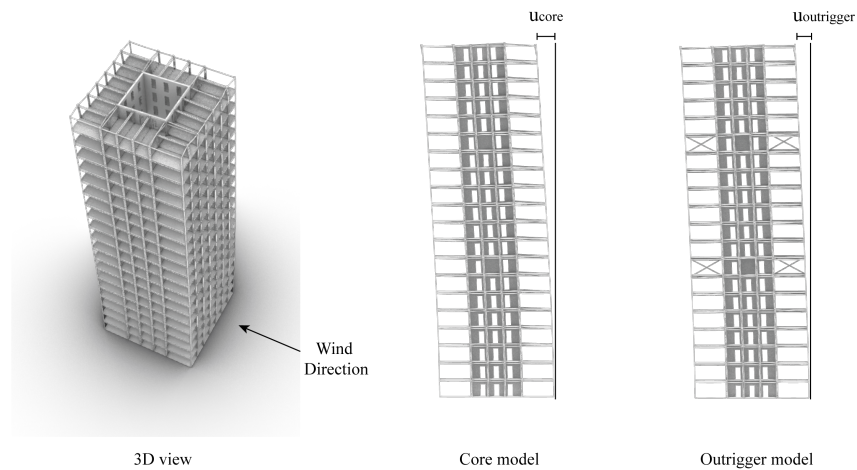
Figure 6.30: Overview of top deflection.

Table 6.13 compares the top displacement values retrieved from the global analysis in Section 6.5.1.

Table 6.13: Top displacement comparison between the *core-only* and proposed *outrigger* model.

Model	Top Displacement [m]
Core-only	0.101
Outrigger (floors 7–14)	0.088

The addition of outriggers reduces the top displacement by $13.5\,\%$, from $0.101\,\mathrm{m}$ to $0.088\,\mathrm{m}$. This value remains within the top displacement limit of $67.7/750 = 0.0903\,\mathrm{m}$, confirming that the model satisfies the lateral deflection criterion.

Displacement-Based Height Evaluation

As the *core-only* model exceeds the allowable top displacement, an important question is up to what height this configuration remains feasible.To explore this, a *parametric* study was performed in which all parameters were held constant except for the total building height.

The *core-only* model reached the serviceability limit of $0.072\,\mathrm{m}$ at a height of $54.2\,\mathrm{m}$, indicating limited applicability for taller buildings. In contrast, the proposed *outrigger* model remained within allowable limits up to $67.7\,\mathrm{m}$, confirming its feasibility for structures approaching the target height of $70\,\mathrm{m}$.

6.6.2. Tie-rod Capacity Criteria

Under load combination L$_{02}$, the maximum axial tension force observed in the tie-rod system is $187\,kN$. This value defines the minimum required capacity for the tie-rod configuration and is highlighted as a red dashed line in the following figures.

Figure 6.31 shows how both yield and ultimate tensile capacity increase with diameter for a fixed steel grade (8.8).
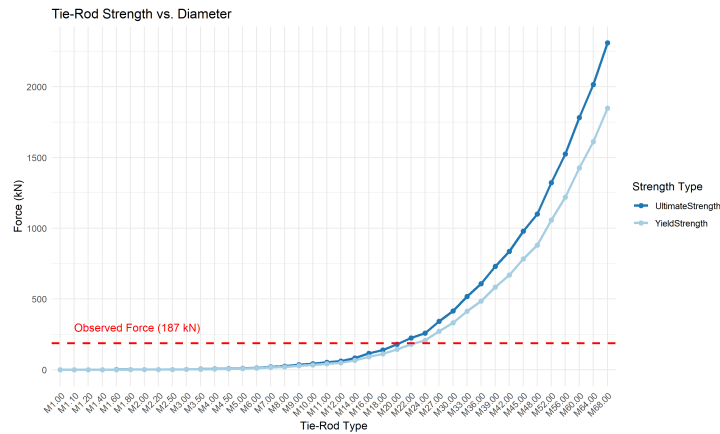
Figure 6.31: Tie-rod yield and ultimate strength vs. diameter for steel grade 8.8.

Based on the plot, tie-rods of M22 or smaller fail to meet the $187\,kN$ requirement, while an M24 rod in grade 8.8 marginally satisfies the yield criterion.

Figure 6.32 compares the yield strength of tie-rods across different steel grades (4.8–12.9) for selected diameters.
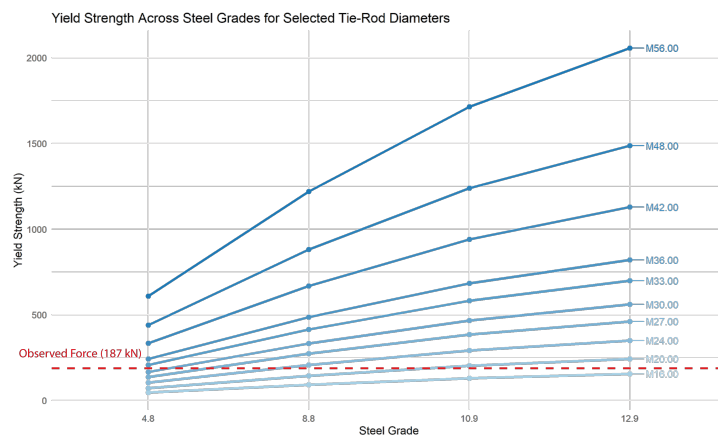
Figure 6.32: Yield strength across steel grades for selected tie-rod diameters.

To safely withstand a maximum tensile force of 187 kN: For steel grade 8.8, a tie-rod of at least M24 is required and for higher steel grades (e.g. 10.9 or 12.9), M20 may suffice.

In the current structural model, the elongation of tie-rods under tension is not explicitly captured. Since axial elongation may reduce the effectiveness of the outrigger system, this simplification may lead to an overestimation of lateral stiffness. To investigate the influence of this phenomenon, a dedicated analysis was carried out in Section 6.7.1.

6.6.3. Utilisation Criteria

The structural utilisation of components in the case study model is assessed based on the methodology outlined in Section 5.2.3. As defined, the utilisation factor (η) expresses the ratio between the applied design action and the corresponding design resistance. To ensure structural safety, this factor should remain below unity:

$$\eta = \frac{S_{\text{Ed}}}{S_{\text{Rd}}} < 1.0 \tag{6.4}$$

Utilisation values were calculated with the *Karamba3D Utilisation*-component for all primary structural members, considering the governing load combinations L_{01} and L_{02}. An explanation of the underlying theory of this component, along with a validation example, is provided in Appendix K.

Table 6.14 summarises the average maximum utilisation values per component type and load case.

Component	Material	Steel Grade	Cross-section	Thickness (cm)	Uti L_{01}	Uti L_{02}
Modular Unit Elements						
Column	Steel	S355	SHSH 120×12	–	0.635	0.513
Top Beams (Big)	Steel	S355	IPE160	–	0.077	0.058
Top Beams (Small)	Steel	S355	IPE160	–	0.133	0.133
Bottom Beams (Big)	Steel	S355	IPE220	–	0.058	0.045
Bottom Beams (Small)	Steel	S355	IPE220	–	0.075	0.069
Outrigger Elements						
Column	Steel	S355	SHSH 120×12.5	–	0.573	0.484
Diagonal	Steel	S355	SHSH 200×10	–	0.184	0.154
Top Beam	Steel	S355	SHSH 220×10	–	0.113	0.107
Bottom Beam	Steel	S355	SHSH 200×10	–	0.114	0.107
Core Elements						
Walls	Concrete	C50/60 CR	–	30	**2.113**	**2.407**
Floors	Concrete	C50/60 CR	–	30	0.578	0.508

Table 6.14: Summary of component utilisations under load combinations L_{01} and L_{02}

While most structural components exhibit safe utilisation levels well below the critical threshold of 1.0, an exception is observed in the concrete core walls. Under load combination L_{01}, the maximum utilisation reaches 2.113, increasing to 2.407 under L_{02}. These values indicate local overstressing and highlight the need for further investigation.

Overutilisation in Core Walls

To investigate these overtulisation of the core walls, the distribution of utilisation values across the wall mesh are analysed.

Table 6.15 presents the statistical summary of the core utilisation.

Table 6.15: Statistical summary of core utilisation values for L_{01} and L_{02}.

Load Combination	Count	Min	Max	Mean	Median	SD
L_{01}	40,776	0.004	2.113	0.132	0.084	0.160
L_{02}	40,776	0.002	2.407	0.152	0.089	0.191

Although the mean and median values remain well below 0.2, the relatively high standard deviation and elevated maximum values suggest a strongly right-skewed distribution.

This distribution is visualised in Figure 6.33, which shows that most mesh elements remain well within safe limits, while a small subset exhibits significantly elevated values.
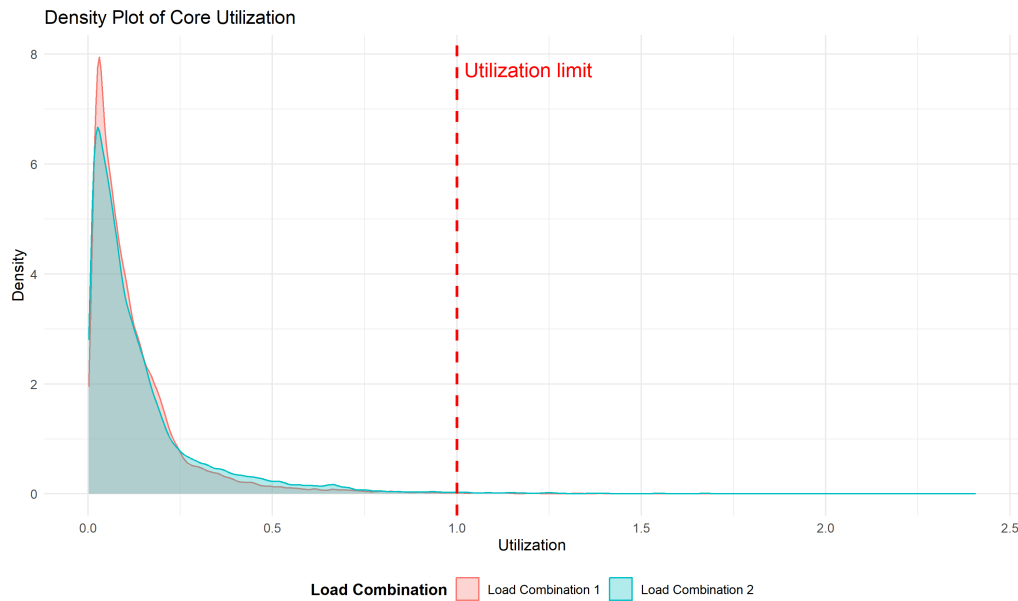
Figure 6.33: Density plot of core utilisation values under L_{01} and L_{02}.

The overutilisation in the core walls is not uniformly distributed but confined to a limited number of distinct locations. Figure 6.34 highlights the mesh vertices, encircled in green, where the utilisation exceeds 1.0.
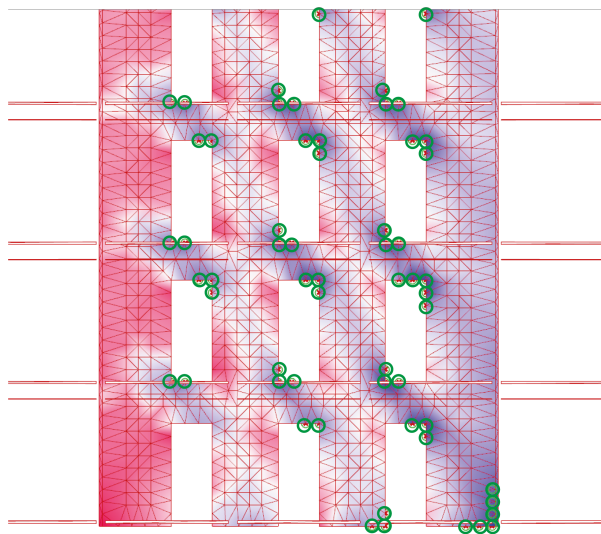
Figure 6.34: Localisation of mesh vertices with utilisation values exceeding 1.0 (green circles).

Figure 6.34 highlights that these peaks are concentrated around geometric discontinuities, such as wall openings, support zones, and sharp or re-entrant corners.

These elevated values are typical artefacts in finite element analysis and are not uncommon in models with geometric irregularities or abrupt boundary conditions. They do not reflect actual structural failure but represent localised overestimations inherent to linear FEM simulations. This phenomenon is especially common near re-entrant corners, point supports, or stiffness discontinuities, where stress concentrations arise that are sensitive to mesh density. These stress concentrations can be managed with improved modelling [57].

Recommendations

To reduce mesh-sensitive overutilisation, several refinements could be done. First, geometric transitions, particularly at re-entrant corners and around openings, could be smoothed with fillets or rounded edges, reducing artificial stress peaks [57]. Second, concentrated supports and loads could be replaced with distributed representations to better approximate realistic boundary conditions. Finally, the use of non-linear material models, particularly elastic-plastic formulations, is recommended in regions where stress concentrations are expected. Such models can more accurately capture local redistribution effects and prevent unrealistically high utilisation values that are common in purely linear analyses [57].

Conclusion

The observed overutilisation in the core walls is limited to a few localised areas and is attributable to mesh-sensitive stress concentrations at geometric discontinuities. These peaks do not compromise the global performance of the structure.

6.7. Feasibility Assessment

This section evaluates the feasibility of the proposed structural concept based on four key aspects: tie-rod elongation, connection design, vertical displacement differences between modules, and expert feedback from Daiwa House Modular Europe.

6.7.1. Elongation of the Tie-rods

An important aspect in assessing the feasibility of the proposed structural concept is the elongation of the tie-rods and how this influences the effectiveness of the outriggers. The tie-rods are responsible for transferring the tensile forces induced by the outrigger beams, and are therefore subject to axial elongation under load.

To approximate this behaviour, the vertical connection between stacked modules should act as a tie-rod under tension and as a column under compression. However, since *Karamba3D* and *Grasshopper* do not support material non-linearity or direction-dependent stiffness, it is not possible to assign different elastic moduli (E) based on the direction of internal force. As a result, the elongation effect could not be directly implemented in the original *2D* and *3D* models. However, to approximate its influence on structural behaviour, a simplified modelling strategy was developed.

Modelling Strategy for Tie-rod Elongation
First, the vertical connections where tension forces occur were manually identified in the model. Figure 6.35 shows the locations of these connections, which are subjected to axial tension under load.
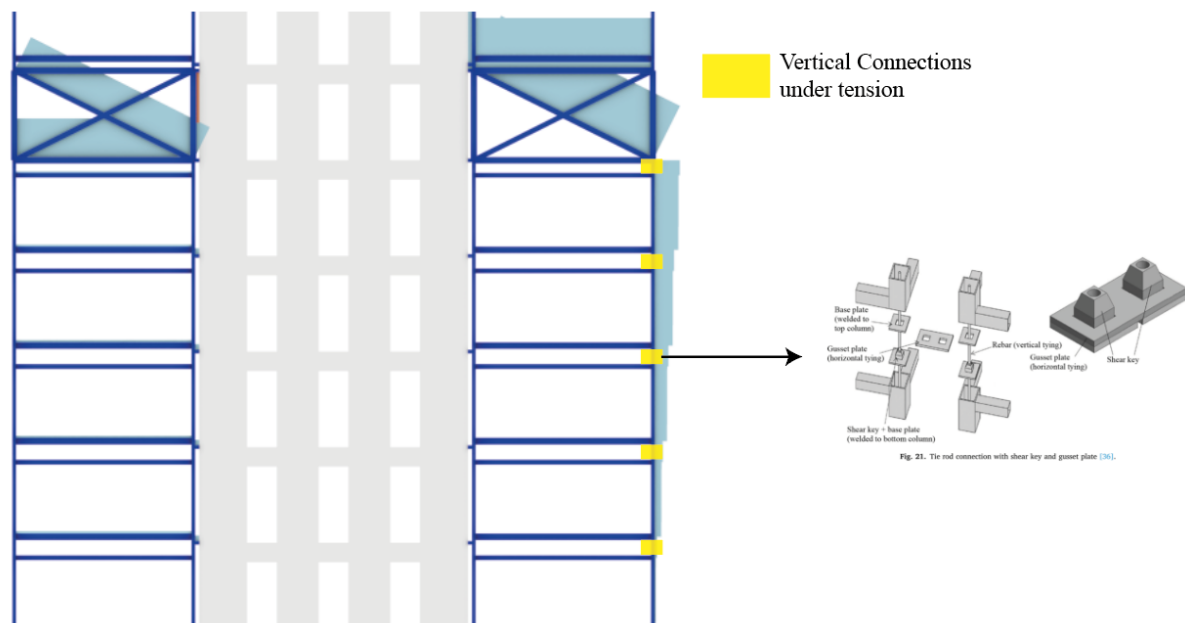
Figure 6.35: Overview of vertical connections under tension (highlighted in yellow).

Next, the identified vertical connections were replaced with artificial cross-sections that simulate the axial elongation of a full-length tie-rod of $3.2\,m$, while remaining in their original model length of $0.2\,m$.

Figure 6.36 illustrates this transformation strategy.

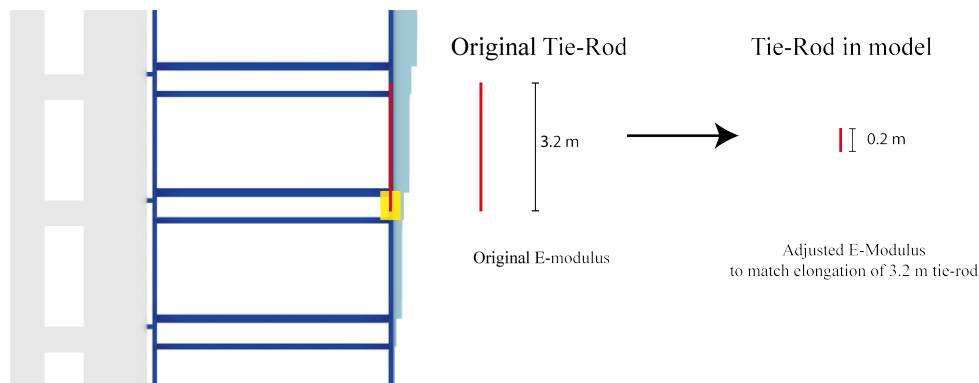**Figure 6.36:** Transformation strategy: tie-rod elongation of $3.2\,m$ is modelled in a $0.2\,m$ element.

To replicate the correct deformation behaviour, the elastic modulus of these artificial elements was reduced through reverse-engineering. This adjustment ensured that the axial deformation under load matched that of a $3.2\,m$ tie-rod with identical cross-section and material properties. A detailed explanation of the calculation procedure and the equivalent elastic modulus values for various tie-rod diameters is provided in Appendix L.

Although tie-rods in reality primarily carry axial forces and exhibit negligible bending stiffness, the physical connections between modules do provide some degree of rotational rigidity. To preserve a realistic global deformation pattern and avoid artificial softening of the lateral stiffness in the model, the replacement elements were assigned the same moment of inertia values (I_{yy} and I_{zz}) as the module columns.

The outcome of this adjustment is shown in Figure 6.37, which compares the original model with the modified version in which tensioned vertical connections were replaced by equivalent tie-rod elements.
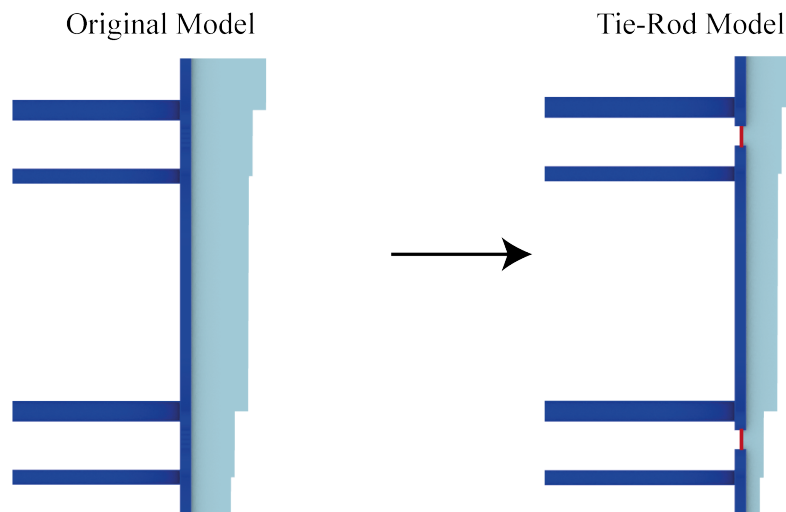
Figure 6.37: Comparison between original model and updated model with equivalent tie-rod elements.

This modelling approach enabled the elongation effect to be approximated within the overall structural analysis and allowed its influence on the building's deformation behaviour to be quantified.

Result Analysis and Feasibility Evaluation

To evaluate the impact of tie-rod elongation, several tie-rod diameters (M24, M30, M40, M50, and M68) were analysed. The analyses were conducted using the Opti-2 *2D* model introduced in Section 5.4.1.

The results are summarised in Table 6.16, which lists the top displacement (w_{top}) for each configuration.

Table 6.16: Top displacements for *core-only* and proposed *outrigger* system with varying tie-rod diameters

Tie-rod	Core w_{top} (m)	Outrigger w_{top} (m)	Reduction Δw_{top} (%)
None	0.153	0.122	20.3%
M24	0.153	0.130	15.0%
M30	0.153	0.129	15.7%
M40	0.153	0.128	16.3%
M50	0.153	0.127	17.0%
M68	0.153	0.126	17.6%

The results in Table 6.16 demonstrate that the apparent effectiveness of the proposed *outrigger* system is highly sensitive to the way tie-rods are modelled. When elongation is neglected (i.e., tie-rods are assumed perfectly rigid in tension), the model predicts a 25.4% reduction in top displacement compared to the core-only configuration. However, this idealised condition significantly overestimates the actual stiffness contribution of the outriggers.

By introducing realistic elongation behaviour, the displacement reduction decreases to 17.7% for M24 tie-rods and gradually increases with larger diameters, reaching 21.4% for M68. This trend illustrates that stiffer (larger diameter) tie-rods can partially recover the lost efficiency, but the maximum benefit remains notably lower than in the idealised case. The observed differences are attributed to axial deformations in the tie-rods under tensile loading, which delay the transfer of lateral forces from the outriggers to the core, thereby reducing the coupling efficiency.

From a structural feasibility perspective, this analysis highlights that tie-rod stiffness is a governing parameter in the effectiveness of the proposed *outrigger* system. To achieve the maximum effectiveness of the proposed *outrigger* system, the design must ensure that tie-rod elongation remains limited, for example by increasing the cross-sectional area when elongation becomes excessive.

6.7.2. Connection Feasibility Assessment

This section evaluates whether the internal forces from the *case-study* model remain within realistic strength limits for practical connection design. Where possible, experimental studies and literature are used as benchmarks. Due to limited availability of directly comparable data, the references do not always reflect a one-to-one match but serve as indicative benchmarks to determine whether the predicted internal forces fall within a reasonable and achievable range for modular construction.

The focus lies on the horizontal inter-modular connections and the connections to the core. Vertical inter-modular connections are not considered here, as their feasibility was addressed in Section 6.7.1.

A. Horizontal Connection (HC)

The horizontal connections (HC) are divided into two categories: module-to-module and outrigger-to-module. Figure 6.38 illustrates both connection types.
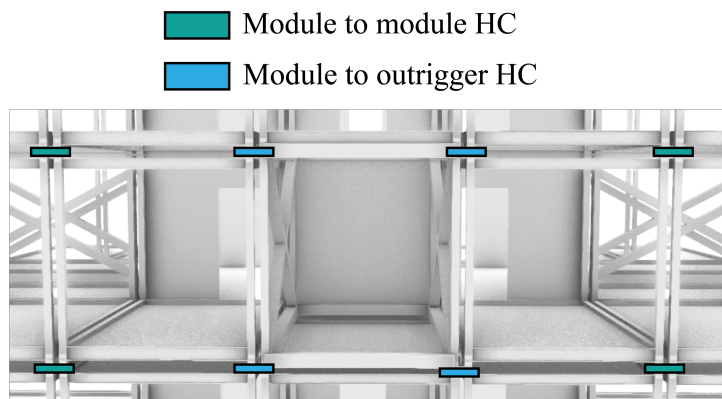
Figure 6.38: The two types of HC

The analysis begins by identifying the most critical connection location where the connection is subjected to the highest forces. The internal forces at this location are then compared with the (theoretical) capacities of similar connection types to assess their structural feasibility.

Maximum Axial Force

Figure 6.39 shows the locations of the HC's subjected to the highest axial tension forces.
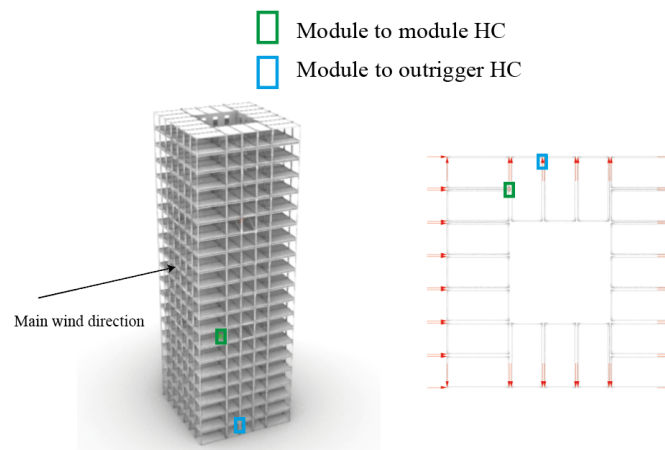
Figure 6.39: Location of the governing HCs based on axial tension force.

The maximum axial tension in the module-to-module connection is $56\,\text{kN}$, while the outrigger-to-module connection reaches a slightly higher value of $62\,\text{kN}$. Both peak values occur under load combination L_{01}.

Maximum Shear Force V_y

Figure 6.40 shows the locations of the HC's subjected to the highest shear forces.
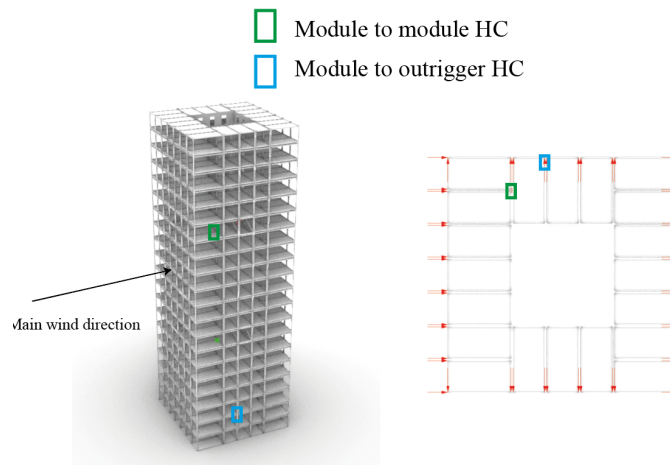
Figure 6.40: Location of the governing HC based on shear force.

The maximum shear force in the module-to-module connection is $27\,\text{kN}$, whereas the HC connecting to the vertical outrigger stack experiences a larger shear force of $-51\,\text{kN}$. Both peak values are observed under load combination L_{01}.

Feasibility Assessment of HC Based on Reference Study

In the proposed modular mid-rise structure, the horizontal connections (HCs) between modules are conceptualised as tie-rod-based systems. However, there is limited experimental data in the literature validating the structural performance of such systems under realistic loading conditions. To address this gap and assess the feasibility of the internal forces derived from the global model, results from a experimental study on a novel steel inter-modular connection are used as a benchmark [58].

Figure 6.41 shows the general layout of the reference connection.
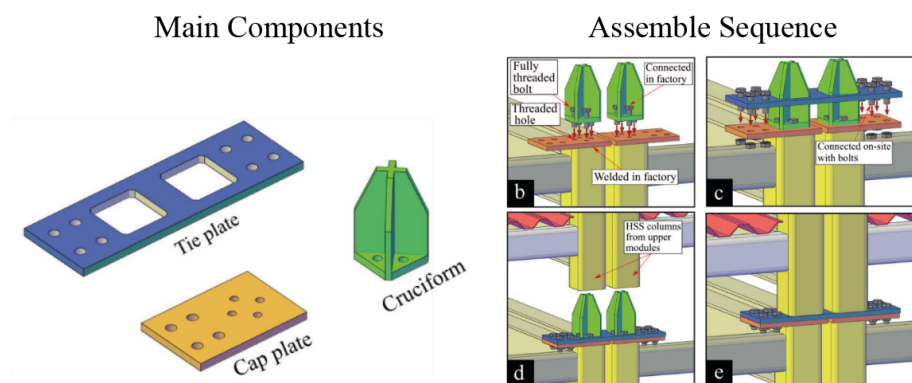
Figure 6.41: Reference connection (retrieved from [58] (Adjusted)).

This reference study introduces a vertically unconstrained inter-modular connection intended for gravity force-resisting (GFR) modules. The design comprises a tie plate and cruciform male–female components, which together provide axial and shear continuity between adjacent modules. The system is specifically developed to reduce on-site assembly time and eliminate the need for uplift-constraining mechanisms in modules that do not experience vertical tension under lateral loading[58]).

It is important to note a key difference between the modelled HC in the *case-study* model and the configuration tested in the reference study. The reference study assumes a gravity-only load path and does not require the connection to resist uplift or significant tension forces. In contrast, the *case-study*

model, particularly in the vertical outrigger-aligned stacks, relies on the full vertical continuity of the inter-modular tie-rod connection to transfer tensile forces as part of the lateral load-resisting system. As a result, the two connection types are not directly comparable.

Nonetheless, both systems employ a horizontal tie-plate to connect adjacent modules. When focusing solely on this horizontal component, the experimental findings from the reference study provide a relevant basis for assessing whether the internal forces in the *case-study* model fall within the range of achievable connection capacities.

Maximum Tension Force of Reference

The axial performance of the horizontal tie plate was investigated through a series of full-scale experiments, in which tensile forces were applied via ceiling beams (specimens C1 to C4). Figure 6.42 presents the experimental set-up and the corresponding load–elongation results for the net section of the tie plate.

A) Test set-up

B) Axial force in the tie plate vs. elongation of the net section of the tie plate.
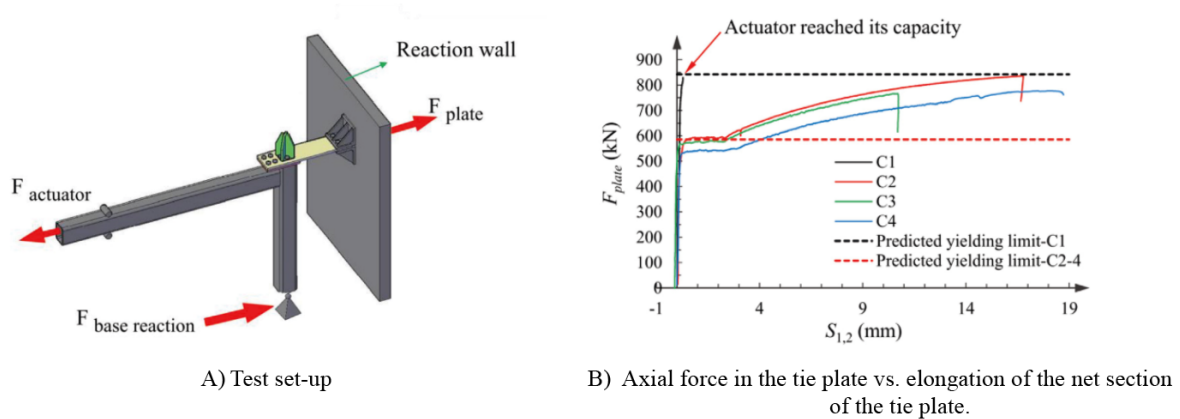
Figure 6.42: Experimental set-up (left) and axial force versus elongation response of the tie plate (right) (retrieved from [58] (Adjusted)).

The results show that slip between the tie plate and cap plate initiated at load levels between approximately 310 and $400\,\text{kN}$, depending on bolt configuration and surface conditions. Yielding in the net section of the plate occurred at higher loads, with ultimate tensile capacities ranging from 585 to $843\,\text{kN}$. In all cases, the connection demonstrated stable and ductile behaviour, without indications of brittle failure [58].

Maximum Shear Force of Reference

Figure 6.43 presents the simulated force–displacement behaviour of the reference tie plate under in-plane shear loading, comparing configurations with and without cruciform connectors.
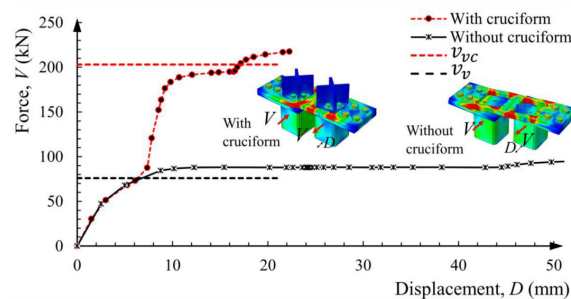
Figure 6.43: Force–displacement response of the tie plate under in-plane shear loading (Retrieved from [58]).

The in-plane shear behaviour was evaluated through finite element simulations calibrated against experimental data. Shear failure of the tie plate occurred at a load of approximately $217\,\text{kN}$, which slightly

exceeded the $203\,\mathrm{kN}$ predicted by plastic analysis. Initial slip between the tie plate and cap plate was observed at roughly $88\,\mathrm{kN}$, while sliding between the cruciform and the plate initiated at around $192\,\mathrm{kN}$ [58].

Reflection and Comparison to Model Forces

The internal forces observed in the *case-study* model fall well within the experimentally validated strength ranges from the reference tests. The maximum axial force in the module-to-module HC is $56\,\mathrm{kN}$, and in the outrigger-to-module HC, $62\,\mathrm{kN}$. These values are approximately one order of magnitude lower than the ultimate axial capacities measured in the reference study, which ranged from 585 to $843\,\mathrm{kN}$.

Similarly, the maximum in-plane shear force is $27\,\mathrm{kN}$ for the module-to-module HC and $-51\,\mathrm{kN}$ for the outrigger-to-module HC. Both remain well below the shear failure load of $217\,\mathrm{kN}$ and even the initial slip threshold of $88\,\mathrm{kN}$.

These comparisons indicate that the internal forces predicted by the global structural model are comfortably within realistic strength limits for practical connection design. Although the reference connection differs in some respects from the modelled HC in the *case study* model, the results provide a relevant basis for concluding that the internal forces fall within the range of achievable connection capacities.

B. Core Connections (CC)

The core connections (CC) are also categorized into two types: module to core and outrigger to core. Figure 6.44 presents the two types of core connections.
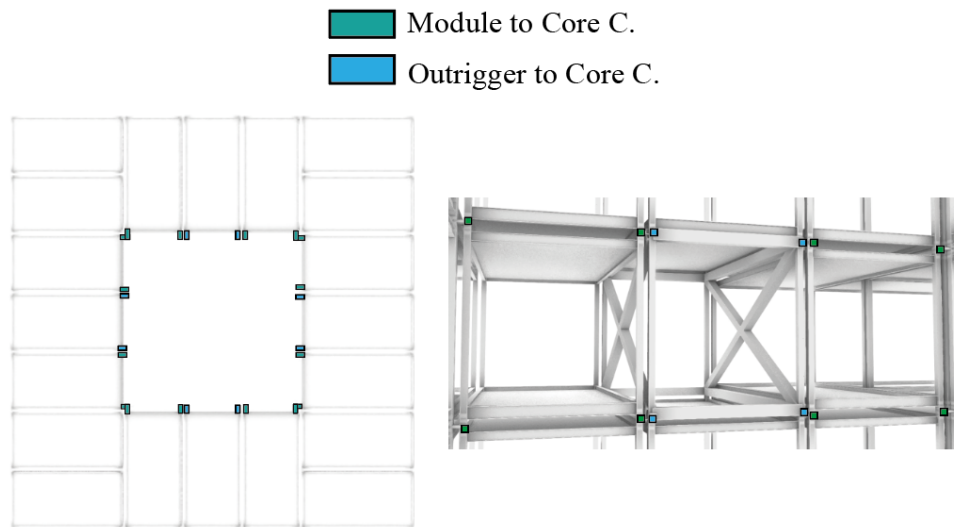
Figure 6.44: The two types of core connections (CC)

In contrast to the HC, the CC cannot be assessed as a single group. The structural behaviour and detailing of the module to core and outrigger to core connections differ too significantly to be treated together. The module to core connection transfers gravity and lateral loads from the units to the central core, while the outrigger to core connection is designed to handle higher forces from the outrigger system. Because of these differences, a separate feasibility assessment is carried out for each connection type. First, the module to core connection is discussed, followed by the outrigger to core connection.

B1. module to core Connection (MC)

Maximum Axial Force

Figure 6.45 shows the location of the module to core Connection (MC) subjected to the highest axial tension force.
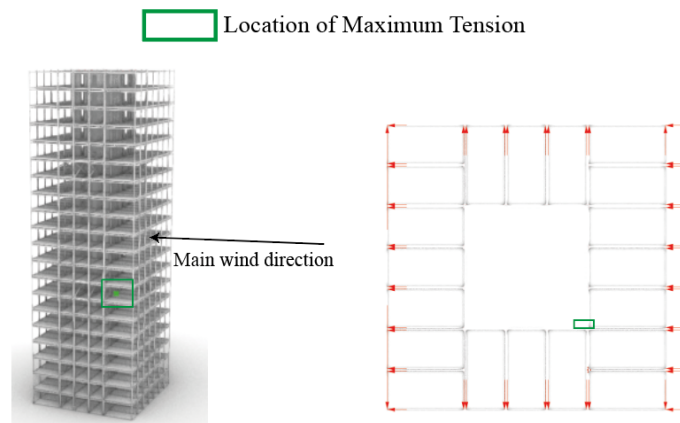
Figure 6.45: Location of the governing MC based on axial tension force.

The maximum axial tension force in the MC is $73\,\text{kN}$, occurring under load combination L_{02}.

Maximum Out-of-Plane Shear Force (V_z)

Figure 6.46 shows the location of the MC subjected to the highest vertical (out-of-plane) shear force.
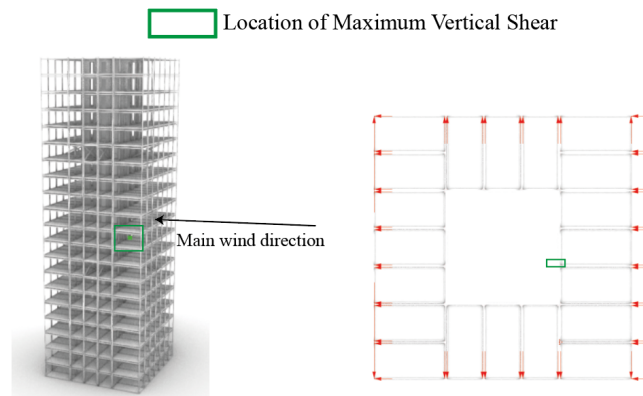
Figure 6.46: Location of the governing MC based on out-of-plane shear force.

The maximum out-of-plane shear force in the MC is $62\,\mathrm{kN}$, observed under load combination L_{01}.

Maximum In-Plane Shear Force (V_y)

Figure 6.47 shows the location of the MC subjected to the highest horizontal (in-plane) shear force.
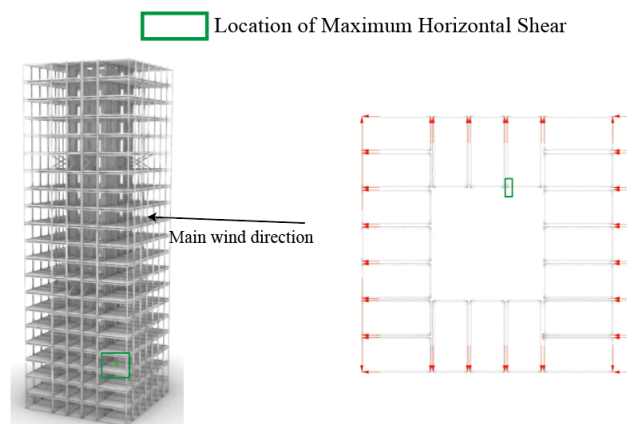
Figure 6.47: Location of the governing MC based on in-plane shear force.

The maximum in-plane shear force in the MC is $25\,\mathrm{kN}$, occurring under load combination L_{01}.

Feasibility Assessment of MC Based on Reference Study

In the *case-study* model, the module to core wall connections (MCs) are responsible for transferring both gravity and lateral loads from the steel-framed modules to the central concrete core. Since no test data is available for the specific connection detail used in this project, the internal forces derived from the global model are compared with the performance of an experimentally validated connection proposed by Shan and Mou (2024) [53].

The reference study introduces an innovative module to core wall connection developed for modular high-rise buildings. As shown in Figure 6.48 shows the connections used for the feasibility assessment of the MC in the *case-study* model.

(a) Schematic view (b) Installation steps
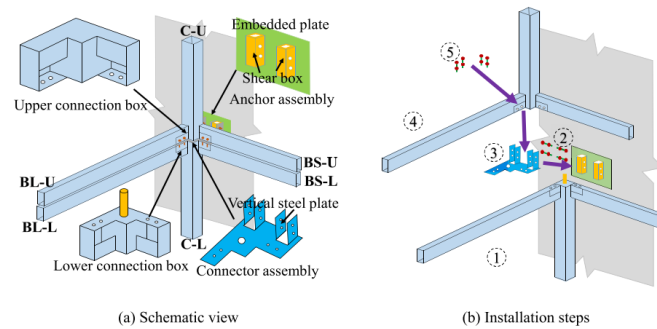
Figure 6.48: Reference module to core wall connection (retrieved from [53]).

The connection is designed for rapid assembly and minimal on-site welding. The lower module is positioned first, followed by the installation of an anchored embedded plate into the core wall. The L-shaped connector is bolted to the embedded plate and aligned between the upper and lower modules. A shear key forged into the lower module fits into the connection box of the upper module. Once in place, the system is secured using four high-strength bolts, resulting in a rigid but demountable connection [53].

The mechanical behaviour of the system was investigated through detailed finite element simulations, calibrated against both monotonic and cyclic loading tests. Figure 6.49 shows the load–displacement responses under three critical load cases: axial tension, vertical shear, and horizontal shear.

(b) Vertical shear (d) Horizontal shear (e) Axial loading

(a) Vertical shear (c) Horizontal shear (d) Axial load
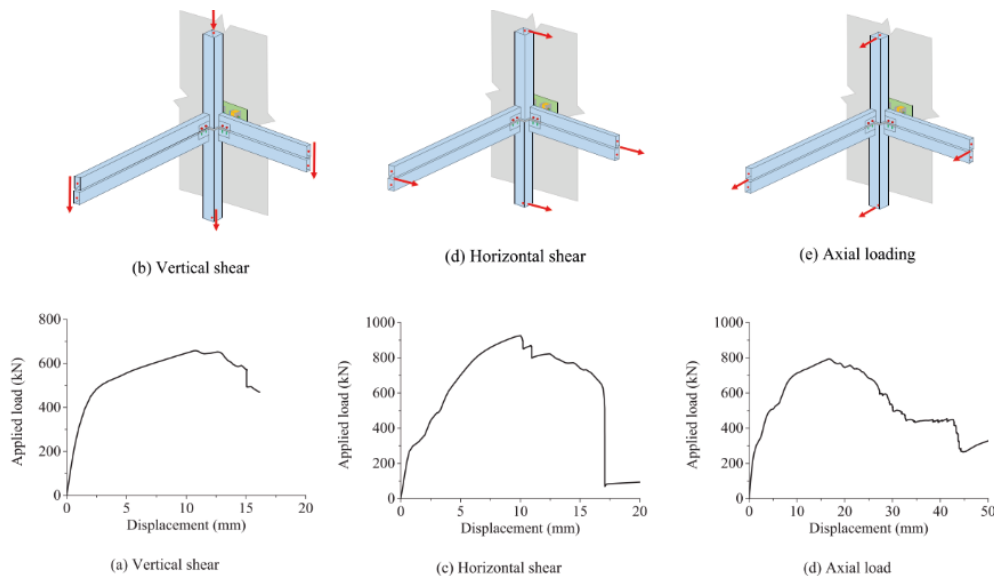
Figure 6.49: Load–displacement curves of the reference MC under axial tension, vertical shear, and horizontal shear [53].

The ultimate capacities recorded in the reference study were $793\,\text{kN}$ in axial pull-out, $658\,\text{kN}$ in vertical shear (V_z), and $926\,\text{kN}$ in horizontal shear (V_y).

Comparison with Model Forces and Reflection

The *case-study* model shows a maximum axial tension of $73\,\mathrm{kN}$, vertical shear of $62\,\mathrm{kN}$, and horizontal shear of $25\,\mathrm{kN}$ in the module-to-core connection. These values are substantially lower than the ultimate capacities reported in the reference study: $793\,\mathrm{kN}$ in axial pull-out, $658\,\mathrm{kN}$ in vertical shear, and $926\,\mathrm{kN}$ in horizontal shear. This indicates that the modelled forces remain well below $10\,\%$ of the tested failure thresholds.

While the comparison is based on ultimate limit states rather than service-level criteria, the considerable margin provides a meaningful indication of structural safety. It supports the conclusion that the internal forces predicted by the global model fall well within realistic capacity limits for practical connection design.

B2. Outrigger to Core Connection (OC)

Maximum Axial Force

Figure 6.50 shows the location of the OC subjected to the highest axial tension force.
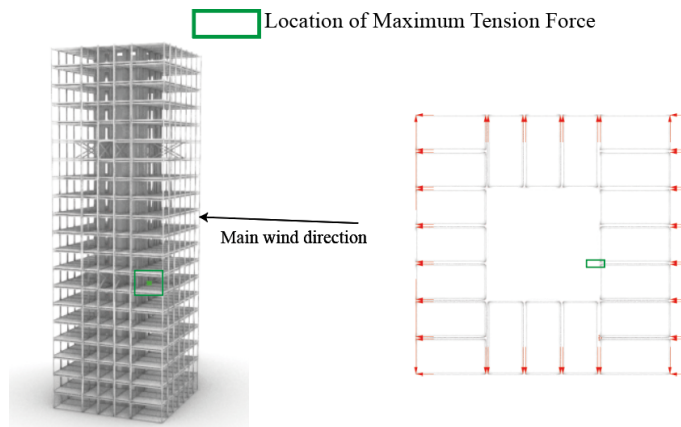
Figure 6.50: Location of the governing OC based on axial tension force.

The maximum axial tension force in the OC is $336\,\text{kN}$, occurring under load combination L_{01}.

Maximum Vertical Shear Force (V_z)

Figure 6.51 indicates the location of the OC experiencing the highest vertical (out-of-plane) shear force.
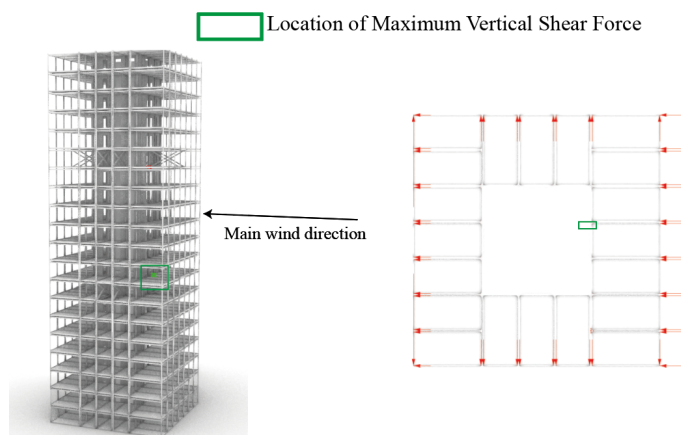
Figure 6.51: Location of the governing OC based on vertical shear force.

The maximum vertical shear force in the OC is $68\,\text{kN}$, observed under load combination L_{01}.

Maximum Horizontal Shear Force (V_y)

Figure 6.52 shows the location of the OC subjected to the highest horizontal (in-plane) shear force.
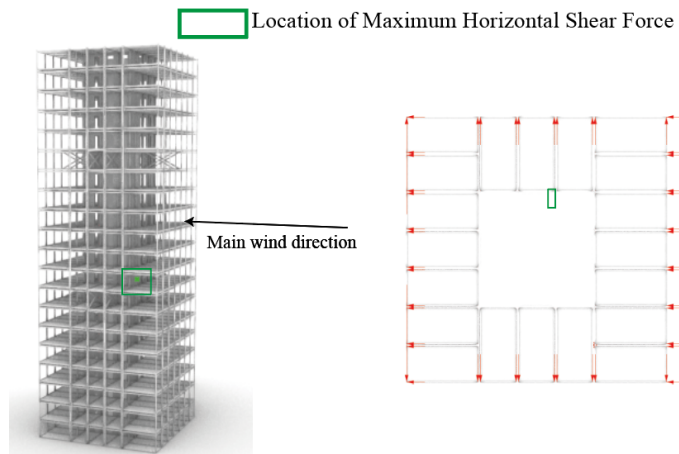
Figure 6.52: Location of the governing OC based on horizontal shear force.

The maximum horizontal shear force in the OC is $20\,\text{kN}$, occurring under load combination L_{01}.

Feasibility Assessment of OC Based on Reference Study

SCI Publication P416 [59] provides design guidance for cast-in plate connections, a connection type commonly used to anchor steel components, such as beams or outriggers, into reinforced concrete walls. Figure 6.53 illustrates a typical outrigger to core connection layout as referenced in the publication.
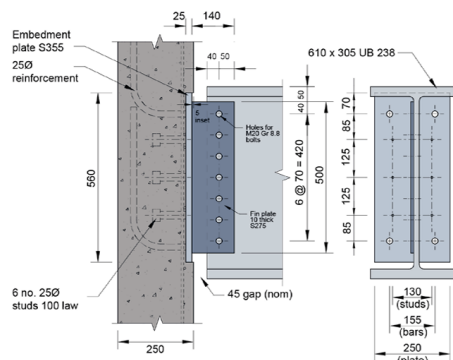
Figure 6.53: Reference outrigger to core wall connection (adapted from [59]).

These systems generally consist of a steel plate cast into the concrete wall, fitted with headed studs for anchorage and welded shear tabs or cleats for connecting structural steel elements. The connection transfers force through a combination of bearing pressure, weld resistance, stud anchorage, and concrete breakout capacity. Design resistances are presented in SCI P416 for a range of cast-in plate configurations, derived from analytical calculations and component-based modelling. For the purpose of this feasibility assessment, one representative configuration is selected as the reference case. It consists of a $10\,\text{mm}$ thick S355 steel plate, four T20 headed studs, and four M20 grade 8.8 bolts embedded in C40/50 concrete.

This reference configuration is shown to resist axial forces up to approximately $450\,\text{kN}$. The vertical shear resistance, governed primarily by the capacity of the headed studs and concrete breakout, is calculated at approximately $160\,\text{kN}$. The horizontal shear resistance, which depends largely on bolt strength and anchorage detailing, reaches approximately $140\,\text{kN}$. These values are based on worked verification examples and tabulated checks included in the publication, and incorporate appropriate partial safety factors. All values assume monolithic, uncracked concrete and sufficient confinement and edge distances [59].

Comparison with Model Forces and Reflection

In the *case-study* model, the outrigger to core connection is subjected to a maximum axial force of $336\,\text{kN}$, a vertical shear force of $68\,\text{kN}$, and a horizontal shear force of $19\,\text{kN}$. All of these forces fall within the design capacities cited in SCI P416 for typical cast-in plate connections.

However, an important distinction must be made regarding the type of concrete core used in the current model. Whereas the reference values in P416 assume a cast-in-situ, monolithic concrete wall, the case study assumes a prefabricated core made of cracked C50/60 concrete. This difference has two key implications. First, although the concrete grade is higher, the presence of pre-existing cracks may reduce both the anchorage performance of the headed studs and the overall breakout resistance. Second, the prefabricated nature of the wall may introduce construction tolerances, joint discontinuities, or misalignments that could affect the mechanical behaviour of the embedded plate.

Conclusion
This section has evaluated the feasibility of the main structural connections in the proposed modular mid-rise design. For all four connection types, the internal forces obtained from the global model are within realistic strength limits for practical connection design.

The reference connections used in this assessment do not represent a one-to-one match with the case study model in terms of detailing, material behaviour, or construction method. However, they provide a reliable bandwidth against which the internal forces can be compared. Within this range, the results show that the modelled connection forces remain below critical limits, supporting the structural viability of the proposed system.

6.7.3. Vertical Displacement Reduction

A critical aspect in assessing the feasibility of the proposed structural system is the vertical displacement mismatch identified in Section 6.5.1. These differential displacements between vertically stacked modules pose significant practical challenges, particularly with regard to the alignment of floors, the integrity of interior finishes, and the performance of inter-modular connections.

The primary source of these mismatches lies in the current modelling assumption for the horizontal inter-modular connections, which are idealised as pinned joints without rotational stiffness. This simplification prevents the redistribution of internal forces and permits notable relative movement between adjacent module stacks.

This section investigates a potential design strategy to mitigate these effects. The analysis focuses on introducing rotational stiffness at horizontal connection points, with the aim of improving vertical deformation compatibility and reducing displacement differences across stacked modules.

Current Situation

As outlined in Section 6.5.1, two main sources of vertical displacement differences can be identified in the current configuration. The first is related to horizontal core deformation, which induces vertical displacement mismatches between modules that are directly connected to the core and those that are not. The second source is the result of the presence of an outrigger in the vertical stack of modules.

Figure 6.54 identifies the critical zones where the largest vertical displacement differences occur on both the windward and leeward sides of the structure.
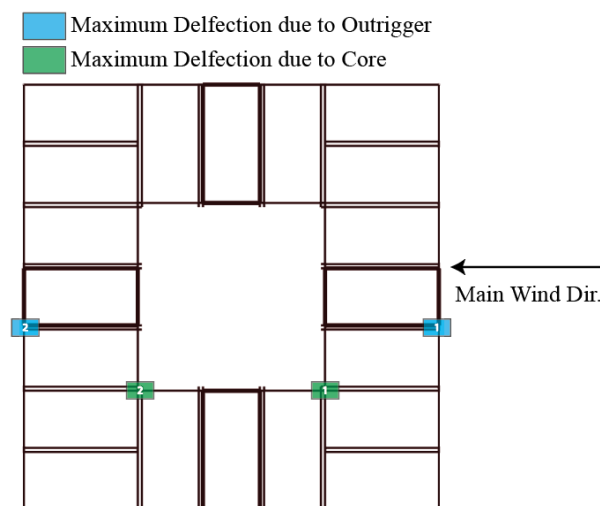
Figure 6.54: Location of maximum vertical displacement differences (1: Windward, 2: Leeward).

These locations represent the most critical points for deformation compatibility and are key targets for potential design improvements in the horizontal inter-modular connections.

Table 6.17 provides a summary of the maximum measured vertical displacement differences, separated by their underlying cause (core deformation or outrigger presence).

Table 6.17: Summary of maximum vertical displacement differences.

Location	Due to Outrigger [m]	Due to Core [m]
Windward (1)	0.0013	0.0020
Leeward (2)	-0.0070	0.0170

Figure 6.55 shows the current design of the horizontal connection between modules.
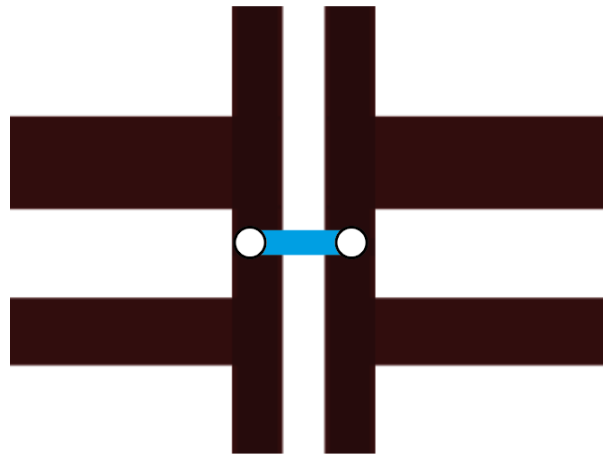
Figure 6.55: Current horizontal connection setup: pin-ended HC.

The connection consists of a flat steel plate (FL12×15 mm), attached to adjacent modules using pin sup-
ports at both ends. As such, it provides no rotational restraint and allows relative angular displacement
between modules. This absence of rotational stiffness limits the structural interaction between vertically
stacked modules and is a main contributor to the observed vertical displacement differences.

Adjusted Rotational Stiffness
To assess the impact of rotational stiffness in horizontal inter-modular connections on vertical displace-
ment differences, a *parametric* study was conducted using the *case-study* model. In this analysis, the
idealised hinge connection was replaced by a rotational spring at one end of each horizontal connection,
as illustrated in Figure 6.56.
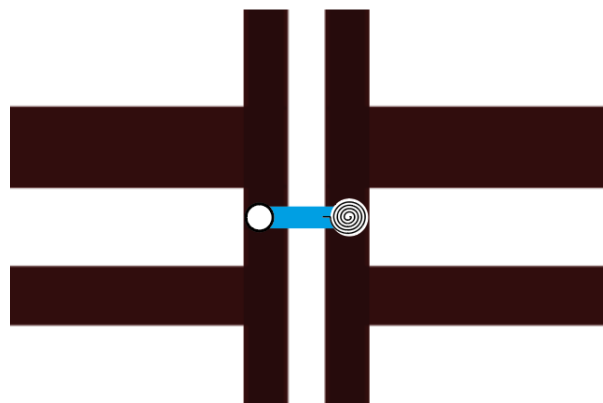
Figure 6.56: Modified horizontal connection: pinned at one end, rotational stiffness at the other.

This modelling approach is based on the mechanical behaviour observed in practical tie-plate (or shear
plate) systems used in modular construction. When vertical movement occurs in one module while the
adjacent module remains stationary, the tie-plate often develops rotational restraint primarily on one side
due to frictional effects.

In the analysis, the rotational stiffness was varied from $0\,\mathrm{kNm/rad}$, representing a fully pinned connection, up to $500\,\mathrm{kNm/rad}$, representing increased rotational restraint. Figure 6.57 shows the resulting absolute vertical displacement differences for four critical module groups, plotted as a function of applied rotational stiffness.
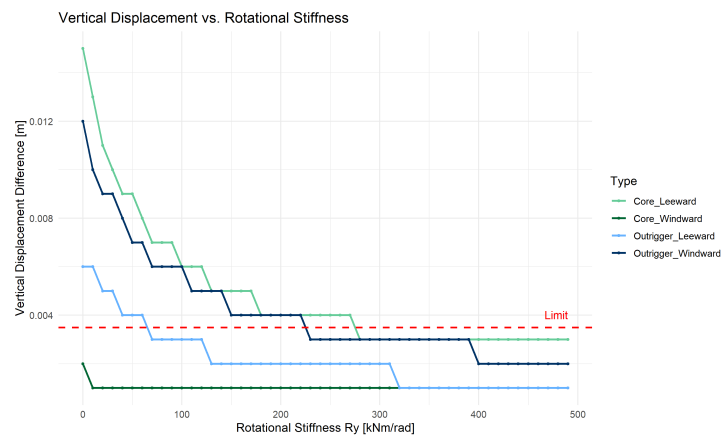
Figure 6.57: Effect of rotational stiffness on vertical displacement differences across module groups.

The results are categorised by the two primary causes of differential displacement: core deformation (green) and outrigger-induced effects (blue). Darker tones represent values on the windward side; lighter tones correspond to the leeward side. A red dashed line indicates the maximum acceptable vertical mismatch of $3\,\mathrm{mm}$. This value marks a practical design goal beyond which vertical deformation compatibility can be considered acceptable for architectural and structural detailing.

The graph shows a consistent reduction in displacement differences as rotational stiffness increases. Most of the reduction occurs between 0 and $100\,\mathrm{kNm/rad}$; beyond this range, additional stiffness yields diminishing returns. Notably, the leeward-side displacement due to core deformation (light green) initially exceeds the $3\,\mathrm{mm}$ limit, but falls below it as stiffness increases. A similar trend is observed for the windward outrigger group (dark blue). In contrast, the remaining two groups, core deformation on the windward side (dark green) and outrigger effect on the leeward side (light blue), remain within acceptable limits regardless of stiffness. Only when rotational stiffness reaches approximately $270\,\mathrm{kNm/rad}$ do all four critical cases fall below the $3\,\mathrm{mm}$ threshold.

Figure 6.58 visually illustrates the improvement in vertical alignment between adjacent modules as rotational stiffness increases from a pinned state to a partially fixed state.

R = 0 kNm/rad   R = 270 kNm/rad
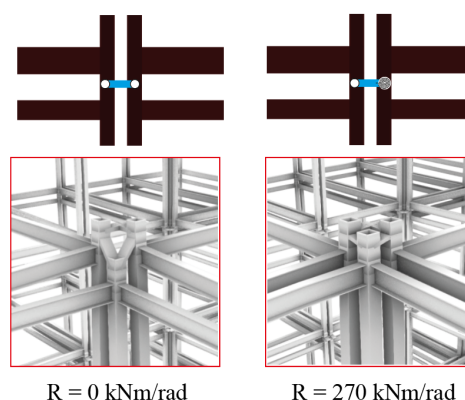
Figure 6.58: Reduction in vertical misalignment with increasing rotational stiffness.

This analysis demonstrates that implementing partial rotational stiffness in horizontal connections significantly improves deformation compatibility between module stacks. A target stiffness of approximately $270\,\mathrm{kNm/rad}$ is sufficient to keep all relevant displacement differences within acceptable tolerances. Therefore, adopting a partially rigid connection offers a practical alternative to fully pinned joints.

Reflection on Required Rotational Stiffness

While the introduction of rotational stiffness is effective in reducing vertical displacement differences between module stacks, it is not without structural consequences and practical challenges. It must be verified whether the required rotational stiffness, estimated at approximately $270\,\mathrm{kNm/rad}$ based on the case study, can realistically be achieved within typical modular construction constraints. Currently, no direct literature or experimental studies confirm the feasibility of attaining this target stiffness in inter-modular connections.

Further research is therefore recommended, including targeted experimental testing or advanced numerical modelling of potential connection types. These investigations should consider both the mechanical performance and the practical limitations associated with manufacturing and on-site assembly.

Moreover, increasing rotational stiffness alters the structural behaviour of the system. When stiffness is introduced at horizontal inter-modular connections, these interfaces may begin to attract bending moments and vertical shear forces from neighbouring stacks. This could lead to unintended force redistribution, resulting in increased demands on local connections.

In the adjusted *case-study* model, the introduction of rotational stiffness up to $270\,\mathrm{kNm/rad}$ did not result in governing axial forces in the adjacent vertical stacks. The global structural response remained stable, and no significant alterations in the load path were observed. Notably, the adjacent stacks to the outrigger locations did not experience significant force redistribution. Nevertheless, further investigation is recommended to assess the effects of increased rotational stiffness in more detail.

6.7.4. Expert Review: Daiwa

As the final step in the feasibility assessment of the proposed structural concept, a review session was held with Daiwa House Modular Europe on 25 April 2025. The meeting was conducted with Mr. Jojan Verbeek, who acted as the primary representative of Daiwa. During this session, the structural concept was presented in detail, and a set of targeted questions was discussed to evaluate the constructability and practical feasibility of the design from the perspective of an experienced modular contractor.

The discussion was structured around four key topics: the general feasibility of the concept, the proposed outrigger configuration, the vertical tie-rod connections, and the selected floor plan layout.

General Feasibility

A key advantage of the proposed hybrid concept, as noted by Mr. Verbeek, is that the additional structural components, specifically the outrigger elements, can be prefabricated alongside standard modules in the factory. This ensures alignment with core modular construction principles: reducing on-site complexity, improving quality control, and optimising logistics.

Mr. Verbeek highlighted that the inclusion of two outrigger levels naturally divides the building into three construction segments: ground floor to first outrigger, first to second outrigger, and second outrigger to the roof. These segments support a logical, phased construction strategy.

Figure 6.59 illustrates this phased approach.
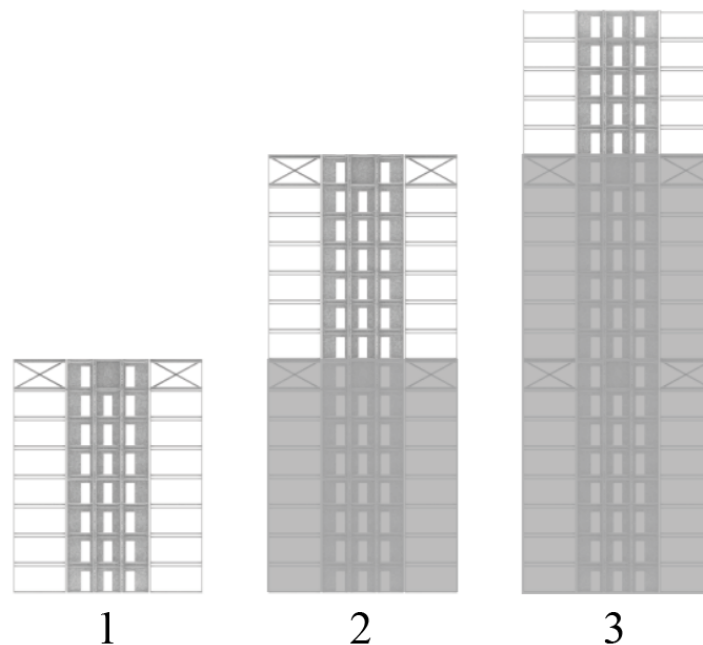
Figure 6.59: Phased building process aligned with outrigger levels

Each segment can be fully prefabricated and then assembled on site, with the outrigger floors acting as both structural and logistical transition points. This segmentation allows factory production and on-site assembly to proceed in parallel: while the first segment is being installed, the next can already be under production. The staggered sequence reduces production downtime and enhances supply chain coordination.

Moreover, since outrigger floors are likely to require additional on-site time for integrating complex details such as wet joints or tie-rod connections, the phased approach creates a natural buffer. This allows the factory sufficient time to produce the next building segment, ensuring continuous production even if on-site progress is temporarily delayed.

Outrigger Configuration

The proposed placement of outriggers on levels 7 and 14 was considered beneficial from a logistical perspective.

Mr. Verbeek noted that the inclusion of outriggers inevitably reduces the usable residential area on those floors due to the space occupied by structural elements. However, this drawback can be mitigated by repurposing these zones as technical areas for HVAC, electrical, lighting, or IT infrastructure. This adaptive reuse not only compensates for the loss of living space but also facilitates the integration of building services that would need to be accommodated in the structure regardless.

A key strength of the concept is the decision to connect the outriggers to a single vertical stack of modules adjacent to the core. By activating only this stack, the tension forces from the outriggers can be concentrated within one line vertical inter-modular connections. This eliminates the need to distribute tie-rods across the entire structure. The selective application simplifies the design, reduces material and labour costs, and shortens on-site installation time. Mr. Verbeek considered this a cost-efficient and execution-friendly solution.

The resulting tie-rod layout is shown in Figure 6.60, where the single vertical stack of modules directly connected to the outriggers is highlighted in blue.
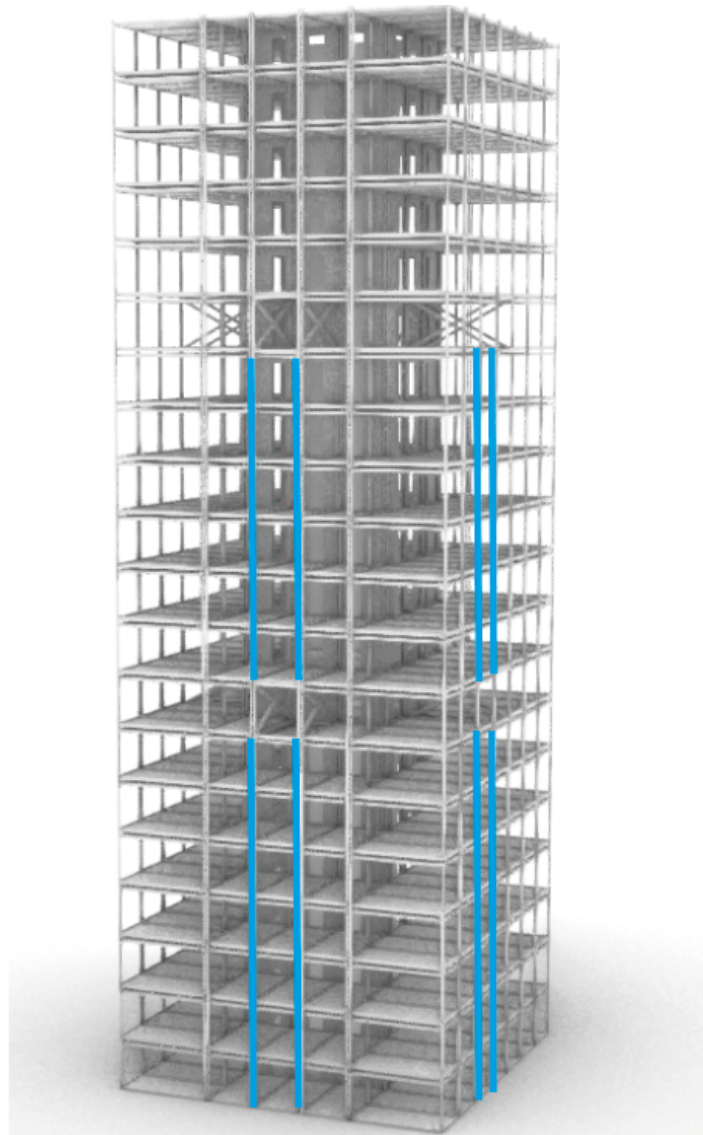
Figure 6.60: Vertical stacks of modules directly connected to outriggers.

Tie-rod Connections

Regarding the vertical tie-rods, Mr. Verbeek raised concerns about the precision required for their installation, particularly at significant heights. Although their structural function is clear, he emphasized that the on-site placement would introduce greater risk due to tight tolerance requirements, limited accessibility, and the logistical challenges of handling heavy components during vertical assembly.

Floorplan Design

The proposed floorplan, based on a symmetrical layout with standard module dimensions of 6–6.22 by 3 metres, was evaluated positively. The vertical stacking of bedrooms and the horizontal alignment of kitchens and living areas reflect a layout suggested by Mr.Verbeek and are consistent with modular construction logic. The resulting organisation of spaces is shown in Figure6.61.
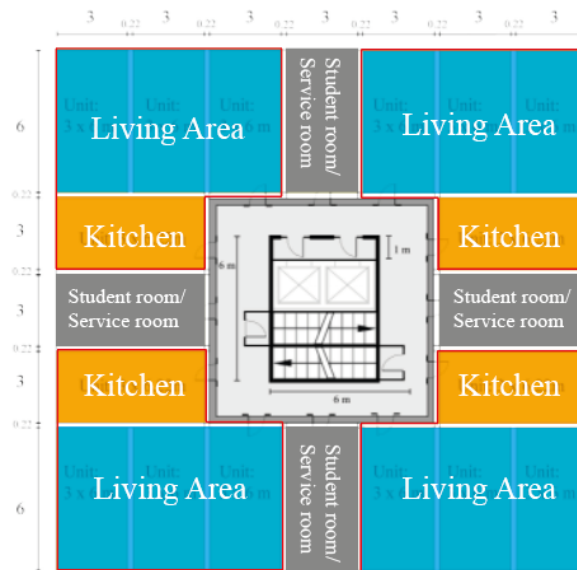
Figure 6.61: Proposed floorplan with room and apartment divisions

Mr. Verbeek added that, in real-world projects, floorplans are often shaped by the vision of the architect, who may prefer a more varied and expressive layout. While the current design is structurally efficient, it may limit architectural freedom. The proposed configuration relies on just two module types, which is ideal for manufacturers like Daiwa, who seek to minimise variability between units. However, if a more irregular layout is introduced, adjustments to the dimensions of corner-supported modules may be required to ensure fit and structural continuity. This could complicate the design process and reduce both manufacturing efficiency and the structural effectiveness of the proposed concept.

Conclusion

The expert review confirmed that the proposed structural concept aligns well with the principles and practicalities of modular construction. Mr. Verbeek highlighted several key advantages, including the logical construction phasing introduced by the outrigger levels, the integration of prefabricated stability components, the targeted use of tie-rods in a single vertical stack, and the efficient floorplan enabled by limited module variation. At the same time, he raised concerns about the precision required for vertical tie-rod installation at height, and the potential impact of architectural customisation on standardisation and structural efficiency. If these challenges are addressed through careful detailing and planning, the concept presents a viable, cost-efficient, and execution-friendly solution within the scope of industrial modular construction.

6.8. Conclusion

This chapter evaluated the structural and practical feasibility of implementing a hybrid outrigger to core system within a modular mid-rise structure, using the Tang Tower as a representative case study. The primary objective was to determine whether such a system could extend the achievable height of modular buildings while preserving structural integrity and constructability.

Introducing outriggers at levels 7 and 14 enhanced the lateral stiffness of the structure, resulting in a reduction in top displacement of 13.5%. This improvement enabled the modular system to reach a total height of $67.7\,\mathrm{m}$. The associated tie-rod system was found to be structurally feasible, with the internal forces observed in the *case-study* model remaining within realistic strength limits for practical connection design.

As a final analysis of the feasibility of the proposed concept, four key aspects were investigated: the effect of tie-rod elongation, vertical displacement differences, connection capacity, and expert validation. First, the influence of tie-rod elongation was studied *parametrically* in the *2D* model. The results showed that elongation of the tie-rods reduced the lateral stiffness contribution of the outriggers, underscoring the importance of providing tie-rods with sufficient cross-sectional area to maximise the effectiveness of the proposed concept. Second, vertical displacement differences between stacked modules were evaluated. Initial gaps of up to $17\,\mathrm{mm}$ exceeded typical tolerances but were reduced to below $3\,\mathrm{mm}$ by introducing rotational stiffness in the horizontal inter-modular connections. Third, the main connection types were benchmarked against experimental references and design guidance, confirming that the proposed detailing provides sufficient strength and stiffness. Finally, expert feedback from Daiwa House Modular Europe validated that the concept aligns with modular construction principles and logistical practice.

7

Discussion

This chapter reflects on the methodology, assumptions, and findings of the research. While the results presented in the previous chapters indicate that the proposed hybrid structural concept offers promising potential for modular mid-rise construction, these findings must be interpreted in light of the modelling simplifications and scope limitations under which they were obtained.

7.1. Evaluation of Modelling Approach

The structural analyses in this thesis were carried out using a *parametric* workflow implemented in *Grasshopper*, with *Karamba3D* serving as the structural analysis tool. This approach facilitated rapid iteration and efficient variation of key design parameters, including module dimensions, core stiffness, tie-rod configuration, number and placement of outriggers, and cross-section optimisation. Moreover, it enabled seamless integration between geometric modelling and structural evaluation. *Karamba3D* delivered immediate visual and numerical outputs, which were used to assess key performance indicators such as lateral drift, internal forces, member utilisation, and vertical displacements. While *Karamba3D* proved effective for concept-level analysis and comparison of design options, it showed several limitations when more detailed structural modelling was required. These limitations are summarised below:

- Tasks that are considered standard in conventional finite element software, such as identifying the most critical members or exporting internal force diagrams, are not readily supported through built-in components. For example, locating the member with the highest axial force or utilisation requires custom scripting or manual post-processing. Unlike tools such as *SCIA Engineer*, *SAP2000*, or *RFEM*, *Karamba3D* does not have a built-in result browser or automatic summaries.

- Similarly, internal force diagrams, cannot be exported in tabular form. Although approximate visualisation is possible within *Grasshopper*, this remains primarily a graphical tool and is not sufficient for design documentation or detailed comparisons between design variants. As a result, in-depth interpretation of force distributions or local performance trends becomes time-consuming.

- Modelling of connections had to be strongly idealised. All joints were simplified as either pinned, rigid, or with assigned rotational stiffness. This allowed for comparative studies, but could not capture local effects such as bolt slip, weld deformation, or bearing pressure. These limitations are discussed further in Section 7.2, which elaborates on the impact of connection modelling assumptions.

- A further limitation is the software's inability to model material non-linearity. The vertical connections between modules should act as tie-rods in tension and as module columns in compression. However, *Karamba3D* does not support tension-only elements or non-linear material models. As a workaround, tie-rod elongation was approximated by manually replacing the vertical elements subjected to tension with elements of artificially reduced axial stiffness to mimic tie-rod behaviour. The effect of this limitation is discussed in Section 7.2 under the assumptions regarding tie-rod behaviour.

This thesis shows that *Grasshopper* in combination with *Karamba3D* can serve as a practical tool for assessing the structural feasibility of modular mid-rise buildings during the design phase. The *parametric* workflow allowed for fast iteration, direct visual feedback, and meaningful comparison between different configurations. Although the results are based on simplifications, the *parametric* modelling approach proved well-suited for concept development. More detailed validation, including non-linear effects and realistic connection behaviour, should be carried out in follow-up studies using more advanced structural analysis software.

7.2. Key Assumptions

The results in this thesis are based on a number of simplifying assumptions made to allow for *parametric* modelling, fast computation, and a clear setup. These assumptions were acceptable for a concept-level feasibility study, but they do affect the accuracy and broader applicability of the outcomes. This section outlines the most important assumptions and explains how they may have influenced the findings.

- Simplified Connection Behaviour: All structural connections were idealised using rigid, pinned, or rotational spring models. While this allowed for *parametric* comparison of joint stiffness at the system level, it does not capture local effects such as slip, friction, bolt deformation, or weld flexibility. These simplifications are particularly relevant for modular construction, where connection stiffness and ductility have a strong influence on overall performance. The global stiffness, force distribution, and vertical displacement mismatches are highly sensitive to inter-modular and core connection assumptions. The effectiveness of the proposed concept may therefore be over- or underestimated depending on how accurately these connection behaviours were approximated.

- Tie-Rod Elongation and Directional Stiffness: In reality, vertical tie-rods only engage under tension, resulting in directional stiffness behaviour. Since *Karamba3D* does not support non-linear material behaviour, elongation was approximated in the *2D* model by assigning artificially reduced axial stiffness to selected members. This approximation could not be applied in the more complex *3D* model. As a result, the reported 13.5% reduction in top displacement in the *case-study* model likely overestimates the actual performance. Accurate simulation of tie-rod behaviour in a full *3D* context would require non-linear material modelling in advanced software such as *DIANA* or *ABAQUS*.

- Monolithic Core Modelling: The precast core was modelled as a continuous monolithic structure with a reduced Young's modulus (E) to approximate the behaviour of precast concrete. This simplification ignores the presence of joints and the reduced continuity typical of precast construction. As a result, the core stiffness was likely overestimated, which may have led to overly optimistic performance in the *core-only* model and affected the force distribution in the proposed concept. This assumption is especially relevant for the interaction between the outriggers and the core, where it could have influenced both displacement results and internal forces.

- Fixed Base Support Conditions: The structural models assume fully fixed base supports, neglecting soil-structure interaction, foundation flexibility, and differential settlement. Although a stricter displacement criterion ($H/750$) was applied to partially compensate for this, it does not replace a detailed foundation model. This assumption may have led to an underestimation of top displacements and inter-storey drifts, as well as vertical displacement differences between module stacks due to settlement variations in the foundation.

- Limited Load Cases and Absence of Dynamic Effects: The structural analysis was restricted to two static load combinations (L_{01} and L_{02}). Dynamic actions, such as fluctuating wind loads, vibrations from occupants, or seismic events, were not considered. While this simplification is acceptable for an early-stage feasibility study, it limits the applicability of the results to static conditions only. In practice, such dynamic effects can be critical in modular buildings due to their lighter mass, stiffer connections, and segmented structural paths. Neglecting them may therefore underestimate serviceability issues like sway, resonance, or joint fatigue.

- Use of Non-Identical Reference Connections: Connection feasibility was assessed by comparing modelled internal forces with data from experimental studies and design guides. However, the referenced connections differ in geometry, materials, and detailing from those in the *case-study* model. While the comparisons suggest that the predicted forces remain within realistic capacity limits for practical connection design. As a result, the findings are indicative rather than conclusive, since the reference connections do not represent a one-to-one match with the actual designs.

Together, these assumptions define the key boundaries within which the results of this research should be interpreted. While they were appropriate for the scope and objective of a feasibility study, future research should aim to reduce or eliminate these limitations.

7.3. Interpretation of Key Findings

This section reflects on the key findings of the research, interpreting their relevance in light of the limitations and assumptions outlined in previous section.

Effectiveness of the Outrigger and Tie-Rod Concept

The structural concept, consisting of a precast concrete core, strategically placed outriggers, and vertical tie-rods, proved effective in improving lateral stability. In the *case-study* model, the introduction of outriggers led to a noticeable reduction in top displacement compared to the *core-only* configuration. The maximum lateral displacement was reduced by 13.5%, remaining within the serviceability limit of $H/750$.

That said, this reported reduction assumes negligible tie-rod elongation. *Parametric* studies in the *2D* model showed that when tie-rod elongation is taken into account, the effectiveness of the system decreases. This suggests that the performance of the proposed concept is highly sensitive to the axial stiffness of the tie-rods. To maintain the desired structural benefit, it may be necessary to use tie-rods with increased cross-sectional area.

Insights from 2D vs. 3D Modelling

While the *2D parametric* studies were instrumental in exploring design strategies and identifying effective outrigger configurations, they were inherently limited to planar behaviour. The transition to *3D* modelling revealed several important spatial effects that could not be captured in the *2D* models.

- One key insight was the occurrence of differential vertical displacements between adjacent stacks of modules. These mismatches, caused by core deformation and the presences of the outriggers, led to vertical misalignments of up to $17\,\mathrm{mm}$ between neighbouring stacks. Such displacements are critical for the fit and finish of modular assemblies. Although tie-rod elongation was not included in the *3D* model due to time constraints, the results from the *2D* analysis suggest that incorporating elongation effects would likely increase these vertical differences even further.

- Additionally, the *3D* analysis provided a more detailed representation of the internal load paths. It confirmed that vertical and lateral forces introduced by the outriggers were primarily transmitted through the module stacks aligned directly beneath them, as intended in the design. Adjacent vertical stacks were largely unaffected by the presence of the outriggers. This concentration of forces and validation of the intended load path could not be assessed in the *2D* models.

These findings demonstrate the importance of *3D* modelling. While *2D* studies are valuable for early-stage optimisation, they should be complemented by *3D* simulations to fully capture spatial interactions.

Feasibility of the $70\,\mathrm{m}$ Target Height

The results suggest that the proposed hybrid concept is structurally capable of achieving the target height of $70\,\mathrm{m}$, whereas the *core-only* model did not meet the performance criteria at this height.

However, the feasibility of the system is highly sensitive to several factors, including tie-rod elongation, connection performance, and the balance of stiffness between the core and the outriggers. While the analysis indicates that the $70\,\mathrm{m}$ goal is achievable in principle, additional validation is required before practical implementation. Recommendations for further research are presented in Section 8.2.

8
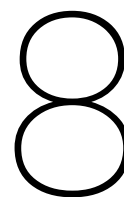
Conclusion and Recommendations

This final chapter concludes the research by reviewing the main findings and outlining suggestions for further study. It begins with a structured summary of each research phase, showing how the sub-questions build towards answering the central research question. The chapter then reflects on the study's limitations and presents recommendations for future research.

8.1. Conclusion

This thesis set out to investigate whether a modular mid-rise building can feasibly reach heights of up to 70 meters while still satisfying structural demands. The key challenge lies in ensuring sufficient lateral stability and load transfer within the constraints of modular construction. To tackle this challenge, the research was divided into four consecutive phases: 1. A preliminary feasibility study, 2. The development of a hybrid structural concept, 3. Detailed structural analysis of the proposed concept, and 4. *Case-study* application. Each phase addressed a specific sub-question that contributed to answering the central research question.

Main research question:

How can the integration of hybrid stability systems be applied to the concept of modular units and precast concrete to build a mid-rise structure up to 70 meters?

After addressing each sub-question in the order of the four phases, the chapter concludes with a comprehensive answer to the main research question, followed by recommendations for future research.

Phase 1: Preliminary Research and Feasibility Assessment

The goal of this phase was to understand the current state of modular mid- and high-rise construction, assess the structural feasibility of such systems up to 70 meters, and identify limitations in current stability strategies.

Sub-question Phase 1:

What are the key structural limitations and possibilities of modular systems up to 70 meters, and which solutions are already proposed in literature and design practice?

To answer this question, literature was reviewed on modular design strategies, structural systems, and realized high-rise projects. Additionally, simplified *parametric* models and hand calculations were used to gain an initial understanding of the structural feasibility of modular systems at a height of up to 70 meters.

Case studies such as Apex House and B2 Tower demonstrated that modular construction is feasible at high-rise scale, but also highlighted limitations, particularly in relation to vertical load transfer and overall stability. Hand calculations based on Eurocode showed that steel corner columns must resist axial forces up to $1152\,kN$ in a 70 meter structure. Only a limited number of profiles, such as SHS 140/10 (cold-formed) and SHS 120/10 (hot-formed), meet this requirement without buckling.

Lateral stability in modular mid-rise structures was found to be critical. Literature identified various types of stability systems that can be implemented to improve lateral performance. *Parametric* models were used to compare four configurations: unbraced, braced, core, and core with outriggers. Among these, the outrigger system showed the lowest lateral displacements and the most uniform deformation. The effect increased when multiple outriggers were added. Integrating an outrigger system into a precast core-based approach proved effective in compensating for the reduced stiffness of precast concrete, by connecting the central core to perimeter columns, thereby reducing sway and optimizing load distribution.

Connection behaviour was studied using *Karamba3D*. Simulations showed that pinned horizontal connections led to significantly higher displacements than rigid ones, highlighting the strong dependence of modular structures on connection stiffness. Literature also indicated that tie-rod connections can significantly improve vertical connectivity between modules. These connections increase module stiffness, resist tensile forces, and reduce lateral deflections. By enhancing overall module stability, tie-rod connections show strong potential as a complementary component to an outrigger system.

Based on these findings, it was concluded that while modular construction up to 70 meters is structurally feasible, key limitations relate to vertical load capacity and lateral stability. Addressing these challenges requires integration of enhanced connection strategies and additional stability systems. Among the proposed design options, a hybrid system combining a precast core, outriggers, corner-supported steel modules, and vertical tie-rod connections showed the most potential. These insights formed the basis for the conceptual design developed in Phase 2.

Phase 2: Concept Development and Initial Modelling
This phase focuses on developing the conceptual design, which consists of the three key components: a corner-supported steel module system, vertical tie-rod connections, and a precast concrete core with integrated outriggers.

Sub-question Phase 2:

How can outrigger systems and tie-rod connections be integrated into the conceptual design of modular buildings up to 70 meters, and to what extent does this integration enhance structural performance?

To answer this question, a first iteration of the concept was developed. The concept was initially established through a *3D* structural layout and then translated into a simplified *2D* model to enable efficient structural analysis at this stage of the research.

Structural performance was evaluated under both vertical and horizontal loading. Outriggers were introduced at floor levels 7, 14, and 20. This configuration led to a notable increase in lateral stiffness, reducing maximum top displacements by approximately 30% compared to the *core-only* system. The distribution of axial forces showed that the outriggers successfully engaged the perimeter columns, enabling the modules to participate in the lateral load-resisting system and resulting in a more balanced and efficient load path.

The influence of connection behaviour was also examined. Increasing rotational stiffness at the module-to-core interface led to substantial reductions in lateral displacement, up to a threshold of 10^5 kNm/rad. Beyond this value, additional stiffness had minimal effect. Stress concentrations at the outrigger-to-core interface identified this as a critical location in the connection design.

Validation against analytical and matrix-frame models showed that the *parametric* approach yielded a sufficiently accurate representation of the structural behaviour.

Overall, this phase demonstrated that the proposed hybrid concept provides adequate lateral stability for mid-rise modular buildings. These insights formed the foundation for more detailed evaluation in the next phase.

Phase 3: Detailed Structural Analysis
This phase focuses on evaluating the structural performance of the proposed concept in more detail. The aim is to assess how the system behaves under realistic loads and to identify where the design can be improved.

Sub-question Phase 3:

How can a detailed structural analysis be used to evaluate the performance of the proposed modular mid-rise concept and guide its design optimizations?

The original configuration with three outriggers improved performance over the *core-only* system but did not meet the stricter deflection limit of $H/750$. To guide the optimisation, an analytical estimation was made of the required global flexural stiffness of the structure. By applying analytical models, the minimum global stiffness needed to satisfy the displacement criterion at $70\,\mathrm{m}$ height was calculated as $EI_{\mathrm{req}} = 2.12 \times 10^9\,\mathrm{kNm^2}$.

Through *parametric* analysis, an optimised configuration with two outriggers at levels 7 and 16 was identified as the most efficient and practical solution for reaching the target height. Additional design improvements included upgrading column steel grade from S235 to S355, resizing column cross-sections, and increasing tie-rod capacity by selecting larger diameters. Further investigation into stiffness distribution revealed that the core plays a dominant role in lateral performance. While outriggers contributed to reduced displacement, their effect was limited compared to increasing the core's stiffness. The benefit of outriggers diminished when core rigidity was high, underscoring the importance of balance between core and outrigger design to reach the full potential of the system.

These findings confirm that the structural concept is feasible for modular applications up to $70\,\mathrm{m}$, provided that an improved configuration is used with two optimally placed outriggers, enhanced material choices, and upgraded tie-rod capacity. The required stiffness calculated in this phase was used as a reference in the next and final stage, where the optimised concept is applied in a *3D* case study.

Phase 4: Case Study Application – Tang Tower

This final phase applies the optimized structural concept to a real-world case study to test and validate the research findings in a *3D* model. The Tang Tower project serves as a practical context to evaluate the applicability and performance of the proposed concept under realistic conditions.

Sub-question Phase 4:

How can the structural concept be applied in the context of the Tang Tower to validate the proposed design solution, and what is the result of this?

To answer this sub-question, the optimized structural concept was applied to the Tang Tower, a real-world-inspired modular mid-rise case study. In contrast to earlier *2D* based analyses, this phase employed a fully developed *3D parametric* model to evaluate the structural performance of the system under realistic geometric conditions and to investigate effects that could not be captured in *2D*.

The results confirmed that the transition to a *3D* analysis provided additional insights into spatial behaviour, including inter-story drift and differential vertical displacement between module stacks, phenomena that could not be captured in the *2D* models. The outrigger system improved lateral stiffness, reducing top displacement by 13.5% and extending the feasible building height to $67.7m$ while satisfying the $H/750$ deflection criterion. tie-rod forces remained within feasible design limits, though axial elongation reduced their contribution to lateral stiffness. Vertical displacement mismatches of up to $17mm$ were observed between adjacent modules.

To assess the overall feasibility of the system, four additional evaluations were carried out. First, a dedicated analysis of tie-rod elongation confirmed that axial deformation significantly reduces the contribution of the tie-rods to lateral stiffness. This underlined the importance of using larger diameters to limit elongation effects and to increase the effectiveness of the proposed concept.

Second, the internal forces in critical connection zones, namely module-to-module, module-to-outrigger, module-to-core, and outrigger-to-core, were found to remain within realistic capacity limits when compared to available experimental references and design guidelines.

Third, the introduction of rotational stiffness in the horizontal inter-modular connections proved to be an effective design strategy to reduce vertical misalignments between adjacent module stacks.

Finally, an expert review by Daiwa House Modular Europe validated the practical alignment of the concept with current modular construction practices. However, it also highlighted potential execution risks, particularly in the installation of tie-rods and managing architectural creativity across the module layout.

The case study implementation confirmed that the design strategies developed during the *2D* phase also led to improved lateral performance under realistic *3D* conditions. Internal force levels remained within practical design limits, and the optimised configuration met all performance criteria. At the same time, the *3D* model revealed new challenges, such as vertical misalignments between module stacks and limitations in connection modelling, that were not apparent in earlier phases.

Main Research Question

This section will conclude with the answer to the main research question and the contribution of this research. The central research question of this thesis is:

How can outrigger systems and tie-rod connections be integrated into the structural design of modular buildings up to 70 meters, and to what extent does this integration improve structural performance and feasibility?

Before this research, the structural stability of modular high-rise buildings above ten storeys largely depended on precast or in-situ concrete cores. Although the literature review showed the potential of outrigger elements and tie-rod connections to enhance performance, their combined use in a modular mid-rise context had not yet been fully explored.

This thesis bridges that gap by developing, analysing, and validating a hybrid structural concept in which corner-supported steel modules contribute directly to lateral stability. Through the integration of tie-rods and outrigger elements, the modules are no longer limited to vertical load transfer but become active components within the overall stability system. This represents a clear shift from conventional modular practice, where structural stability typically depends on cores or internal bracing, and modules play a largely passive role.

A central outcome of this research is the demonstrated performance gain achieved by integrating outriggers. By connecting the core to perimeter modules, the outrigger system enables more efficient distribution of lateral forces. In the *3D* case study, this resulted in a 13.5% reduction in top displacement and enabled the structure to reach a height of $67.7\,m$ while satisfying the $H/750$ top displacement limit. *Parametric* optimisation identified outrigger placement at levels 7 and 14 as the most effective configuration, offering an optimal balance between structural stiffness and practical feasibility.

The study established capacity limits for both the tie-rods and the steel corner columns. Only a limited number of cross-sections with S355 steel, such as SHS 140/10 (CF), SHS 120/10 (HF), and RHS 180×100/10 (HF), were found to meet the Eurocode buckling criteria at a building height of $70\,m$. For the tie-rods, the diameter was identified as a critical parameter. Axial elongation under load significantly reduced the overall effectiveness of the structural system. When using M24 tie-rods, the outriggers achieved a relative stiffness gain of only 17.7%, compared to 25.4% in the idealised case without elongation. Increasing the tie-rod diameter to M50 improved the effectiveness to 20.5%, demonstrating that larger diameters can enhance the performance of the proposed concept.

The effectiveness of outriggers was shown to depend strongly on the stiffness of the core. *Parametric* analysis revealed that when the core was relatively flexible, the inclusion of outriggers reduced lateral displacement by over 30%. However, as core stiffness increased, this benefit diminished to below 10%, underscoring the importance of a balanced stiffness distribution between core and outriggers to maximise the effectiveness of the proposed concept.

An in-direct contribution of this research was the application of *parametric modelling*, which proved to be an effective tool for structural exploration. By developing a flexible model, this method enabled rapid testing and optimisation of different design configurations, offering advantages over conventional software workflows. However, as discussed in Section 7.1, the approach also introduced certain limitations that must be considered in future applications.

The findings of this research provide practical design guidelines and performance benchmarks for a potential modular hybrid mid-rise concept. The following section outlines recommendations for further research, based on the limitations and challenges identified throughout the study.

8.2. Recommendations for Further Research

To build on the findings of this research, the following directions are recommended for future studies:
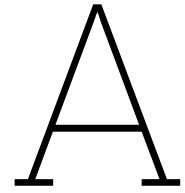
- The tie-rod elements were modelled using simplified assumptions and did not account for tension-compression asymmetry or nonlinear material behaviour in the case study. In future research, a more advanced numerical modelling approach should be employed, using software that supports direction-dependent stiffness properties, such as *ABAQUS* or *DIANA*, to more accurately simulate tie-rod elongation effects, particularly in a *3D* environment.

- Although existing experimental studies were used to verify the plausibility of internal forces in the structural connections, no physical testing was conducted on the specific intermodular tie-rod connection proposed in this research. It is recommended that full-scale laboratory tests be performed to evaluate the capacity, stiffness and tolerance sensitivity of this critical connection detail.

- The concrete core was modelled as a monolithic element with a reduced modulus to approximate segmental behaviour. However, this is a simplification. Future research should model the core as a segmented precast system with realistic joint properties to evaluate its influence on global stiffness and outrigger effectiveness.

- The analysis in this thesis was conducted using linear elastic modelling. Further research could focus on the effect of nonlinear behaviour, including concrete cracking, plastic deformation in steel components, and second-order effects, to assess the robustness of the concept under extreme loading conditions.

- Only two load combinations were considered in the current analysis. A broader evaluation of structural performance under dynamic loads such as wind excitation, vibration, and seismic action is recommended, especially for taller or asymmetrical variations of the proposed concept.

- The current structural model assumes fixed base supports. In reality, foundation flexibility and soil-structure interaction can significantly influence both lateral and vertical response. Future work should investigate the implications of realistic support conditions on global behaviour.

- While the technical feasibility was the primary focus of this research, the economic and environmental performance of the proposed concept remains unexplored. It is recommended that future studies evaluate the cost-efficiency and embodied carbon of the outrigger–tie-rod system in comparison to conventional modular or hybrid structural solutions. Since modular construction is often promoted for its economic and sustainability benefits, it is important to assess whether the proposed hybrid concept aligns with these core values.

References

[1] Rijswaterstaat. *900.000 nieuwe woningen om aan groeiende vraag te voldoen*. URL: `https://www.rijksoverheid.nl/onderwerpen/volkshuisvesting/nieuwe-woningen`.

[2] *Vergrijzing en de krappe woningmarkt: meer integraal denken en betere samenwerking vereist - Wyzer*. URL: `https://www.wyzer.nl/kennisartikel/vergrijzing-en-de-krappe-woningmarkt-meer-integraal-denken-en-betere-samenwerking-vereist/`.

[3] *Dalend aantal mensen per woningen - woningsplitsen biedt kansen*. URL: `https://vastgoedinsider.nl/dalend-aantal-mensen-per-woningen-woningsplitsen-biedt-kansen/`.

[4] *Wat zijn de gevolgen van stikstof voor bouwprojecten? • Jurable*. URL: `https://www.jurable.nl/blog/2022/07/25/gevolgen-stikstof-voor-bouwprojecten/`.

[5] *Modulair en industrieel bouwen: dé oplossing voor de wooncrisis*. URL: `https://www.stedenbouw.nl/artikel/modulair-en-industrieel-bouwen-de-oplossing-voor-de-wooncrisis/`.

[6] Huu Tai Thai, Tuan Ngo, and Brian Uy. *A review on modular construction for high-rise buildings*. Dec. 2020. DOI: `10.1016/j.istruc.2020.09.070`.

[7] Nick Bertram et al. *Modular construction: From projects to products*. Tech. rep. 2019.

[8] *Modular construction advantages and disadvantages*. URL: `https://www.hm-ec.com/blog-posts/modular-construction-advantages-and-disadvantages-hm`.

[9] R. Mark Lawson, Ray G. Ogden, and Rory Bergin. "Application of Modular Construction in High-Rise Buildings". In: *Journal of Architectural Engineering* 18.2 (June 2012), pp. 148–154. ISSN: 1076-0431. DOI: `10.1061/(asce)ae.1943-5568.0000057`.

[10] Ryan E Smith, James Timberlake, and Faia Smith. *PREFAB ARCHITECTURE*. Tech. rep. URL: `www.itac.utah.edu`.

[11] Andrew William Lacey et al. *Review of bolted inter-module connections in modular steel buildings*. May 2019. DOI: `10.1016/j.jobe.2019.01.035`.

[12] Jiahao Peng, Chao Hou, and Luming Shen. "Progressive collapse analysis of corner-supported composite modular buildings". In: *Journal of Building Engineering* 48 (May 2022), p. 103977. ISSN: 2352-7102. DOI: `10.1016/J.JOBE.2021.103977`.

[13] Ar Ravi and Prakash Mishra. "Review of Prefabricated Prefinished Volumetric Construction and Its Application in India". In: *International Journal of Research Publication and Reviews* 3.1 (2022), pp. 568–573. URL: `www.ijrpr.com`.

[14] Christos Hannides. *Modular Construction*.

[15] Si Hwa Heng et al. "Computational Modelling of Intra-Module Connections and Their Influence on the Robustness of a Steel Corner-Supported Volumetric Module". In: *Modelling* 5.1 (Mar. 2024), pp. 392–409. ISSN: 2673-3951. DOI: `10.3390/modelling5010021`. URL: `https://www.mdpi.com/2673-3951/5/1/21`.

[16] Zhihang Ye et al. *State-of-the-art review and investigation of structural stability in multi-story modular buildings*. Jan. 2021. DOI: `10.1016/j.jobe.2020.101844`.

[17] Robert Mark Lawson and Jane Richards. "Modular design for high-rise buildings". In: *Proceedings of the Institution of Civil Engineers: Structures and Buildings* 163.3 (2010), pp. 151–164. ISSN: 17517702. DOI: `10.1680/stbu.2010.163.3.151`.

[18] Bahareh Maleki et al. "Integrated Value Model for Sustainable Assessment of Modular Residential Towers: Case Study: Ten Degrees Croydon and Apex House in London". In: *Sustainability (Switzerland)* 16.2 (Jan. 2024). ISSN: 20711050. DOI: `10.3390/su16020497`.

[19] Will Mann. *World's tallest modular scheme approved - Construction Management*. URL: `https://constructionmanagement.co.uk/worlds-tallest-modular-development-gets-planning-a/`.

[20] Aluminium & Glass Facades Ltd. *Apex House, Wembley*. URL: `https://www.agf.uk.com/projects/apex-house-wembley/`.

[21] HTA Design LLP. *Apex house*. URL: `https://www.skyscrapercenter.com/building/apex-house/27396`.

[22] NLA. *Londons Built Environment Community*. Jan. 2025. URL: `https://nla.london/projects/ten-degrees`.

[23] David Farnsworth. *Modular Tall Building Design at Atlantic Yards B2 大厦大厦大厦B2 大厦大厦大厦大厦大厦大厦大厦大厦*. Tech. rep. URL: `www.arup.com`.

[24] Archinspires. *The Mini Sky City – How architects built a 57-story skyscraper in just 19 days*. Sept. 2023. URL: `https://archinspires.com/2023/09/06/the-mini-sky-city-how-architects-built-a-57-story-skyscraper-in-just-19-days/`.

[25] Eoghan Macguire. *The Chinese firm that can build a skyscraper in a matter of weeks*. June 2015. URL: `https://edition.cnn.com/2015/06/26/asia/china-skyscraper-prefabricated/index.html`.

[26] *Dimensions of Design – 2D, 3D & Hybrid components - Built Offsite*. URL: `https://builtoffsite.com.au/emag/issue-02/dimensions-design-2d-3d-hybrid-components/`.

[27] J. Y.R. Liew, Y. S. Chua, and Z. Dai. "Steel concrete composite systems for modular construction of high-rise buildings". In: *Structures* 21 (Oct. 2019), pp. 135–149. ISSN: 23520124. DOI: `10.1016/j.istruc.2019.02.010`.

[28] R. M. Lawson and R. G. Ogden. "'Hybrid' light steel panel and modular systems". In: *Thin-Walled Structures* 46.7-9 (July 2008), pp. 720–730. ISSN: 0263-8231. DOI: `10.1016/J.TWS.2008.01.042`.

[29] B. Shirokov and T. Belash. "Parametric Studies of Intra-Modular". In: *International Conference on Construction, Architecture and Technosphere Safety* (Mar. 2023). URL: `https://link.springer.com/book/10.1007/978-3-031-21120-1`.

[30] Xiaodun Wang et al. "Lateral stiffness of modular steel joint with semi-rigid bolted intra-module connection". In: *Journal of Building Engineering* 97 (Nov. 2024), p. 110668. ISSN: 2352-7102. DOI: `10.1016/J.JOBE.2024.110668`.

[31] Sandor Kaliszky -Budapest et al. *Semi-rigid connections in structural steelwork.* Tech. rep. 2000.

[32] Feng Wei Shi et al. "Seismic behavior of high-rise modular buildings with simplified models of inter-module connections". In: *Journal of Constructional Steel Research* 221 (Oct. 2024). ISSN: 0143974X. DOI: `10.1016/j.jcsr.2024.108867`.

[33] Betül Karacalı and Merve Sağıroğlu Maali. *Review of Interconnection in Modular Structures*. Tech. rep.

[34] Andrew William Lacey et al. *Review of bolted inter-module connections in modular steel buildings*. May 2019. DOI: `10.1016/j.jobe.2019.01.035`.

[35] Daiwa Modular Europe. *Internal Information Exchange with Daiwa Modular Europe (Confidential)*. Tech. rep. 2024.

[36] Heshachanaa Rajanayagam et al. "A-State-Of-The-Art review on modular building connections". In: *Structures* 34 (Dec. 2021), pp. 1903–1922. ISSN: 23520124. DOI: `10.1016/j.istruc.2021.08.114`.

[37] Hi Sun Choi et al. *Title: Outrigger System Design Considerations High-Rise Buildings Outrigger System Design Considerations*. Tech. rep. 3. 2012, pp. 237–246. URL: `www.ctbuh.org`.

[38] R M Lawson and Masce Acgi. *Building Design Using Modules*. Tech. rep.

[39] Feng Fu. "Shear Wall, Core, Outrigger, Belt Truss, and Buttress Core System for Tall Buildings". In: *Design and Analysis of Tall and Complex Structures* (Jan. 2018), pp. 81–107. DOI: `10.1016/B978-0-08-101018-1.00003-4`.

[40] B. G. Kavyashree, Shantharam Patil, and Vidya S. Rao. "Evolution of Outrigger Structural System: A State-of-the-Art Review". In: *Arabian Journal for Science and Engineering* 46.11 (Nov. 2021), pp. 10313–10331. ISSN: 21914281. DOI: `10.1007/S13369-021-06074-9/TABLES/1`. URL: `https://link.springer.com/article/10.1007/s13369-021-06074-9`.

[41] Akshay Khanorkar et al. "Outrigger and Belt Truss System for Tall Building to Control Deflection: A Review". In: *GRD Journal for Engineering |* 1.6 (2016). ISSN: 2455-5703. URL: `www.grdjournals.com`.

[42] *EN 1993-1-1: Eurocode 3: Design of steel structures - Part 1-1: General rules and rules for buildings*. Tech. rep.

[43] *EN 1991-1-4: Eurocode 1: Actions on structures - Part 1-4: General actions - Wind actions*. Tech. rep. 2010.

[44] H H Snijder, H M G M Steenbergen, and Steel Design. *Structural basics Annex for The Netherlands*. Tech. rep. 2019. URL: `www.bouwenmetstaal.nl`.

[45] Mick Bosse. *MSc Thesis Calculation Method for the Lateral Deflection of Multi-Storey Timber Modular Buildings*. Tech. rep. URL: `http://repository.tudelft.nl/.`.

[46] Thomas Leung et al. *PREDICTING LATE RAL DEFLECTION AND FUNDAMENTAL NATURAL PERIOD OF MULTI-STOREY WOOD FRAME BUILDINGS*. Tech. rep.

[47] Tianyao Ping, Wei Pan, and Ben Mou. "An innovative type of module-to-core wall connections for high-rise steel modular buildings". In: *Journal of Building Engineering* 62 (Dec. 2022). ISSN: 23527102. DOI: `10.1016/j.jobe.2022.105425`.

[48] Sriskanthan Srisangeerthanan et al. "Numerical study on the effects of diaphragm stiffness and strength on the seismic response of multi-story modular buildings". In: *Engineering Structures* 163 (May 2018), pp. 25–37. ISSN: 18737323. DOI: `10.1016/j.engstruct.2018.02.048`.

[49] Y. S. Chua, J. Y.Richard Liew, and S. D. Pang. "Modelling of connections and lateral behavior of high-rise modular steel buildings". In: *Journal of Constructional Steel Research* 166 (Mar. 2020). ISSN: 0143974X. DOI: `10.1016/j.jcsr.2019.105901`.

[50] P Ham and K.C. Terwel. *Structural calculations of High Rise Structures*. Tech. rep. Apr. 2017.

[51] Aditya Kumar Tiwary. "Different types of outrigger system in high-rise buildings: a preliminary comparative seismic analysis in a 40-story RC building". In: *Innovative Infrastructure Solutions* 7.6 (Dec. 2022). ISSN: 23644184. DOI: `10.1007/s41062-022-00946-1`.

[52] Victokr Castlen Rist and Stefan Svensson. *TALL BUILDING DESIGN Steel, Concrete, and Composite Systems*. Tech. rep. Faculty of Engineering LTH, Lund University, June 2016.

[53] Sidi Shan and Ben Mou. "Development of an innovative module-to-core wall connection for steel-framed modular high-rise buildings". In: *Journal of Constructional Steel Research* 214 (Mar. 2024). ISSN: 0143974X. DOI: `10.1016/j.jcsr.2024.108494`.

[54] C.R. Braam, Paul Lagendijk, and W.C. Dees. *Constructieleer gewapend beton - cement en beton 2*. 6th. Aeneas Media B.V, Apr. 2010.

[55] *NEN-EN 300*. Tech. rep.

[56] J Zhou, G B Bu, and K N Li. *Calculation Methods for Inter-Story Drifts of Building Structures*. Tech. rep.

[57] IDEA STATICA. *IDEA Statica: Kennisbank Singulariteiten vs. spanningsconcentraties*. 2025. URL: `https://www.ideastatica.com/nl/support-center/singulariteiten-vs-spanningsconcentraties`.

[58] E. Bazarchi et al. "Experimental and numerical investigation of a novel vertically unconstrained steel inter-modular connection". In: *Thin-Walled Structures* 183 (Feb. 2023). ISSN: 02638231. DOI: `10.1016/j.tws.2022.110364`.

[59] Richard Henderson. *THE DESIGN OF CAST-IN PLATES*. Tech. rep. SCI (The Steel Construction Institute), 2017.

[60] A. V. Beek. *Advanced Engineering Design*. 8th ed. Delft: Delft University of Technology, 2006.

[61] Karamba 3D. *Karamaba3D: In depth Component Reference*. Feb. 2025. URL: `https://manual.karamba3d.com/3-in-depth-component-reference/3.5-algorithms/3.5.8-optimize-cross-section`.

A

Appendix: Column Capacities

An Excel sheet containing the calculated capacities of all columns used in this study is available in the supplementary materials. This file provides detailed data on column capacities for various configurations and can be accessed via the following GitHub repository:

```
https://github.com/ScheltoBlankenTU/TU-Delft-Thesis-Supplements
```

Figure A.1 illustrates the location of the file containing the Excel sheet with the column capacities on the GitHub repository.
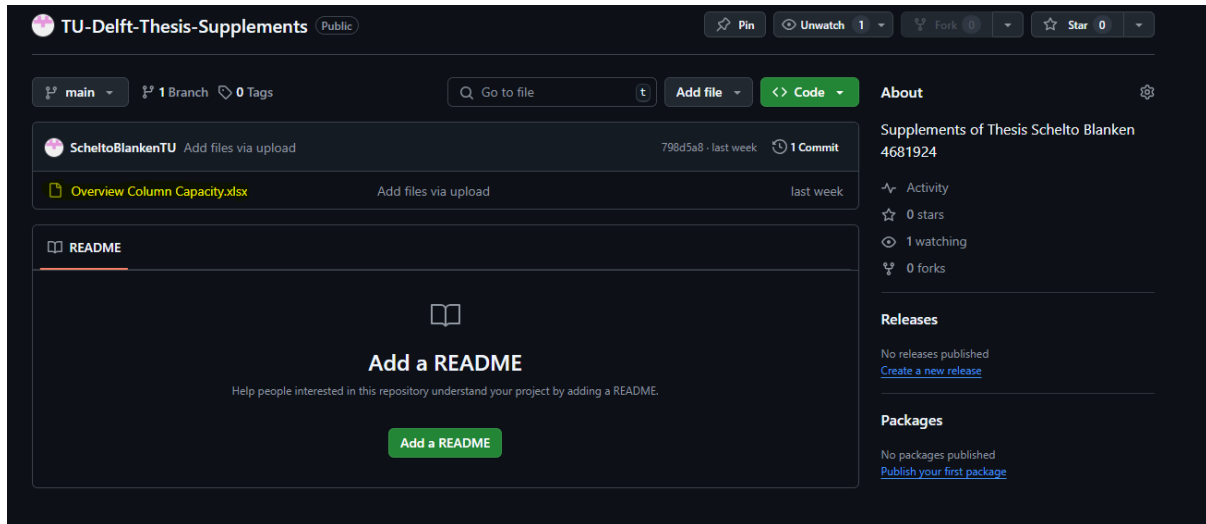
Figure A.1: Location of the column capacity sheet on GitHub

B

Appendix: Matrix Frame Results Rigid frame

This appendix presents the results of a rigid frame representing the portals on the short side of a module. A dummy load of 10 kN/m is applied on the left side of the structure in the positive x-direction.

Figure B.1: Normal Force Rigid Portal

Figure B.2: Shear force Rigid Portal
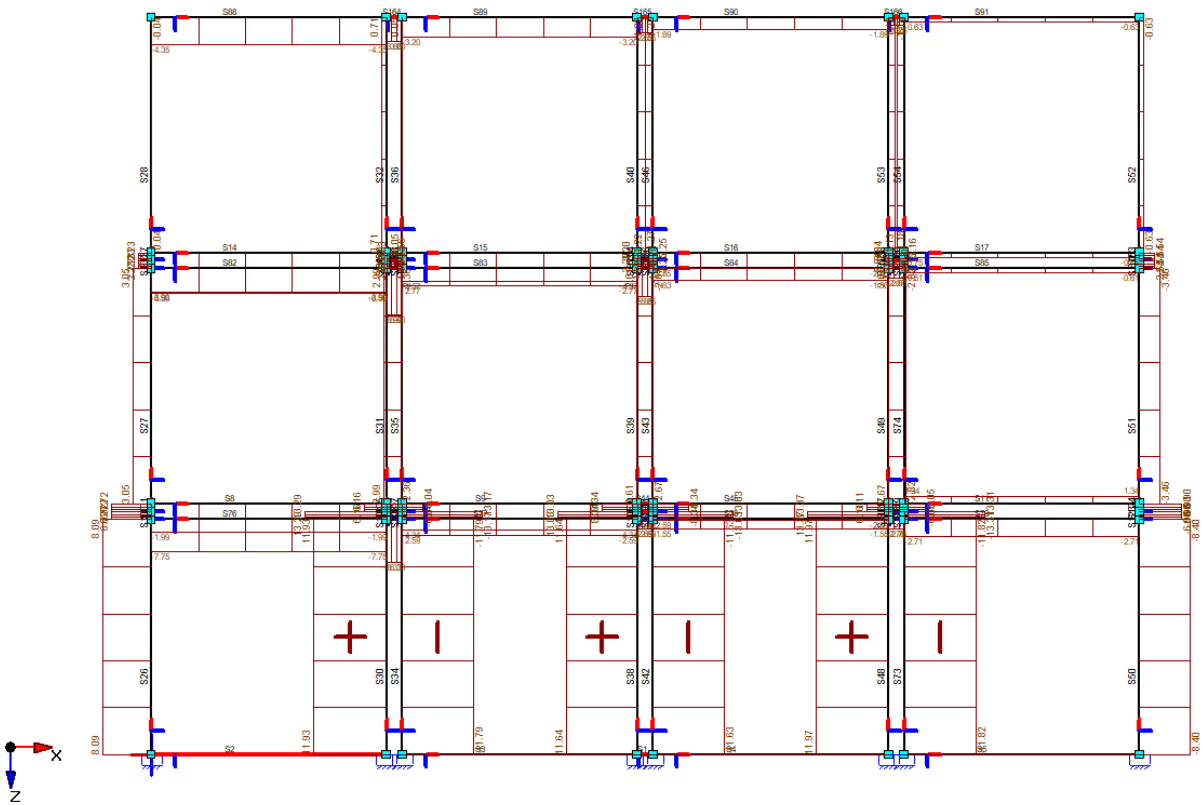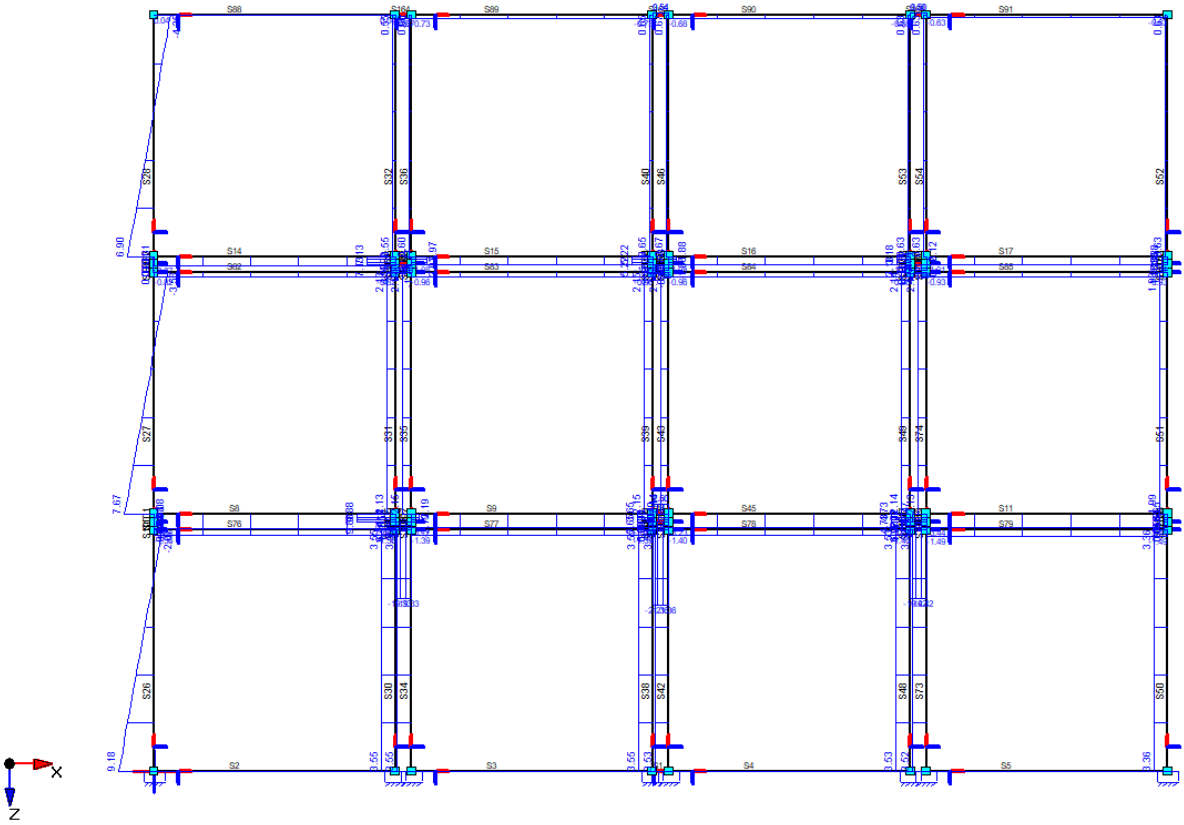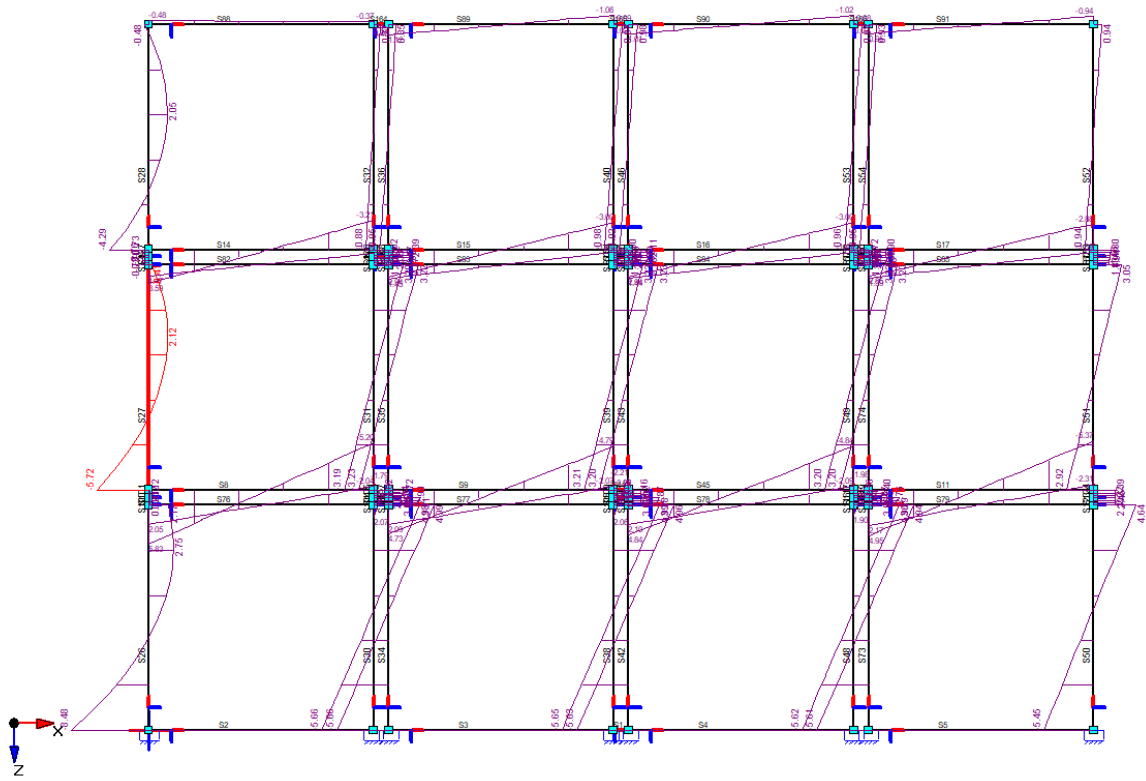
Figure B.3: Moment line Rigid Portal

C

Appendix: Validation Using Different Modelling Software

This appendix presents a comparative validation of the structural analysis results obtained from three different modelling software tools used in this thesis. The comparison focuses on the short-side portal frame of a single module in a two-dimensional configuration. The software packages used are *Karamba3D*, *Technosoft*, and *Matrix-Frame*.

Figure C.1 displays the normal force, shear force, and bending moment diagrams generated by each software package for the same module configuration.
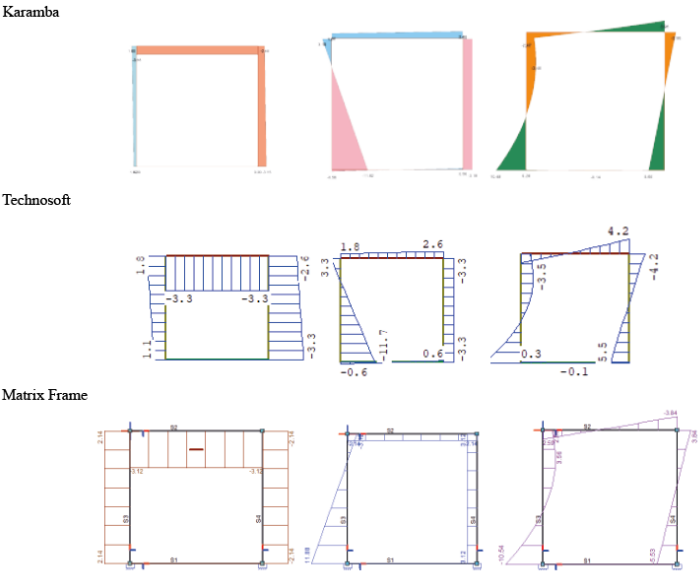
Figure C.1: Comparison of normal force, shear force, and bending moment diagrams for a single module portal frame using different software

In addition, Figure C.2 shows the horizontal displacements of the portal frame, as calculated by the three modelling environments.
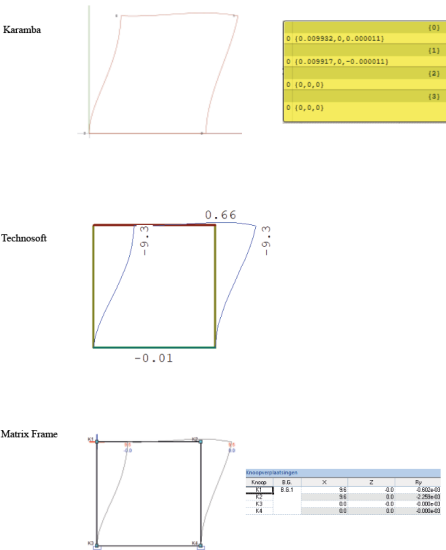
Figure C.2: Comparison of horizontal displacements for the same portal frame across different software

As illustrated in the figures, the analysis results are largely consistent across all three platforms. Minor differences are observed, which can be attributed to variations in modelling assumptions, numerical solvers, and internal element formulations. Nevertheless, the discrepancies remain within an acceptable range, confirming the reliability of the *Karamba3D* results used in this thesis.

D

Appendix: Frame Validation

Normal force Diagram
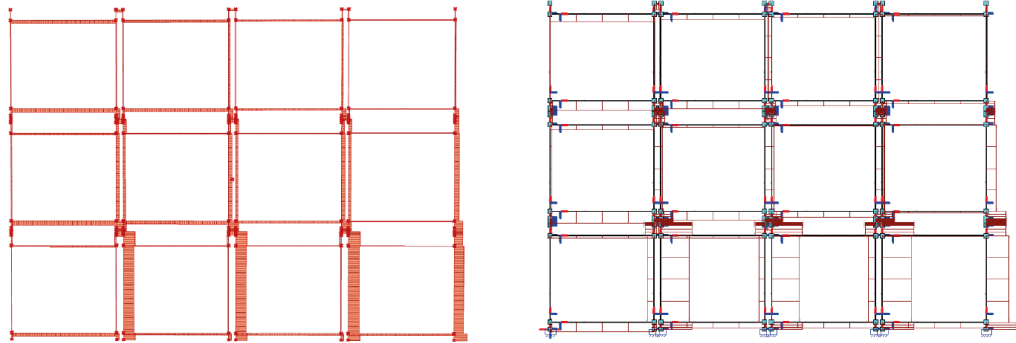
Shear force Diagram
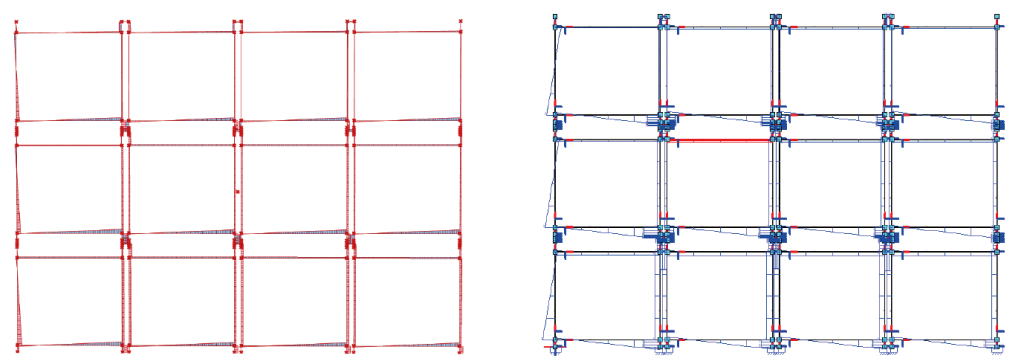
Moment force Diagram
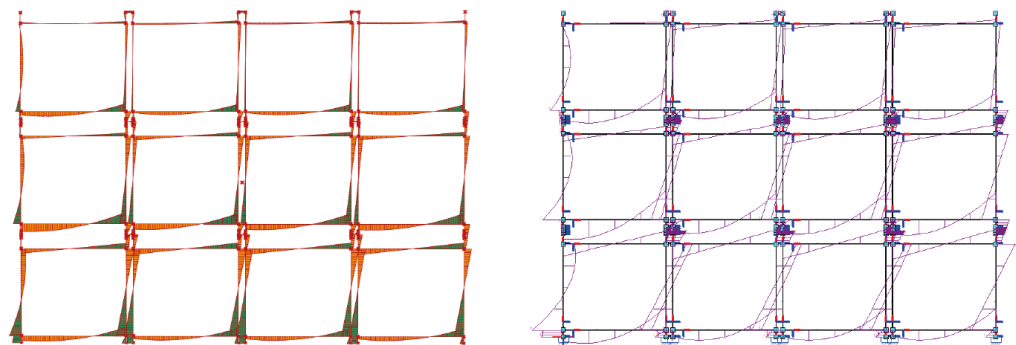
Displacement force Diagram
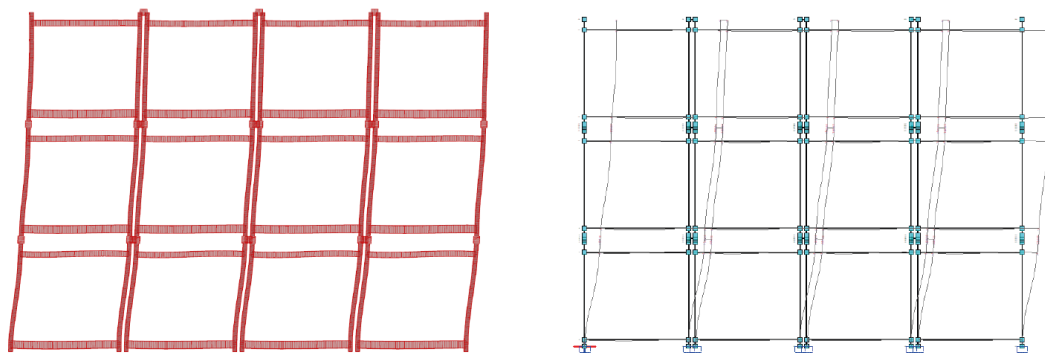
Figure D.1: Overview of Model diagrams Rigid frame

Normal force Diagram
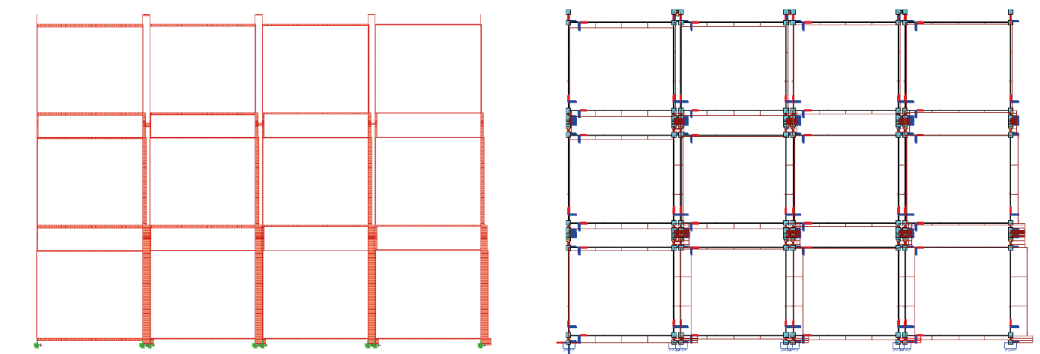
Shear force Diagram
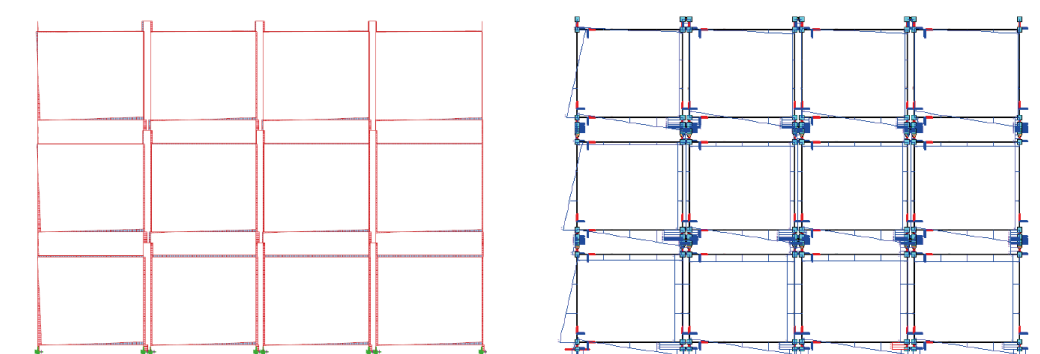
Moment force Diagram
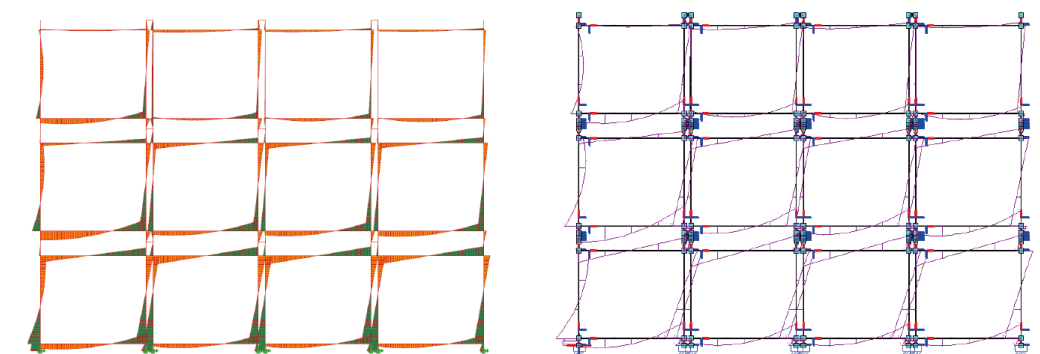
Displacement force Diagram
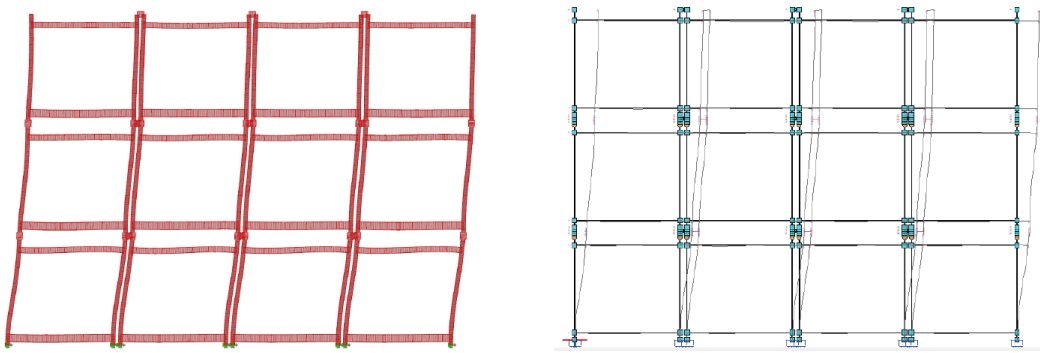
Figure D.2: Overview of Model diagrams independent frame

E

Appendix: Enlarged Figures

This appendix presents enlarged figures illustrating the force distribution and utilization of columns of the modules in both the core system and the original outrigger configuration.

Figures E.1 and E.2 show the normal force distribution for all four column groups in the core system and the original outrigger configuration, respectively, under load combination L_{01}.

Normal Force Distribution for Core System

(a) Normal force group 1

(b) Normal force group 2

(c) Normal force group 3

(d) Normal force group 4
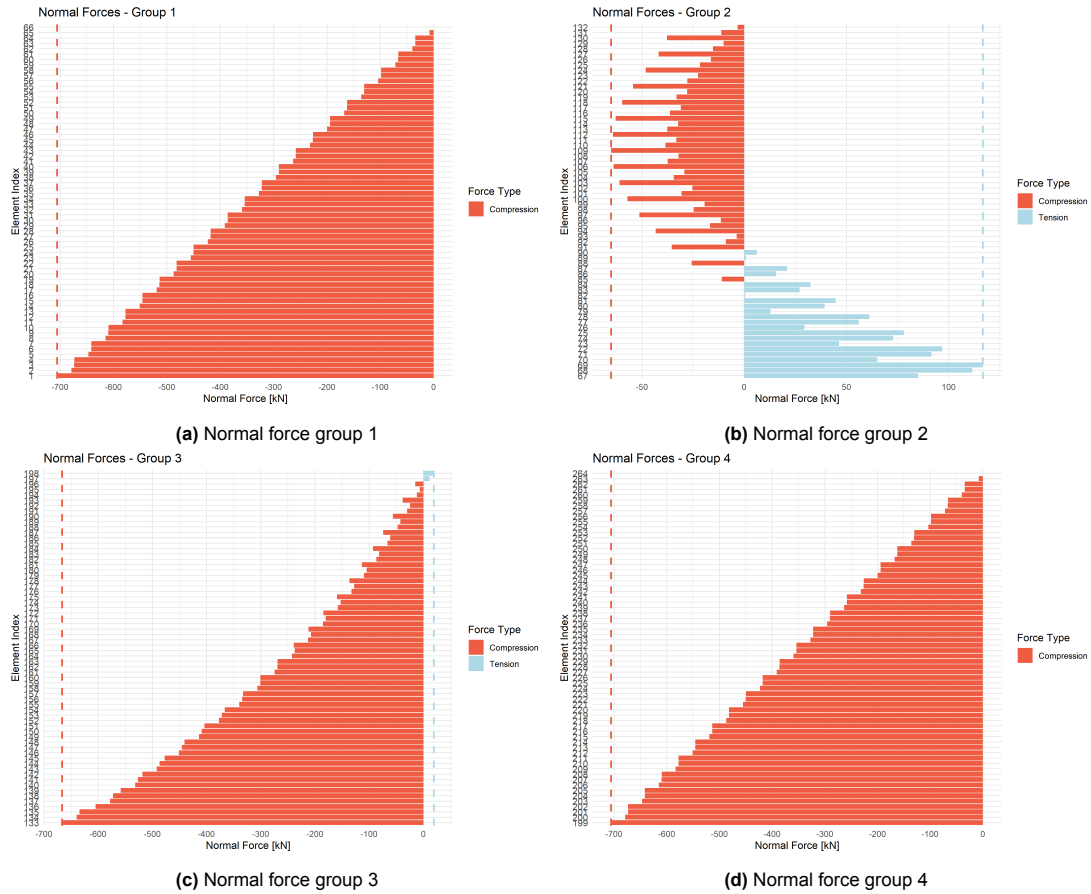
Figure E.1: Normal force distribution for all four groups in the core system (L_{01} load combination)

Normal Force distribution of the Original Outrigger Configuration

(a) Normal force group 1

(b) Normal force group 2

(c) Normal force group 3

(d) Normal force group 4
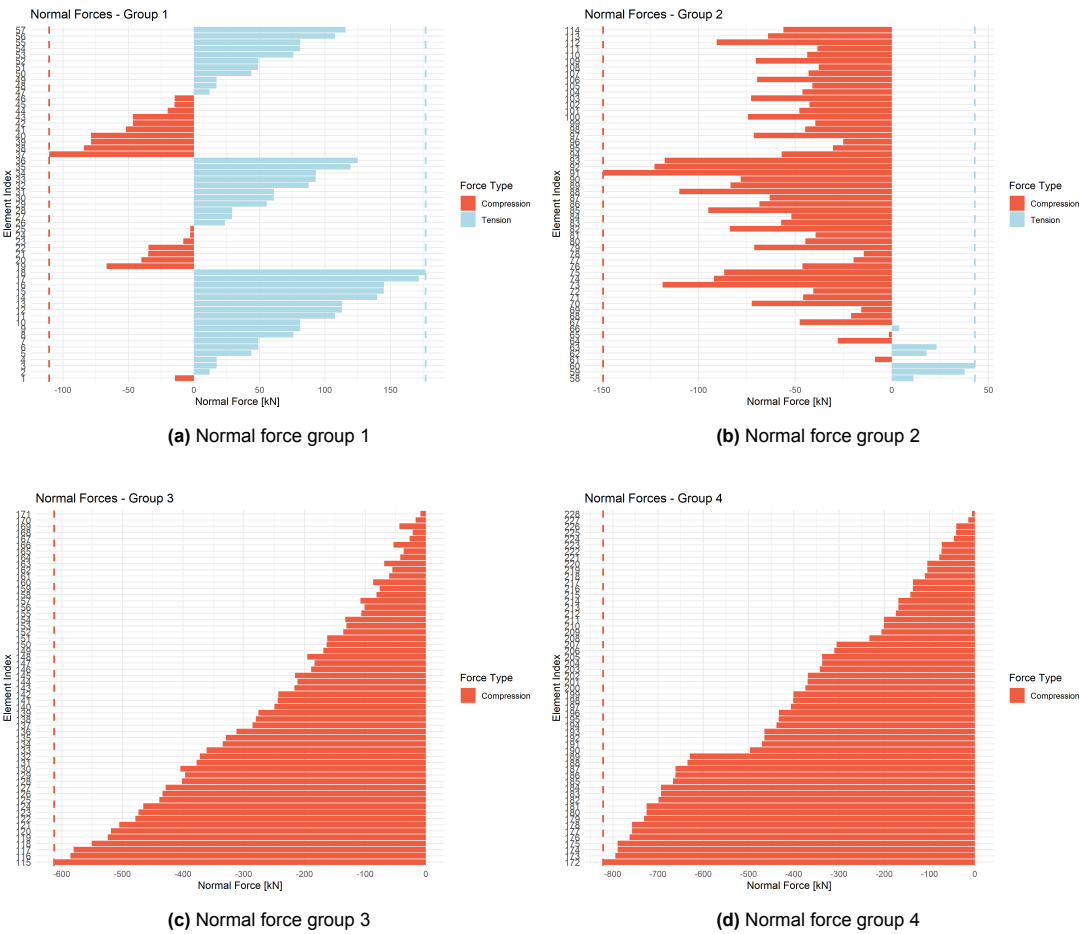
Figure E.2: Normal force distribution for all four groups original outrigger configuration (L_{01} load combination)

Figures E.3 and E.4 present the utilization of the column members for all four groups in the core system and the original outrigger configuration, respectively.

Utilization of the Column Members of the Core System

(a) Utilization group 1

(b) Utilization group 2

(c) Utilization group 3

(d) Utilization group 4
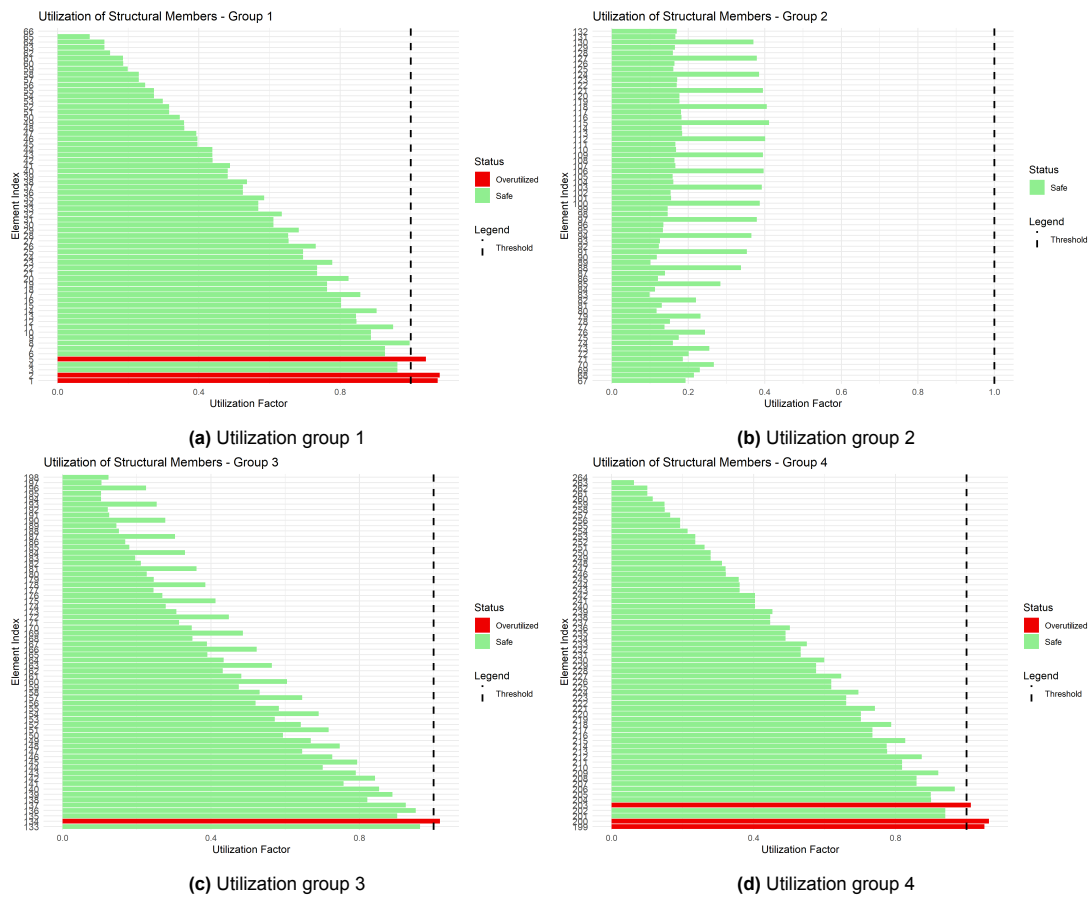
Figure E.3: Utilization for all four groups for the Core system (L_{01} load combination)

Utilization of the Original Outrigger Configuration

(a) Utilization group 1

(b) Utilization group 2

(c) Utilization group 3

(d) Utilization group 4
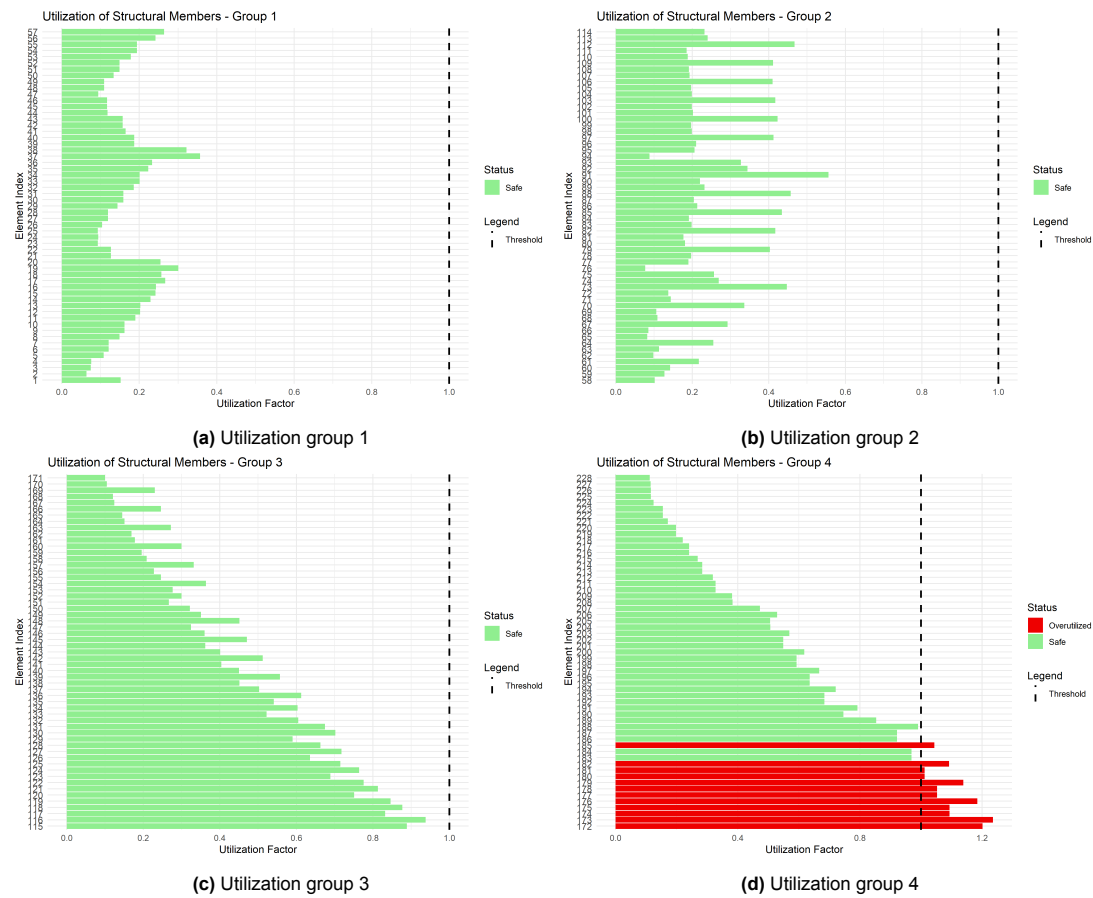
Figure E.4: Utilization for all four groups Original Outrigger (L_{01} load combination)

F

Appendix: Mesh Sensitivty Study

To ensure numerical accuracy of the finite element model, a mesh sensitivity study was performed. The purpose of this analysis is to determine the influence of element size on the calculated top displacement of the structure and to justify the mesh resolution used in the final simulations.

A range of meshes was considered with element sizes varying between $1.2\,\mathrm{m}$ and $0.25\,\mathrm{m}$. For each mesh, the average top displacement was extracted from the analysis results.

Figure F.1 shows the relation between mesh size and average top displacement. As expected, the displacement increases with decreasing mesh size, which is consistent with the underlying theory: finer meshes introduce more degrees of freedom (DOFs), allowing the structure to deform more realistically and with less artificial stiffness. Coarser meshes, on the other hand, tend to overconstrain the system, leading to underestimated deformations.
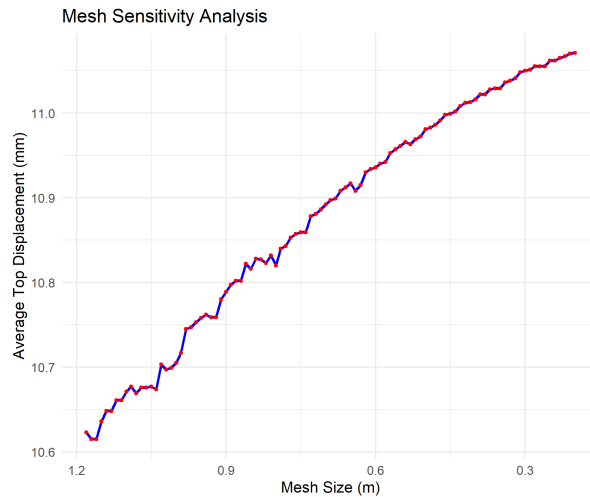
Figure F.1: Average top displacement as a function of mesh size. Mesh size decreases from left to right.

In Figure F.2, the same data is plotted on a logarithmic x-axis to better visualise the rate of convergence. The curve gradually flattens, indicating diminishing sensitivity of the output to further mesh refinement.
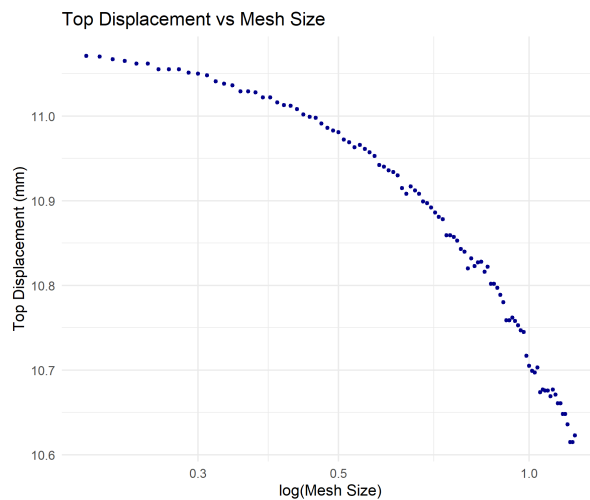
Figure F.2: Top displacement plotted against mesh size using a logarithmic x-axis.

Based on these results, it is concluded that a mesh size of $0.3\,\mathrm{m}$ provides a good balance between accuracy and computational efficiency. At this resolution, the top displacement is within $0.021\,\mathrm{mm}$ of the value obtained using the finest mesh, which is considered acceptable for the purpose of this study.

G

Appendix: Tie-rod Dimensions

Figure G.1 illustrates the geometric properties of the tie-rods considered in this study, including diameters and relevant cross-sectional dimensions.

$$H= 0.86603P \quad h_3= 0.61343P \quad H_1= 0.54127P \quad R= H/6$$

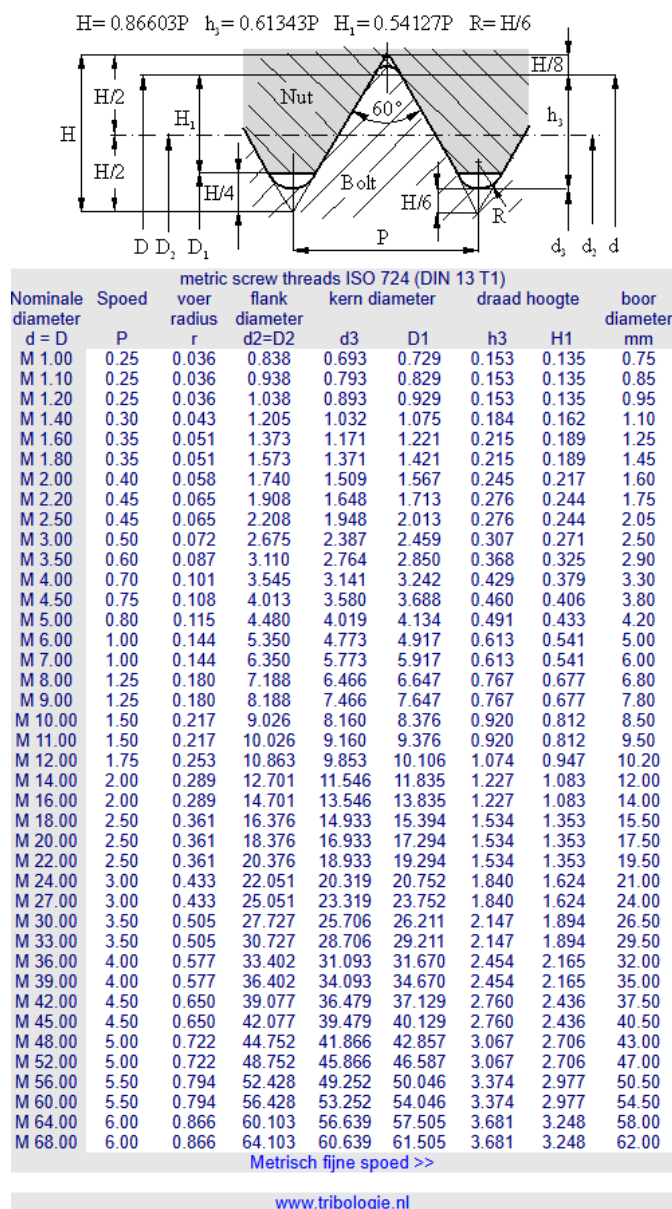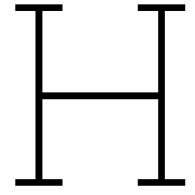| metric screw threads ISO 724 (DIN 13 T1)								
Nominale diameter $d = D$	Spoed P	voer radius r	flank diameter d2=D2	kern diameter		draad hoogte		boor diameter mm
				d3	D1	h3	H1	
M 1.00	0.25	0.036	0.838	0.693	0.729	0.153	0.135	0.75
M 1.10	0.25	0.036	0.938	0.793	0.829	0.153	0.135	0.85
M 1.20	0.25	0.036	1.038	0.893	0.929	0.153	0.135	0.95
M 1.40	0.30	0.043	1.205	1.032	1.075	0.184	0.162	1.10
M 1.60	0.35	0.051	1.373	1.171	1.221	0.215	0.189	1.25
M 1.80	0.35	0.051	1.573	1.371	1.421	0.215	0.189	1.45
M 2.00	0.40	0.058	1.740	1.509	1.567	0.245	0.217	1.60
M 2.20	0.45	0.065	1.908	1.648	1.713	0.276	0.244	1.75
M 2.50	0.45	0.065	2.208	1.948	2.013	0.276	0.244	2.05
M 3.00	0.50	0.072	2.675	2.387	2.459	0.307	0.271	2.50
M 3.50	0.60	0.087	3.110	2.764	2.850	0.368	0.325	2.90
M 4.00	0.70	0.101	3.545	3.141	3.242	0.429	0.379	3.30
M 4.50	0.75	0.108	4.013	3.580	3.688	0.460	0.406	3.80
M 5.00	0.80	0.115	4.480	4.019	4.134	0.491	0.433	4.20
M 6.00	1.00	0.144	5.350	4.773	4.917	0.613	0.541	5.00
M 7.00	1.00	0.144	6.350	5.773	5.917	0.613	0.541	6.00
M 8.00	1.25	0.180	7.188	6.466	6.647	0.767	0.677	6.80
M 9.00	1.25	0.180	8.188	7.466	7.647	0.767	0.677	7.80
M 10.00	1.50	0.217	9.026	8.160	8.376	0.920	0.812	8.50
M 11.00	1.50	0.217	10.026	9.160	9.376	0.920	0.812	9.50
M 12.00	1.75	0.253	10.863	9.853	10.106	1.074	0.947	10.20
M 14.00	2.00	0.289	12.701	11.546	11.835	1.227	1.083	12.00
M 16.00	2.00	0.289	14.701	13.546	13.835	1.227	1.083	14.00
M 18.00	2.50	0.361	16.376	14.933	15.394	1.534	1.353	15.50
M 20.00	2.50	0.361	18.376	16.933	17.294	1.534	1.353	17.50
M 22.00	2.50	0.361	20.376	18.933	19.294	1.534	1.353	19.50
M 24.00	3.00	0.433	22.051	20.319	20.752	1.840	1.624	21.00
M 27.00	3.00	0.433	25.051	23.319	23.752	1.840	1.624	24.00
M 30.00	3.50	0.505	27.727	25.706	26.211	2.147	1.894	26.50
M 33.00	3.50	0.505	30.727	28.706	29.211	2.147	1.894	29.50
M 36.00	4.00	0.577	33.402	31.093	31.670	2.454	2.165	32.00
M 39.00	4.00	0.577	36.402	34.093	34.670	2.454	2.165	35.00
M 42.00	4.50	0.650	39.077	36.479	37.129	2.760	2.436	37.50
M 45.00	4.50	0.650	42.077	39.479	40.129	2.760	2.436	40.50
M 48.00	5.00	0.722	44.752	41.866	42.857	3.067	2.706	43.00
M 52.00	5.00	0.722	48.752	45.866	46.587	3.067	2.706	47.00
M 56.00	5.50	0.794	52.428	49.252	50.046	3.374	2.977	50.50
M 60.00	5.50	0.794	56.428	53.252	54.046	3.374	2.977	54.50
M 64.00	6.00	0.866	60.103	56.639	57.505	3.681	3.248	58.00
M 68.00	6.00	0.866	64.103	60.639	61.505	3.681	3.248	62.00
Metrisch fijne spoed >>								
www.tribologie.nl								

Figure G.1: Dimensions of various Tie-Rods [60]

H

Appendix: Cross-section Division

This appendix provides an overview of the column cross-section division used in the structural design.

Figure H.1 illustrates the selected cross-sections, showing the varying wall thicknesses with a fixed outer profile.
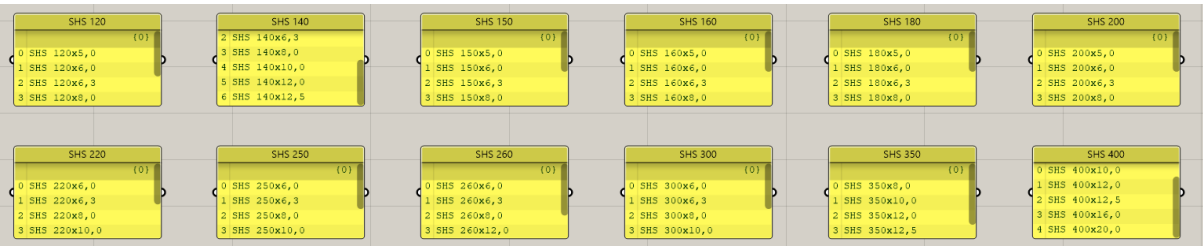

**Figure H.1:** Column cross-section division with the same thickness

Appendix: Tie-rod Dimensions Excel

An *Excel* sheet containing the calculated Tie-rods capacities used in this research is available and can be accessed via the following GitHub repository:

`https://github.com/ScheltoBlankenTU/TU-Delft-Thesis-Supplements`

Figure I.1 illustrates the location of the file containing the *Excel* sheet of the tie-rods on the GitHub repository.
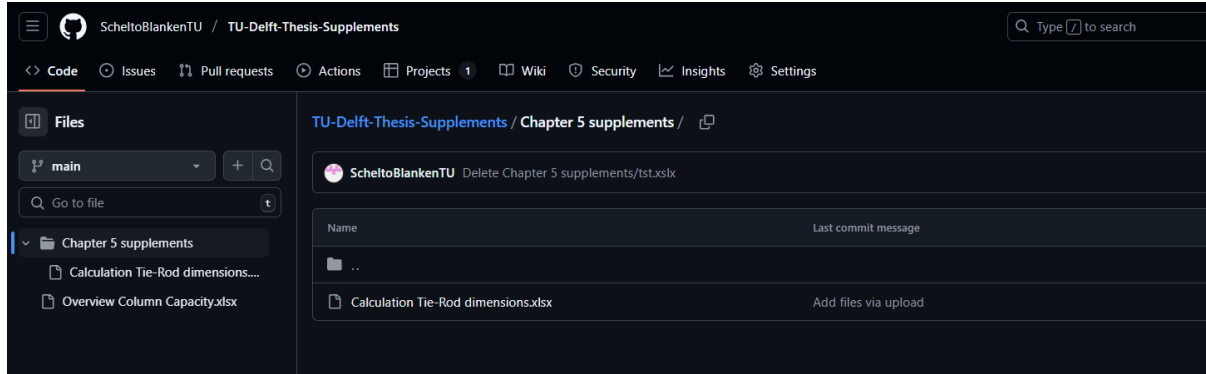
Figure I.1: Location of the Tie-Rod *Excel* on GitHub

J

Appendix: Concrete Strength and SHS Cross-Sections

This appendix provides reference data used in the parametric stiffness analysis discussed in Section 5.4.4. Table J.1 lists the modulus of elasticity for various concrete strength classes, both in cracked and uncracked conditions.

Table J.1: Modulus of elasticity for concrete of various strength classes (cracked and uncracked) [54]

Concrete Strength Class	$E_{cd,\text{cracked}}$ (N/mm^2)	$E_{cd,\text{uncracked}}$ (N/mm^2)
C20/25	9987	19975
C25/33	10492	20984
C30/37	10946	21891
C35/45	11359	22718
C40/50	11740	23480
C45/55	12094	24189
C50/60	12426	24852
C55/67	12738	25476
C60/75	13033	26067
C70/85	13581	27162
C80/95	14081	28163
C90/105	14544	29087

Table J.2 presents an overview of the hot-formed square hollow section (SHS) profiles considered in the outrigger design studies.

Table J.2: Overview of SHS cross-sections (Hot-Formed) used per dimension group

SHS 120	SHS 140	SHS 150	SHS 160
SHS 120x5,0	SHS 140x5,0	SHS 150x5,0	SHS 160x5,0
SHS 120x6,0	SHS 140x6,0	SHS 150x6,0	SHS 160x6,0
SHS 120x12,0	SHS 140x12,0	SHS 150x12,5	SHS 160x12,5
SHS 120x12,5	SHS 140x12,5	SHS 150x16,0	SHS 160x16,0
SHS 180	**SHS 200**	**SHS 220**	**SHS 250**
SHS 180x5,0	SHS 200x5,0	SHS 220x6,0	SHS 250x6,0
SHS 180x6,0	SHS 200x6,0	SHS 220x6,3	SHS 250x6,3
SHS 180x12,5	SHS 200x12,5	SHS 220x16,0	SHS 250x12,5
SHS 180x16,0	SHS 200x16,0		SHS 250x16,0
SHS 260	**SHS 300**	**SHS 350**	**SHS 400**
SHS 260x6,0	SHS 300x6,0	SHS 350x8,0	SHS 400x10,0
SHS 260x6,3	SHS 300x6,3	SHS 350x10,0	SHS 400x12,0
SHS 260x12,5	SHS 300x12,5	SHS 350x12,5	SHS 400x16,0
SHS 260x16,0	SHS 300x16,0	SHS 350x16,0	SHS 400x20,0

K

Appendix: Supplementary Utilisation Checks

Theoretical Background of Utilisation Checks

Utilisation checks for structural members are performed using the *Karamba3D Utilisation*-component. This tool evaluates member performance according to Eurocode 3 (EN 1993-1-1), which provides the basis for assessing steel structures under combined loading conditions [61].

Within the elastic design domain, the combined utilisation factor η accounts for axial force and biaxial bending moments, including their interaction. The general form of the check is given by:

$$\eta = \frac{N_{\text{Ed}}}{\chi_y N_{\text{Rd}}} + \frac{k_{yy} M_{y,\text{Ed}}}{\chi_{LT} M_{y,\text{Rd}}} + \frac{k_{zz} M_{z,\text{Ed}}}{M_{z,\text{Rd}}} \tag{K.1}$$

where N_{Ed}, $M_{y,\text{Ed}}$, and $M_{z,\text{Ed}}$ are the design axial force and bending moments; N_{Rd}, $M_{y,\text{Rd}}$, and $M_{z,\text{Rd}}$ are the corresponding resistances; χ_y and χ_{LT} are reduction factors for buckling and lateral-torsional buckling; and k_{yy}, k_{zz} are interaction factors.

Manual Calculation Example

To verify the accuracy of the values generated by the *Karamba3D Utilisation*-component, a manual utilisation check is performed for a modular steel column subjected to load combination L_{01}.

The column experiences a compressive axial force of $N = -679.63$ kN, a minor bending moment $M_y = 0.556$ kNm, and a shear force $V_y = -0.046$ kN.

The following section properties and resistance parameters are used in the verification:

- $N_{\text{Rd}} = 1152$ kN
- $M_{y,\text{Rd}} = 39.6$ kNm
- $\chi_y = 0.8354$, $\chi_{LT} = 1.0$
- $k_{yy} = 1.1987$, $k_{zz} = 1.1987$
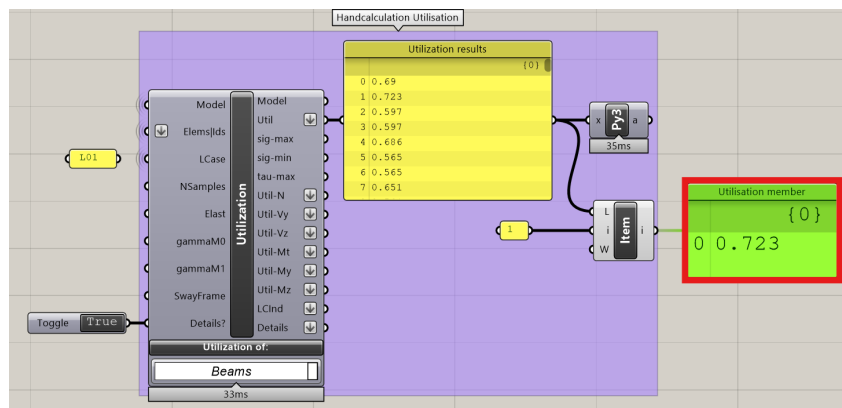
The utilisation components are calculated as follows:

$$\eta_N = \frac{678.80}{0.8354 \cdot 1152} = 0.706$$
$$\eta_{My} = \frac{1.1987 \cdot 0.556}{1.0 \cdot 39.6} = 0.01683$$
$$\eta_{Mz} = 0 \quad (\text{since } M_z = 0)$$

Summing the contributions gives the total utilisation:

$$\eta = \eta_N + \eta_{My} + \eta_{Mz} = 0.706 + 0.01683 + 0 = 0.723 \tag{K.2}$$

Figure K.1 presents the corresponding result from the *Karamba3D Utilisation*-component.

Figure K.1: Utilisation result (red box) from the *Karamba3D Utilisation* component.

The result from the manual calculation matches the output from the *Karamba3D Utilisation* component, confirming the accuracy and reliability of its computational implementation for the utilisation assessment in this research.

Appendix: Equivalent Elastic Modulus Calculation for Tie-Rod Elements

Equivalent Elastic Modulus Calculation for Tie-Rod Elements

To investigate the effect of the axial elongation of tie-rods in the structural model, an equivalent elastic modulus (E_{eq}) was calculated for a selected range of standard metric thread sizes (M20 to M68). The goal is to replace short model elements (0.2 m in length) with artificially reduced stiffness such that their axial elongation under load matched that of a full-length tie-rod (3.2 m) with identical geometry and material.

The calculation assumes a homogeneous isotropic steel with an elastic modulus of:

$$E_{steel} = 210{,}000 \text{ N/mm}^2 = 2.1 \times 10^8 \text{ kN/m}^2$$

For each tie-rod diameter the core diameter was used to determine the net tensile cross-sectional area A and then the elongation w of a 3.2 m long tie-rod under a 206 kN tensile load was calculated using Hooke's law:

$$w = \frac{F \cdot L}{E \cdot A}$$

To simulate this elongation in a model element of length 0.2 m, an equivalent elastic modulus E_{eq} was computed:

$$E_{eq} = \frac{F \cdot L_{model}}{w \cdot A}$$

This ensures that each short model element reproduces the same axial deformation as the full tie-rod under tension. The table L.1 shows the calculated values for a range of tie-rod sizes.

Tie-Rod (M)	Equivalent E_{eq} (kN/cm^2)
M20	16,819.10
M22	20,593.68
M24	24,750.04
M27	31,700.45
M30	39,509.88
M38	62,401.11
M40	62,951.08
M50	102,389.12
M68	175,484.80

Table L.1: Equivalent elastic moduli for tie-rod diameters

M

Appendix: Grasshopper Files

The main Grasshopper files used in this study, are available in the supplementary materials. These files include parametric models developed for the structural analyses. The archive can be accessed via the following GitHub repository:

$$\texttt{https://github.com/ScheltoBlankenTU/TU-Delft-Thesis-Supplements}$$

Figure M.1 shows the location of the Grasshopper files within the GitHub repository.
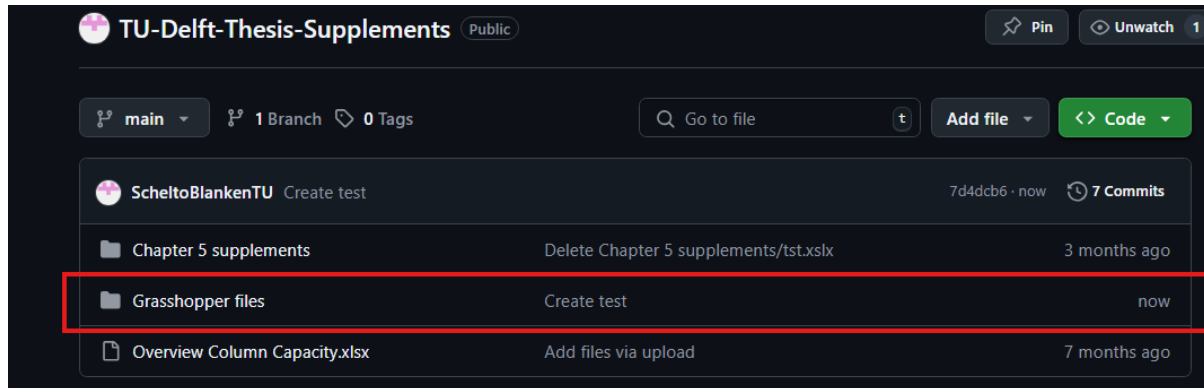
Figure M.1: Location of the Grasshopper files on GitHub

This page is intentionally left blank.